AD-A010 672

SPECIALISTS MEETING ON WING-WITH-STORES FLUTTER

Advisory Group for Aerospace Research and Development
Paris, France

April 1975

AGARD-CP-162

AGARD-CP-162

AGARD

ADVISORY GROUP FOR AEROSPACE RESEARCH & DEVELOPMENT

7 RUE ANCELLE 92200 NEUILLY SUR SEINE FRANCE

AGARD CONFERENCE PROCEEDINGS No. 162

Specialists Meeting on

Wing-With-Stores Flutter

NORTH ATLANTIC TREATY ORGANIZATION

DISTRIBUTION AND AVAILABILITY
ON BACK COVER

NORTH ATLANTIC TREATY ORGANIZATION

ADVISORY GROUP FOR AEROSPACE RESEARCH AND DEVELOPMENT

(ORGANISATION DU TRAITE DE L'ATLANTIQUE NORD)

AGARD Conference Proceedings No.162

Specialists Meeting on

WING-WITH-STORES FLUTTER

Papers presented at the 39th Meeting of the Structures and Materials Panel in Munich, Germany, 6–12 October 1974.

THE MISSION OF AGARD

The mission of AGARD is to bring together the leading personalities of the NATO nations in the fields of science and technology relating to aerospace for the following purposes:

- Exchanging of scientific and technical information;
- Continuously stimulating advances in the aerospace sciences relevant to strengthening the common defence posture;
- Improving the co-operation among member nations in aerospace research and development;
- Providing scientific and technical advice and assistance to the North Atlantic Military Committee in the field of aerospace research and development;
- Rendering scientific and technical assistance, as requested, to other NATO bodies and to member nations in connection with research and development problems in the aerospace field;
- Providing assistance to member nations for the purpose of increasing their scientific and technical potential;
- Recommending effective ways for the member nations to use their research and development capabilities for the common benefit of the NATO community.

The highest authority within AGARD is the National Delegates Board consisting of officially appointed senior representatives from each member nation. The mission of AGARD is carried out through the Panels which are composed of experts appointed by the National Delegates, the Consultant and Exchange Program and the Aerospace Applications Studies Program. The results of AGARD work are reported to the member nations and the NATO Authorities through the AGARD series of publications of which this is one.

Participation in AGARD activities is by invitation only and is normally limited to citizens of the NATO nations.

Published April 1975

533.695.9:533.6.013.422

Printed by Technical Editing and Reproduction Ltd
Harford House, 7–9 Charlotte St. London. W1P 1HD

FOREWORD

There has been a considerable increase in interest for predicting and preventing flutter on fighter aircraft carrying stores. Because of the importance of the application to the NATO countries' air forces, the Structures and Materials Panel of the NATO Advisory Group for Aerospace Research and Development (AGARD) held a one-half day Specialists' Meeting on "Wing-with-Stores Flutter" at the Structures and Materials Panel's 39th Meeting in Munich on 9 October 1974.

The addition of the stores significantly changes the dynamic characteristics and often adversely affects the flutter properties through drastically reduced flutter speeds. Flutter speed placards are thus frequently required thereby severely restricting potential speeds and mission performances. Moreover, many different stores can be carried at each carriage station requiring evaluation of a very high number of potentially flutter critical store combinations. The purpose of this meeting was to discuss the latest state-of-the-art in the various countries, and optimum methods for avoiding restrictive placards and for rapidly and economically evaluating the many store combinations. These proceedings contain the papers presented.

The AGARD Structures and Materials Panel expresses its appreciation to the authors and to the Specialists' Meeting Chairman, Mr O.Sensburg of M.B.B., Germany, for their significant contributions to this important fighter and ground support aircraft topic.

Walter J.Mykytow
Chairman, Working Group on
Aeroelasticity and Unsteady Aero-Dynamics

CONTENTS

CALCULATION METHODS FOR THE FLUTTER OF AIRCRAFT WINGS AND EXTERNAL STORES

by

Ll. T. Niblett and J. C. A. Baldock
Structures Department
Royal Aircraft Establishment
Farnborough, Hampshire
England

SUMMARY

This paper reports theoretical work at RAE on the wing-with-stores problem which has been in the fields of structural representation, the solution of the flutter equations and the prediction of flutter characteristics from structural properties.

The subjects covered in some detail are:

(a) a comparison of the normal modes calculated for a wing-with-stores from some of the normal modes of the bare wing and discrete-load modes with those calculated from the full flexibility matrix;

(b) the basis of a computer program which traces the loci of constant flutter speeds when two structural parameters vary; and

(c) the interpretation of the loci of constant flutter speed in terms of modal shapes and frequencies with the object of assessing the most critical store combinations.

1 INTRODUCTION

This paper describes work that has been done on a few of the techniques of the theoretical treatment of the flutter of wings with stores favoured at RAE.

Among the data needed for wing-with-stores flutter calculations is a description of the structural properties of the wing which is adequate enough to give its distortions under a wide variety of store inertia forces yet economic in computing time and space. That such a description is given by a combination of normal and discrete-load modes has been shown by some calculations which will be described.

Since this combination will give the distortions of the wing under practically any store inertia forces from only comparatively few coordinates it is very suitable for use with a computer program which automatically follows contours of constant flutter speed against two of the mass and/or stiffness properties of the store. Such contours are useful in that they give the most critical store combinations and the basis of an automatic contour-following program is given.

The contours will indicate critical combinations of store parameters. A method is given for a rapid assessment of the physical basis for this combination.

2 DISCRETE-LOAD MODES

Comparable calculations have been made of the normal modes of an encastré wing with stores. The structural system consisted of the bare wing, two flaps with beams connecting them to the bare wing structure and two stores with pylons connecting them to the bare wing structure (see Fig.1). The object of the calculations was to discover how close an approximation to the 'true' modes of the wing with stores, defined as the results of calculations using all the information available, was obtained if only a limited number of the normal modes of the wing-without-stores together with appropriate 'discrete-load' modes of the wing were used. The 'discrete-load' modes (sometimes known as 'junction' modes) are the deflection shapes taken up by the wing when it is loaded statically at the pylon attachment points by the types of load the stores generate dynamically which give significant distortions of the wing, i.e. heaving force and rolling- and pitching-moments. These modes are proportional to the columns of the flexibility matrix for the wing which pertain to those particular types of loads acting at the pylon attachment points.

Thus an allowed displacement of the wing can be written

$$z_a = [Q_{ab}, \gamma F_{aa} P_{ac}]\{q_b, q_c\} \qquad (1)$$

where z_a is a vector of wing displacements,

Q_{ab} is the rectangular matrix of wing displacements in the normal modes whose generalised coordinates are q_b,

F_{aa} is the wing flexibility matrix,

P_{ac} is a non-square permutation matrix which selects from F_{aa} the columns appropriate to the discrete-load modal coordinates q_c,

and factoring by γ simply replaces the dimensions of flexibility by the dimensions of displacement.

The inertia matrix, if the mass matrix associated with the wing deflection points is A_{aa}, is

$$\begin{bmatrix} Q_{ba} \\ \gamma P_{ca} F_{aa} \end{bmatrix} A_{aa} \left[Q_{ab}, \gamma F_{aa} P_{ac} \right] = \begin{bmatrix} \hat{a}_b & \gamma Q_{ba} A_{aa} F_{aa} P_{ac} \\ \text{sym} & \gamma^2 P_{ca} F_{aa} A_{aa} F_{aa} P_{ac} \end{bmatrix} \tag{2}$$

where $\hat{a}_b$ is a diagonal matrix of the normal mode inertias, and the stiffness matrix is given by

$$\begin{bmatrix} Q_{ba} \\ \gamma P_{ca} F_{aa} \end{bmatrix} F_{aa}^{-1} \left[Q_{ab}, \gamma F_{aa} P_{ac} \right] = \begin{bmatrix} \hat{e}_b & \gamma Q_{ba} P_{ac} \\ \text{sym} & \gamma^2 P_{ca} F_{aa} P_{ac} \end{bmatrix} . \tag{3}$$

If the initial data is in the form of a stiffness matrix, E_{dd}, rather than a flexibility matrix, the discrete load modes, Q_{dc}, are given by the solution of an equation such as

$$E_{dd} Q_{dc} = \gamma Q_{da} P_{ac} \tag{4}$$

the rhs giving the generalised forces in the stiffness modes due to the discrete loads. The total stiffness matrix is then given by

$$\begin{bmatrix} Q_{bd} \\ Q_{cd} \end{bmatrix} E_{dd} \left[Q_{db}, Q_{dc} \right] = \begin{bmatrix} Q_{bd} \\ \gamma P_{ca} Q_{ad} E_{dd}^{-1} \end{bmatrix} E_{dd} \left[Q_{db}, \gamma E_{dd}^{-1} Q_{da} P_{ac} \right] = \begin{bmatrix} \hat{e}_b & \gamma Q_{bd} Q_{da} P_{ac} \\ \text{sym} & \gamma^2 P_{ca} Q_{ad} E_{dd}^{-1} Q_{da} P_{ac} \end{bmatrix} . \tag{5}$$

This is not possible if E_{dd} is singular. One of the usual methods of overcoming this type of problem is to split the coordinates q_d into coordinates, q_f say, which involve distortion of the structure and coordinates, q_r say, which describe rigid-body displacements. The inertia matrix

$$A_{dd} = \begin{bmatrix} A_{ff} & A_{fr} \\ A_{rf} & A_{rr} \end{bmatrix}$$

and the stiffness matrix

$$E_{dd} = \begin{bmatrix} E_{ff} & 0 \\ 0 & 0 \end{bmatrix} \tag{6}$$

The q_d coordinates are replaced by $q_{\bar{f}}$ coordinates using the transformation

$$q_d = \begin{bmatrix} q_f \\ q_r \end{bmatrix} = \begin{bmatrix} I \\ -A_{rr}^{-1} A_{rf} \end{bmatrix} q_{\bar{f}} = \begin{bmatrix} I \\ Q_{r\bar{f}} \end{bmatrix} q_{\bar{f}} \quad \text{(say)} \tag{7}$$

where the $q_{\bar{f}}$ coordinates are fewer than the q_d coordinates by the number of rigid body freedoms present. The constraints on the $q_{\bar{f}}$ modes are the equivalent of the addition of rigid-body deflections to the q_f modes such that the new modes are orthogonal to further rigid-body deflections. Eq.(4) transformed and premultiplied by $[I, Q_{\bar{f}r}]$ is

$$\left[I, Q_{\bar{f}r} \right] \begin{bmatrix} E_{ff} & 0 \\ 0 & 0 \end{bmatrix} \begin{bmatrix} I \\ Q_{r\bar{f}} \end{bmatrix} Q_{\bar{f}c} = \gamma \left[I, Q_{\bar{f}r} \right] \begin{bmatrix} Q_{fa} \\ Q_{ra} \end{bmatrix} P_{ac} \tag{8}$$

which multiplied out and transformed back gives

$$Q_{dc} = \gamma \begin{bmatrix} I \\ Q_{r\bar{f}} \end{bmatrix} E_{ff}^{-1} (Q_{fa} + Q_{\bar{f}r} Q_{ra}) P_{ac} \tag{9}$$

An approximate description of the system could be obtained by adding some of the natural modes, including all the rigid-body modes to these. This has not been tested numerically.

Some simple exploratory calculations have been made in the case of 'discrete-constraint' modes, which is another approach useful when the stiffness matrix is singular. The term is used to denote the fundamental modes of the system described by the equation

$$\left(\omega^2 A_{dd} - E_{dd}\right)q_d = 0 \tag{10}$$

which each of the constraint equations, collectively described by

$$C_{ra}Q_{ad}q_d = 0 \quad , \tag{11}$$

used separately as a subsidiary equation. The constraints applied are the equivalents for the discrete loads on the actual system, i.e. a discrete-load mode under a force is replaced by a discrete-constraint mode with position constraint at the point of action of the force. The constraints can be applied before or after the system is transformed to one orthogonal to the body freedoms.

The 'true' modes of the wing with flaps and stores were obtained by setting up the dynamical equations for the wing primary structure, the flap beams and flaps and the pylons and stores and solving them simultaneously. The wing primary structure, which originally had 98 degrees of freedom, was approximated to by its lowest 70 normal modes and 6 discrete-load modes. Each flap beam had 2 distortion modes and the flaps had 30 degrees of freedom *in toto*. The pylons each had 3 distortion degrees of freedom covering motions in pitch, roll and torsion. The total number of degrees of freedom subsequent to the application of continuity constraints was 112. The approximate systems were made up of up to 10 normal modes for the bare wing and flap, 6 discrete-load modes of the wing primary structure, with the coefficients modified to take account of the flaps, and 6 pylon distortion modes, adding up to a maximum of 22 modes. The frequencies of the first 10 modes of these systems were compared with those of the true system. For the biggest approximate system the maximum error was found to be 0.04%. The errors were not all of the same sign which suggested that the theoretical accuracy of the approximation was greater than the numerical accuracy with which the modes were calculated. Were the differences in frequencies larger it might have been necessary to formulate other criteria of accuracy. A comparison of the frequencies obtained when fewer normal and discrete-load modes were used showed that the modes were dominated by the effect of the heavy stores. A good indication of this was that the approximations with 6 discrete-load modes only were better than those with 10 normal modes only apart from those which had a large flap or beam content. Also the approximations were significantly worse when the discrete-load modes for the outer pylon fixing points were excluded. There is no reason to believe however that the method would not give good approximations with lighter stores and it certainly works in the no-stores case. It would appear that, in the case of the structure considered here at least, accurate results can be achieved by including all the discrete-load and pylon modes and normal modes up to and including the first whose frequency is above the maximum frequency of interest. Further details of the calculations are given in Ref.1.

The approximate method used here has wider applications in the representation of substructures. For instance, from some further calculations that have been made[1], it can be surmised that fewer modes of the wing primary structure and flaps would have been needed to calculate the wing-with-flaps normal modes if some of the modes for the wing primary structure had been the modes under discrete loads at the flap beam junctions and some of the modes for the flaps had been discrete-constraint or -load modes for the beam junctions.

3 CONTOURS OF CONSTANT FLUTTER SPEED

A representation of the wing structure such as the above is useful for providing data for computer programs which calculate contours of constant flutter speed against two store mass or pylon stiffness parameters for the aerodynamic coefficients for one set of modes will cover an infinite variety of store/pylon conditions. The contour program used at RAE is based on inverse iteration and circular extrapolation.

The form of the flutter equations generally used in the UK can be written

$$\left[A\lambda^2 + (B + D\nu^{-1})\lambda + C + E\nu^{-2}\right]q = 0 \tag{12}$$

where A, D and E are real matrices associated with the structural properties of the system, B and C are real matrices associated with the aerodynamic properties, λ is the (imaginary) frequency parameter, ν the speed parameter, and q the latent vector.

An abbreviated form of Eq.(12) is

$$\left[A\lambda^2 + \bar{B}\lambda + \bar{C}\right]q = 0 \tag{13}$$

which can be written in linear form as

$$\begin{bmatrix} -A^{-1}\bar{B} & -A^{-1}\bar{C} \\ I & 0 \end{bmatrix}\begin{bmatrix} p \\ q \end{bmatrix} = \lambda\begin{bmatrix} p \\ q \end{bmatrix} \tag{14}$$

where $p = \lambda q$.

Iteration according to the equation

$$\begin{bmatrix} A^{-1}\bar{B} + \pi I & A^{-1}\bar{C} \\ -I & \pi I \end{bmatrix} \begin{bmatrix} p_{s+1} \\ q_{s+1} \end{bmatrix} = -(\lambda - \pi) \begin{bmatrix} p_s \\ q_s \end{bmatrix} \tag{15}$$

results to convergence to the latent root nearest π .

Eq.(15) can be replaced by two equations

$$\pi q_{s+1} = p_{s+1} - (\lambda - \pi) q_s \tag{16}$$

and

$$(\pi A + \bar{B}) p_{s+1} + \bar{C} q_{s+1} = -(\lambda - \pi) A_{ps} \quad . \tag{17}$$

Substituting for q_{s+1} in Eq.(17) from Eq.(16) and multiplying by π gives

$$(\pi^2 A + \pi \bar{B} + \bar{C}) p_{s+1} = (\lambda - \pi)(\bar{C} q_s - \pi A q_s) \tag{18}$$

Once one point on the contour has been found the stability at any point near to it can be found by making the appropriate modifications to the coefficient matrices and iterating using Eq.(18) and Eq.(16) with the frequency parameter at the known point on the contour as the pole π . The sign of the real part of $(\lambda - \pi)$ determines which side of the contour the trial point lies.

The choice of where to search for the contour is based on the assumption that an arc of a circle will be a good approximation over a limited range. In general three previous points on the contour will be available (say A, B and C of Fig.2). A circle is drawn through these points and the positions of the last two points are defined in terms of the angles (α,β) between the radii through them and the first point and the next point is searched for, using Muller interpolation, along a radius which is at the same angle to the radius through the last point as that is to the radius through the point before ($\gamma = \beta - \alpha$). The search is commenced on the circle (at D1) and continues until $(\lambda - \pi)$ has a small enough real part or until it is predicted that the contour lies more than a limited distance from D1. If the latter is the case the value of γ is halved and this can happen a number of times if the contour proves difficult to find. On the other hand if the contour proves easy to find the value of γ used for the next point may be made greater subject to maximum limits, one of which is part of the data and the other rt of the program. Thus the intervals between points on the contours vary constantly with the tortuosity of the contour. One of the main objects in writing the programs has been to reduce the amount of human intervention to the minimum. Further details of the program are given in Refs.2 and 3.

The method does not cater for the exact lining-up of assumed and calculated frequency parameter but if it is so wished the aerodynamic coefficient matrices can be made consistent with π .

4 INTERPRETATION OF CONTOURS OF CONSTANT FLUTTER SPEED

Fig.3 shows the diagram from a typical output of the contour program. The store mass parameters are the mass and the square of the radius of gyration of a store on an inboard pylon. This output was preceded by conventional solutions for the system roots versus airspeed at the mass parameter points shown on Fig.3, in order to find critical flutter speeds, which were used as starting values for the loci of flutter speeds versus one mass parameter with the other mass parameter held constant. These solutions were obtained by one of the options built in to the contour program, and they themselves are used for starting values for finding the contours.

It may be seen from Fig.3 that there is a sharply critical combination of store mass and radius of gyration. The physical basis for this critical combination is of obvious interest, particularly for assessing the likely change in the critical mass parameters for a change in another parameter, such as pylon stiffness. Diagnostic procedures are available[4] for interpreting flutter conditions, but the number of parameters in a wing-with-stores calculation is so large, and some of the stiffness data so uncertain in the early stages of design, that a very rapid and easily obtained indicator is desirable. The frequencies at zero airspeed of the modes involved in the flutter solutions are easily found, and variations of these with one mass parameter can be helpful. Fig.4 shows the zero airspeed frequencies versus store mass for a value of store radius of gyration close to that of the most critical store combination. Comparing Fig.3 and Fig.4, it may be seen that the most critical store mass combination is associated with the proximity of the second and third normal mode frequencies. Alternatively, it may be possible to divide the system of equations into a set of predominantly 'bending' modes (e.g. wing vertical bending, store pylon lateral bending) and a set of predominantly 'torsion' modes (e.g. wing torsion, pylon pitching) and the variation of the zero airspeed frequencies from these sets separately may be plotted against a store mass parameter. Fig.5 is an example of this presentation for the same system as in Figs.3 and 4. It may be seen that on Fig.5, the critical store mass combination is associated with the proximity of the frequencies of the second 'bending' mode and the first 'torsion' mode.

Obviously, a serious study of the flutter coupling should involve the shapes of the modes of the system, but the large number of specific configurations of potential interest in a wing-with-stores analysis can easily lead to a bulk of mode shape results that is difficult to assimilate. Modal frequency results are more compact and can provide a useful quantitative guide to the effects of parameters, so that the plotting of mode shapes can be confined to a bare minimum of the most important specific configuration cases.

5 REFERENCES

1 Ll. T. Niblett. Structural representation of a wing with stores in normal-mode calculations. (1974) RAE Technical Report 74019

2 Ll. T. Niblett. Methods of solving the flutter equations in use at RAE. (1969) ARC Current Paper 1046

3 Ll. T. Niblett. A flutter-speed contour program. Unpublished. ('971) RAE Technical Memorandum

4 J.C.A. Baldock. A technique for analysing the results of a flutter calculation. (1973) RAE Technical Report 73168

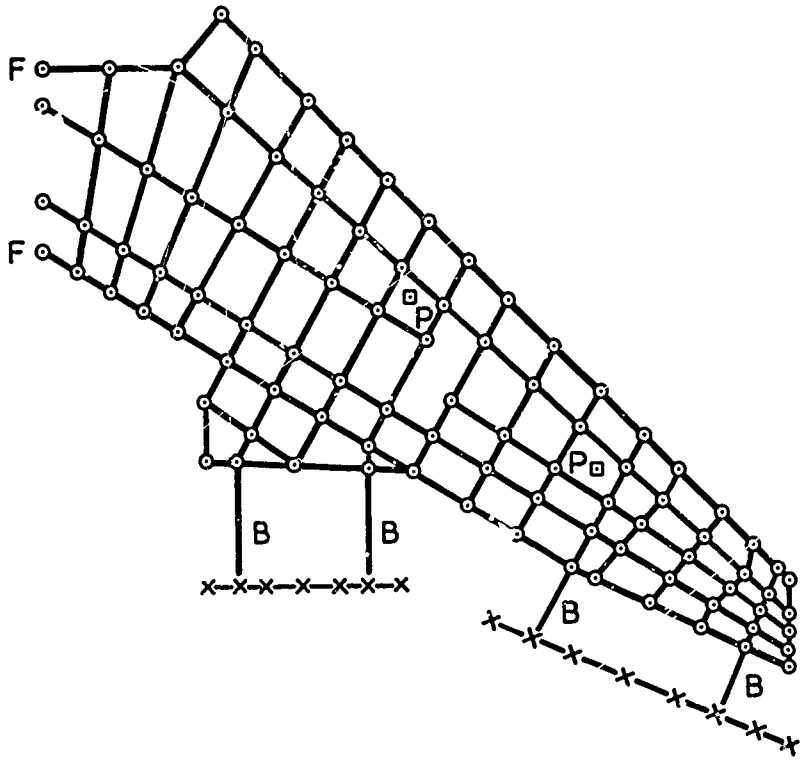

FIG.1 WING AND FLAP GRID POINTS

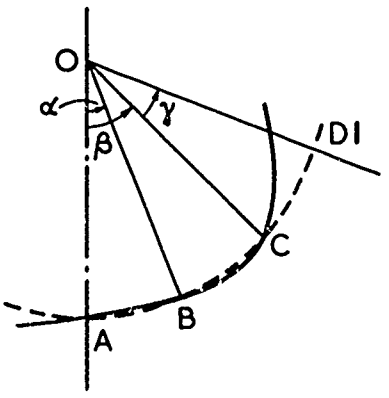

FIG.2 CIRCULAR EXTRAPOLATION

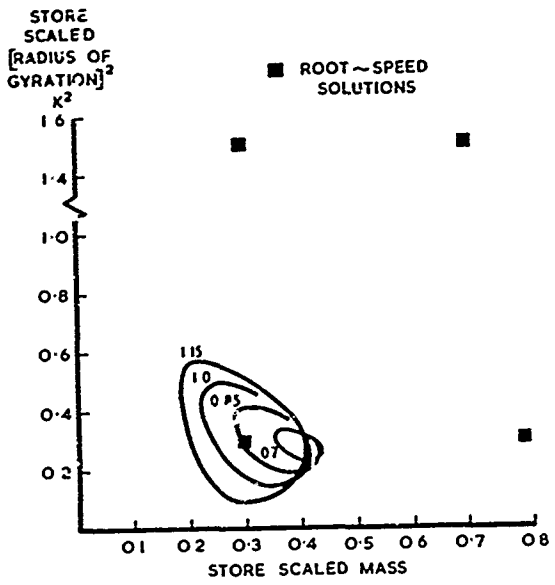

FIG. 3

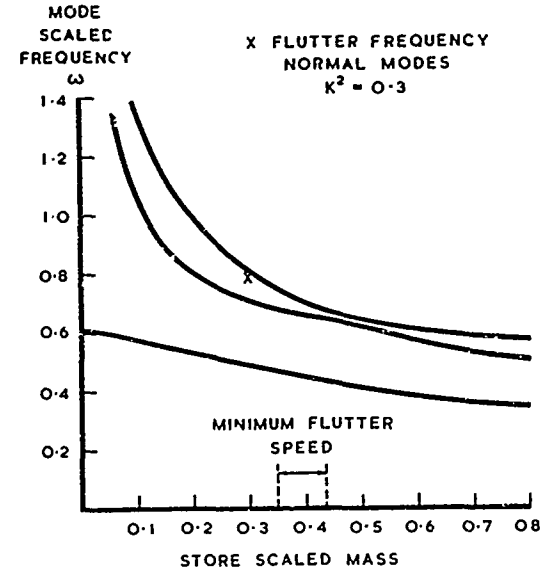

FIG. 4

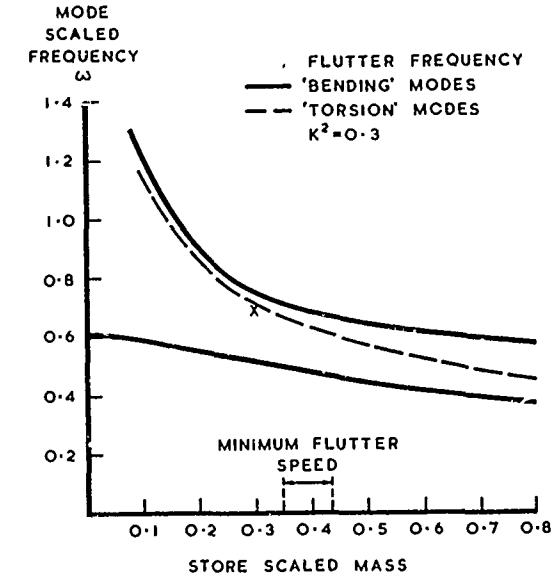

FIG. 5

U.K. JAGUAR EXTERNAL STORE FLUTTER CLEARANCE

by

C.G.LODGE and M.ORMEROD

British Aircraft Corporation Limited,
Military Aircraft Division,
Warton Aerodrome,
WARTON. Nr.Preston. Lancashire.

SUMMARY :

The paper describes the flutter clearance of U.K. Jaguar using a combination of mathematical modelling, ground resonance and flight testing leading ultimately to clearance of a wide range of under wing stores. Some improvements in modal modelling techniques are outlined. These should enable reductions in future ground and flight testing times to be made.

1. INTRODUCTION

Modern military aircraft are expected to carry a wide range of external stores, many of these on flexible underwing pylons. For a relatively small aircraft such as Jaguar where external stores are carried on two underwing pylons and an underfuselage pylon (Figure 1) and the masses of the heavier stores are of the same order as the wing itself, it is evident that the structural modes and hence the flutter status of the aircraft will change considerably from one store combination to another. On Jaguar, further complications arise because multiple stores can be carried on a "tandem beam" and side by side carriers, which are fitted to the underwing pylons, and these introduce additional flexibility.

The resulting problem of clearing for flutter a wide range of "different" aircraft has been approached by a combination of theoretical calculations, ground and flight tests. This report describes the procedures followed concentrating on the techniques employed and discusses some of the results obtained.

2. CLEARANCE PROCEDURE

It was decided that the most efficient and economical method of demonstrating the clearance was by utilising as extensively as possible a theoretical model of the aircraft structural modes and their associated aerodynamics. The calculated modes could be checked against the appropriate ground resonance test data and if necessary modified to achieve a successful match. With the structural representation thus validated, flutter behaviour could be rechecked by calculation and the critical configurations identified for investigation in flight tests. Hopefully, these flight tests would :

(a) achieve a flight flutter clearance for these critical configurations

(b) provide reliable measured data on critical structural mode behaviour to corroborate predictions and hence,

(c) justify an analogous clearance by calculation for all other non-critical stores without the need for further specific instrumented flight tests.

This approach aims to derive maximum benefit from extensive but relatively cheap calculations in order to confine flight testing by a few key configurations. It hinges crucially upon :

(a) a confident choice of the key configurations for flight tests,

and

(b) Measuring modal data, in flight, which is extensive and reliable enough to allow meaningful comparison with predictions in order to support the analogous clearance.

Its final success depends upon a good correlation from (b)

3. THEORETICAL MODELLING

Thus the underwing stores flutter clearance program relied fundamentally on the quality and efficiency of the theoretical calculations. It was recognised that these must not only predict potentially critical store combinations with sufficient accuracy but must also:

(a) allow the key structural and aerodynamic parameters to be identified

(b) allow flutter status of any new stores to be established quickly

A theoretical model has been set up using a combination of branch modes for :

(i) clean aircraft, and

(ii) pylon/stores.

This component set has several advantages over the normal modes of the aircraft including underwing stores :

(a) The clean aircraft modes and flutter behaviour is well understood and validated from clean aircraft ground resonance tests and flight flutter clearance data.

(b) The pylon modes have been chosen so that modal stiffnesses can be inserted easily from static stiffness test data. These in turn can be verified by calculating the associated normal modes and comparing these with rig mounted pylon-stores resonance test data.

(c) The modal generalised inertias are computed once for all for each store on each pylon and combinations constructed by appropriate additions.

(d) As many pylon modes as required can be introduced, to represent E.R.U. effects, tandem beams, side by side carriers etc.

(e) The model generalised aerodynamics neglect contributions from pylon and stores, and hence can be computed once for all and are independent of store configuration. So far as can be judged from calculation and test data, this simplification introduces errors within about 5% on flutter speeds.

Theoretically derived modes were used for the basic aircraft representation. These were computed from wing, tail and fuselage branch modes and in the initial, pre G.R.T. stages were confined to fixed root wing modes. Although this sacrifices some accuracy in flutter speed prediction, the basic store flutter couplings are unchanged and the much reduced number of modes allowed a significant economy in computation and eased interpretation of the calculation output. This allows a better understanding of the fundamental couplings and sensitivities. Finally the full aircraft free-free theoretical modes were incorporated into the model and have been used to match aircraft G.R.T., to define the flight flutter test configurations, and provide comparison with flight data.

4. FLUTTER CALCULATIONS

It was clear at the outset that fuel tank sequencing would need particular attention. Two possible flutter couplings were identified with the prototype fuel sequencing system, using fixed root wing modes (Figure 3), and these survive when outboard stores are introduced. (Figure 4). Corresponding calculations using complete aircraft modes showed that although these wing-store flutter speeds changed, the flutters still occurred at similar frequency, with the same store mass properties but were milder in type. (Figure 5).

Detailed inspection of the flutter mode shapes revealed that these wing flutters arise from couplings between modes which resemble fundamental wing bending and torsion.

Further, it can be shown that :

(a) component modes of wing bending, inboard and outboard pylon lateral bending combine to produce three "wing bending" modes

(b) component modes of wing torsion, inboard and outboard pylon pitch combine to produce three "wing torsion" modes.

The wing store flutters which have been found for a wide range of stores all arise from couplings between modes of these types. These effects can be illustrated most clearly for the case with inboard tank alone (Figure 6) when the two types of flutter are both associated with the first "wing torsion" mode frequency coinciding with first and second "wing bending" modes.

Similar relationships can be identified in the more complex inboard tank/outboard bomb case (Figure 7). It is clear that pylon mode stiffnesses are the key structural feature in wing-store flutter. The stores which are predicted to be most critical will change if pylon stiffnesses change, and some further evidence of this is given in Figure 8. Note that these trends are characteristic of frequency coincidence.

5. GROUND RESONANCE TESTING

The reliance on theoretical calculations and their sensitivity to pylon stiffnesses dictated rig mounted stiffness and resonance tests on inboard and outboard pylons for a representative range of store mass properties. Subsequently, a few complete aircraft resonance tests were completed with a typical store,

(a) on inboard pylon only

(b) on outboard pylon only

(c) in combination

to verify the overall mathematical model and in particular the important pylon stiffnesses. All the normal modes were measured, up to and including the highest frequency pylon induced wing bending/torsion mode which might be a source of flutter coupling, based on the theoretical review.

The measured normal modes were compared with the appropriate predictions (Figure 9), where labels have been attached which describe the predominant structural motion in that mode. The correspondence is good when only the inboard or only the outboard store is fitted, but relatively poor when these are in combination. An alternative set of pylon stiffness values was derived (Calc.2) which provide a better match for all three configurations. These adjustments were small for the inboard pylon but up to 0.5x the values established by rig tests for the outboard pylon.

It was conjectured that the 6 wing normal modes which were retained in the clean aircraft representation might be insufficient to define local wing distortion near to the pylon-wing attachment. Failure to account for these effects would be consistent with compensation via a reduction in pylon stiffnesses, as evidenced by the aircraft ground resonance test matching. Further evidence for this is presented in Figure 10. This demonstrates the accuracy of calculating wing-store modes (for a rigid pylon) from a finite number of clean Jaguar wing modes. From this there are substantial inaccuracies at low frequencies even with twelve clean wing modes. These can however, be avoided even with only 3 clean wing modes, provided that additional wing modes are introduced which are the statically distorted wing shapes for unit vertical shear, bending moment and pitching moment applied at each pylon-wing attachment. Such discrete load modes clearly retain significant local distortion effects which are discarded in the higher order clean wing modes, and they retain the concept and economy of the component mode approach.

For subsequent applications, it might be expected that the increased accuracy of predictions will allow the critical store configuration to be confidently defined prior to ground resonance testing, given some test data on pylons. In addition, it might be considered sufficient in future only to resonance test one configuration, eg. with both pylons loaded.

6. SELECTION OF MOST CRITICAL STORES

The basis of selection on Jaguar is juxtaposition of wing bending and torsion type mode frequencies, supported by representative flutter calculations for each possible region of coincidence.

Inboard stores only

Figure 11 shows the frequency of the normal modes of bending and torsion types which fall within the important frequency range for a wide range of projected stores. It is evident that for all these stores, the bending and torsion mode frequencies are substantially independent and uniquely related to pylon lateral bending and pitch mode generalised inertias, respectively; that is, to store mass and to store pitching inertia. Superimpositon of Figures 11(a), 11(b) reveals two potential flutter couplings:

(1) B1/T1 (10 Hz) - for heavy, slender stores, eg. full fuel tank

(2) B2/T1 (10 Hz) - for medium weight, short stores, eg. bombs/part full fuel tank.

Flutter calculations are already available in these classifications; the mild flutter on Figure 3 is B1/T1 and the severe flutter is B2/T1.

Updated flutter calculations with new pylon stiffnesses confirm that the latter is more important, and reveal that the fuel tank with prototype fuel sequencing system is still the most critical store for this type of flutter. Similarly, the fuel tank is most critical for the alternative, milder type.

Outboard Stores only

Similar modal frequency characteristics can be identified for outboard stores only (Figure 12). Superimposition in this case reveals :

(1) B1/T1 coupling - medium weight, slender stores, outside the present range.

(2) B2/T1 coupling - for most of the stores in the current inventory

Thus, flutter calculations were necessary for nearly all the projected outboard single stores. These revealed that only the B1/T1 coupling is potentially critical. Very mild couplings and no flutter resulted from the B2/T1 frequency coincidence. Thus, none of the stores in the current inventory are critical when carried alone on outboard pylon.

Inboard and Outboard Stores

The problem becomes more complicated now, as there are three bending modes and two torsion modes to consider. Figure 13 shows the possible bending mode frequencies and Figure 14 the possible torsion mode frequencies as a function of inboard and outboard store inertia properties. Observe that there are six possible sources of coupling :

(a) B1/T1 flutter is only possible when heavy slender stores are carried on the inboard pylon. The most critical combination is with a small light outboard store. (eg. full fuel tank in Figure 6).

(b) B1/T2 flutter would require store mass and inertia outside the range considered at present.

(c) B2/T1 is most likely for store combinations with moderately heavy stores on the inboard pylon and light stores on the outboard pylon. (the 50% full fuel tank case in Figure 6).

(d) B2/T2 flutter would require an unrealistic store mass and inertia combination.

(e) B3/T1 is most critical for a combination of inboard and outboard stores which are similar in weight (eg. the 50% fuel tank plus outboard bomb flutter in Figure 7).

(f) B3/T2 is most critical for heavy outboard stores. (The full fuel tank plus outboard bomb flutter in Figure 7).

The most critical store combinations were established for flutter calculations in each of these regions. From these the potentially critical flutters occur when the fuel tank is carried on the inboard pylon both with and without outboard pylon stores. Types B1/T1 and B2/T1 have higher flutter speeds than the inboard only stores case, and B3/T1 and B3/T2 have the lowest flutter speeds of all.

SUMMARY

From this review, the following projected store configurations emerge as critical, in order of concern :

(1) tank inboard plus bomb outboard

(2) tank inboard only

(3) tandem beam stores inboard plus outboard bomb

(4) tandem beam stores inboard only

and these were selected for flight flutter testing.

The multiple carried stores were predicted to be less critical for flutter than the fuel tank, but there was a possibility of significant structural response in several poorly damped, local beam modes.

7. FLIGHT TESTING

Strategy:

Calculations have shown the inboard fuel tank was the most critical store for flutter. It was decided to flutter test this alone initially, anticipating that the experience and data gained would help considerably in interpreting the more complicated and most critical configuration, according to prediction, with outboard bomb.

This approach was also adopted with tandem beams inboard. In each case (4 configurations) specific excitation and instrumentation was fitted.

Finally, on successfully completing the above programme, single flights were planned with less critical stores, which were confidently expected to be flutter free. In these flights, no specific excitation was attempted, other than pilot opinion of vibration response to turbulence, manoeuvring etc., en route to the design clearance speed.

Excitation was effected via electrical inputs to the main taileron actuators (inherited from the clean aircraft clearance) covering an appropriate frequency range. This proved to be more effective than bonking the wing or providing electrical inputs via wing spoilers.

Acceleration transducers were mounted on the stores and on fuselage, wing and tail. Signals from these could be recorded on magnetic tape during the flight.

Analysis:

Raw time histories of the response signals allowed a watching brief to be kept on real events. Computer analysis of the signals yielded power spectra which assisted in the subsequent interpretation of these events. Final quantitative analysis provided modal data for justifying flight envelope expansion and for correlation with predictions.

RESULTS

Some results are included here from flight tests on the most critical inboard tank/outboard bomb combination.

A typical spectral variation is shown in Figure 15. For this, a large number of samples, each of short duration were taken. These particular results are taken from the tank nose vertical transducer and demonstrate in a striking way how the two wing torsion mode frequencies develop as fuel is used from the tank. Because of short sampling times, these spectra cannot be used to obtain accurate dampings but taken together they give a very clear picture of frequency trends eg. Figure 16. Note that all the potential flutter couplings are excited and that the critical condition will be close to 60% tank fuel.

More accurate estimates of frequency and damping were obtained by further analysis of the impulse response, derived by spectral division and inverse fourier transformation using spectra taken from longer data samples.

Frequencies and dampings obtained in this way are shown in Figure 17 for the potential flutter mode of the tank/outboard bomb store combination. There is some scatter in the results but the overall trend in frequency and damping is clear. Also included in the plot are the predicted trends for this mode. If 3% critical damping increase is introduced from the structure (where about 2% could be expected from GRT results) then a good match follows. Observe that 60% fuel state is indeed the most critical condition.

In general, the comparison with predictions was acceptable for the form configurations tested, and no flutter limitations were encountered.

8. CONCLUSIONS

At this stage :

(a) a theoretical model has been established, and

(b) validated by ground resonance test on key configurations.

(c) the most critical store configurations have been successfully cleared by flight test to the full flight envelope of M = 0.95/Sea Level

(d) good correlation between flight tests and predictions has been achieved over a wide range of store configurations.

We therefore claim that clearance can be justified, by analogy, for all other projected stores, without a need for specific flight flutter tests. In the course of subsequent flights to assess handling/performance of non-critical stores, there have been no indications of any flutter problems.

Thus, from flutter tests on 4 configurations, a full flight envelope clearance has been achieved for 85 possible combinations of known stores.

FIG.1

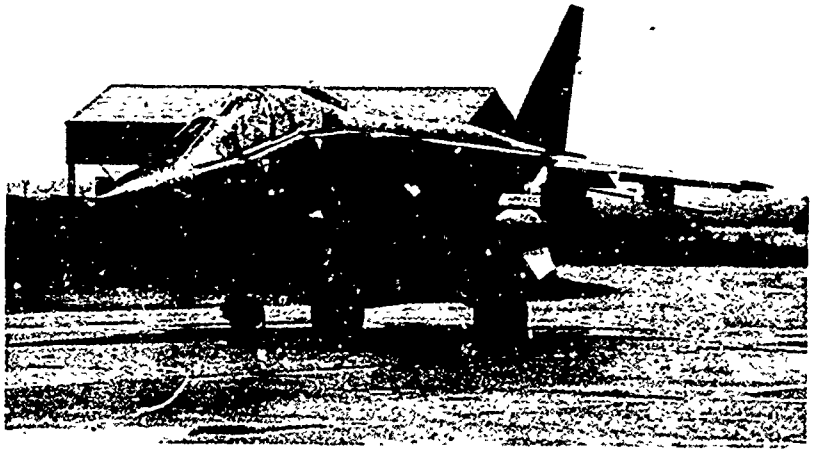

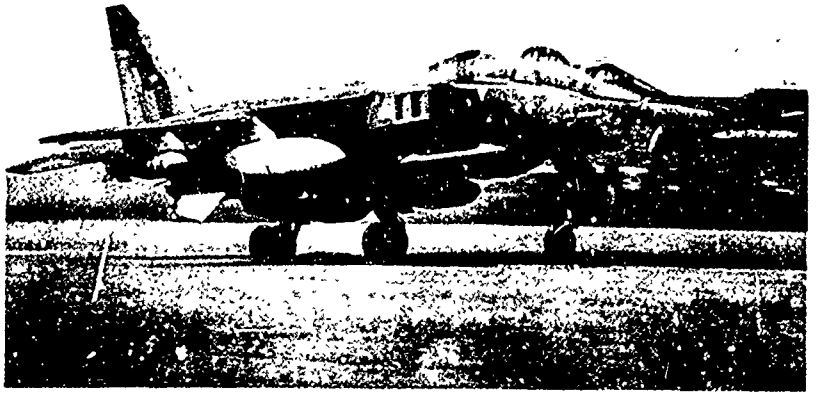

FIGURE 2

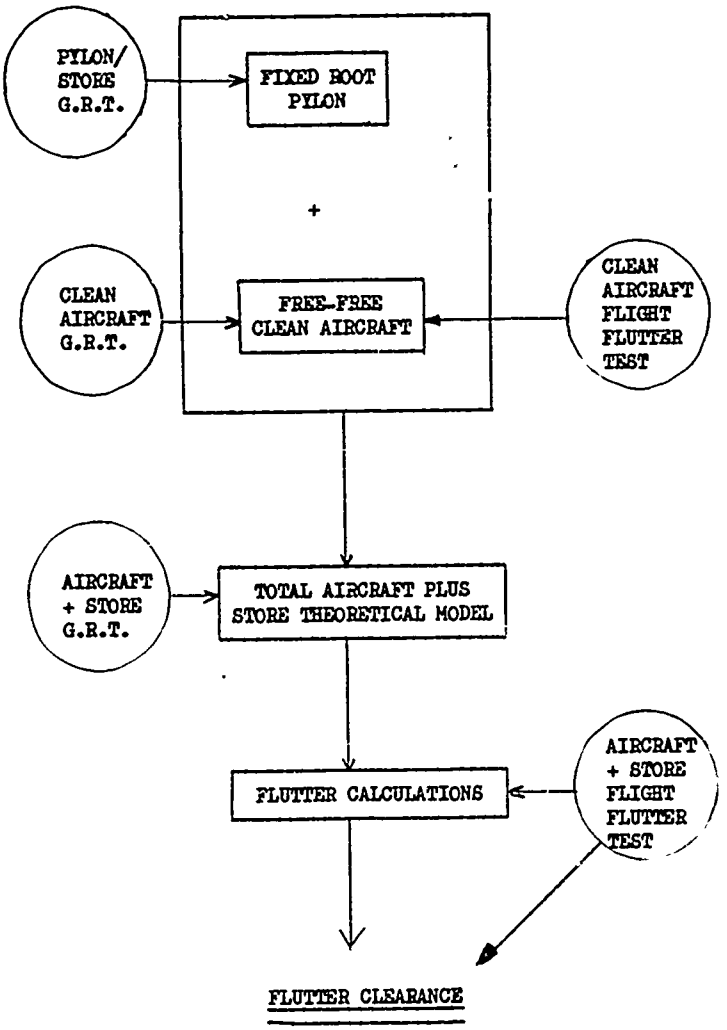
PYLON/
STORE
G.R.T.
FIXED ROOT
PYLON
+
CLEAN
AIRCRAFT
G.R.T.
FREE-FREE
CLEAN AIRCRAFT
CLEAN
AIRCRAFT
FLIGHT
FLUTTER
TEST
AIRCRAFT
+ STORE
G.R.T.
TOTAL AIRCRAFT PLUS
STORE THEORETICAL MODEL
FLUTTER CALCULATIONS
AIRCRAFT
+ STORE
FLIGHT
FLUTTER
TEST
FLUTTER CLEARANCE

FIG. 3

FUEL TANK ON INBOARD PYLON

CALCULATED CHARACTERISTICS.

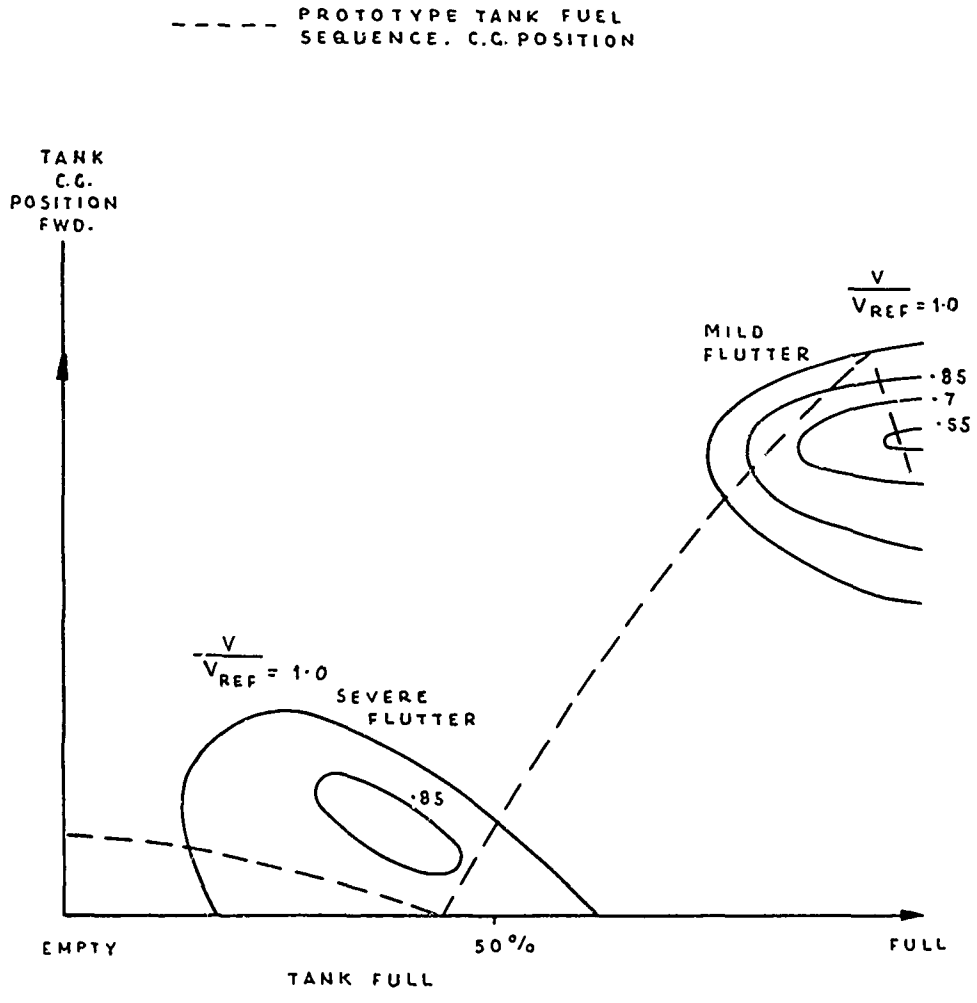

FIG 4

FUEL TANK ON INBOARD PYLON STORES ON OUTBOARD PYLON
FIXED ROOT WING

CALCULATED CHARACTERISTICS.

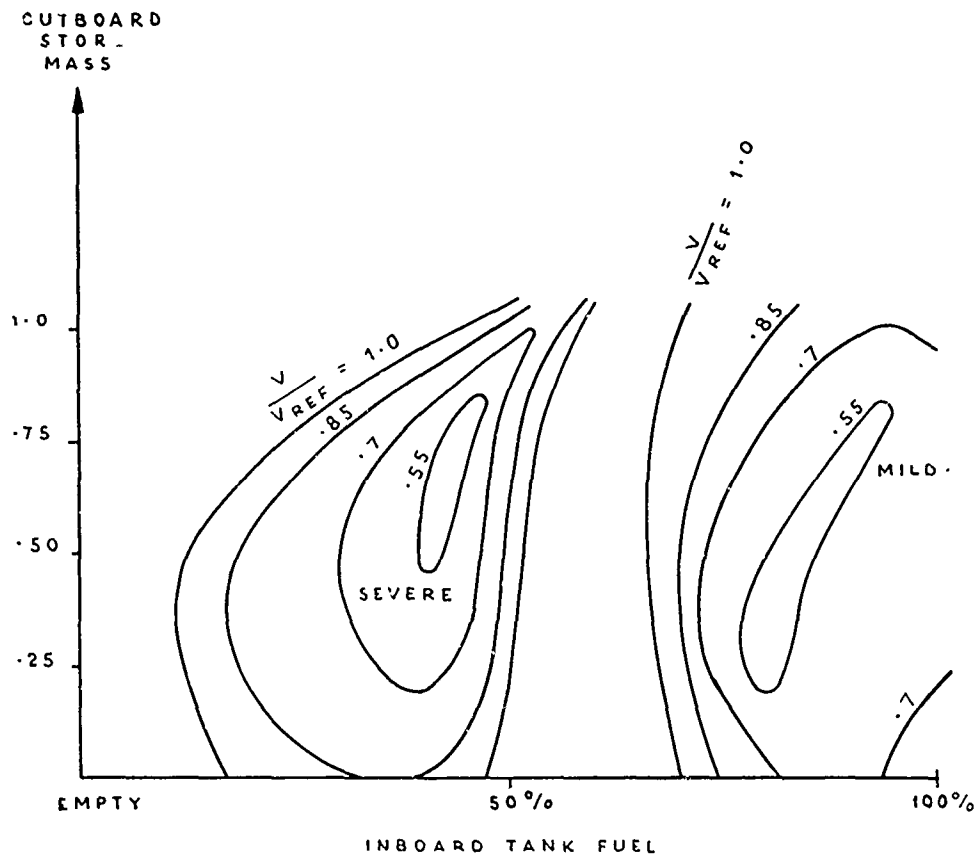

FIG. 5.

FUEL TANK ON INBOARD PYLON

CALCULATED CHARACTERISTICS.

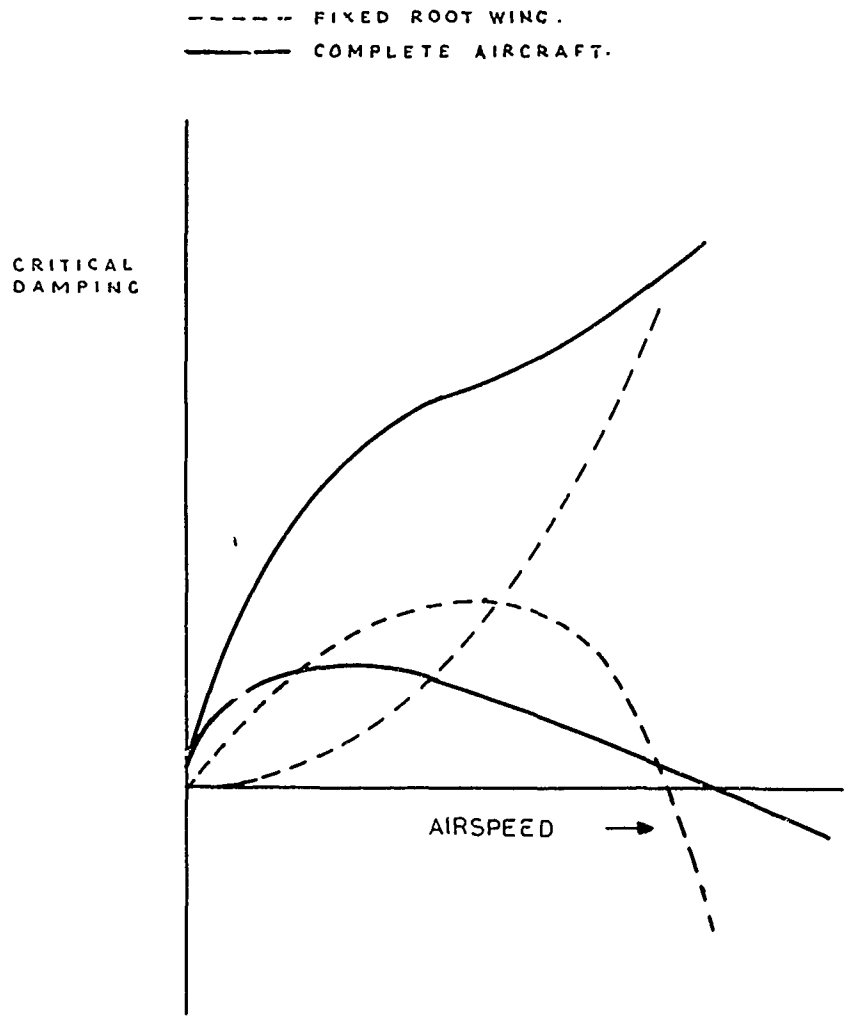

FIG. 6

1200 LITRE TANK ON INBOARD PYLON

CALCULATED CHARACTERISTICS.

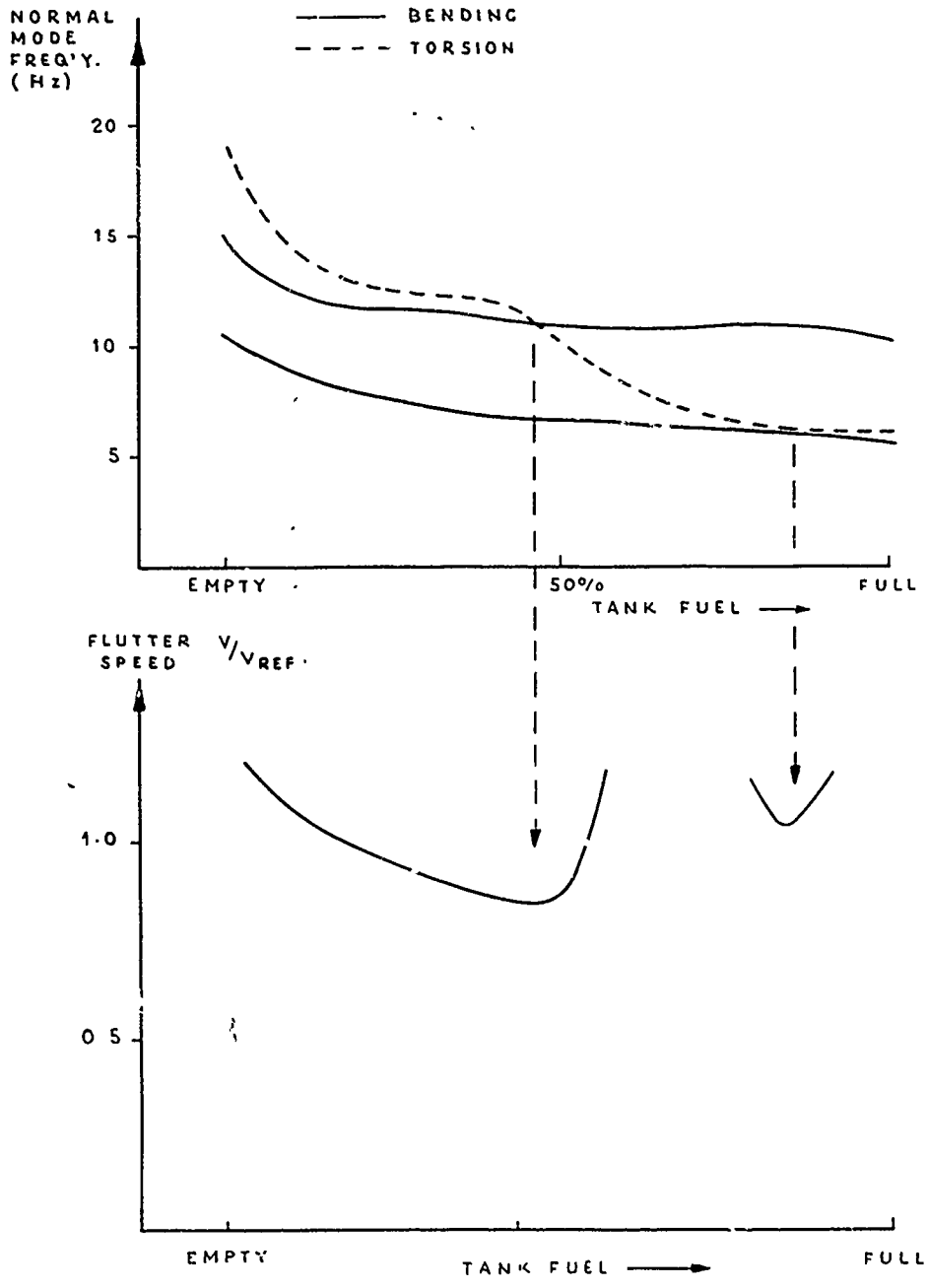

FIG. 7

1200 LITRE TANK ON INBOARD PYLON
1000LB BOMB ON OUTBOARD PYLON

CALCULATED CHARACTERISTICS.

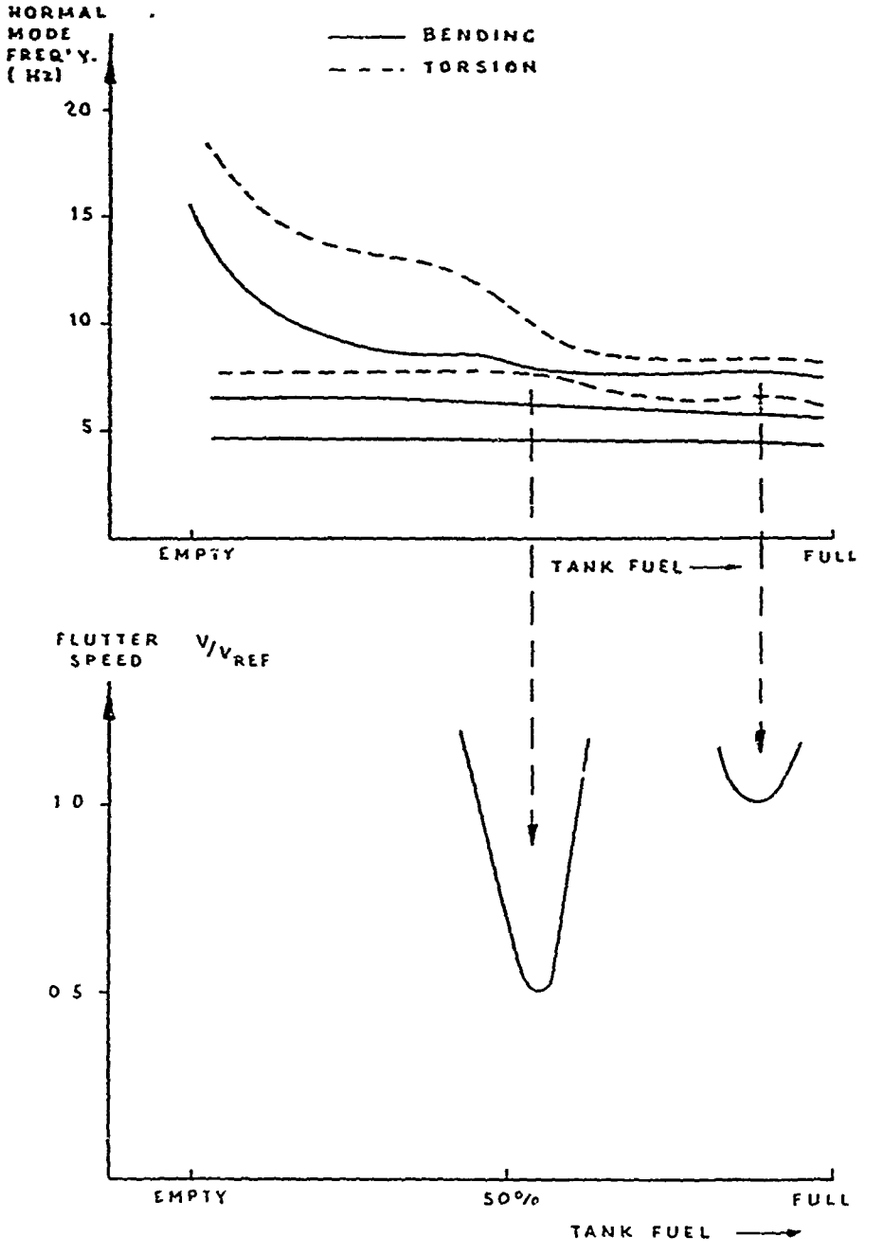

FIG. 8.

FLUTTER SPEEDS INBOARD FUEL TANK (55% FUEL)
OUTBOARD BOMB.

CALCULATED CHARACTERISTICS.

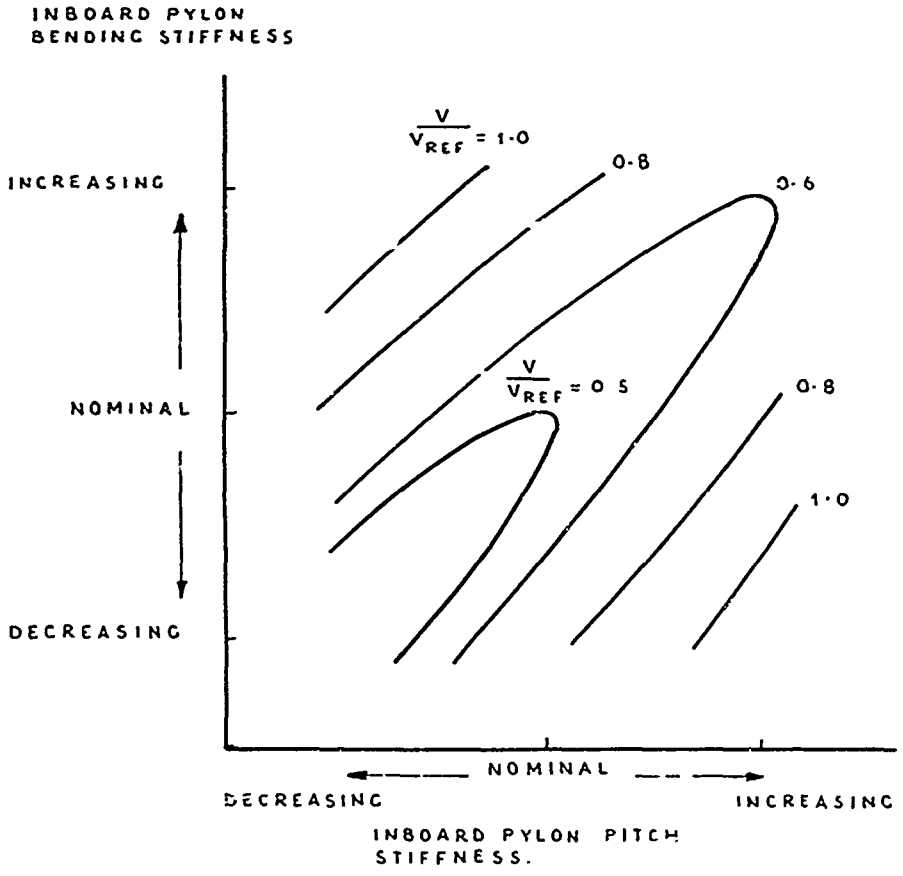

FIG.9

COMPLETE AIRCRAFT GROUND RESONANCE TEST.

MODE	CALC 1	CALC 2	TEST	CONFIGURATION
$W + \phi_I$	6·7	6·8	7·1	INBOARD TANK ONLY
$W - \phi_I$	9·4	9·5	9·1	
ψ_I	10·5	11·0	11·5	(60% FULL)
α_I	13·2	12·8	12·8	
$W + \phi_o$	5·2	4·9	4·8	OUTBOARD BOMB ONLY
$W - \phi_o$	7·3	6·9	7 1	
α_o	8·5	7·3	7·8	
ψ_o	14·0	11·6	12·4	
$W + \phi_I + \phi_o$	5·7	5·6	5·0	INBOARD TANK WITH OUTBOARD STORE.
$W + \phi_I - \phi_o$	7·9	7·7	7·1	
$W - \phi_I - \phi_o$	10·7	8·9	8·3	
$\alpha_I + \alpha_o$	10 0	9·5	9·4	
ψ_I	10·5	11·0	11·2	
$\alpha_I - \alpha_o$	14·6	15·7	15·1	
ψ_o	20·2	18·7	16·7	

CALC 1 PYLON STIFFNESSES EX. RIG G R T.

CALC 2 CALC. 1 VALUES FACTORED TO MATCH A/C G.R.T.

W = WING BENDING α = PYLON PITCH

ϕ = PYLON BENDING ψ = PYLON YAW

FIG.10.

ACCURACY OF WING STORE MODE CALCULATIONS

Full calculation	12 wing modes plus incremental mass	3 wing modes plus 3 load modes	CONFIGURATION
7.3	7.3	7.3	I/B STORE ONLY
10.3	11.0	10.3	
15.4	21.6	[illegible]4	
21.5	26.4	21.5	
37.9	40.6	38.6	
51.7	52.1	55.1	
4.2	4.3	4.2	O/B STORE ONLY
6.2	6.6	6.2	
9.5	12.4	9.5	
26.7	28.7	26.8	
48.6	56.4	51.2	
55.2	57.3	56.6	
4.0	4.1	4.0	I/B AND O/B STORE
6.1	6.4	6.1	
8.3	10.3	8.3	
13.9	16.9	13.9	
15.4	26.7	15.4	
25.2	33.3	25.2	
34.3	49.9	34.6	

FIG. 11.

AIRCRAFT MODE FREQUENCIES FOR STORES ON IN BOARD PYLON.

CALCULATED CHARACTERISTICS.

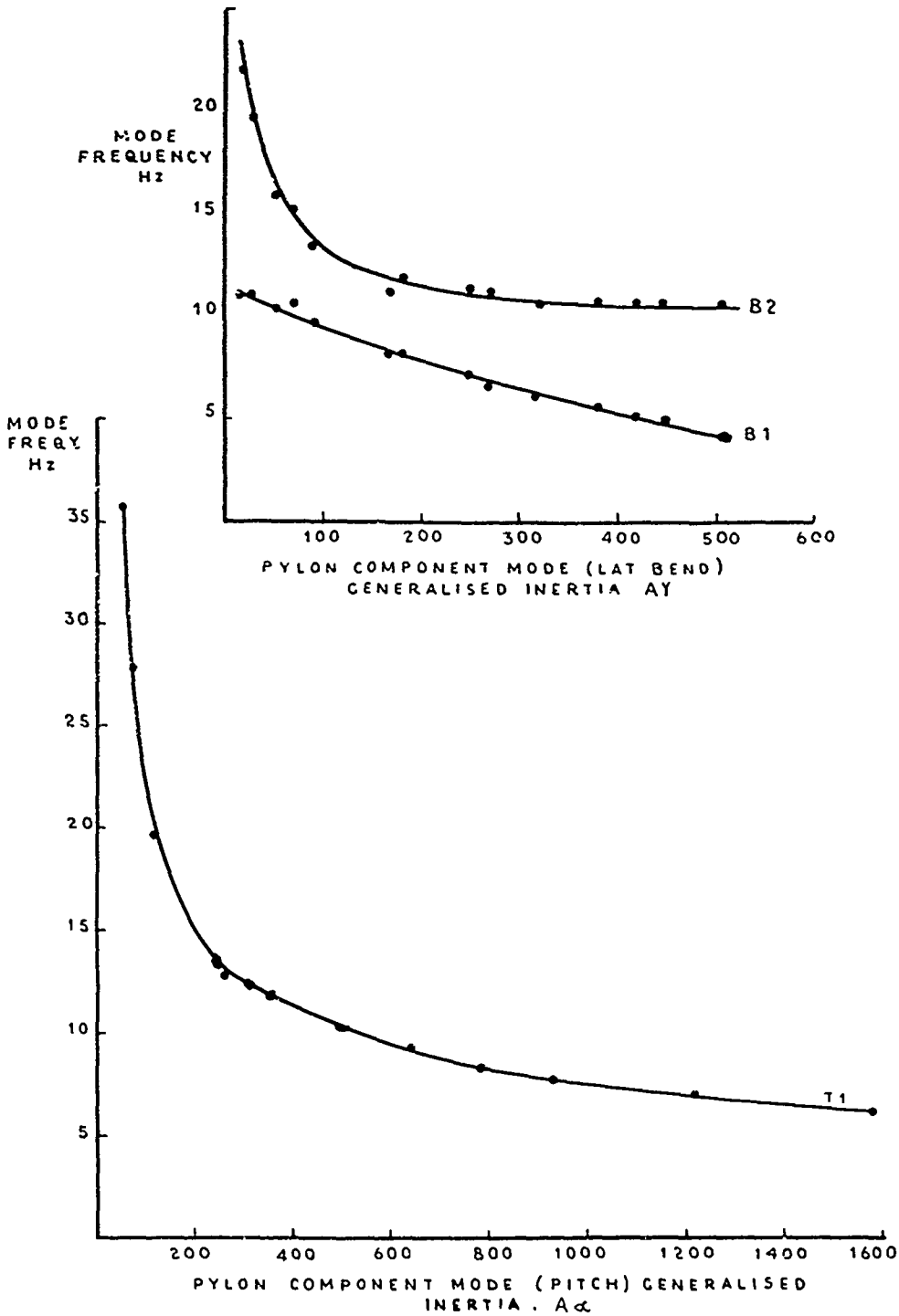

FIG 12.

AIRCRAFT MODE FREQUENCIES FOR STORES ON OUTBOARD PYLON.

CALCULATED CHARACTERISTICS.

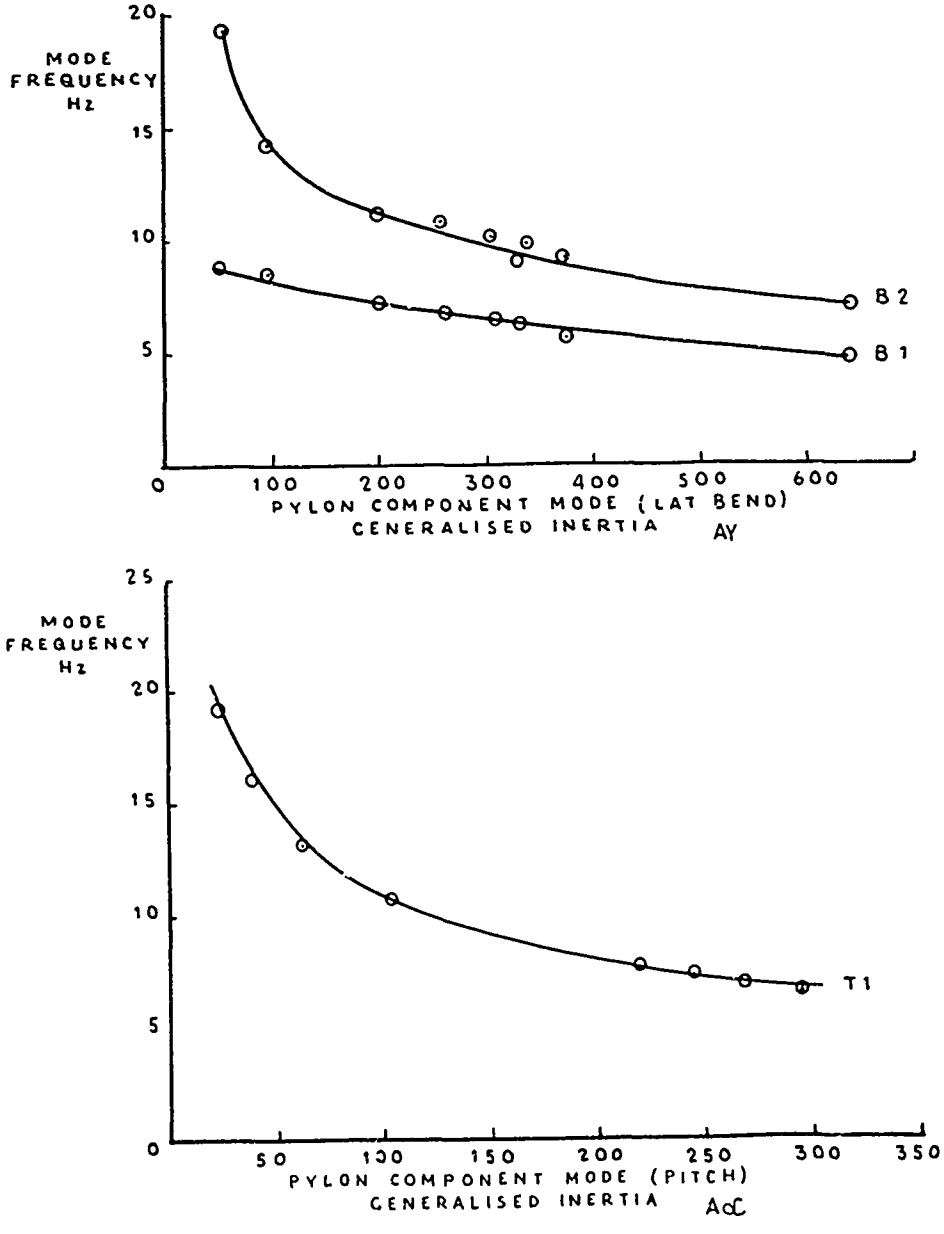

FIG. 13.

AIRCRAFT BENDING MODE FREQUENCIES,
FOR STORES ON INBOARD AND OUTBOARD PYLONS

CALCULATED CHARACTERISTICS.

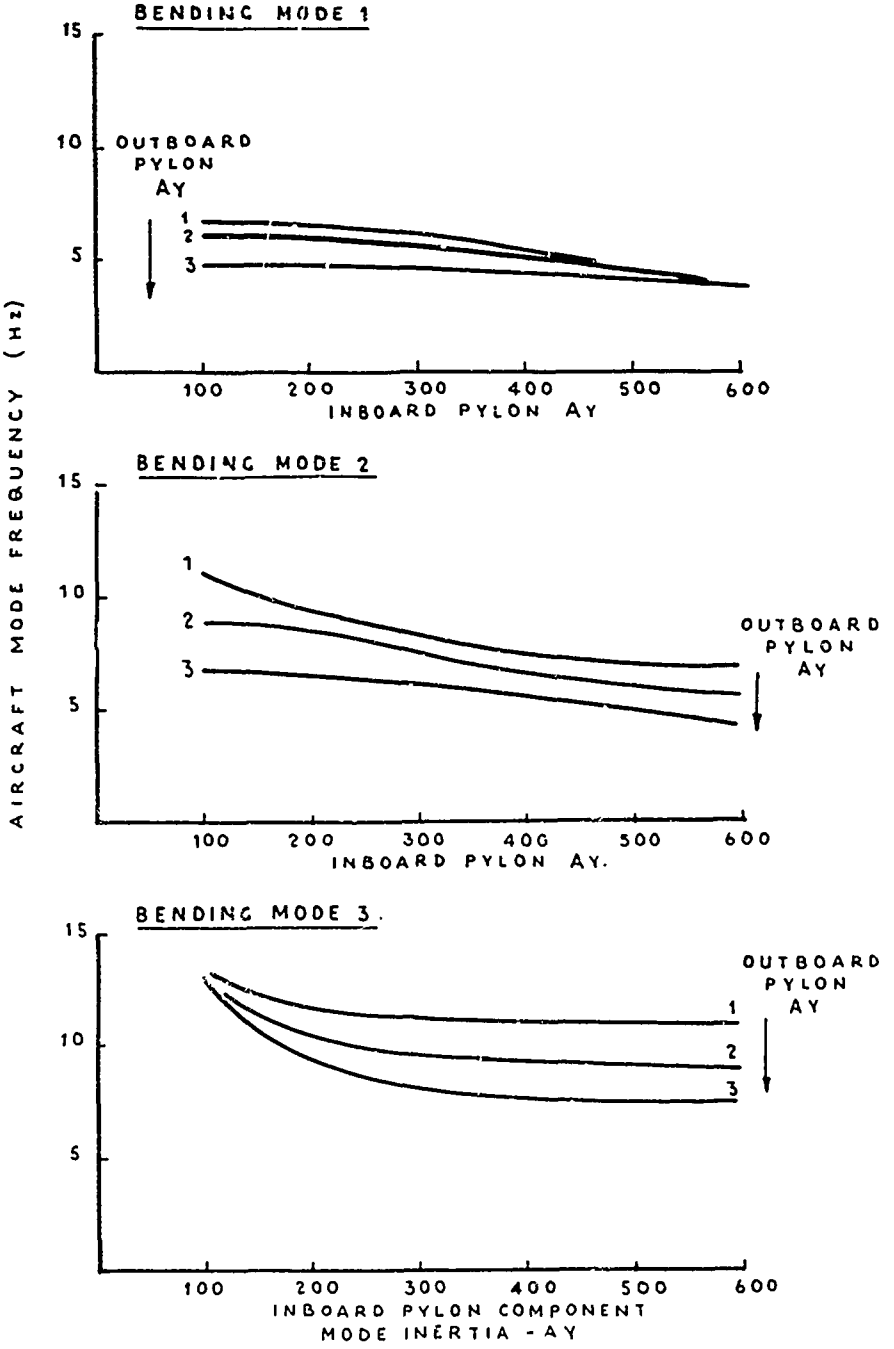

FIG . 14.

AIRCRAFT TORSION MODE FREQUENCIES FOR STORES ON INBOARD AND OUTBOARD PYLON

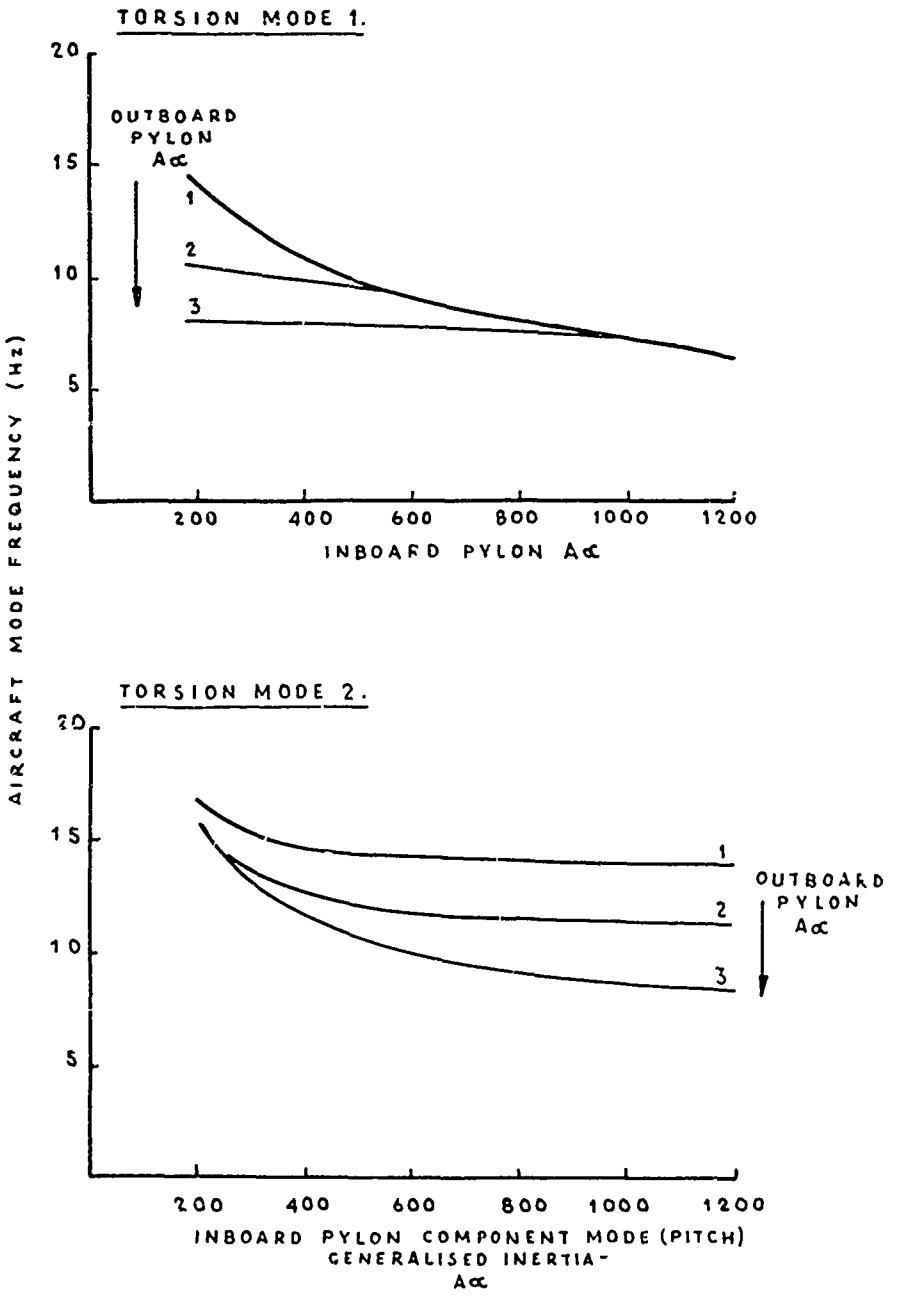

FIG 15.

EXAMPLE OF SEQUENTIAL SPECTRA FROM FLIGHT

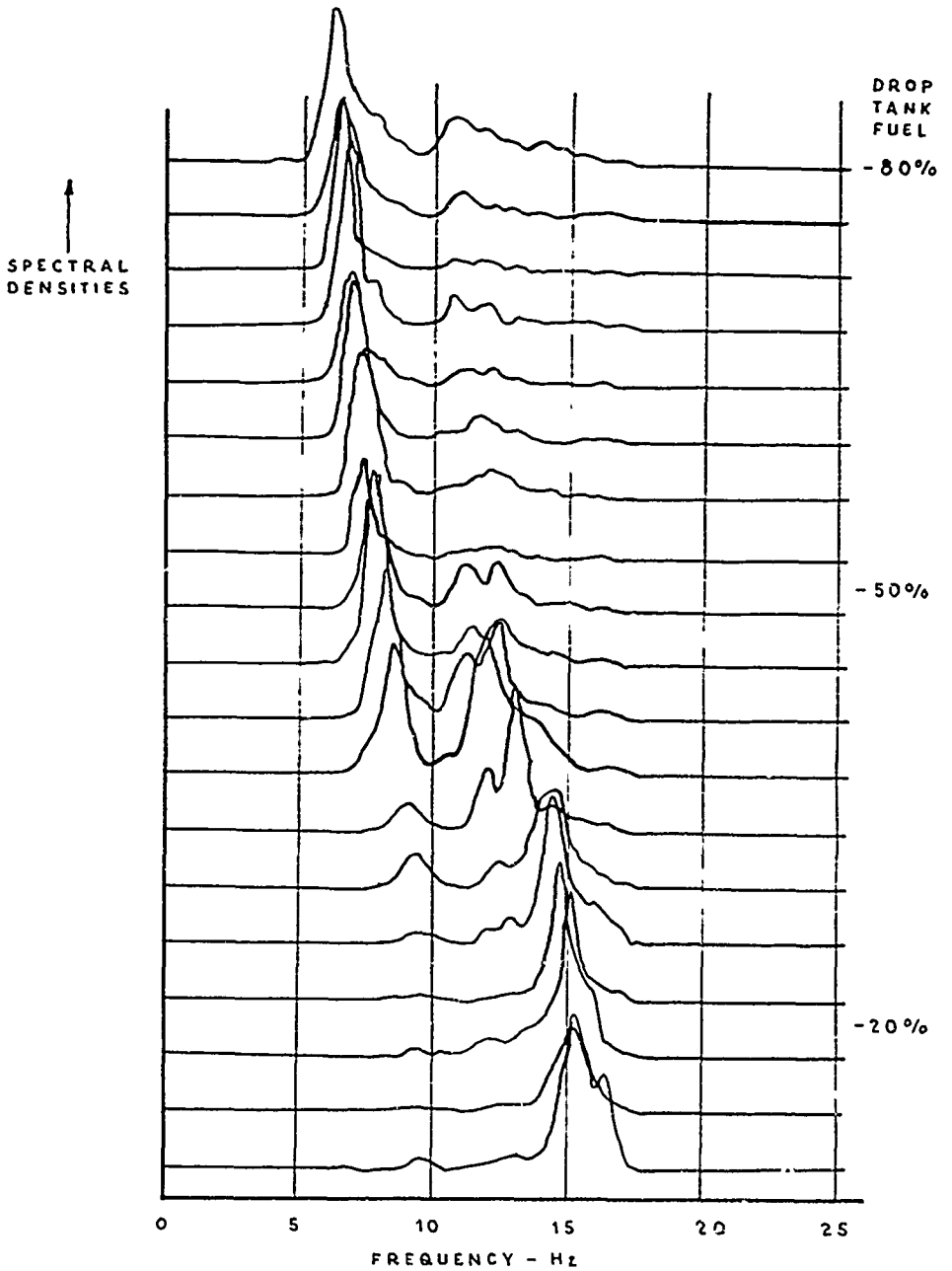

FIG. 16

FLIGHT TEST RESULTS COMPARED WITH PREDICTIONS

INBOARD FUEL TANK OUTBOARD BOMB.

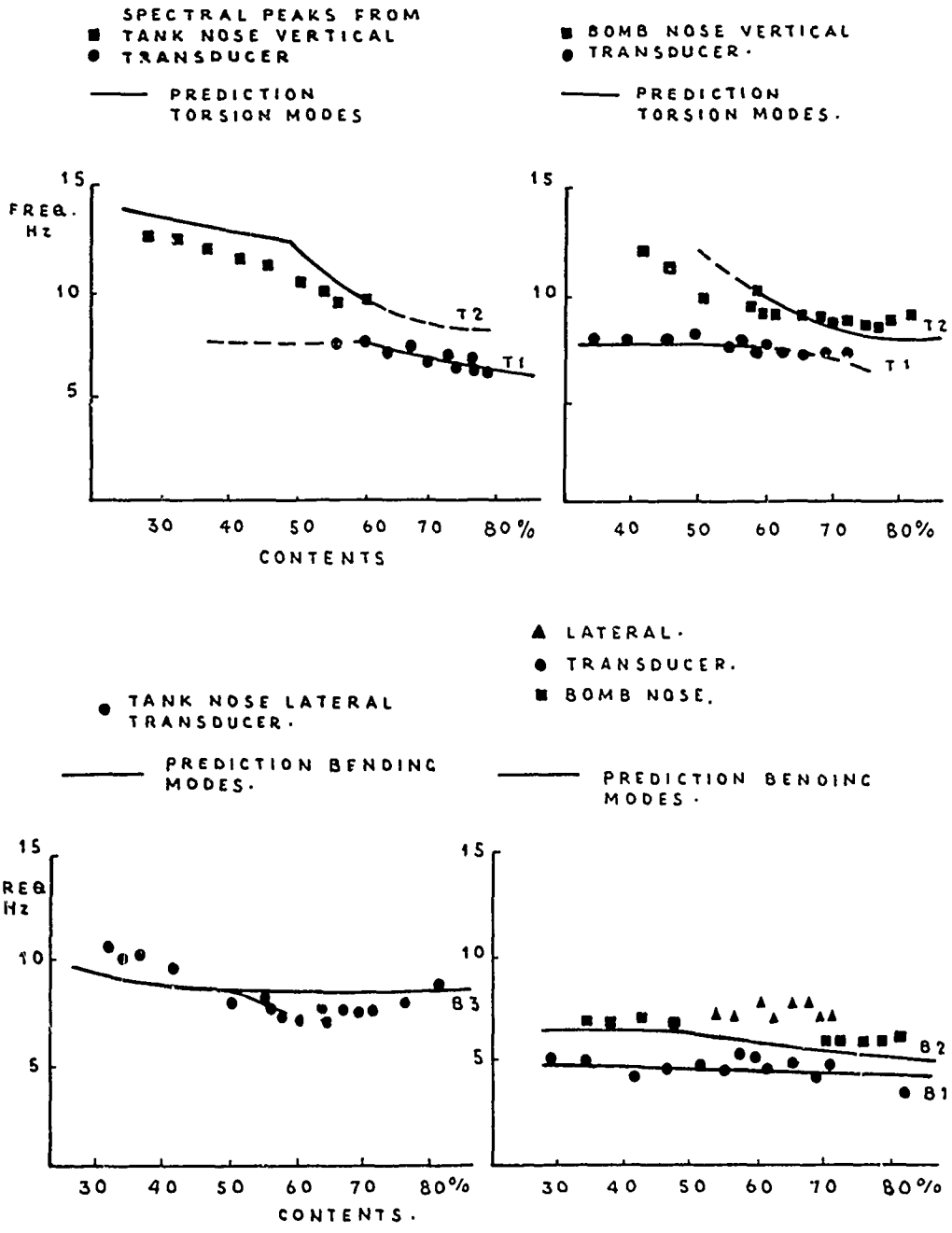

FIG.17

MEASURED DAMPING LEVELS IN THE PREDICTED FLUTTER MODE INBOARD FUEL TANK OUTBOARD BOMB.

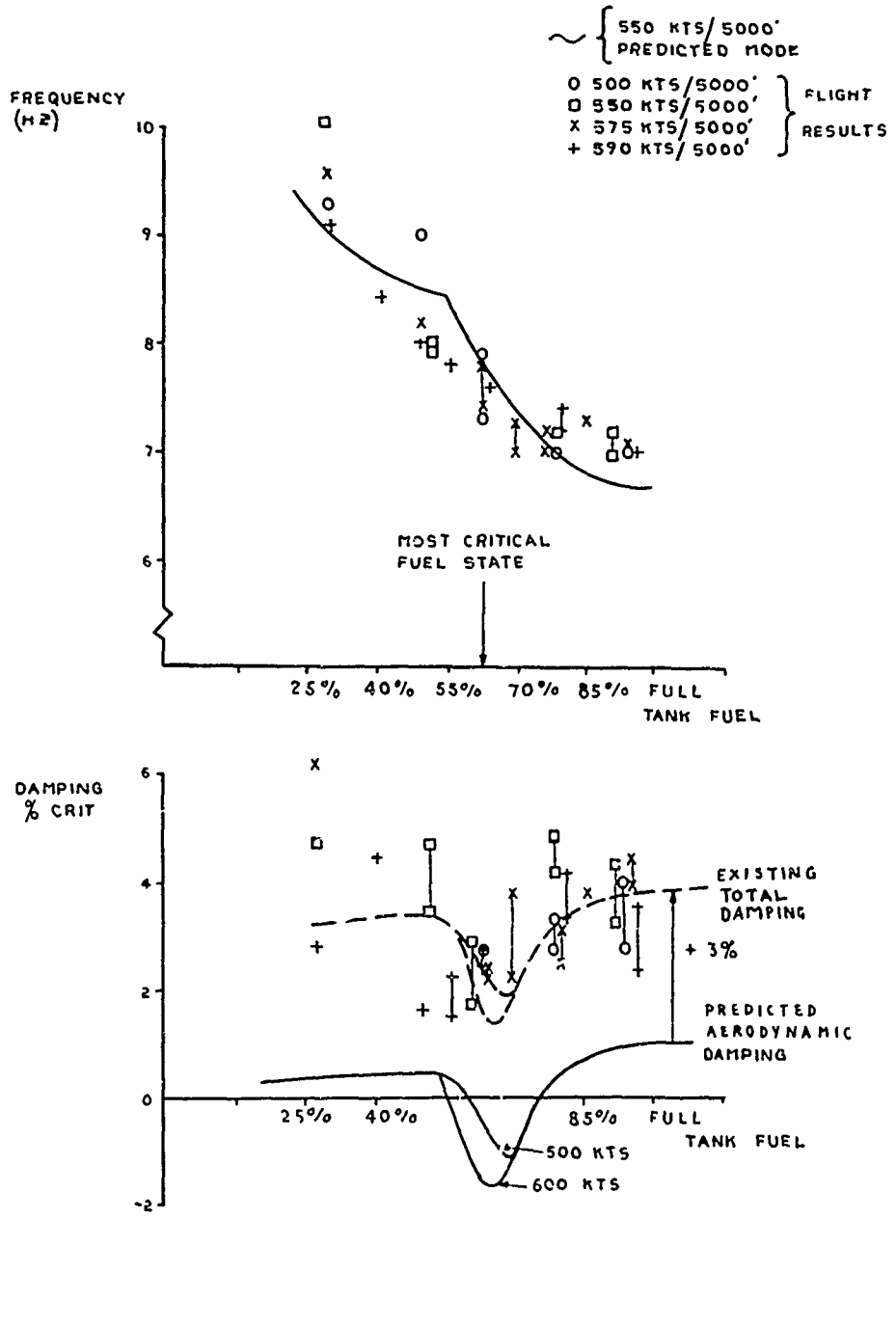

FLOTTEMENT D'AILES EQUIPEES DE MOTEURS EN NACELLE

par R. Destuynder

Office National d'Etudes et de Recherches Aérospatiales (ONERA)
92320 Châtillon (France)

Résumé

Le calcul et les mesures des forces aérodynamiques instationnaires effectués en écoulement subsonique sur une maquette équipée d'un réacteur en nacelle montrent que l'interaction entre le réacteur et l'aile reste négligeable. Par contre les forces aérodynamiques induites sur le réacteur lui-même par son propre mouvement sont importantes et jouent un rôle non négligeable dans le bilan des forces généralisées.

Le réacteur en nacelle a donc pu être traité séparément. Il a été assimilé à un cylindre à paroi mince avec écoulement interne et externe.

Une application à un cas de flottement a été faite montrant l'importance des forces sur le réacteur ; un bon recoupement a été établi entre théorie et expérience à Mach = 0,80.

FLUTTER OF WINGS EQUIPPED WITH LARGE ENGINES IN POD

Summary

Calculations and measurements of unsteady aerodynamic forces performed in subsonic flow on a model equipped with an engine in pod showed that the interference between engine and wing remains negligible.

It was also shown that the aerodynamic forces induced on the engine itself by its own oscillation are important and give a significant contribution to the generalized forces.

Account was taken of these two remarks and the aerodynamic forces were calculated separately on the engine which was assimilated to a thin walled cylinder with internal and external flow in the axial direction.

An application to a flutter case shows the importance of the contribution of the forces on the engine. A good agreement was obtained between theory and experiment at Mach number M = 0.80.

I.- INTRODUCTION

A la suite de désaccords observés dans l'évolution des paramètres de fréquences et d'amortissements théoriques et expérimentaux, sur une maquette aéroélastique de voilure équipée d'un réacteur en nacelle, il a paru intéressant d'étudier l'influence de ce dernier sur les forces aérodynamiques instationnaires.

Les résultats ont montré que les pressions instationnaires induites sur l'aile par un mouvement du réacteur restaient négligeables, bien que mesurables.

Par ailleurs les forces aérodynamiques instationnaires induites sur le réacteur lui-même par sa propre oscillation se sont révélées très importantes. C'est ainsi que pour une oscillation de l'ensemble aile réacteur autour d'un axe passant au voisinage des mi-cordes, le moment des forces aérodynamiques agissant sur la nacelle, par rapport à l'axe d'oscillation est égal au quart du moment total.

On a pu en conclure que les calculs d'aéroélasticité ne pourraient pas négliger l'influence du réacteur, mais pourraient être effectués sans tenir compte du couplage avec l'aile, c'est-à-dire que les forces aérodynamiques agissant sur le réacteur pourraient être évaluées séparément.

A la suite de cette remarque des calculs dans lesquels le réacteur en nacelle est assimilé à un ou deux cylindres circulaires concentriques à paroi mince, ont été développés d'une part par une méthode de doublet (calcul développé par le N.L.R.) d'autre part par une méthode de surface portante (calcul élaboré par l'ONERA).

Les résultats fournis par les théories se recoupent très bien entre eux et correctement avec l'expérience et traduisent bien, entre autres, l'effet du réacteur sur les limites de flottement.

L'étude était d'autant plus justifiée que cet effet s'est révélé défavorable.

II.- DETERMINATION EXPERIMENTALE DES FORCES AERODYNAMIQUES INSTATIONNAIRES

La maquette, qui comprend une demi-voilure rigide, munie ou non de son réacteur en pod, était fixé sur un support qui permettait de la faire osciller sinusoïdalement.

L'incidence moyenne pouvait être réglée, ce qui a permis de réaliser deux séries d'essais :

- une série dans laquelle l'écoulement stationnaire était supercritique (à M = 0,88) référence [1],
- une série dans laquelle l'incidence moyenne (- 45 mn) et le nombre de Mach maximum ($M \leqslant 0,8$) avaient été choisis de telle façon que l'écoulement reste subcritique sur tout le profil.

Cet article concerne uniquement la deuxième série d'essais.

Le réacteur en nacelle était lié rigidement à l'aile et solidaire de celle-ci dans son mouvement d'oscillation. L'axe d'oscillation était situé à 52 % des cordes.

Des capteurs de pression répartis sur l'aile et sur la nacelle ont permis de déterminer la répartition des coefficients de pression instationnaire et d'obtenir, par intégration, les coefficients sans dimensions qui expriment les forces et les moments pour le mouvement d'oscillation considéré.

La comparaison des résultats obtenus avec et sans réacteur a permis de séparer l'influence de ce dernier.

II.1 - Description du montage

L'aile dont la forme en plan est donnée par les figures 1 et 2 était équipée de capteurs de pression à court temps de réponse répartis sur cinq cordes distribuées en envergure suivant une loi de Kulthopp.

Les amplitudes angulaires du mouvement de tangage étaient réglables entre 10 et 45 minutes. L'aile était considérée comme rigide, les premières fréquences propres se situant à 66 Hz en flexion et 185 Hz en torsion.

Le rappel élastique était fourni par une lame de rigidité réglable par valeurs discrètes, montée sur un arbre porté par des lames en croix dans le prolongement de l'axe de tangage. L'excitation était réalisée à l'aide de 4 pots électrodynamiques, portés par le même arbre et délivrant un moment maximum de 20 Nm. Afin de réduire les mouvements parasites de flexion, l'axe de rotation était imposé, à l'extrémité de l'aile, par des câbles d'acier tendus à travers la veine. Les fréquences d'essai, à divers nombre de Mach, étaient de 35 à 48 Hz dans les deux configurations (avec ou sans réacteur). Des mesures ont été réalisées également en stationnaire (fréquence nulle).

Lors des essais dynamiques on mesurait en outre le moment aérodynamique instationnaire global autour de l'axe d'oscillation.

L'équipement de mesure des pressions instationnaires permettait l'analyse, en temps réel, des signaux délivrés simultanément par dix capteurs de pression. Après analyse ces signaux étaient moyennés pendant dix secondes pour réduire les effets parasites dus à la turbulence de la soufflerie.

La chaîne de mesure entièrement automatique, demandait moins d'une minute pour l'acquisition et le traitement de l'ensemble des résultats (70 paramètres complexes).

II.2 - Effet du réacteur en nacelle sur la voilure

Les pressions instationnaires sont présentées sous la forme de coefficients sans dimension, C_p, définis :

$$C_p = \frac{\Delta p}{q\theta} = C'_p + i\,C''_p$$

avec Δp = affixe de la pression locale , q = pression dynamique
θ = affixe de l'angle d'oscillation, pris parallèlement à l'écoulement.

La fréquence réduite est définie par $\omega_R = \frac{\omega s}{aM}$ (s étant la demi-envergure de l'aile). A la fréquence nulle (stationnaire) la distribution de pression expérimentale a été déduite des champs de pression statique mesurés pour les incidences de zéro et moins 45 minutes.

Les figures 3, 4, 5 et 6 présentent les répartitions de C_p aux nombres de Mach M = 0,60 et M = 0,80, pour les configurations avec et sans moteur et pour les sections les plus caractéristiques (sections 2 et 3).

Ces sections sont les seules concernées par l'effet d'interaction entre réacteur et voilure ainsi qu'on peut le constater, par exemple, sur la figure 7 qui représente la distribution de C_p M = 0,80, avec et sans réacteur, pour la section n° 5, à 88 % de l'envergure de l'aile.

On peut observer que l'effet d'interaction reste toujours faible et qu'il est localisé sur le bord d'attaque de l'aile. Il n'affecte pratiquement que la partie réelle des coefficients C_p. La comparaison avec la distribution de C_p stationnaire sans moteur montre que les coefficients sont très peu sensibles à la fréquence réduite dans la gamme de fréquence étudiée.

Un calcul d'interaction aérodynamique, effectué par le National Lucht en Ruimtevaartlaboratorium d'Amsterdam, par la méthode des doublets, référence [2], confirme bien cette évolution.

Pour les cordes situées entre l'emplanture de l'aile et le réacteur, l'effet du réacteur sur l'aile crée une légère déportance tandis que l'effet inverse est observé pour les sections au-delà du réacteur.

Calcul et expérience sont en bon accord et montrent que l'interaction du réacteur sur l'aile est très locale et d'intensité suffisamment faible pour pouvoir être négligée dans les calculs de flottement.

II.3 - Effet du réacteur sur lui-même

L'étude a montré l'importance relative des efforts instationnaires sur le réacteur lui-même comparés aux efforts exercés sur la voilure dans un mouvement de tangage de l'ensemble.

Les efforts sur le réacteur ont été déterminés de deux façons :

- par différence des moments de tangage déduits de l'évolution de la fréquence propre sur la maquette avec et sans réacteur
- par pesée du réacteur.

II.3.1 - Détermination à partir des fréquences

Les forces aérodynamiques dépendent linéairement de l'angle d'oscillation et ont pour effet de faire varier la fréquence propre et l'amortissement du mode d'oscillation de la maquette. Le montage comportant un seul degré de liberté, les formules qui expriment la variation de fréquence et la variation d'amortissement en fonction du coefficient complexe de moment sont simples et peuvent être exploitées pour déterminer ce coefficient à partir des fréquences et des amortissements mesurés en soufflerie.

$m_\theta = m'_\theta + i m''_\theta$ étant le coefficient de moment autour de l'axe d'oscillation, pour une amplitude angulaire de 1 radian, on a :

$$m'_\theta = \frac{k(f^2 - f_0^2)}{P_s\, \gamma\, M^2}$$

où f_0 et f sont les fréquences propres d'oscillation sans vent et avec vent

k un coefficient incluant la masse généralisée du montage et le volume de référence

P_s la pression statique de l'écoulement, γ le rapport des chaleurs spécifiques, M le nombre de Mach.

Sur la figure 8 a été porté le coefficient m'_θ relatif à l'aile avec et sans réacteur, en fonction du nombre de Mach, pour différentes fréquences réduites d'essai. La courbe de la figure 9 montre l'importance relative des forces sur le réacteur.

Le coefficient k est donné par

$$k = \frac{m'_{\theta\ \text{global}} - m'_{\theta\ \text{aile seule}}}{m'_{\theta\ \text{global}}}$$

La valeur de k est de l'ordre de 25 % et dépend peu du nombre de Mach et de la fréquence réduite.

Dans le cas d'un mode de vibration de "tangage moteur" d'une aile flexible, l'amplitude angulaire du moteur serait plus importante que celle de l'aile et la valeur relative du moment dû à la nacelle s'en trouverait accrue.

Ce coment agit à l'inverse des forces élastiques, qui tendent toujours à ramener la structure vers sa position d'équilibre, et il a en général un effet défavorable sur le flottement (effet de raideur négative).

Son importance s'explique par l'écoulement à l'intérieur de la nacelle. Celle-ci, en effet, se comporte comme une aile annulaire dont les oscillations engendrent des variations de pression importantes au voisinage de la section d'entrée.

II.3.2 - Détermination par pesée

Du fait de la faible variation du coefficient k avec la fréquence réduite et le nombre de Mach des mesures comparatives par pesée ont pu être effectuées en stationnaire et à faible vitesse (incompressible), dans une petite soufflerie de Laboratoire, en faisant varier l'incidence entre - 3° et + 3°.

Ces mesures ont montré que le foyer était situé très en avant du réacteur et que l'effet portant était localisé au voisinage de la section d'entrée d'air.

Le coefficient de moment qui a été trouvé représente la différence m'_{θ} global - m'_{θ} aile seule et permet d'évaluer le rapport de moment k défini dans le paragraphe II.3.1.

La valeur obtenue, qui est égale à 23,2 %, recoupe bien la valeur déterminée à partir des variations de fréquence (paragraphe II.3.1).

III - CALCUL DES FORCES AERODYNAMIQUES SUR LE REACTEUR EN NACELLE

L'étude expérimentale de l'aile avec réacteur en nacelle a montré que la plupart des problèmes d'aéroélasticité pouvaient être traités en calculant les forces aérodynamiques sur l'aile et sur le réacteur séparément, sans tenir compte des interactions.

Le calcul des forces sur l'aile ou le réacteur par la théorie des doublets ou de la surface portante est donné dans les références [2] et [6].

Nous nous bornons ici à présenter les résultats.

III.1 -

Le calcul fournit les coefficients K_1, K_2, K_3 et K_4 qui expriment la portance et le moment aérodynamiques sur la nacelle, par rapport à un axe de référence choisi à 50 % de la longueur du cylindre qui la schématise dans le calcul. Ces coefficients sont définis par l'équation matricielle :

$$\begin{bmatrix} F L \\ M \end{bmatrix} = \frac{1}{2} \rho V^2 L^3 \begin{bmatrix} k_1 & k_2 \\ k_3 & k_4 \end{bmatrix} \begin{bmatrix} \delta/L \\ \alpha \end{bmatrix}$$

où F est l'affixe de la portance

M est l'affixe du moment autour de l'axe de référence oy normal à l'emplanture

δ et α définissent le mouvement d'oscillation : δ est l'affixe de la translation au niveau de l'axe de référence, et α l'affixe de l'angle d'oscillation.

Les coefficients K_1, ... K_4 sont complexes et ils dépendent du nombre de Mach et de la fréquence réduite.

K_1 détermine la portance due à une oscillation de translation verticale.

K_2 détermine la portance due à une oscillation de tangage autour de l'axe oy.

K_3 détermine le moment dû à une oscillation de translation verticale.

K_4 détermine le moment dû à une oscillation de tangage autour de oy.

III.1.1 - Comparaison avec la théorie de l'écoulement bidimensionnel

En considérant un cylindre dont le diamètre 2R est grand devant la longueur 2L on doit trouver des résultats comparables aux coefficients donnés par la théorie de l'écoulement bidimensionnel. Pour le vérifier, on a effectué une application à un cylindre de 24 mètres de rayon et de 1,2 mètre de longueur, à ω_R faible (0,05) et à Mach 0,5. Les resultats sont présentés dans le tableau ci-après. Les coefficients donnés par la théorie du cylindre ne sont pas rigoureusement égaux aux coefficients de l'écoulement bidimensionnel, ce qui est normal puisque le rapport R/L n'est pas ∞ , mais les différences sont relativement faibles.

	Bidimensionnel	Théorie du cylindre
K_1	0,023 + j 0,1	0,016 + j 0,11
K_2	2,02 - j 0,29	2,2 - j 0,27
K_3	- 0,012 - j 0,05	- 0,009 - j 0,05
K_4	- 1,006 + j 0,205	- 0,995 + j 0,160

Pour cette comparaison les coefficients K_1, ... K_4 ont été ramenés aux conventions de l'écoulement bidimensionnel.

III.1.2 - Comparaison avec la méthode des doublets de la référence [2]

Un calcul a été fait à Mach 0,8 sur un cylindre de rayon 0,0315 m et de longueur 0,113 m animé d'un mouvement de tangage autour du centre du cylindre. Les résultats ont été comparés avec ceux obtenus par R. Roos, au MLR en employant la méthode de la référence [2].

La concordance est très bonne. La seule divergence, très faible d'ailleurs, se manifeste sur le moment, la position du centre de poussée étant légèrement différente.

	Méthode des doublets	Théorie du cylindre
	ω_R = 0,045	
K_2	3,837 + 0,42 j	3,915 + 0,387 j
K_4	- 3,23 + 0,144 j	- 3,48 + 0,138 j
	ω_R = 0,0675	
K_2	3,837 + 0,633 j	3,920 + 0,600 j
K_4	- 3,243 + 0,210 j	- 3,48 + 0,210 j

III.1.3 - Influence de la pulsation et du Mach

Sur un cylindre de rayon 0,034 m et de longueur 0,113 m simulant la forme en plan du réacteur utilisé dans les essais des calculs ont été effectués à différents nombres de Mach. A l'examen des résultats on s'aperçoit que l'évolution en Mach est très faible, ainsi d'ailleurs que l'évolution en fréquence réduite, sauf pour certains coefficients nuls à $\omega_R = 0$ comme R (K_1) ou R (K_3)

ω_R = 0

Mach	R (K_2)	R (K_4)
0,2	4,57	- 3,63
0,5	4,586	- 3,75
0,6	4,59	- 3,80
0,7	4,597	- 3,915
0,8	4,60	- 4,08

ω_R = 0,10

Mach	R (K_2)	R (K_4)	R (K_1)	$\frac{J(K_2)}{\omega_R}$	$\frac{J(K_4)}{\omega_R}$
0,2	4,626	- 3,682	- 0,060	9,07	2,50
0,5	4,644	- 3,809	- 0,062	9,37	2,819
0,6	4,65	- 3,88	- 0,0645	9,58	3,03
0,7	4,663	- 3,984	- 0,0648	9,80	3,285
0,8	4,665	- 4,09	- 0,068	10,10	3,67

ω_R = 0,50

Mach	R (K_2)	R (K_4)	R (K_1)	$\frac{J(K_2)}{\omega_R}$	$\frac{J(K_4)}{\omega_R}$
0,2	5,473	- 4,594	- 1,732	10,31	2,56
0,5	5,644	- 4,785	- 1,803	10,80	3,10
0,7	5,924	- 5,306	- 1,893	11,44	3,80

III.1.4 - Comparaison avec l'expérience

Pour valider la schématisation du réacteur par un cylindre creux, on a comparé en incompressible stationnaire (la faible variation théorique des coefficients en fonction de ω_R et du Mach permettant de se limiter à cette comparaison) la valeur des coefficients de portance et de moment.

	R (K_2)	R (K_4)
Calcul	4,57	- 3,63
Essai	4,15	- 1,80

Le coefficient de portance est estimé correctement.

Une différence relative plus importante se manifeste sur le coefficient de moment du fait que l'axe de référence est relativement près du foyer aérodynamique. Cette imprécision n'apporte pas d'erreur notable dans le calcul du paragraphe 2.3.1 parce que, dans ce cas, l'axe d'oscillation est situé très en arrière du réacteur.

La variation de la partie imaginaire du moment induit sur l'aile par le réacteur était suffisamment faible pour rester dans la dispersion des mesures. Si l'on effectue la même comparaison à partir des coefficients théoriques on trouve que pour une fréquence de 50 Hz à M = 0,8 la partie imaginaire du moment sur le réacteur n'apporte qu'une variation de 2 à 3 % sur le terme de moment global aile + réacteur.

L'influence des termes dus au réacteur, sur les forces globales de l'aile a également été calculée.

Un calcul a été fait sur une aile, pour un mouvement de tangage autour de l'axe de rotation de l'aile à une fréquence de 36 Hz. Les valeurs comparées sont celles de la partie réelle du coefficient $\mathcal{M}$ donné par

$$M = \frac{1}{2} \rho V^2 \mathcal{M}$$

	Aile seule	Aile + Réacteur	Aile seule	Aile + Réacteur
	M = 0,6		M = 0,8	
Calcul	$- 10,4\ 10^{-3}$	$- 13,4\ 10^{-3}$	$- 10,95\ 10^{-3}$	$- 13,99\ 10^{-3}$
Essai	$-9,698\ 10^{-3}$	$-12,682\ 10^{-3}$	$- 10,97\ 10^{-3}$	$- 14,32\ 10^{-3}$

Si l'on fait le rapport $\frac{\text{Moment réacteur}}{\text{Montant global (Aile + réacteur)}}$

comme il a été fait au paragraphe 2.3.1, on trouve une valeur identique en calcul et en essai

22,4 % à partir des valeurs théoriques

23 % à partir des valeurs expérimentales.

Ces résultats montrent la bonne concordance des méthodes théoriques de calcul des forces aérodynamiques sur les ailes et sur le cylindre avec les valeurs expérimentales, pour un terme direct de moment de tangage à une fréquence déterminée.

IV - ESSAIS DE FLOTTEMENT

Pour montrer l'influence défavorable du réacteur sur les limites de flottement, la maquette a été montée à l'emplanture sur un support à deux degrés de liberté (tangage et roulis) qui permet d'obtenir un flottement dans le domaine de la soufflerie.

Deux configurations ont été essayées :

- une configuration dans laquelle l'aile est équipée du réacteur en nacelle, avec écoulement interne,
- une configuration dans laquelle le réacteur en nacelle est remplacé par un corps fuselé de même masse, même inertie et même centre de gravité, de façon à ne pas modifier les fréquences propres, les masses généralisées et les déformées des deux modes propres.

Les évolutions dans le vent des deux fréquences propres et des amortissements ont été déterminées à partir des enregistrements de réponse de la maquette à la turbulence, par la méthode de Cole (Réf. [4]). Cette méthode permet d'obtenir les réponses impulsionnelles de la maquette (fig. 10).

Les limites de flottement ont été déterminées par extrapolation, à partir des fréquences et des amortissements mesurés alors que la maquette était encore loin du domaine d'instabilité par la méthode de Zimmerman [5]. Dans cette méthode, on détermine un paramètre de stabilité, F, qui s'annule à l'entrée en flottement et qui

évolue suivant une parabole, en fonction de la pression génératrice P_i , pour une évolution à Mach constant.

Le paramètre est donné par :

$$F = \left[\frac{\omega_2^2 - \omega_1^2}{2} + \frac{\beta_2^2 - \beta_1^2}{2}\right]^2 + 4\,\beta_1\beta_2\left[\left(\frac{\omega_2^2 + \omega_1^2}{2}\right) + 2\left(\frac{\beta_2 + \beta_1}{2}\right)^2\right] - \left[\frac{\beta_2 - \beta_1}{\beta_2 + \beta_1}\left[\frac{\omega_2^2 - \omega_1^2}{2}\right] + 2\left(\frac{\beta_2 + \beta_1}{2}\right)^2\right]^2$$

où ω_1 et ω_2 sont les deux pulsations propres, $\beta_1 = \omega_1\alpha_1$ et $\beta_2 = \omega_2\alpha_2$, α_1 et α_2 étant les amortissements réduits.

Les courbes $F(P_i)$ déterminées à partir des fréquences et des amortissements théoriques et expérimentaux ont été représentées sur les figures (11) et (12) pour les nombres de Mach 0,60 et 0,80.

On voit que l'influence relative du réacteur est plus importante à Mach 0,60 qu'à 0,80, ce qui est logique, puisque le moment dû au réacteur est peu sensible au Mach, tandis que le moment dû à l'aile subit un accroissement considérable entre Mach 0,60 et Mach 0,80.

Les courbes expérimentales ont été lissées par une méthode de moindres carrés autour d'une parabole.

Dans l'ensemble, les courbes théoriques et expérimentales présentent un décalage qui correspond à une erreur de l'ordre de 10 % sur la pression génératrice.

On constate que la pression d'entrée en flottement, qui correspond à F = 0, est plus faible avec le réacteur qu'avec le corps fuselé sans écoulement interne, d'environ 15 %. Cette influence défavorable est correctement prévue par la théorie.

V - CONCLUSION

La mesure des forces aérodynamiques instationnaires sur une maquette équipée d'un réacteur en nacelle, en subsonique, a montré que la portance et le moment induits sur le réacteur lui-même, par ses propres oscillations, étaient très importants.

Ces forces ne doivent pas être négligées dans les calculs de flottement des avions, car elles peuvent abaisser sensiblement les limites de flottement par effet de "rigidité négative" sur les modes de torsion de voilure et surtout de "tangage de moteur".

On a pu observer également :

- que les forces aérodynamiques sur le réacteur sont peu sensibles au Mach et à la fréquence réduite,
- que l'interaction aérodynamique réacteur-voilure peut être négligée.

En se fondant sur cette dernière remarque on a utilisé une théorie qui permet de traiter séparément le moteur en nacelle en le schématisant par un tube cylindrique à paroi mince avec écoulement subsonique de même vitesse à l'intérieur et à l'extérieur.

La comparaison des résultats théoriques et expérimentaux est satisfaisante.

REFERENCES

[1] N.C. Lambourne, H.C. Garner and B.L. Welsh - Some measurements of oscillatory leading and related semi-empirical predictions on a wing in supercritical flow. T.M. Aero 1541 Oct. 1973.

[2] R. Roos and R.J. Zwan - Calculation of instationary pressure distributions and generalized aerodynamic forces with the doublet lattice method. NLR TR 720 37 U Nov. 1972.

[3] E. Albano and W.P. Rodden - A Doublet lattice method for calculating left distributions on oscillating surfaces in subsonic flows. AIAA J Vol 7 n° 2 Feb. 1969 p 279-285.

[4] H.A. Cole Jr. - On line failure detection and damping measurement of aerospace structures by random decrement signatures. NASA CR 2205 March 1973.

[5] N.H. Zimmerman and J.T. Weissenberger - Rediction of flutter onset speed based on flight testing at subcritical speeds. J. Aircraft July-August 1964 p 190-202.

[6] J. Angélini - S. Chopin - R. Destuynder - Calcul des forces aérodynamiques en écoulement subsonique sur un cylindre creux. N.T. ONERA 1152 Mai 1974.

[7] R. Roos and R.J. Zwaan - The effect of a pylon-mounted nacelle on the flutter behavior of a wing-pylon-nacelle configuration. NLR TR 74125 U.

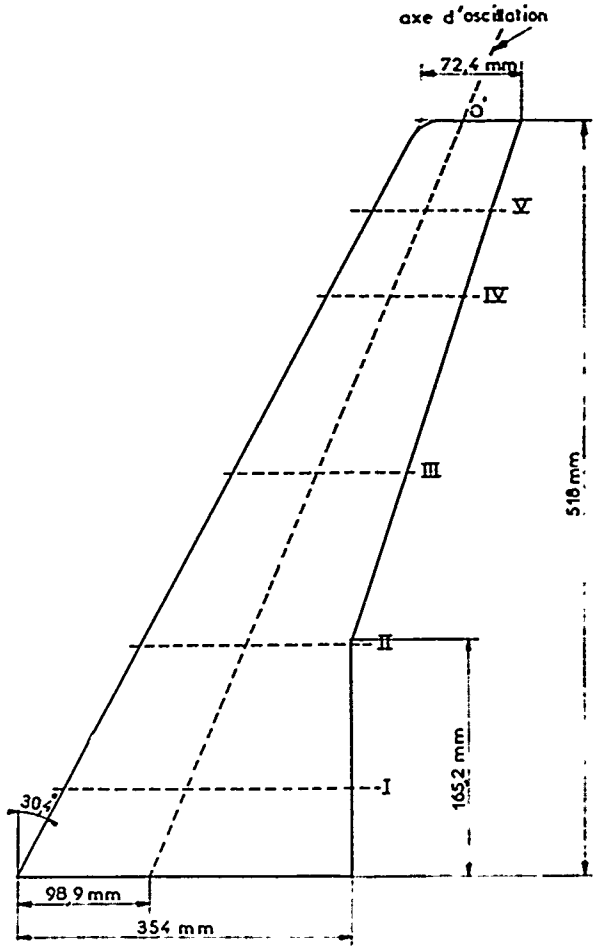

Fig 1 · Repartition des cordes de mesure des pressions et axe d'oscillation

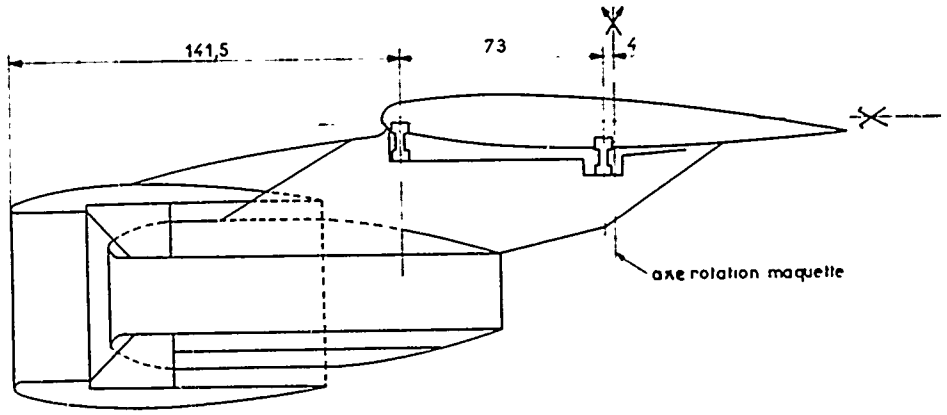

Fig 2 Détail de la position relative du réacteur et de l'aile

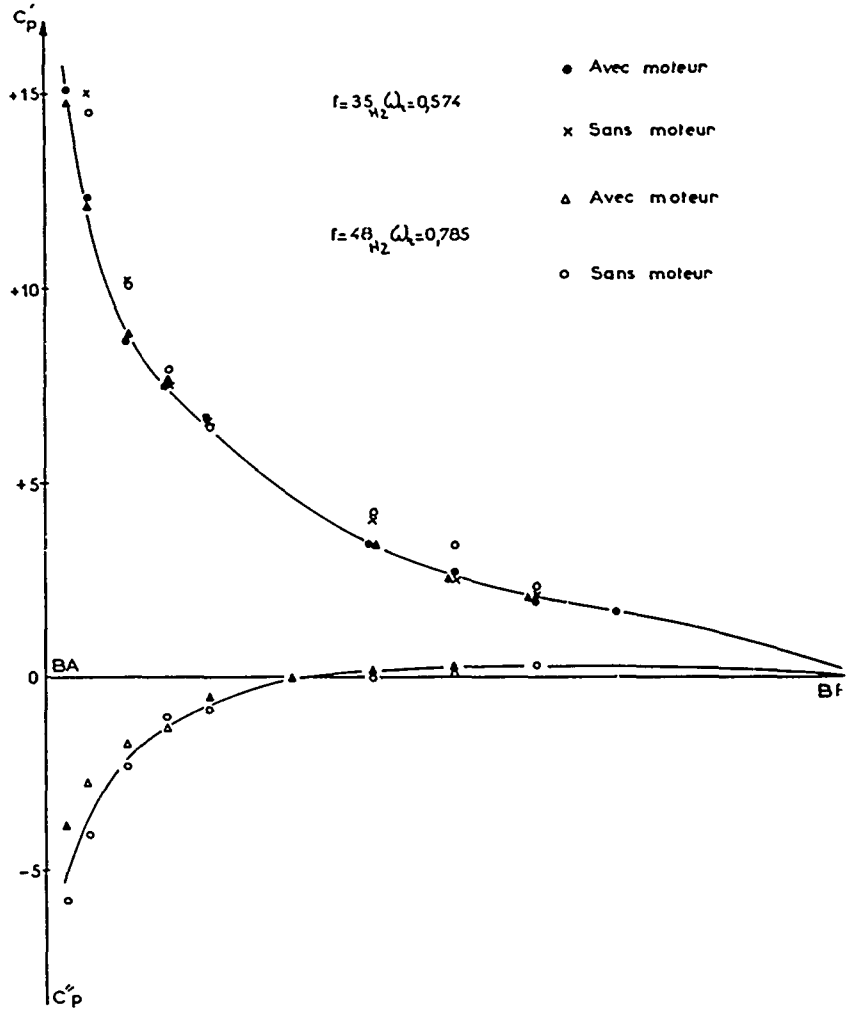

Fig 3 : Répartition de pression instationnaire en corde (coefficient complexe Cp) M = 0,60, η = 0,308

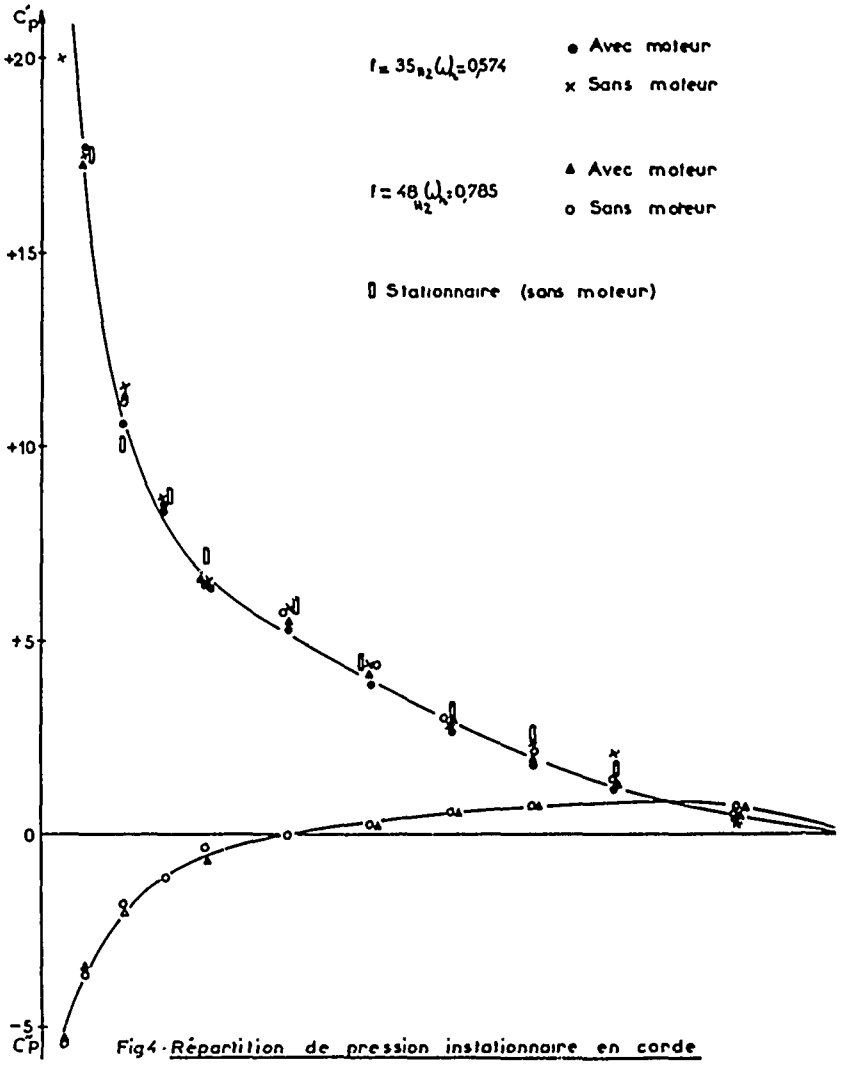

Fig 4 · Répartition de pression instationnaire en corde
M=0,60 , η = 0,535

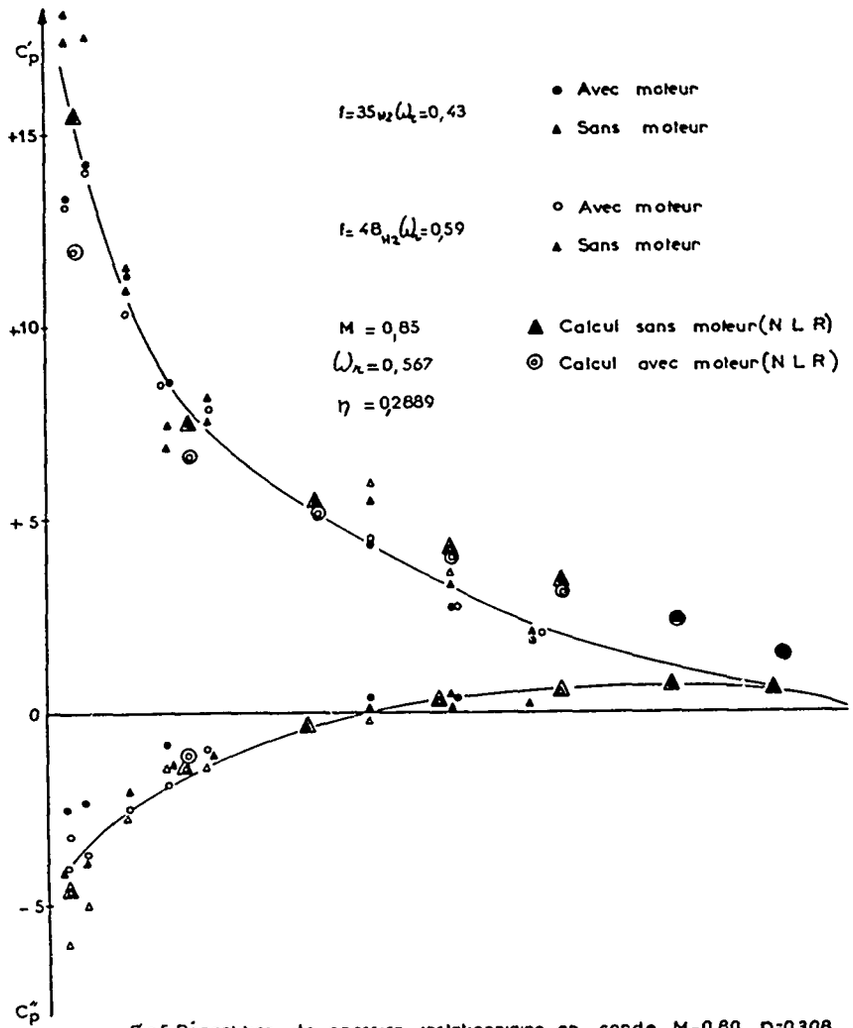

Fig 5 Répartition de pression instationnaire en corde M=0,80, η=0,308

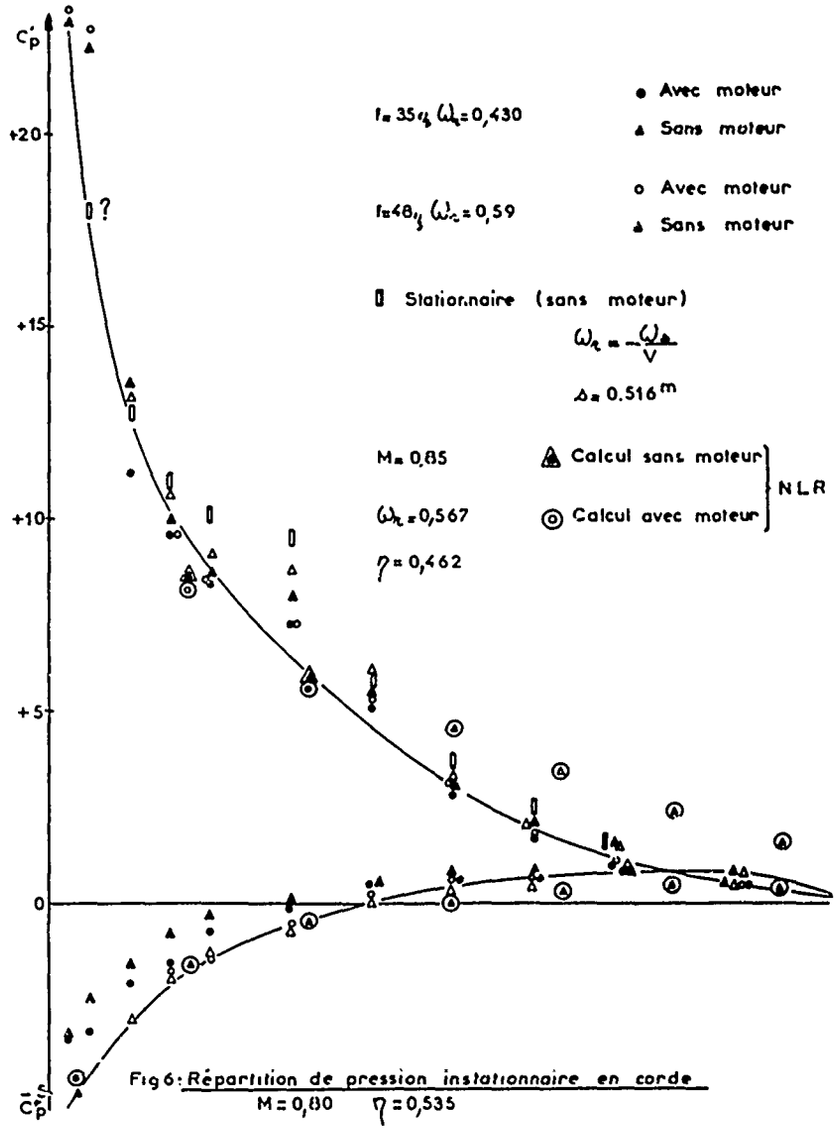

Fig 6: Répartition de pression instationnaire en corde
M = 0,80 η = 0,535

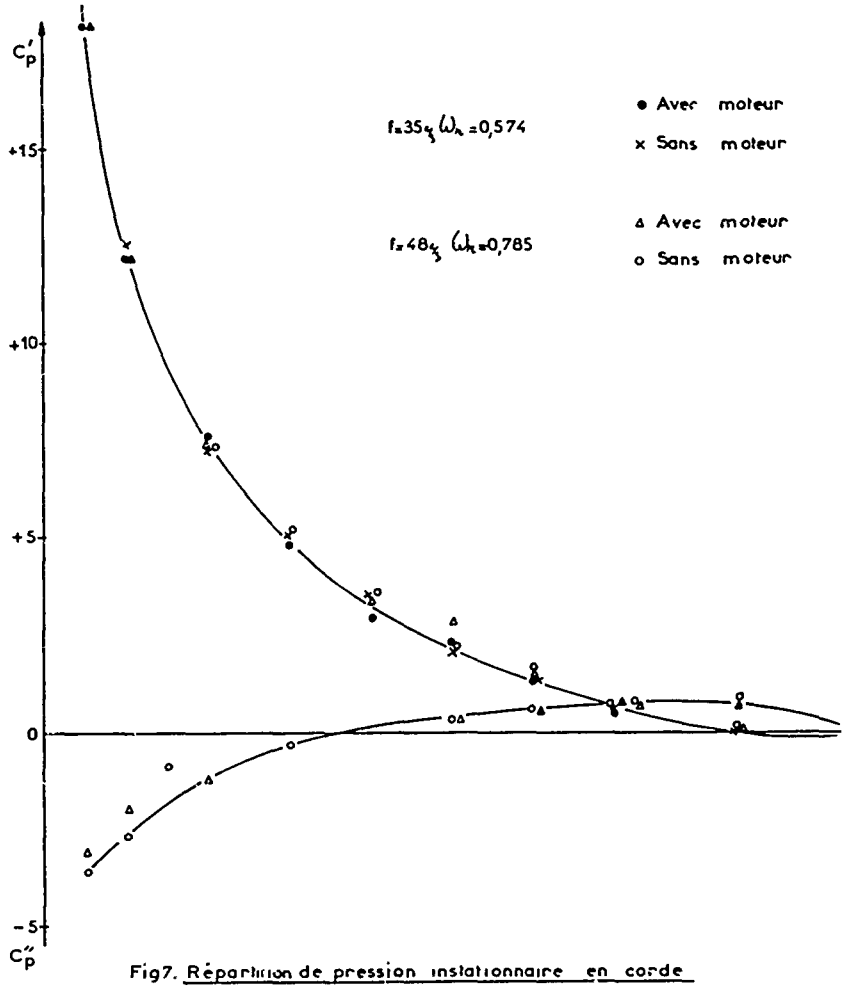

Fig7. Répartition de pression instationnaire en corde
M = 0,60 η = 0,882

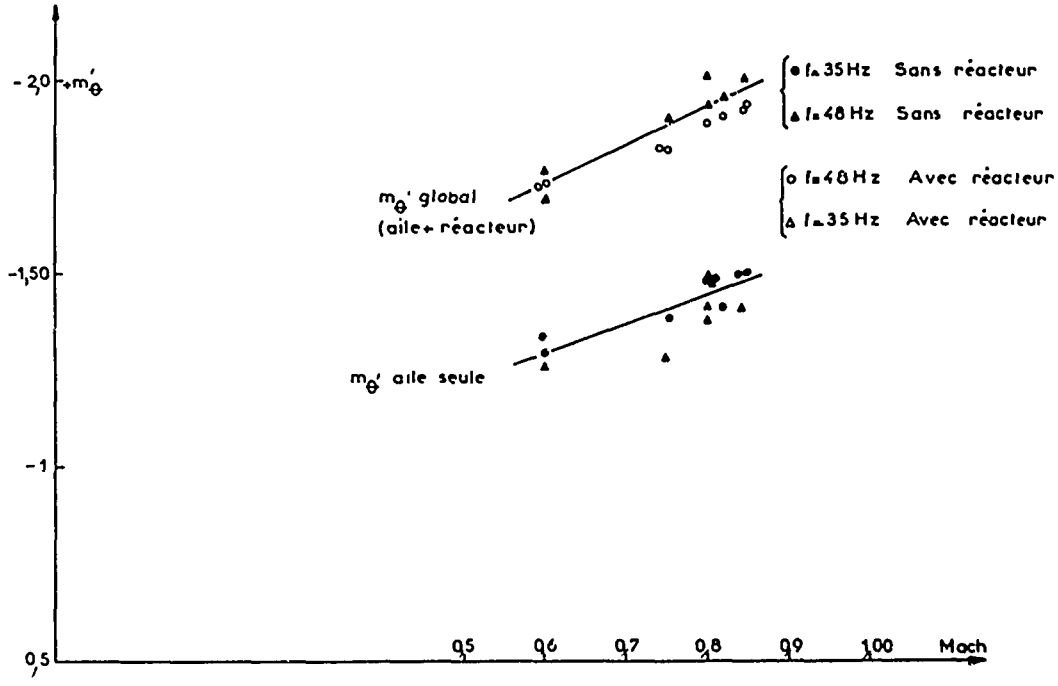

Fig 8 Moment aérodynamique global avec et sans réacteur partie réelle du coefficient m_θ

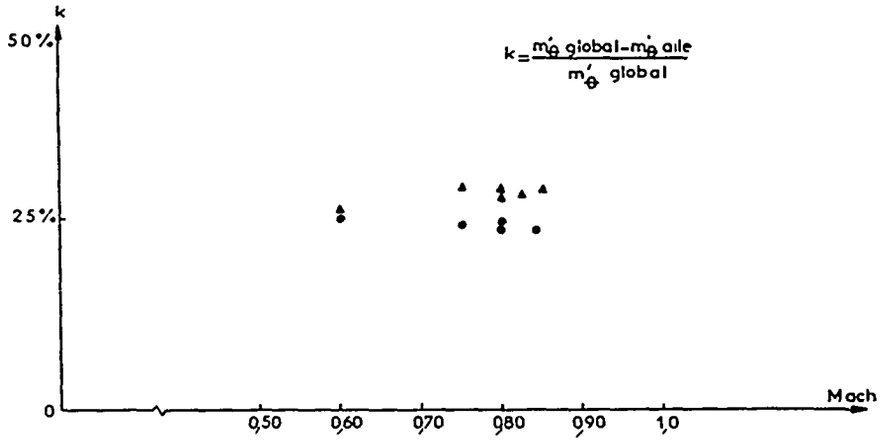

Fig9: Influence du réacteur sur le moment global

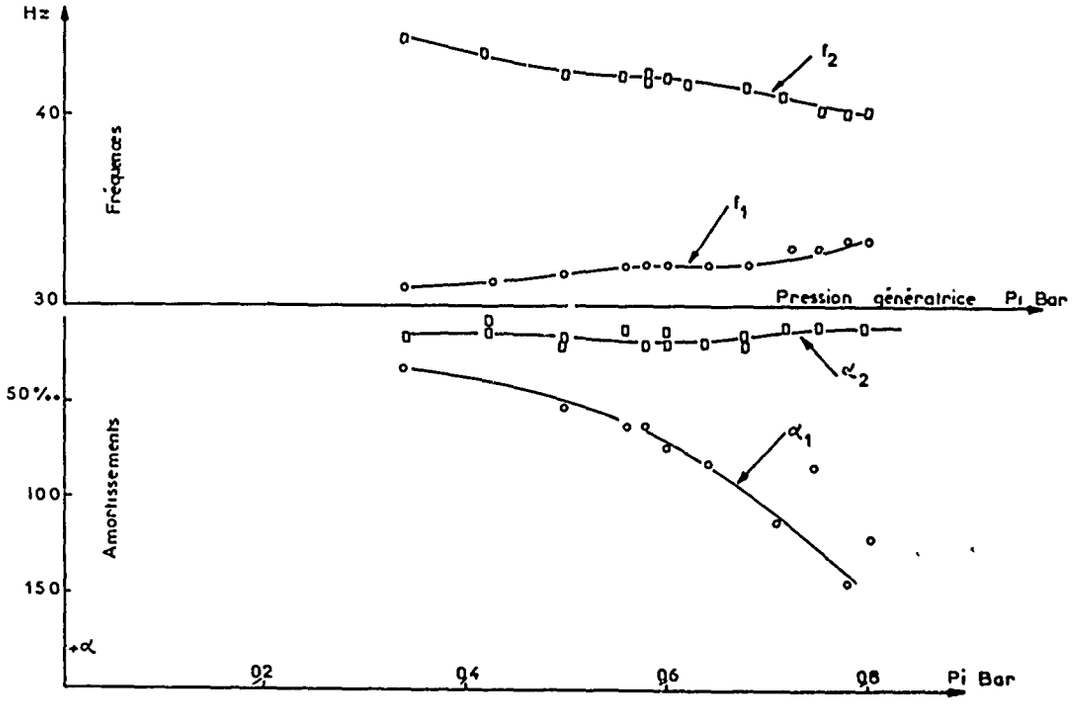

Fig 10: Essai de flottement : évolution des fréquences et des amortissements M=0,80 avec réacteur

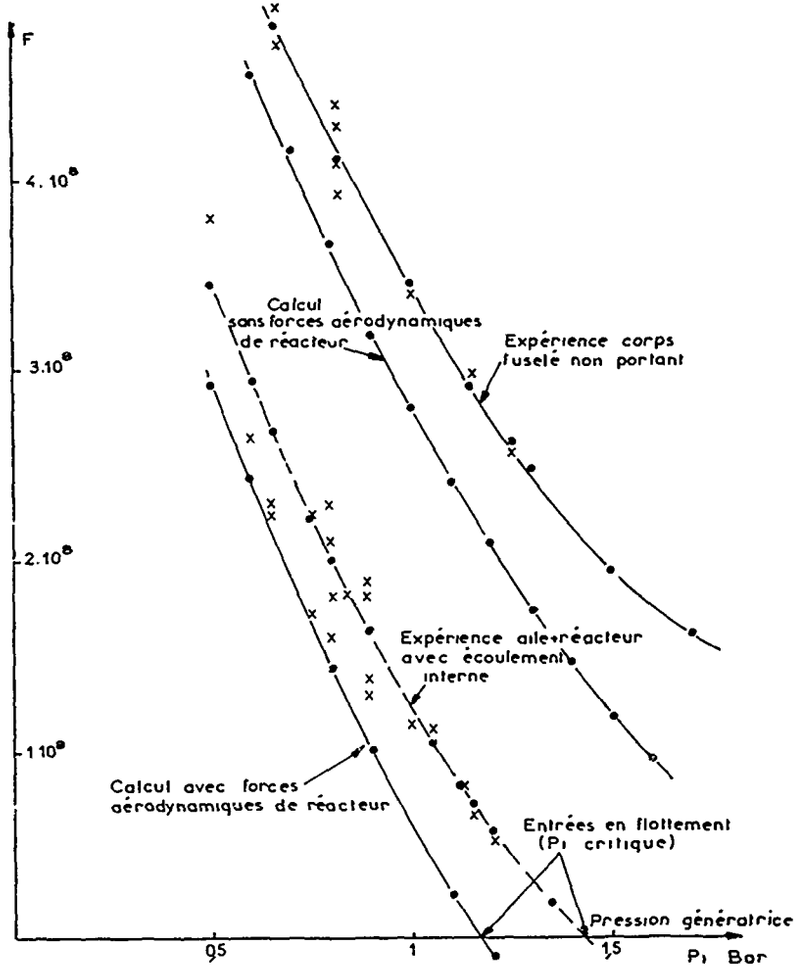

Fig 11: Application de la méthode de Zimmerman. Evolution du paramètre de stabilité F en fonction de la pression génératrice Mach 0,6

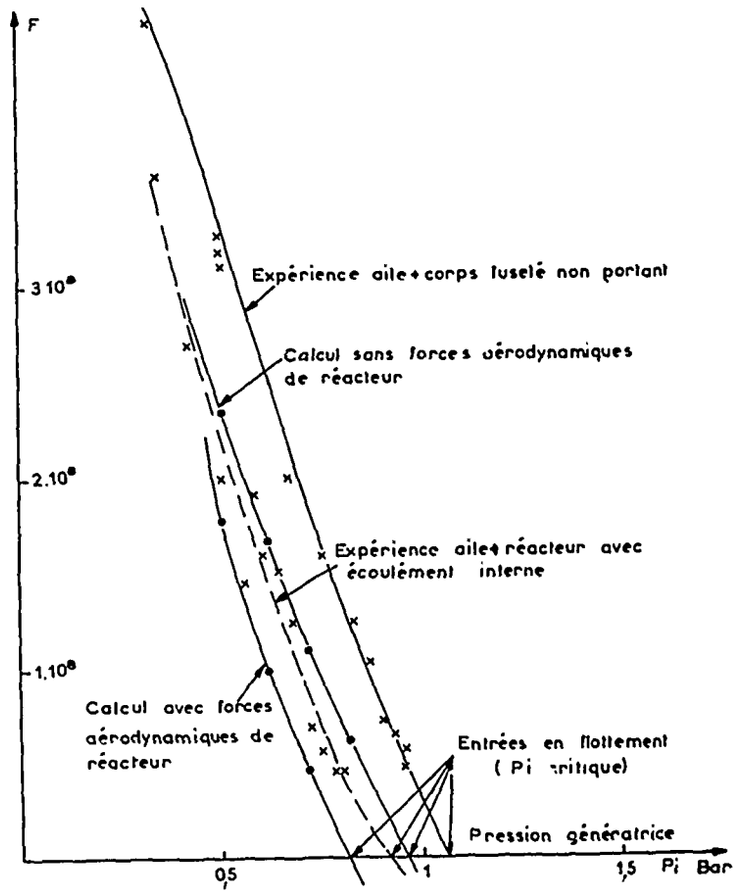

Fig12 · Application de la méthode de Zimmermar, Evolution du paramètre de stabilité de F en fonction de la pression génératrice Mach 0,8

CALCULATION OF AERODYNAMIC LOADS ON OSCILLATING WING/STORE COMBINATIONS IN SUBSONIC FLOW*)

by

B. Bennekers, R. Roos and R.J. Zwaan
National Aerospace Laboratory NLR
Anthony Fokkerweg 2
Amsterdam-1017
The Netherlands

SUMMARY

A method for the calculation of aerodynamic loads on wing-store configurations oscillating in subsonic flow is presented. In this method the linearized equation for subsonic compressibl. flow is transformed into two sets of integral equations for the steady and a superimposed unsteady flow field.

The wing loads are represented by dipole distributions (wing thickness is neglected) and the store loads by source distributions. Discretizing these distributions into lifting lines and source panels of constant strength results into a set of algebraic equations. These are solved for the unknown distributions by forcing the flow to be tangential to the surfaces of the oscillating wings and bodies in - set of control points.

The solution enables the calculation of pressure distributions on the wings and stores and of generalized aerodynamic coefficients. Calculated results are presented and compared with experiments.

CONTENTS

LIST OF SYMBOLS

A^{ij}	influence coefficient	
a	velocity of sound	(L/T)
C_p	pressure coefficient	
k	reduced frequency	
k_n	wave number	
ℓ, m, n	components of the normal vector $\vec{n}$	
M_∞	Mach number	
N	number of panels	
$\vec{n}$	normal vector	
$\vec{q}$	velocity vector	(L/T)
$\vec{r}$	position vector	(L)
r_c	distance between collocation point i and the centroid of panel j	(L)
$\vec{r}_e$	displacement vector	(L)
S	surface of wing or body	(L^2)
t	time	(T)
t	longest panel diagonal	(L)
U, V, W	components of the velocity vector	(L/T)
x, y, z	right-handed cartesian co-ordinate system	(L)
x_e, y_e, z_e	components of the displacement vector	(L)
ΔC_p	pressure jump between lower and upper wing surface	
$\Delta C_p/A$	normalized pressure jump over the wing surface	
α	angle of attack	(degrees)
β	$(1 - M^2)^{1/2}$	
γ	specific heat ratio	
δ	angular co-ordinate on tip tank	(degrees)
μ	dipole strength on the wing camber surface	(L^2/T)

*)This investigation was carried out under contract for the Scientific Research Branch, Air Materiel Directorate, RNLAF.

ξ, η, ζ	right-handed cartesian co-ordinate system	(L)
σ	source strength	(L/T)
ϕ	velocity potential	(L^2/T)
φ	disturbance velocity potential	(L^2/T)
ω	oscillation frequency	(1/T)
$\Delta\varphi$	dipole strength on the wake surface	(L^2/T)

Subscripts

B	referring to the body
C	" " " camber surface
D	" " " lifting surface
n	" " steady (n = 0) and unsteady (n = 1) flow field
W	" " the wake
o	" " the steady reference position
1	" " " unsteady flow field
∞	" " " free-stream condition

Superscripts

B	referring to the body
D	" " " lifting surface
*	" " " time-independent quantity

1 INTRODUCTION

Many modern military aircraft are equipped with ever larger stores under the wing and at the wing tips. A problem which arises in the investigation of the aeroelastic characteristics of such aircraft (flutter, gust response and manoeuvring loads) is how to obtain reliable estimates of the aerodynamic loads introduced by these stores. Important questions in this context are: What does the presence of a store do to the unsteady aerodynamic loads on the wing and what are the aerodynamic loads on the store itself in the presence of the wing?

Until some time ago the aerodynamic loads on these stores and their influence on the wing were neglected or were approximated for instance by using slender body theory only. However, to the knowledge of the authors the value of this application of slender body theory has not yet been tested conclusively in a comparison between theory and experiment.

A more thorough attempt to determine wing-body interference effects on harmonically oscillating configurations was recently made by Kalman, Rodden and Giesing (Ref.1). Using the doublet lattice method they assumed the body to be a cylindrical ring wing and thus were able to approximate the interference effects on the wing due to the proximity of the body. Although such calculations might give a reasonable prediction of these interference effects, it is clear that the diversion of the flow by the body is not accounted for and that forces on the body cannot be determined in this way. To alleviate this problem they incorporated slender body theory (Ref.2), and to overcome the problem of large systems of equations they introduced an image system in the body representing the interference effects (Ref.3). This way a method was obtained, capable of handling configurations consisting of lifting surfaces and bodies, which gives satisfactory results in the calculation of aerodynamic coefficients.

A few years ago an extensive research program was started at the NLR to investigate airloads on oscillating wing-store configurations. Recently detailed pressure measurements were completed on a wing-tiptank-store configuration, as reported by Renirie (Ref.4). Another part of the research program was the development of a method for the calculation of aerodynamic loads on oscillating wing-store configurations in subsonic flow. The purpose of such a method was twofold:

1 calculation of air forces on wing-store configurations for aeroelastic analysis;
2 support of wind tunnel measurements through the calculation of detailed pressure distributions.

The method presented here was set up in an effort to meet the above requirements. It combines the elements of four existing methods into one general method for the calculation of steady and unsteady pressure distributions on wing-body configurations. The steady flow field is described with the vortex lattice method and the panel method of Hess and Smith (Ref.5). The unsteady field is modelled with the doublet lattice method and a new panel method, which is partially based on the work of Hess (Ref.6) on the calculation of acoustic fields about arbitrary bodies. In the following the part of the method describing the steady flow field will be called the NLRS-method, while the part in which the steady and unsteady fields are combined will be referred to as the NLRI-method.

This paper gives a description of the method and presents some preliminary calculated results on a wing-tiptank configuration in comparison with experimental data.

2 OUTLINE OF THE THEORY

The present description of unsteady airloads on wing-store combinations involves airforces on rather thin lifting surfaces (wing, pylons, tail surfaces) and on streamlined closed stores, both influencing each other through interference effects.

For the calculation of aerodynamic forces on lifting surfaces several effective methods are known. In the theory presented here the lifting surfaces are treated with the doublet lattice method (DL-method), since it is very flexible in handling different configurations (Ref.7). Recently the reliability of the DL-method was shown again by Roos and Zwaan (Ref.8) in calculations of the unsteady aerodynamic loads used in the determination of the flutter behaviour of a wing-pylon-nacelle wind tunnel model.

Considering the large experience with the NLR-panel method for steady flow (see for example reference 9), the unsteady flow field about the stores was chosen to be described with an unsteady source panel method.

This implies that the surface of the body is discretized into panels each containing a time-varying source distribution of constant yet unknown strength over the panel. The wake behind the store is assumed to be represented with an extension of the lifting surface into the store. This is a rather crude simplification, but appropriate experimental evidence is lacking. However, as in steady calculation methods this simplification leads to good results, it seems to be a reasonable assumption. The boundary conditions are enforced in the control point of each panel on lifting surfaces and stores.

Let the inviscid flow around an oscillating arbitrary wing-store configuration be described with a velocity potential

$$\Phi \langle x,y,z,t \rangle = U_\infty x + V_\infty y + W_\infty z + \varphi \langle x,y,z,t \rangle \tag{1}$$

in which U_∞, V_∞ and W_∞ are the components of the free-stream velocity vector $\vec{q}_\infty$ and φ is the disturbance velocity potential. The use of a small disturbance potential implies the assumption that the body does not disturb the free stream significantly. For the region of the stagnation points the validity of this assumption will have to be verified afterwards. Assuming that V_∞ and W_∞ are small as compared to U_∞ and that φ is small in comparison with $U_\infty x$ the general equation for Φ reduces to a linearized equation for φ

$$\beta^2 \varphi_{xx} + \varphi_{yy} + \varphi_{zz} - \frac{1}{a_\infty^2} \varphi_{tt} - 2 \frac{M_\infty}{a_\infty} \varphi_{xt} = 0 \tag{2}$$

with $M_\infty = U_\infty / a_\infty$ and $\beta^2 = 1 - M_\infty^2$. The Mach number is taken to be constant throughout the flow field, which consequently makes the value of the method doubtful in the near-transonic Mach range.

The surface of an oscillating arbitrary configuration can be described in general with the functional:

$$S \langle x,y,z,t \rangle = 0 \tag{3}$$

The boundary condition requiring the flow to be tangential to the moving surface is then given by:

$$\frac{DS}{Dt} = \frac{\partial S}{\partial t} + \vec{q} \cdot \vec{\nabla} S = 0 \qquad \text{on } S = 0 \tag{4}$$

In Appendix 1 the general solution of equation (2) is derived for a harmonic motion of small amplitude. In principle this solution includes the effects due to the thickness and the wake of the wing in about the same way as does the theory presented recently by Morino and Kuo (Refs.10, 11). However, it is also agued there that in practice an accurate consideration of the wake effects complicates the calculation substantially. Recalling the purpose of the method and realizing that lifting surface theories, although they neglect thickness effects, are quite accurate already as demonstrated in references 7 and 12, the wing is assumed to be infinitely thin. Thus, a method is obtained of which the set-up is described earlier in this section. In Appendix 1 this set-up is formulated; the pertinent expressions for the velocity potential φ are repeated here.

$$\varphi \langle x,y,z,t \rangle = \varphi_o \langle x,y,z \rangle + \varphi_1 \langle x,y,z \rangle \, e^{i\omega t} \tag{5}$$

with for the body:

$$\varphi_n^B \langle x,y,z \rangle = -\frac{1}{4\pi} \iint_{S_B} \sigma_n \langle \xi_B, \eta_B, \zeta_B \rangle \, e^{ik_n M_\infty (x-\xi_B)} \frac{e^{-ik_n r}}{r} \, dS \tag{6}$$

in which

$$r = \left[(x - \xi_B)^2 + \beta^2 (y - \eta_B)^2 + \beta^2 (z - \zeta_B)^2 \right]^{1/2} \tag{7}$$

and for the lifting surface

$$\varphi_n^D \langle x,y,z \rangle = \frac{q^2}{8\pi U_\infty} \iint_{S_D} \Delta C_{p_n} \langle \xi_D, \eta_D, \zeta_D \rangle \, K_n \langle x,y,z,\xi_D,\eta_D,\zeta_D,M_\infty,\omega \rangle \, dS \tag{8}$$

in which

$$K_n = e^{-in\omega(x-\xi_D)/U_\infty} \int_{-\infty}^{x-\xi_D} \frac{\partial}{\partial n} \left[\frac{e^{-in\omega(\tau - M_\infty r)/U_\infty \beta^2}}{r} \right] d\tau \tag{9}$$

and

$$r = \left[\tau^2 + \beta^2 (y - \eta_D)^2 + \beta^2 (z - \zeta_D)^2 \right]^{1/2} \tag{10}$$

In the above expressions the disturbance potential φ_n is written in terms of a source distribution of strength σ_n on the body surface S_B and a pressure dipole distribution of strength ΔC_{p_n} on the thin lifting surface S_D. The subscript n can have the values 0 and 1, indicating the steady and unsteady potential.

The description of the surface of an oscillating arbitrary body is not as simple as it might look from expression (3), because the functional form of S is not known in general. However, often the time-dependent position of the individual points of the surface can be expressed in terms of a reference position and a time-dependent amplitude $\vec{r}_e$. Assuming that this amplitude is small such that $\varphi_1 \ll \varphi_o \ll U_\infty x$, the boundary condition on the surface, as given by (4), can be divided into a steady and an unsteady part, as shown in Appendix 2. For the steady φ_o this results in the classical condition*)

$$(\vec{q}_\infty + \vec{\nabla}\varphi_o) \cdot \vec{n} = 0 \qquad \text{on} \quad S_o \langle x,y,z \rangle = 0 \tag{11}$$

*) the normal vector $\vec{n}$ is directed outside the body.

and for the unsteady φ_1

$$\vec{\nabla}\varphi_1\Big|_o.\vec{n} - i\omega\vec{r}_e^{\,*}.\vec{n} - (\vec{q}_\infty+\vec{\nabla}\varphi_o).(\ell\vec{\nabla}_o x_e^* + m\vec{\nabla}_o y_e^* + n\vec{\nabla}_o z_e^*) + \vec{n}.\left[(\vec{r}_e^{\,*}.\vec{\nabla})\vec{\nabla}\varphi_o\right]\Big|_o = 0$$

$$\text{on } S < x,y,z,t > \; = 0 \qquad (12)$$

with $\vec{r}_e^{\,*}$ being the amplitude of the displacement vector having components x_e^*, y_e^* and z_e^*. The components of the normal vector $\vec{n}$ on the body in its stationary position are given by resp. ℓ, m and n. For the thin lifting surfaces the unsteady condition reduces to a simpler form:

$$\vec{\nabla}\varphi_1\Big|_o.\vec{n} - i\omega\vec{r}_e^{\,*}.\vec{n} - \vec{q}_\infty\left[m\vec{\nabla}_o y_e^* + n\vec{\nabla}_o z_e^*\right] = 0 \qquad (13)$$

$$\text{on } S_D < x,y,z,t > \; = 0$$

From (12) it is clear that, while the linearized equation (2) allows for a disconnection of the steady and unsteady fields, as implemented in (5), the boundary condition restores this connection again through second order terms involving first and second order derivatives of the steady disturbance potential φ_o. Including these terms is necessary to obtain a proper representation of the effects due to diversion of the flow as a result of the thickness of the body. Morino and Kuo (Refs. 10, 11) do not indicate this connection in their work on oscillating wings with thickness.

Substitution of the expressions (6) through (10) for φ_n in these boundary conditions leads to the following sets of integral equations for resp. the steady and unsteady flow field:

for n = 0:

$$-\frac{1}{4\pi}\iint_{S_B}\sigma_o<\xi_B,\eta_B,\zeta_B>\left[\vec{\nabla}\frac{1}{r}\right]\Big|_{(x_B,y_B,z_B)}.\vec{n}<x_B,y_B,z_B>\,dS$$

$$+\frac{q_\infty^2}{8\pi U_\infty}\iint_{S_D}\Delta C_{p_o}<\xi_D,\eta_D,\zeta_D>\left[\vec{\nabla}K_o\right]\Big|_{(x_B,y_B,z_B)}.\vec{n}<x_B,y_B,z_B>\,dS = -\vec{q}_\infty.\vec{n}<x_B,y_B,z_B> \qquad (14)$$

$$-\frac{1}{4\pi}\iint_{S_B}\sigma_o<\xi_B,\eta_B,\zeta_B>\left[\vec{\nabla}\frac{1}{r}\right]\Big|_{(x_D,y_D,z_D)}.\vec{n}<x_D,y_D,z_D>\,dS$$

$$+\frac{q_\infty^2}{8\pi U_\infty}\iint_{S_D}\Delta C_{p_o}<\xi_D,\eta_D,\zeta_D>\left[\vec{\nabla}K_o\right]\Big|_{(x_D,y_D,z_D)}.\vec{n}<x_D,y_D,z_D>\,dS = -\vec{q}_\infty.\vec{n}<x_D,y_D,z_D> \qquad (15)$$

and for n = 1:

$$-\frac{1}{4\pi}\iint_{S_B}\sigma_1<\xi_B,\eta_3,\zeta_B>\left[\vec{\nabla}\left(e^{ik_1M_\infty(x-\xi_B)}\,\frac{e^{-ik_1r}}{r}\right)\right]\Big|_{(x_B,y_B,z_B)}.\vec{n}<x_B,y_B,z_B>\,dS$$

$$+\frac{q_\infty^2}{8\pi U_\infty}\iint_{S_D}\Delta C_{p_1}<\xi_D,\eta_D,\zeta_D>\left[\vec{\nabla}K_1\right]\Big|_{(x_B,y_B,z_B)}.\vec{n}<x_B,y_B,z_B>\,dS =$$

$$= i\omega\vec{r}_e^{\,*}<x_B,y_B,z_B>.\vec{n}<x_B,y_B,z_B> + (\vec{q}_\infty+\vec{\nabla}\varphi_o\Big|_{(x_B,y_B,z_B)}).$$

$$.(\ell<x_B,y_B,z_B>\vec{\nabla}_o x_e^*<x_B,y_B,z_B> + m<x_B,y_B,z_B>\vec{\nabla}_o y_e^*<x_B,y_B,z_B>$$

$$+ n<x_B,y_B,z_B>\vec{\nabla}_c z_e^*<x_B,y_B,z_B>) - \vec{n}<x_B,y_B,z_B>.\left[(\vec{r}_e^{\,*}<x_B,y_B,z_B>.\vec{\nabla})\vec{\nabla}\varphi_o\right]\Big|_{(x_B,y_B,z_B)} \qquad (16)$$

$$-\frac{1}{4\pi}\iint_{S_B}\sigma_1<\xi_B,\eta_B,\zeta_B>\left[\vec{\nabla}\left(e^{ik_1M_\infty(x-\xi_B)}\,\frac{e^{-ik_1r}}{r}\right)\right]\Big|_{(x_D,y_D,z_D)}.\vec{n}<x_D,y_D,z_D>\,dS$$

$$+\frac{q_\infty^2}{8\pi U_\infty}\iint_{S_D}\Delta C_{p_1}<\xi_D,\eta_D,\zeta_D>\left[\vec{\nabla}K_1\right]\Big|_{(x_D,y_D,z_D)}.\vec{n}<x_D,y_D,z_D>\,dS$$

$$= i\omega\vec{r}_e^{\,*}.\vec{n}<x_D,y_D,z_D>$$

$$+\vec{q}_\infty.(m<x_D,y_D,z_D>\vec{\nabla}_o y_e^*<x_D,y_D,z_D> + n<x_D,y_D,z_D>\vec{\nabla}_o z_e^*<x_D,y_D,z_D>) \qquad (17)$$

Equations (14) and (15) determine the steady flow field on the body and the lifting surface, while equations (16) and (17) concern the unsteady flow field superimposed on this steady field. The interference effects between the body and the lifting surface are represented in the second integral of equations (14) and (16) and in the first integral of equations (15) and (17).

To solve these integral equations for the unknown source and dipole distributions, these distributions

are discretized. The surface of the body and the lifting surface are respectively divided into N_B and N_D panels. On the body each panel is assumed to contain a source distribution of constant, yet unknown strength. The panels on the lifting surface are taken to contain each a lifting line of constant, also unknown, strength, along the 1/4 -chord line of the panel. Further, each panel possesses one collocation point in which the boundary condition is imposed. That is, in these points the flow is forced to be tangential to the surface. With this discretization the sets of integral equations are transformed into two sets of (N_B+N_D) algebraic equations for the steady and unsteady part of the flow:

$$\left[\sum_{j=1}^{N_B} A_n^{ij}\sigma_n^j + \sum_{j=1}^{N_D} A_n^{1j}\Delta C_{pn}^j = F_n^i\right] \qquad (n=0,1) \qquad (18)$$

$$i=1,2,\ldots\ldots,(N_B+N_D)$$

in which σ_n^j and ΔC_{pn}^j are the unknown source and lifting line strength of each panel of the body and the lifting surface. The term F_n^i is the prescribed normal velocity in the collocation point of the i^{th} panel of either the body or the lifting surface. The influence coefficient A_n^{ij} represents the normal velocity induced by the i^{th} panel with a source distribution or lifting line of unit strength in the collocation point of the j^{th} panel. Their methods of calculation are indicated in section 3. The numerical solution of the sets of algebraic equations is given in section 4 of this paper.

After the steady source and lifting line strength have been calculated, the steady part of the velocity in the collocation points can be determined. The second derivatives of φ_o are obtained by differentiation of the expressions for the velocity. Next, these values are used to determine the right-hand side of the unsteady set of equations, after which the unsteady flow field can be solved as well.

For the lifting surface the strength of the lifting line is taken to be equal to the pressure jump over the surface in the middle of the 1/4 -chord line of the panel. The steady and unsteady pressure distributions on the body follow from the following expressions, derived in Appendix 3:

$$C_{p_o} = \frac{2}{\gamma M_\infty^2}\left\{\left[1 + \frac{(\gamma-1)}{2}M_\infty^2\left(1 - \frac{\vec{q}_o\cdot\vec{q}_o}{q_\infty^2}\right)\right]^{\gamma/(\gamma-1)} - 1\right\} \qquad (19)$$

and

$$C_{p_1} = -\frac{2}{q_\infty^2}\left[1 - \frac{(\gamma-1)}{2}M_\infty^2\left(1 - \frac{\vec{q}_o\cdot\vec{q}_o}{q_\infty^2}\right)\right]^{1/(\gamma-1)} \cdot$$
$$\left[\vec{q}_o\cdot\vec{\nabla}\varphi_1\Big|_o + i\omega\varphi_1\Big|_o + (U_\infty+\varphi_{o_x}\Big|_o)(\vec{r}_e^{\,*}\cdot\vec{\nabla})\varphi_{o_x}\Big|_o\right.$$
$$\left.+(V_\infty+\varphi_{o_y}\Big|_o)(\vec{r}_e^{\,*}\cdot\vec{\nabla})\varphi_{o_y}\Big|_o + (W_\infty+\varphi_{o_z}\Big|_o)(\vec{r}_e^{\,*}\cdot\vec{\nabla})\varphi_{o_z}\Big|_o\right] \qquad (20)$$

in which

$$\vec{q}_o = (U_\infty+\varphi_{o_x}\Big|_o)\vec{i} + (V_\infty+\varphi_{o_y}\Big|_o)\vec{j} + (W_\infty+\varphi_{o_z}\Big|_o)\vec{k} \qquad (21)$$

Figure 1 gives a schematic outline of all necessary calculations.

3 CALCULATION OF THE INFLUENCE COEFFICIENTS

For both the steady and unsteady flow field the influence coefficients A_n^{ij} can be divided into two groups: one A_n^{iD} in which the j^{th} panel lies on a lifting surface and a second A_n^{iB} having the j^{th} panel on the body. For the steady flow field the calculation follows exactly the lines of two well-known methods. The coefficients A_o^{iB} are obtained with the expressions of the panel method of Hess and Smith (Ref.5), after the compressibility factor β has been removed temporarily from (7) with a transformation of the Prandtl-Glauert type. The coefficients A_o^{iD} are evaluated according to the formulations for the vortex lattice method given in reference 13. The calculation of the unsteady coefficients A_1^{iD} does not introduce any new problems either. They are simply obtained from the formulations of the doublet lattice method given in reference 2.

For the unsteady coefficients A_1^{iB} represented by the integral

$$A_1^{iB}\langle x,y,z\rangle = -\frac{1}{4\pi}\iint_{S_B}\left[\vec{\nabla}\left(e^{ik_1M_\infty(x-\xi_B)}\,\frac{e^{-ik_1r}}{r}\right)\right]\cdot\vec{n}\langle x,y,z,\rangle dS \qquad (22)$$

a new calculation method is developed which in part is based on the panel method of Hess (Ref.6) for the determination of acoustic fields around arbitrarily shaped bodies.

To evaluate the above integral five different regions are distinguished based on the ratio $\frac{r_c}{t}$ being the distance between collocation point i and the centroid of the panel j over the longest diagonal t of the panel. In these regions the integral is calculated as follows:

1. $\frac{r_c}{t} \geq 4$, the point i lays far away from panel j; the source distribution on the panel is approximated with a point-source at the centroid of the panel.
2. $4 > \frac{r_c}{t} \geq 1.9$, the point i lays at fairly large distance from panel j; the source distribution is approximated with a two term multi-pole expansion in powers of $(k_1 t)$ and $(\frac{t}{r_c})$ around the centroid.
3. $1.9 > \frac{r_c}{t} \geq 1$, the point i lays at fairly small distance from panel j; the same approximation as in 2., with three terms taken into account instead of two.

4. $1 > \frac{r_c}{t} > 0$, the point i lays close to the centroid of panel j; the integrand is approximated with a one-dimensional Taylor series expansion in powers of $(ik_1 r)$.

5. $\frac{r_c}{t} = 0$, the point i lays at the centroid of panel j; the integrand is expanded similarly as in 4., but now the expressions are simpler.

A detailed description of the above approximations and the resulting expressions is given in reference 14.

In their work Morino and Kuo (Refs. 10, 11) have not introduced such a complicated scheme to calculate the unsteady influence coefficients. For all values of r_c they take the exponent as a constant in front of the integral and then are left with an integration which is identical to the one belonging to a steady source and doublet distribution. Although this gives a good approximation for larger distances, it can be expected that for small $\frac{r_c}{t}$ the result will not be very accurate. On the other hand the possibility exists that this inaccuracy might be compensated by the use of curved panels as recently proposed by Chen, Suciu and Morino (Ref.15).

4 NUMERICAL SOLUTION

After the influence coefficients A_n^{ij} have been calculated, the two sets of equations given by (18) will have to be solved. Making a distinction in these equations between the body and the lifting surface, (18) can be rewritten in matrix form:

$$\begin{bmatrix} A_n^{BB} & A_n^{BD} \\ A_n^{DB} & A_n^{DD} \end{bmatrix} \begin{bmatrix} \sigma_n \\ \Delta C_{p_n} \end{bmatrix} = \begin{bmatrix} F_n^B \\ F_n^D \end{bmatrix} \qquad (n = 0,1) \qquad (23)$$

in which the matrix is partioned into four submatrices, each containing the influence coefficients of a particular type of influence between panels on the body and/or the lifting surface. The advantage of this partitioning is that the submatrix $[A_n^{BB}]$, describing the influence between the panels on the body, is strongly diagonal-dominant. The submatrix $[A_n^{DD}]$ possesses a similar structure, although less pronounced. The two submatrices $[A_n^{BD}]$ and $[A_n^{DB}]$ will not have a specific structure, but in general their elements will be small compared to the diagonal terms in the other two submatrices.
Based on these expected properties with regard to the general structure of the matrix equations the following iterative procedure is used to solve them.

First the set containing $[A_n^{BB}]$ is solved with an iterative Gauss-Seidel process. Then the residue is is determined, which is used to solve the set containing $[A_n^{DD}]$ through a direct Crout-process. The residue is determined again and the process is started from the beginning. This iteration process is repeated several times until the increment, which during each run is added to the solution of σ_n and ΔC_{p_n} has become smaller than a certain value. To overcome the problem of numerical under- or overshoots in the first few iteration steps, the calculation of the residues is performed with a relaxation factor on the correction term.

5 CALCULATED RESULTS

To test the method a configuration is chosen on which extensive steady and unsteady pressure measurements have been performed at NLR (see reference 4). The configuration which is shown in figure 2, consists of a tapered wing with a tip tank and a removable pylon-store attachment.

The panel distribution used for the calculations on the wing-tip tank configuration is designed as follows. The wing is divided into 10 chordwise strips of 10 panels each. The last strip is assumed to continue up to the tip tank axis, such that part of these panels fall within the tip tank. This strip does not contain collocation points and the strength of the singularities is taken to be equal to the ones of the strip next to it. The tip tank is panelled into 27 octagonal sections perpendicular to the axis, totalling a number of 216 panels.

5a Steady results

Figures 3 and 4 show some chorswise distributions of the steady pressure jump ΔC_{p_o} across the wing of the wing-tip tank configuration for $M_\infty = 0.45$ and $\alpha = 0^\circ$. For both sections the agreement between the results of the NLRS-method and the measurements is satisfactory. The leading edge peak visible in both figures is caused by the fact that the wing profile has a drooped nose which extends over the first 40 % of the chord. Corresponding pressure distributions on the tip tank are given in figures 5 and 6. Figure 5 shows a comparison between calculated and measured pressure distributions in the direction along the tip tank axis at a station just above the wing reference plane ($\delta = 202.5^\circ$).

The leading edge peak induced by the wing is clearly visible in the theoretical results but is too local to be discernable in the measurements. Further away from the wing this peak has disappeared also in the calculated results as can be seen in figure 6, which gives the pressure on the outside of the tip tank.

5b Quasi-steady and unsteady results

Unsteady results have been calculated for a pitching oscillation around an axis at 15 % of the root-chord, with a reduced frequency $k = 0.305$ based on the wing semi-span. In figures 7 and 8 a comparison is given for the same wing sections as used in the steady case. The chordwise distributions of the unsteady pressure jump $\Delta C_{p_1}/A$ calculated with the NLRI-method are in good agreement with the experimental data for both the real and imaginary part. In this comparison all distributions are normalized with the same amplitude A. Also shown in these figures is the quasi-steady distribution based on the difference of the results of the NLRS-method for $\alpha = 2^\circ$ and 0°. Apparently the reduced frequency of $k = 0.305$ is still too small to give a significant difference between the quasi-steady results and the real part of the unsteady distribution. A significant difference is found indeed in these figures if the theoretical results of the wing with and without tip tank are compared. Clearly, the presence of the tip tank causes the pressure level on the wing to rise. This interference effect is most prominent in the vicinity of the tip tank, but is still noticable in section 3.

Contrary to the theory these unsteady calculations with the NLRI-method are performed under omission of the second derivatives of φ_0 in the boundary condition (12) and the formula (20) for the pressure distribution on the body (tip tank). During the calculations it was found that, as is assumed in the theory, the computer program of the NLRS-method indeed generates small perturbation velocities on the body. However, the second derivatives of φ_0 do not come out small, but instead are so large that they dominate the solution of the flow field completely. The reason for this is not yet completely understood, but it is believed to be inherent to the coarseness of the panelling. That these second derivatives of φ_0 should be small indeed is partially confirmed by the fact that omitting them leads to the excellent comparison with the measurements on the wing where they enter the calculation through interference with the tip tank. Preliminary calculations of the unsteady pressure on the tip tank indicate that the second derivatives can not be neglected completely.

6 CONCLUSIONS

A method is presented which enables the calculation of unsteady pressure distributions on wing-body configurations. Since the unsteady flow field depends on the steady flow field on which it is superimposed, this steady flow field is calculated as a part of the method. The results of the steady method seem to be in agreement with the measurements except for the calculation of the second derivatives of the disturbance potential. This problem, which is probably caused by a too coarse discretization of the body, is being investigated at the moment.

Theoretical unsteady pressure distributions on the wing show a very good agreement with the experimental ones, while from calculations for the wing only it is found that the interference effects of the tip tank on the wing are not of a negligible magnitude. Preliminary results on the body seem to indicate the importance of an accurate calculation of the second derivatives of the disturbance potential.

7 REFERENCES

1. Kalman, T.P., Rodden, W.P. and Giesing, J.P. — Application of the doublet-lattice method to nonplanar configurations in subsonic flow. J. Aircraft, Vol.8, No.6, 1971, pp. 406-413.
2. Rodden, W.P., Giesing, J.P. and Kalman, T.P. — New developments and applications of the subsonic doublet-lattice method for nonplanar configurations. AGARD Conf. Proc. No. 80-71, Part II, No.4, 1971.
3. Giesing, J.P., Kalman, T.P. and Rodden, W.P. — Subsonic steady and oscillatory aerodynamics for multiple interfering wings and bodies. J. Aircraft, Vol.9, No.10, 1972, pp. 693-702.
4. Renirie, L.T. — Analysis of measured aerodynamic loads on an oscillating wing/store combination in subsonic flow. Paper in AGARD Specialists Meeting on Wing-with-Stores Flutter, Munich, 1974.
5. Hess, J.L. and Smith, A.M.O. — Calculation of potential flow about arbitrary bodies. Progress in Aeron. Sciences, Vol.8, Küchemann, 1967, pp. 1-138.
6. Hess, J.L. — Calculation of acoustic fields about arbitrary three-dimensional bodies by a method of surface source distributions based on certain wave number expansions. Douglas Aircr. Comp., Rep. No. DAC 66901, 1968.
7. Roos, R. and Zwaan, R.J. — Calculation of instationary pressure distributions and generalized aerodynamic forces with the doublet-lattice method. NLR TR 72037 U, Amsterdam, National Aerospace Laboratory NLR, 1972.
8. Roos, R., and Zwaan, R.J. — The effect of a pylon-mounted nacelle on the flutter behaviour of a wing-pylon-nacelle configuration. NLR TR 74125 U, Amsterdam, National Aerospace Laboratory NLR, 1974.
9. Labrujere, Th.E., and Sytsma, H.A. — Aerodynamic interference between aircraft components: the possibility of prediction. ICAS Paper No. 72-49, 8th Congress of the International Council of Aeronautical Sciences, Amsterdam, August 1972.
10. Morino, L. — Unsteady compressible potential flow around lifting bodies: General theory. AIAA Paper No. 73-196, 11th Aerospace Sciences Meeting, Washington, DC, January 1973.
11. Morino, L. and Kuo, C.C. — Unsteady subsonic compressible flow around finite thickness wings. AIAA Paper No. 73-313, Dynamics Specialists Conference, Williamsburg, Virginia, March 1973.
12. Destuynder, R. and Tijdeman, H. — An investigation of different techniques for unsteady pressure measurements in compressible flow and comparison with results of lifting surface theory. AGARD R-617, 1973.
13. Kalman, T.P., Rodden, W.P. and Giesing, J.P. — Aerodynamic influence coefficients by the doublet lattice method for interfering non-planar lifting surfaces oscillating in a subsonic flow. Part I. Douglas Aircr. Comp., Rep. No. DAC 67977, 1969.
14. Roos, R., and Bennekers, B. — Description of a method for the calculation of aerodynamic loads on oscillating wing-body configurations in subsonic flow (NLRI-method). Part I: The theory. To be published.
15. Chen, L.T., Suciu, E.O. and Morino, L. — A finite element method for potential aerodynamics around complex configurations. AIAA Paper No. 74-107, 12th Aerospace Sciences Meeting, Washington, DC, January 1974.
16. Rubbert, P.E., et al. — A general method for determining the aerodynamic characteristics of fan-in-wing configurations. Vol.I: Theory and application. US Army Aviation Mat. Lab., Tech.Rep. No. 67-61A, 1967.

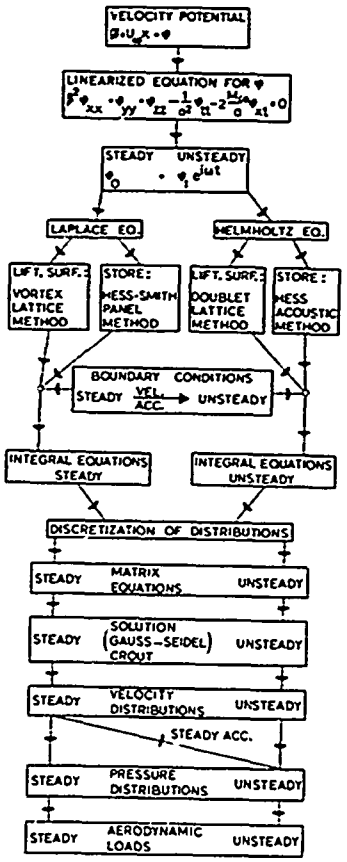

Fig.1 Schematic outline of the calculations

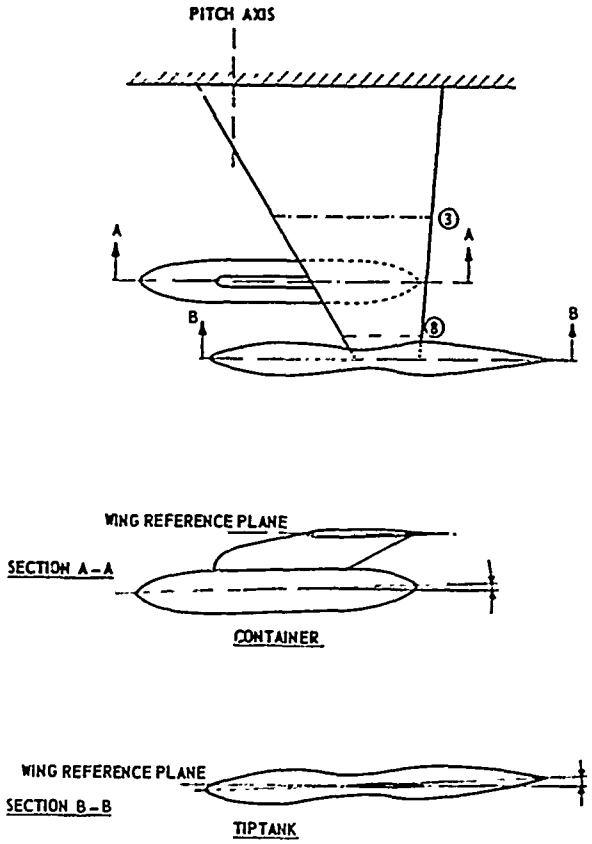

Fig.2 Schematic view of the wing-tip tank store configuration

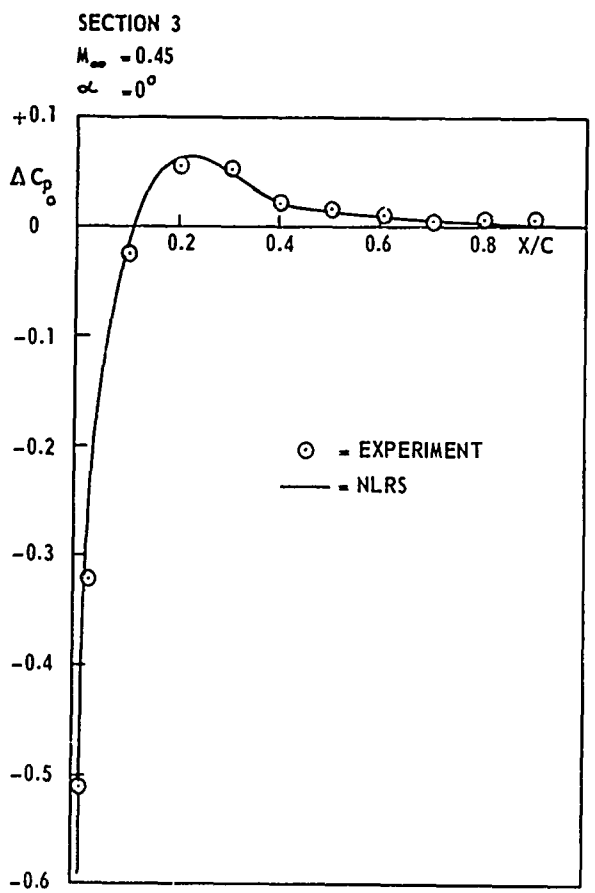

Fig.3 Chordwise distribution of the steady pressure jump across the wing of the wing-tip tank configuration

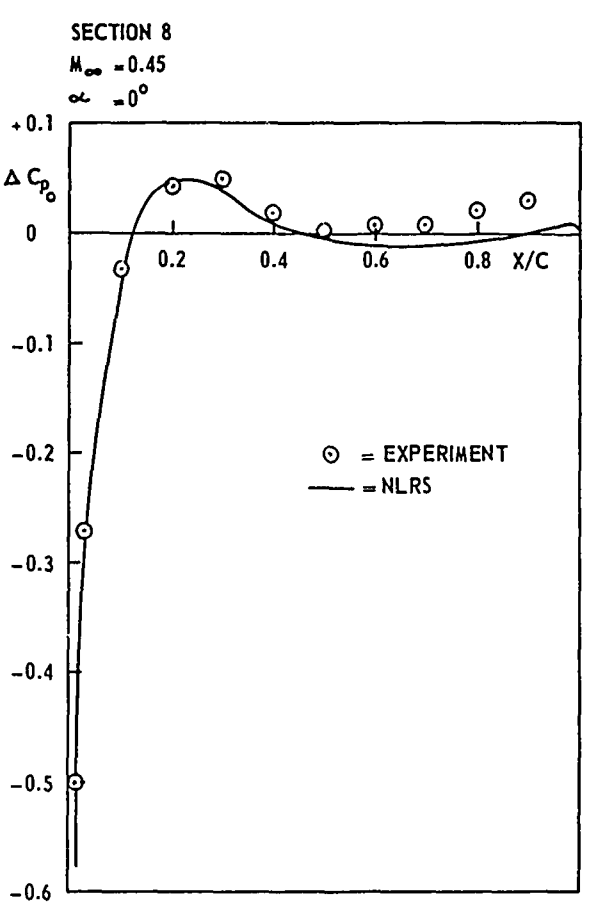

Fig.4 Chordwise distribution of the steady pressure jump across the wing of the wing-tip tank configuration

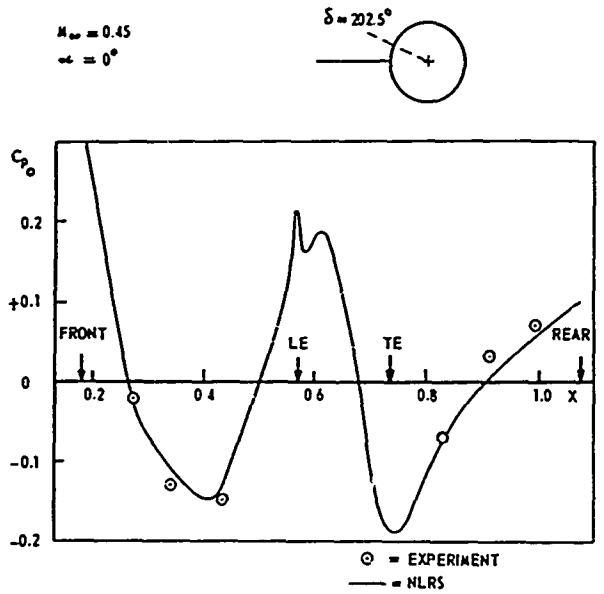

Fig.5 Steady pressure distribution along the tip tank of the wing-tip tank configuration

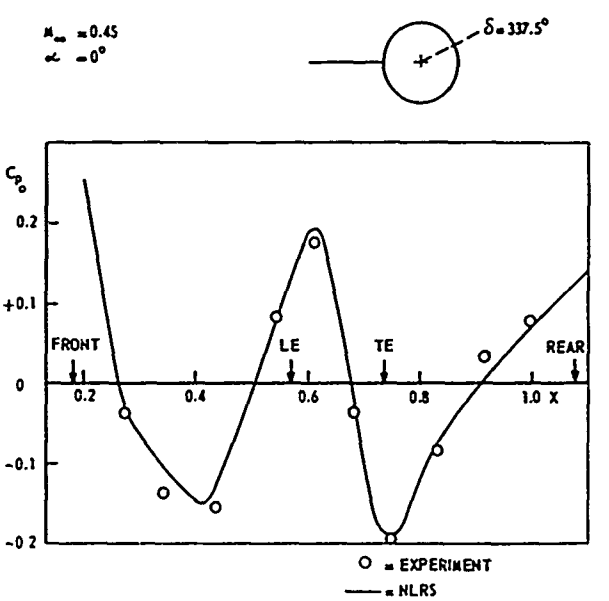

Fig.6 Steady pressure distribution along the tip tank of the wing-tip tank configuration

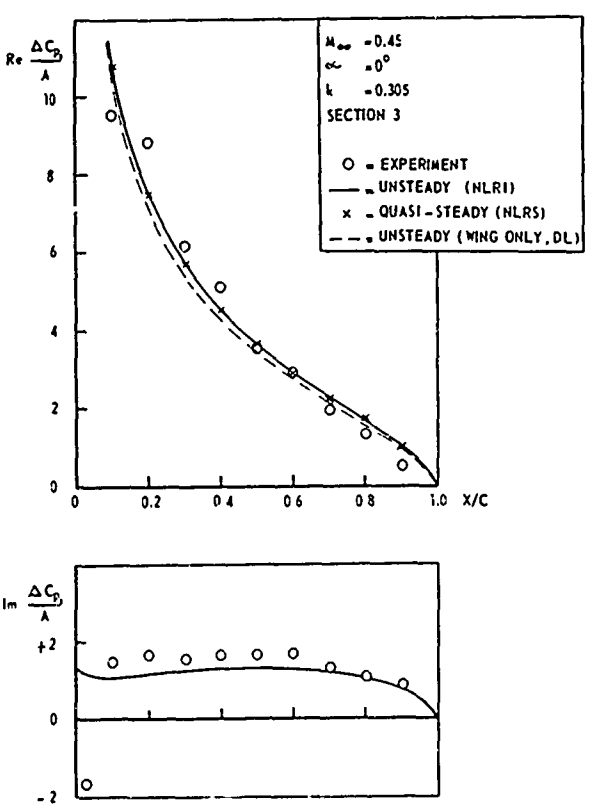

Fig.7 Chordwise distribution of the unsteady and quasi-steady pressure jump across the wing of the wing-tip tank configuration oscillating in a pitch mode

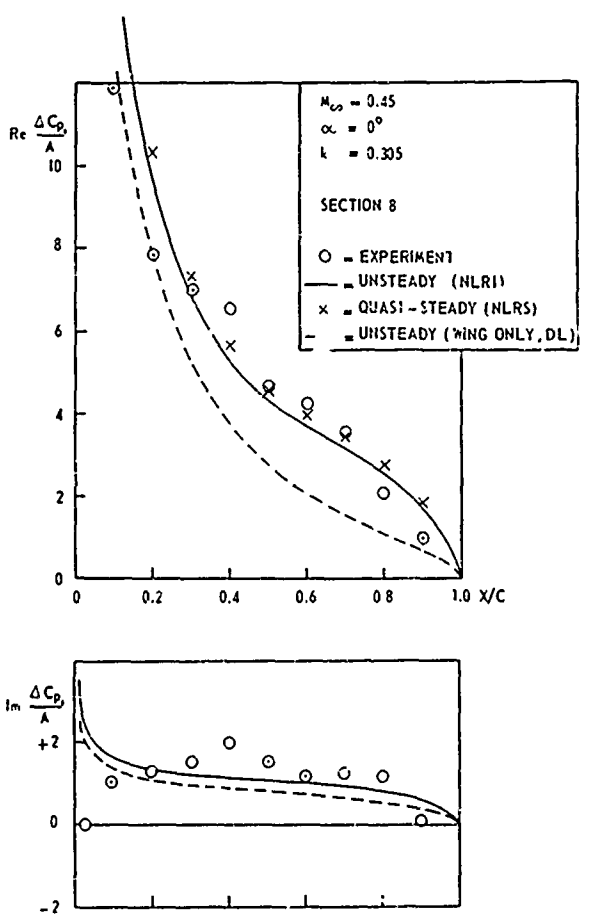

Fig.8 Chordwise distribution of the unsteady and quasi-steady pressure jump across the wing of the wing-tip tank configuration oscillating in a pitch mode

APPENDIX 1

THE GENERAL SOLUTION

The disturbance velocity potential $\varphi \langle x,y,z,t \rangle$ satisfies the equation

$$\beta^2 \varphi_{xx} + \varphi_{yy} + \varphi_{zz} - \frac{1}{a_\infty^2} \varphi_{tt} - 2 \frac{M_\infty}{a_\infty} \varphi_{xt} = 0 \qquad \text{(A1.1)}$$

in which $M_\infty = U_\infty / a_\infty$ and $\beta^2 = 1 - M_\infty^2$. Assuming harmonic variations in time φ can be written as:

$$\varphi \langle x,y,z,t \rangle = \varphi_o \langle x,y,z \rangle + \varphi_1 \langle x,y,z \rangle e^{i\omega t} \qquad \text{(A1.2)}$$

with φ_o being the steady part and $\varphi_1 e^{i\omega t}$ the unsteady part.
Using also the substitutions:

$$\varphi_n \langle x,y,z \rangle = \varphi_n^* \langle x,y,z \rangle e^{ik_n M_\infty x} \qquad (n = 0,1) \qquad \text{(A1.3)}$$

with $k_n = \frac{n\omega}{a_\infty \beta^2}$ and

$$x' = x \quad , \quad y' = \beta y \quad , \quad z' = \beta z \qquad \text{(A1.4)}$$

equation (A1.1) can be transformed into

$$\varphi^*_{n_{x'x'}} + \varphi^*_{n_{y'y'}} + \varphi^*_{n_{z'z'}} + k_n^2 \varphi_n^* = 0 \qquad (n = 0,1) \qquad \text{(A1.5)}$$

A general solution φ_n^* of this equation can be written in terms of a source distribution over the body and a dipole distribution over the wake. To avoid numerical instabilities near the trailing edge, as indicated by Rubbert et al (Ref.16), the dipole distribution over the wake should be extended to the camber surface inside the body. Transforming the result back to an expression for φ_n, one obtains:

$$\varphi_n \langle x,y,z \rangle = -\frac{1}{4\pi} \iint_{S_B} \sigma_n \langle \xi_B,\eta_B,\zeta_B \rangle e^{ik_n M_\infty (x-\xi_B)} \frac{e^{-ik_n r}}{r} dS$$

$$+ \frac{1}{4\pi} \iint_{S_C} \mu_n \langle \xi_C,\eta_C,\zeta_C \rangle e^{ik_n M_\infty (x-\xi_C)} \frac{\partial}{\partial n} \left[\frac{e^{-ik_n r}}{r} \right] dS$$

$$+ \frac{1}{4\pi} \iint_{S_W} \Delta\varphi_n \langle \xi_W,\eta_W,\zeta_W \rangle e^{ik_n M_\infty (x-\xi_W)} \frac{\partial}{\partial n} \left[\frac{e^{-ik_n r}}{r} \right] dS \qquad \text{(A1.6)}$$

for n = 0,1 and

with $$r = \left[(x-\xi)^2 + \beta^2 (y-\eta)^2 + \beta^2 (z-\zeta)^2 \right]^{1/2} \qquad \text{(A1.7)}$$

In (A1.6) σ_n represents the strength of the source distribution on the body surface, μ_n and $\Delta\varphi_n$ the dipole distribution on the camber surface and the surface of the wake.

The calculation of the integral over the wake surface, is rather difficult in practice. Obtaining analytical expressions is hampered by the fact that the stationary position of the wake is not known a priori and thus will have to be determined first with some kind of iteration procedure. Assuming that the unsteady wake coincides with the steady one, which in general is not a plane surface behind the wing, introduces the problem of calculating integrals with oscillating integrands over curved surfaces, practically excluding analytical formulations. The alternative of discretizing the wake sheet and calculating the contribution of the individual elements as proposed by Morino and Kuo (Refs. 10, 11) leads to the question of truncation.

Besides the effects of the wake, the general expression (A1.6) for φ does also include the effects due to wing thickness. However, in this context it is important to realize that lifting surface theory gives already a sufficiently accurate prediction of the aerodynamic forces on the wing, while at the same time the wake effects are incorporated.

Taking into account the above arguments and considering the goal of the method, being the calculation of pressure distributions on stores, of which the wake is not as well defined as that of the wing, the method is simplified. The body is assumed to produce no wake, while the lifting surfaces are taken to be infinitely thin. With these assumptions the expression for the velocity potential due to the body reduces to:

$$\varphi_n \langle x,y,z \rangle = -\frac{1}{4\pi} \iint_{S_B} \sigma_n \langle \xi_B,\eta_B,\zeta_B \rangle e^{ik_n M_\infty (x-\xi_B)} \frac{e^{-ik_n r}}{r} dS \qquad \text{(A1.8)}$$

The velocity potential due to the lifting surfaces can now be given in terms of a pressure dipole as is common in existing lifting surface theories.

APPENDIX 2

THE BOUNDARY CONDITIONS ON AN OSCILLATING SURFACE

The surface of an oscillating body is described by the functional

$$S < \vec{r} > = 0 \tag{A2.1}$$

The vector $\vec{r}$, which determines the position of points on this surface, can be written in the form:

$$\vec{r} = \vec{r} < \vec{r}_o, t > = \vec{r}_o + \vec{r}_e < \vec{r}_o t > \tag{A2.2}$$

where $\vec{r}_o$ represents the stationary reference position and $\vec{r}_e$ the time dependent amplitude of the motion, which also depends on $\vec{r}_o$. The vector $\vec{r}_o$ satisfies the functional

$$S_o < \vec{r}_o > = 0 \tag{A2.3}$$

describing the surface of the body in the reference position.

The boundary condition requiring the flow to be tangential to the moving surface is given by:

$$\frac{DS}{Dt} = \frac{\partial S}{\partial t} + \vec{q}.\vec{\nabla}S = 0 \qquad \text{on } S < \vec{r} > = 0 \tag{A2.4}$$

Except perhaps for some very simple bodies the functionals $S < \vec{r} >$ and $S_o < \vec{r}_o >$ are very difficult to determine. On the other hand the individual point on the oscillating surface can be given in terms of their reference position and the time dependent amplitude $\vec{r}_e$ as is done in (A2.2). Also the normal in these points on their reference position, can be calculated without any problem. Therefore, in the formulation of the boundary condition on the oscillating body the derivatives of S will have to be expressed in terms of the amplitude $\vec{r}_e$ and the normal $\vec{n}$. This can be done as follows.

The components of the vector $\vec{r}$ are

$$\begin{aligned} x &= x < x_o, y_o, z_o, t > \\ y &= y < x_o, y_o, z_o, t > \\ z &= z < x_o, y_o, z_o, t > \end{aligned} \tag{A2.5}$$

Interchanging dependent and independent variables results in:

$$\begin{aligned} x_o &= x_o < x, y, z, t > \\ y_o &= y_o < x, y, z, t > \\ z_o &= z_o < x, y, z, t > \end{aligned} \tag{A2.6}$$

With (A2.6) a point $< x, y, z >$ can be related at any time to its reference position $< x_o, y_o, z_o >$. The functional for the moving surface becomes:

$$\begin{aligned} S_o < \vec{r}_o > &= S_o < x_o < x, y, z, t >, y_o < x, y, z, t >, z_o < x, y, z, t >> \\ &\equiv S < x, y, z, t > = 0 \end{aligned} \tag{A2.7}$$

Assuming that $|r_e| \ll |r_o|$ the following expressions for the derivatives of S can be obtained from (A2.7)

$$\frac{\partial S}{\partial t} \cong -\vec{\nabla}_o S_o \cdot \frac{\partial \vec{r}_e}{\partial t} \tag{A2.8}$$

and

$$\vec{\nabla}S \cong -\vec{\nabla}_o S_o - \left[\frac{\partial S_o}{\partial x_o} \vec{\nabla}_o x_e + \frac{\partial S_o}{\partial y_o} \vec{\nabla}_o y_e + \frac{\partial S_o}{\partial z_o} \vec{\nabla}_o z_e \right] \tag{A2.9}$$

with x_e, y_e and z_e being the components of the displacement vector

$$\vec{r}_e \quad \text{and} \quad \vec{\nabla}_o = \left(\frac{\partial}{\partial x_o}, \frac{\partial}{\partial y_o}, \frac{\partial}{\partial z_o} \right) .$$

The disturbance potential in a point on the moving body can be expressed in the value of the potential in the corresponding point of the surface in the reference position*)

$$\varphi < x, y, z > = \varphi < x_o, y_o, z_o > + (\vec{r}_e \cdot \vec{\nabla}\varphi) \Big|_o + \ldots\ldots \tag{A2.10}$$

Similarly one can write for the disturbance velocities:

$$\vec{\nabla}\varphi = \vec{\nabla}\varphi \Big|_o + (\vec{r}_e \cdot \vec{\nabla}) \vec{\nabla}\varphi \Big|_o + \ldots\ldots \tag{A2.11}$$

Substitution of (A2.8), (A2.9) and (A2.11) in (A2.4) and retaining only terms of first and second order in the amplitude and its derivatives gives

$$-\vec{\nabla}_o S_o \cdot \frac{\partial \vec{r}_e}{\partial t} + (\vec{q}_\infty + \vec{\nabla}\varphi \Big|_o) \cdot (\vec{\nabla}_o S_o - \frac{\partial S_o}{\partial x_o} \vec{\nabla}_o x_e - \frac{\partial S_o}{\partial y_o} \vec{\nabla}_o y_e - \frac{\partial S_o}{\partial z_o} \vec{\nabla}_o z_e) + \vec{\nabla}_o S_o \cdot \left[(\vec{r}_e \cdot \vec{\nabla}) \vec{\nabla}\varphi \Big|_o \right] = 0 \tag{A2.12}$$

*) The symbol $\Big|_o$ indicates that the term preceding it will have to be evaluated on the body in the reference position.

Using the harmonic expansion (A1.2) for φ, a time harmonic amplitude of the form

$$\vec{r}_e \langle x_o, y_o, z_o, t \rangle = \vec{r}_e^{\,*} \langle x_o, y_o, z_o \rangle \; e^{i\omega t} \tag{A2.13}$$

and neglecting products of $\vec{r}_e^{\,*}$ and φ_1 leads to the following two conditions

n = 0:

$$(\vec{q}_\infty + \vec{\nabla}\varphi_o \Big|_o) \cdot \vec{n} = 0 \tag{A2.14}$$

and

n = 1:

$$\vec{\nabla}\varphi_1 \Big|_o \cdot \vec{n} - i\omega \vec{r}_e^{\,*} \cdot \vec{n} - (\vec{q}_\infty + \vec{\nabla}\varphi_o \Big|_o) \cdot (\ell \vec{\nabla} x_e^* + m\vec{\nabla} y_e^* + n\vec{\nabla} z_e^*) + \vec{\nabla}_o S_o \cdot \left[(\vec{r}_e^{\,*} \cdot \vec{\nabla}) \vec{\nabla}\varphi_o \Big|_o \right] = 0 \tag{A2.15}$$

where ℓ, m and n are the components of the normal vector on the body in the reference position defined by $\vec{n} = \dfrac{\vec{\nabla}_o S_o}{|\nabla_o S_o|}$.

APPENDIX 3

DERIVATION OF THE FORMULAS FOR THE PRESSURE ON THE BODY

The pressure in a point on the surface of the body is given by the general formula:

$$C_p = \frac{2}{\gamma M_\infty^2}\left\{\left[1 + \frac{(\gamma-1)}{2} M_\infty^2 \left(1 - \frac{\vec{q}.\vec{q} + 2\,\phi_t}{q_\infty^2}\right)\right]^{\gamma/(\gamma-1)} - 1\right\} \tag{A3.1}$$

Introduction of the disturbance potential φ modifies this into:

$$C_p = \frac{2}{\gamma M_\infty^2}\left\{\left[1 - \frac{(\gamma-1)}{2}\frac{M_\infty^2}{q_\infty^2}\left(2\,U_\infty\varphi_x + 2\,V_\infty\varphi_y + 2\,W_\infty\varphi_z + 2\,\varphi_t + \varphi_x^2 + \varphi_y^2 + \varphi_z^2\right)\right]^{\gamma/(\gamma-1)} - 1\right\} \tag{A3.2}$$

Substitution of (A2.11) for the spatial derivatives and

$$\varphi_t = \varphi_t\Big|_o + (\vec{r}_e \cdot \vec{\nabla})\,\varphi_t\Big|_o + \ldots\ldots \tag{A3.3}$$

for the time derivative of φ, together with the use of (5) and (A2.13) results in the following expression for the pressure:

$$C_p = \frac{2}{\gamma M_\infty^2}\left\{\left[1 - \frac{(\gamma-1)}{2}\frac{M_\infty^2}{q_\infty^2}\left(A + Be^{i\omega t}\right)\right]^{\gamma/(\gamma-1)} - 1\right\} \tag{A3.4}$$

in which:

$$A = 2\left(U_\infty\varphi_{o_x}\Big|_o + V_\infty\varphi_{o_y}\Big|_o + W_\infty\varphi_{o_z}\Big|_o\right) + \left(\varphi_{o_x}\Big|_o\right)^2 + \left(\varphi_{o_y}\Big|_o\right)^2 + \left(\varphi_{o_z}\Big|_o\right)^2 \tag{A3.5}$$

and

$$B = 2\left[\vec{q}_o \cdot \vec{\nabla}\varphi_1\Big|_o + i\omega\varphi_1\Big|_o + \left(U_\infty + \varphi_{o_x}\Big|_o\right)\left(\vec{r}_e^{\,*} \cdot \vec{\nabla}\varphi_{o_x}\right)\Big|_o + \left(V_\infty + \varphi_{o_y}\Big|_o\right)\left(\vec{r}_e^{\,*} \cdot \vec{\nabla}\varphi_{o_y}\right)\Big|_o + \left(W_\infty + \varphi_{o_z}\Big|_o\right)\left(\vec{r}_e^{\,*} \cdot \vec{\nabla}\varphi_{o_z}\right)\Big|_o\right] \tag{A3.6}$$

Since $\varphi_1 << \varphi_o$ and $\vec{r}_e^{\,*}$ is of the same order as φ_1, only terms linear in φ_1 and $\vec{r}_e^{\,*}$ are retained in B, while at the same time it follows that $B << A$. This makes it possible to introduce a two-term binomial expansion in (A3.4):

$$\left[\left(1 - \frac{(\gamma-1)}{2}\frac{M_\infty^2}{q_\infty^2}A\right) - \frac{(\gamma-1)}{2}\frac{M_\infty^2}{q_\infty^2}B\right]^{\gamma/(\gamma-1)} =$$

$$\left[1 - \frac{(\gamma-1)}{2}\frac{M_\infty^2}{q_\infty^2}A\right]^{\gamma/(\gamma-1)} - \frac{\gamma M_\infty^2 B}{2\,q_\infty^2}\left[1 - \frac{(\gamma-1)}{2}\frac{M_\infty^2}{q_\infty^2}A\right]^{1/(\gamma-1)} + \ldots\ldots \tag{A3.7}$$

Substitution of (A3.7) in (A3.4) and decomposing C_p as:

$$C_p = C_{p_o} + C_{p_1}\,e^{i\omega t} \tag{A3.8}$$

leads to the following two expressions for the steady and the unsteady pressure distributions on the body:

$$C_{p_o} = \frac{2}{\gamma M_\infty^2}\left\{\left[1 + \frac{(\gamma-1)}{2} M_\infty^2 \left(1 - \frac{\vec{q}_o.\vec{q}_o}{q_\infty^2}\right)\right]^{\gamma/(\gamma-1)} - 1\right\} \tag{A3.9}$$

and

$$C_{p_1} = -\frac{B}{q_\infty^2}\left[1 + \frac{(\gamma-1)}{2} M_\infty^2 \left(1 - \frac{\vec{q}_o.\vec{q}_o}{q_\infty^2}\right)\right]^{1/\gamma-1} . \tag{A3.10}$$

ANALYSIS OF MEASURED AERODYNAMIC LOADS ON AN OSCILLATING WING-STORE COMBINATION IN SUBSONIC FLOW

by

L. Renirie

NATIONAL AEROSPACE LABORATORY, NLR, Amsterdam, The Netherlands

Paper presented during the specialists meeting on wing-with-stores-flutter in conjunction with the 39th meeting of the Structures and Materials Panel of AGARD, Munich, Germany, 6-12 October 1974.

The extensive investigation, of which some results are presented in this paper, is a joint effort of the following group of specialists at NLR:

J.W.G. van Nunen	R. Roos
R. Poestkoke	P. Schippers
N. Pronk	H. Tijdeman
L. Renirie	R.J. Zwaan

The investigation was carried out under contract for the Scientific Research Branch Air Materiel Directorate of the RNLAF.

SUMMARY

An analysis is given of aerodynamic loads measured with an oscillating wind tunnel model representing a wing with a tip tank and a removable pylon with store. Attention is paid to the interference effects on the wing load and to the pylon store load in low and high subsonic flow.

CONTENTS

LIST OF SYMBOLS

c	local chord	(m)
$\bar{c}$	mean chord ; $\bar{c} = 0.4034$	(m)
C_p	steady pressure coefficient ; $C_p = (p-p_\infty)/q_\infty$	
C_{p_b}	unsteady pressure coefficient ; $C_{p_b} = p_i/(q_\infty \frac{d}{s})$	
C_y	local side force coefficient ; C_y = side force/$q_{\infty_{ref}} \ell$; positive outwards	
C_z	local normal force coefficient ; C_z = normal force/$q_{\infty_{ref}} \ell$; positive upwards	
d	displacement of reference point ($x/c = 0.871$, $y/s = 0.143$)	(m)
f	frequency	(Hz)
k	reduced frequency based on s	
k_b	unsteady lift coefficient in a wing section ($\frac{1}{\pi} C_{z_b}$)	
ℓ_c	length of the pylon store ; $\ell_c = 0.734$	(m)
ℓ_{ref}	reference dimension : wing : $\ell_{ref} = c$ store : ℓ_{ref} = max. diameter = 0.1043	(m)
M	free stream Mach number	
p	steady pressure	(kg/m^2)
p_i	unsteady pressure	(kg/m^2)
q_∞	dynamic pressure	(kg/m^2)
s	model semi-span ; $s = 0.6646$	(m)
x	co-ordinate along local chord or along store	(m)
y	spanwise co-ordinate normal on chord	(m)
α	angle of attack ; positive nose up	(degree)
φ	angular co-ordinate in store cross-section	(degree)

1 INTRODUCTION

Today military aircraft configurations involve frequently wing-attached stores of considerable size. When dealing with aeroelastic problems for such configurations two questions arise, namely:

- what are the unsteady aerodynamic loads on the stores
- what are the interference loads induced by the stores on the wing.

Also the NLR was faced with this question when it got involved in the flutter investigation for a fighter-type aircraft with a number of wing stores, differing in size and position. Appropriate general data concerning aerodynamic loads on oscillating wing-store combinations was not available, so that a research programme was started at the NLR involving wind tunnel measurements on a model of a representative wing-store combination and the development of a method to calculate aerodynamic loads on oscillating wing-store combinations in subsonic flow. The latter subject is reported on in ref.1. In this way a comparison of measured and calculated results is possible and, because of the fact that the wind tunnel model has been scaled to the wing of the aircraft in question, the results can be used as input to practical aeroelastic calculations.

In this paper a brief description is given of the wind tunnel measurements and the analysed results now available are discussed.

2 MODEL DESCRIPTION AND TEST CONDITIONS

A picture of the model installed in the wind tunnel is presented in fig.1. It is a semi-span model equipped with a tip tank and a pylon mounted store. (The full-scale wing can also carry an inboard pylon, but in the wind tunnel model this pylon has been left out because of the expected tunnel wall interference). Some geometrical data concerning the wing and the stores are given in fig.2. The wing has a moderate sweep angle and is strongly tapered. Wing thickness is 4.8 % and the profile, being constant along the span, shows a droop nose.

During the measurements the model was able to perform a pitching oscillation about an axis perpendicular to the wall. The pitching axis could be shifted to locations at 15 % and 50 % of the root chord. The model was driven at a resonance frequency, which could be varied by changing springs in the supporting structure of the pitching axis. However, the pitching frequency was always well below the frequencies at which elastic deformations of the model could be observed. The vibration mode was measured by 12 acceleration pick-ups, of which 6 were installed in the wing, 4 in the pylon store (2 vertical and 2 lateral) and 2 in the tip tank. The vibration mode for which results are presented in this paper, was a nearly pure pitching oscillation ; lateral motion of the pylon store could be neglected.

To gain a detailed pressure distribution over the model surface, the model was provided with 340 pressure taps of which 88 were distributed over both upper and lower wing surface, 86 over the pylon store and 78 over the tip tank. The tap locations on the wing and the pylon store are indicated in fig.3.

The pressure measuring technique was described very recently in ref.2 in an application at high subsonic speeds. In this reference it was demonstrated that the accuracy of the measuring technique is satisfactory. The essence of this method is that through vinyl tubes all pressure taps are connected with a small number of scanning valves outside the test section of the wind tunnel. The measured pressures are corrected using the calibrated transfer functions of the tubes. In the present wind tunnel model the calibration was performed by means of a number of in situ micro miniature pressure transducers, installed in one of the measuring sections. To obtain unsteady pressure coefficients the pressures have been related to a displacement s in a reference point ($x/c = 0.871$; $y/s = 0.143$).

Transition of the boundary layer was assured by carborundum strips on the wing and the stores. On the wing the strips were located at 20 % of the chord on the upper surface and at 40 % on the lower surface. The strips on the tip tank and pylon-store were located at 8.5 % and 11 % of their length, respectively.

The model tests were performed in the large transonic wind tunnel HST. Parameters in the test conditions were: configuration (pylon store and pylon were removable), pitching axis location, frequency, Mach number, stagnation pressure and angle of attack (only in the steady measurements; in the unsteady measurements wing angle of attack was zero).

An analysis of the influence of all these parameters is in process. A part of the results now available is discussed in this paper. They involve pressure distributions on the wing and the pylon store for the configuration shown in fig.1, a pitching axis at 15 %, frequencies of 0,11 and 19 Hz, Mach numbers of 0.45 and 0.8 and a stagnation pressure of 1 atm. In the steady measurements the wing angle of attack is 0° and 3° with respect to the wing reference plane.

3 DISCUSSION OF RESULTS

In the discussions in this section the following line will be pursued. First steady results are presented, next quasi-steady results which have been derived from the steady results for $\alpha = 0^\circ$ and 3° and finally the unsteady results. In doing so attention can be paid separately to the interference effects between wing and pylon store which are essentially of the same kind for the quasi-steady and the unsteady results and to the influence of frequency.

3.1 Results for the wing

3.1.1 Steady and quasi-steady pressure distributions

In figure 4 some steady chordwise pressure distributions are presented, which are typical for this wing model in low subsonic flow ($M = 0.45$) at zero angle of attack. The distributions on both the upper and lower surface of the wing are given for the configurations with and without the pylon-store. On the lower surface near the leading edge they show a large suction peak, which is caused by the droop nose of the wing profile and therefore is characteristics for all steady pressure distributions shown.

The addition of the pylon and store under the wing has a large effect on the flow characteristics around the wing in the neighbourhood of the pylon. The diversion of the flow due to the store causes the local velocity under the wing to speed up, resulting in a considerable change in the pressure distribution on the lower surface. On the upper surface this interference effect is an order of

magnitude smaller, while it is restricted mainly to the vicinity of the pylon-store attachment.

Increasing the freestream Machnumber only pronounces the picture described above. While the wing with tip tank only becomes supercritical between $M = 0.85$ and $M = 0.9$ on the lower surface near the leading edge, the presence of the store lowers it down to just below $M = 0.8$. Figure 5 shows a few chordwise distributions for this Machnumber at zero angle of attack. Clearly the flow over the lower surface of the wing has already become supercritical just inboard of the pylon and a weak shock might have been formed already in that region. Figure 6 presents some quasi-steady chordwise pressure distributions for low subsonic flow ($M = 0.45$). These quasi-steady distributions can be interpreted as the "unsteady" airloads for infinitely slow pitching oscillations.

As in the steady distributions the influence of the store is found to be largest in the vicinity of the pylon. The quasi-steady distributions show interference effects on both the upper and the lower surfaces. On the upper surface a decrease of the quasi-steady pressure is found and on the lower surface an increase with the largest interference on the lower wing surface inboard of the pylon. Outboard of the pylon the pressure change due to the store addition is largest on the upper wing surface.

For high subsonic flow ($M = 0.8$) the quasi-steady distributions are the same qualitatively. The only difference is the appearance of some wiggles caused by the apparent existence of a weak shock on the lower surface near the pylon, which was already noticed in the steady distribution (see fig.7).

3.1.2 Steady and quasi-steady spanwise load distributions

The steady and quasi-steady spanwise load distribution, the latter being derived from the measured steady pressure distributions at $\alpha = 0^{\circ}$ and 3°, are given in figure 8a for $M = 0.45$ and 0.8. For $M = 0.8$ these experimental results are also compared with theoretical calculations performed with the NLR panel method (see reference 3).

From the figure it follows that for all flow conditions the interference between wing, pylon and store results in a considerable decrease in the steady lift along the span of the wing, which is maximal near the position of the pylon. Clearly this effect corresponds with the large change in pressure over the lower wing surface observed in the steady chordwise pressure distributions. The pylon also takes away part of the circulation from the wing, causing at that location a jump in the lift distribution. This jump changes its sign if the angle of attack increases from 0° to 3°, indicating a change in the direction of the side force on the pylon and store.

The influence of the pylon and store on the quasi-steady wing load $\frac{\Delta C_z}{\Delta \alpha}$ is shown in figure 8b. It is characterized by an increase of $\frac{\Delta C_z}{\Delta \alpha}$ inboard of the pylon and a decrease on the outboard side. This can be traced back to the quasi-steady pressure distributions of figure 6, which show a interference effect being different on both sides of the pylon.

Both figures 8a and 8b show that the theory overestimates the lift which probably is caused by the neglect of the viscous effects. However, the trend is predicted rather well.

3.1.3 Unsteady pressure distributions

Figures 9 through 11 show a set of unsteady chordwise pressure distributions which are representative for the model oscillating in subsonic flow. In figures 9 and 10 the pressure distribution in low subsonic flow ($M = 0.45$) on the upper and lower wing surface are given for frequencies of 11 and 19 Hz.

As far as the real part of the unsteady pressures is concerned, the influence of the store is very similar to what is found for the quasi-steady distributions: the pressure on the upper surface shows a decrease, while on the lower surface an increase is found. The effect of frequency appears to be very limited. The imaginary part of the pressure distributions remains more or less uneffected for both frequencies. For high subsonic flow ($M = 0.8$) as shown in figure 11 the picture remains the same qualitatively, except that the distributions in section 5 and 6 at the lower surface show wiggles which are related to the presence of a local supercritical flow.

3.1.4 Unsteady spanwise load distributions

The spanwise unsteady load distribution obtained from the measured pressure distributions are presented in figure 12 for both low and high subsonic flow. For comparison also the quasi-steady distributions have been included.

The influence of the pylon and store is clearly very similar for 0, 11 and 19 Hz. For the frequency range considered the jump in the circulation across the pylon tends to decrease a little with increasing frequency. The magnitude of the interference does not exceed the 15 % of the local lift values for the wing without pylon and store. The total lift coefficient which is obtained through spanwise integration shows an interference effect of less than 5 %. The imaginary part of the unsteady wing load is hardly effected by the pylon-store addition.

3.2 Results for the store

3.2.1 Pressure distributions

Fig.13 shows pressure distributions along the store in 4 sections. These sections are defined by the angle φ. Wing angle of attack is zero. On the left side the results are given for $M = 0.45$, on the right side for $M = 0.8$.

Starting the discussion with $M = 0.45$ the first observation is that the pressure distributions for different φ-angles are very similar. This is due to the fact that the wing angle of attack is zero, so that the presence of the wing is hardly felt. The store has a small negative angle of attack, which is reflected in the positive pressures at the nose being higher for $\varphi = 0^{\circ}$ than for 180°. Two minima occur in each section, clearly related to the transition of the varying cross-section of the nose to the cylindrical part and to the transition of this part to the aft-body.

The observations for $M = 0.8$ are the same. In this case theoretical values have been included calculated with a panel method presented in references. The agreement is very satisfactory. At the end of the cylindrical part the flow becomes slightly supercritical, just below the part of the wing where the flow is also supercritical. Obviously this phenomenon is caused by the geometry of wing-pylon-store, which admits only a narrow passage for the flow.

In fig.14 quasi-steady and unsteady results are presented for the same 4 sections as in fig.13. Mach number is 0.45. The quasi-steady pressure distributions and the real parts of the unsteady pressure distributions show exactly the same tendencies. The magnitudes of the imaginary parts are relatively very small.

In fig.15 analogous results are shown for M = 0.8, where again a comparison between measured and calculated results is possible. The agreement is fairly good ; the differences are largest over the rear half of the store, possibly due to boundary layer and separation effects.

3.2.2 Load distributions

In this section quasi-steady and unsteady results are presented in the form of C_{z_b} - and C_{y_b} -distributions along the store. In fig. 16 the C_{z_b} -distribution is shown for the M = 0.45 and 0.8. The remarks as for fig. 14 can also be made here. A qualitative analysis of the load distribution may be given using the result of slender body theory that the load distribution is proportional to $\frac{\partial}{\partial x}(S(x)\alpha(x))$, where S(x) is the local cross-sectional area and $\alpha(x)$ the local normal wash as functions of the co-ordinate x along the store. The normal wash $\alpha(x)$ is a combination of the geometric angle of attack α and the wing-induced upwash, which increases towards the wing and passes on to a downwash near the leading edge. The resulting downwash distribution along the store thus will have the global shape as sketched in fig.18. The derivative of the product $S(x)\alpha(x)$ then leads to a force upwards on the front part of the store and downwards on the rear part, in accordance with the C_{z_b} -distributions of fig.16.

A final remark concerns the small imaginary parts of C_{z_b} in fig. 16, indicating that the damping effect of the store loads on the oscillatory motion is negligible.

Lastly, fig.17 presents the distribution of the coefficient C_{y_b} along the store for both Mach numbers. Also here the quasi-steady and the real parts of the unsteady results are almost identical. Again slender body theory may be used for a qualitative explanation of the load distribution. Due to the presence of the swept wing the side wash along the store increases gradually towards the tail as is shown qualitatively in fig.18. The resulting side load is pointing outwards nearly all along the store. It is very small over the front part, shows a maximum near the wing leading edge and falls off towards the tail. Through integration of the side load distribution along the store a side force coefficient is found. The modulus of this coefficient is nearly 2 % of the modulus of the lift coefficient if both are made dimensionless in the same way.

4 CONCLUDING REMARKS

In this paper a discussion is given of the aerodynamic loads on an oscillating wing-store combination measured at subsonic speeds during a wind tunnel experiment. Emphasis is put upon the influence of the store on the unsteady airload on the wing and on the loads acting on the store itself.

It is shown that for the configuration under consideration the store has a limited influence on the wing loads. The maximum effect on the local unsteady lift coefficient amounts to about 15 %, while the maximum effect on the overall unsteady lift coefficient is about 5 %.

The real part of the unsteady load on the store resembles very much the quasi-steady load; the imaginary part (damping) appears to be very small. Noteworthy is the wing-induced lateral load on the store. The resulting side force is in the order of 2 % of the unsteady lift force on the wing.

5 REFERENCES

1. Bennekers, B.
   Roos, R.
   Zwaan, R.J.
   Calculation of the aerodynamic loads on oscillating wing-store combinations in subsonic flow.
   Paper in AGARD Specialists Meeting on Wing-with-stores flutter, Munich 1974.

2. Destuynder, R.
   Tijdeman, H.
   An investigation of different techniques for unsteady pressure measurements in compressible flow and comparison with results of lifting surface theory.
   AGARD R-617 (1973). Also:
   NLR MP 73071 U (1973).

3. Labrujere, Th.E.,
   Sytsma, H.A.
   Aerodynamic interference between aircraft components: the possibility of prediction.
   ICAS Paper No. 72-49, 8th Congress of the ICAS, Amsterdam (1972).

Fig. 1 Model of wing with pylon and store mounted in large transsonic wind tunnel H.S.T.

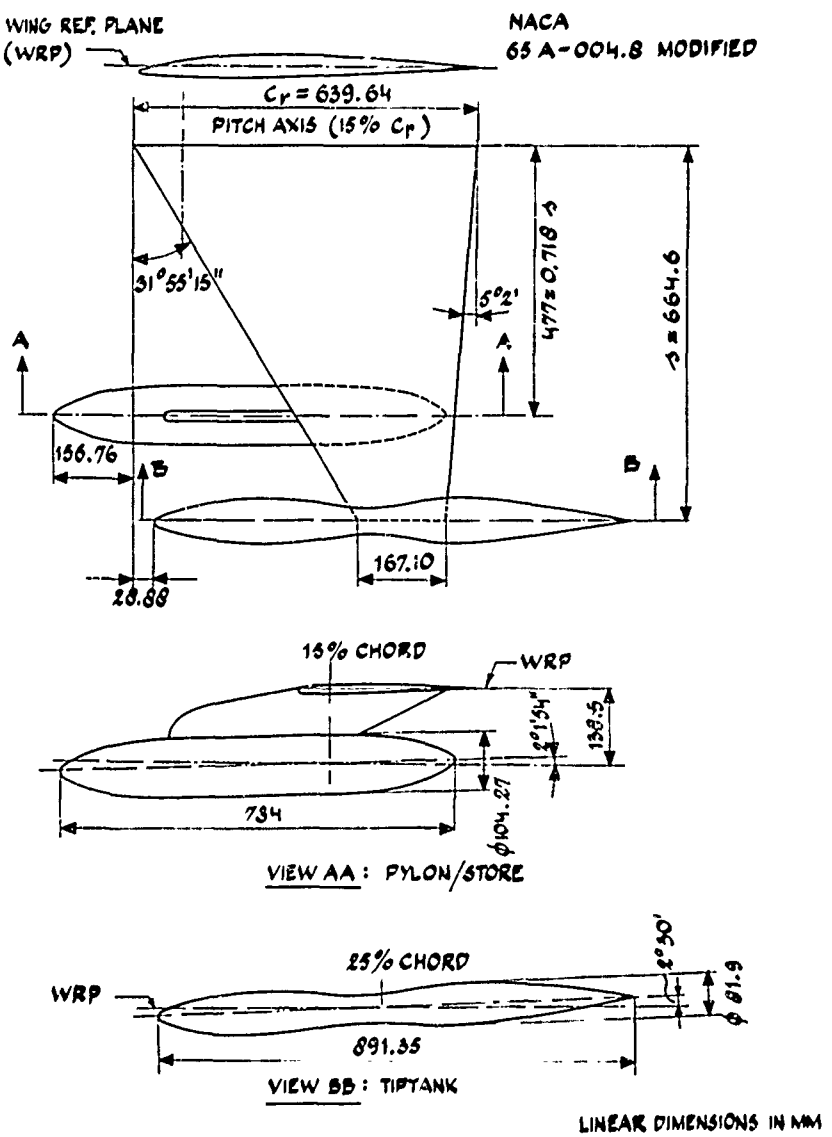

Fig. 2 Characteristic dimensions of the windtunnel model.

WING PRESSURE HOLES ( )

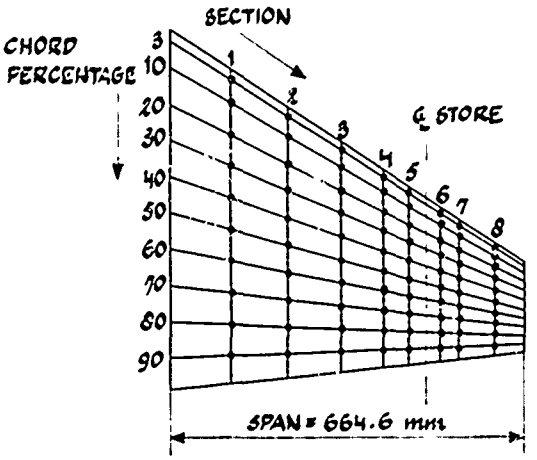

SECTION	% SPAN
1	17.0
2	33.0
3	48.0
4	60.0
5	67.5
6	76.5
7	82.0
8	91.5

STORE PRESSURE HOLES

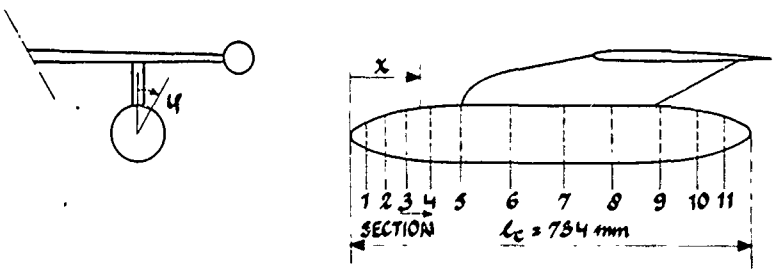

IN EACH SECTION
PRESSURE HOLES AT

φ (°)	*)
0	
30	
90	
150	
180	
210	
270	
330	

*) NO PRESSURE HOLE AT 0° IN SECTION 6,7 AND 8

SECTION	x (% l_c)
1	4.087
2	8.174
3	13.624
4	19.755
5	27.240
6	39.850
7	52.452
8	65.055
9	77.657
10	86.512
11	94.006

Fig.3 Position of pressure holes on the wing and pylon store.

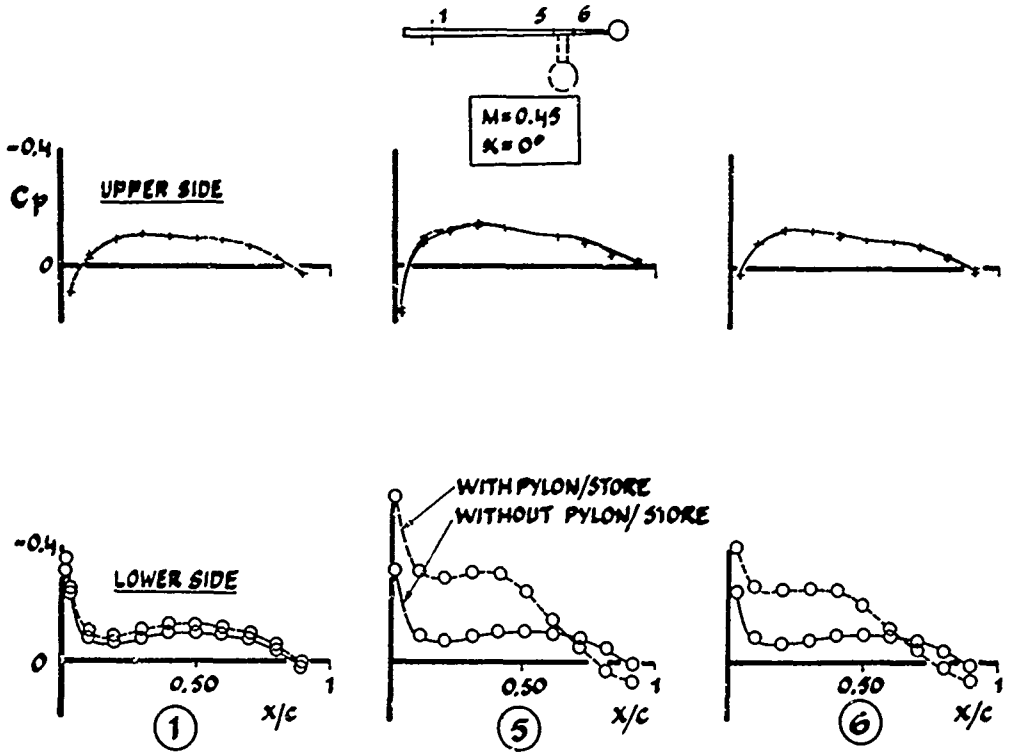

Fig.4 Influence of pylon and store on the steady chordwise pressure distributions on the wing in low subsonic flow.

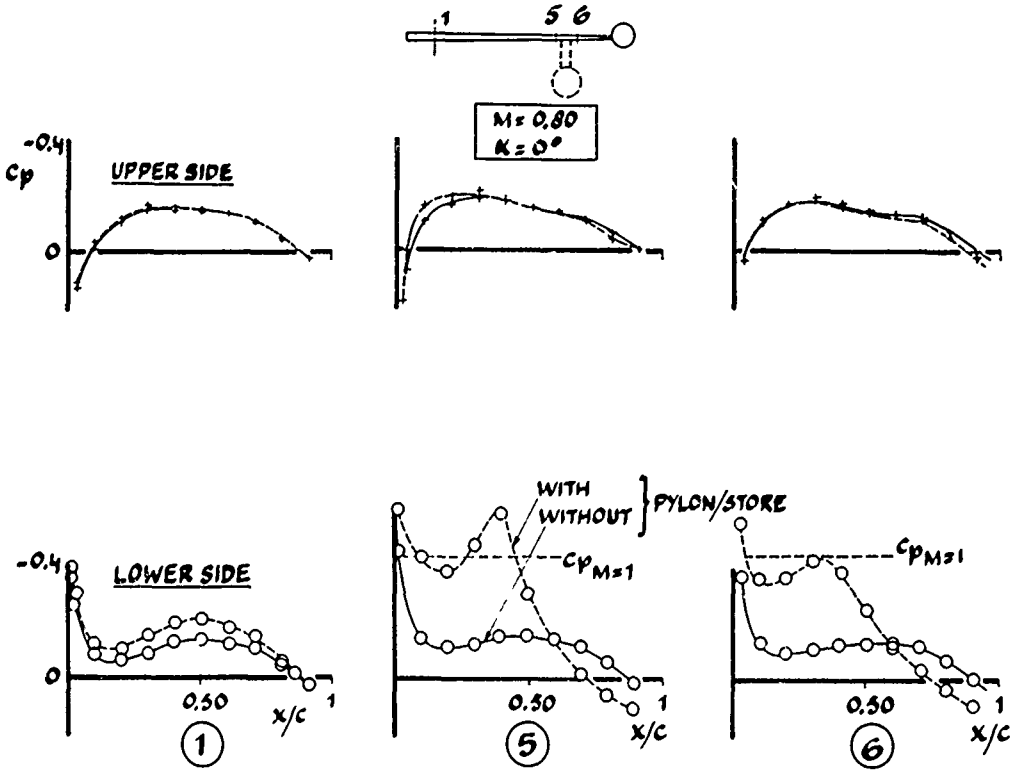

Fig.5 Influence of pylon and store on the steady chordwise pressure distributions on the wing in high subsonic flow.

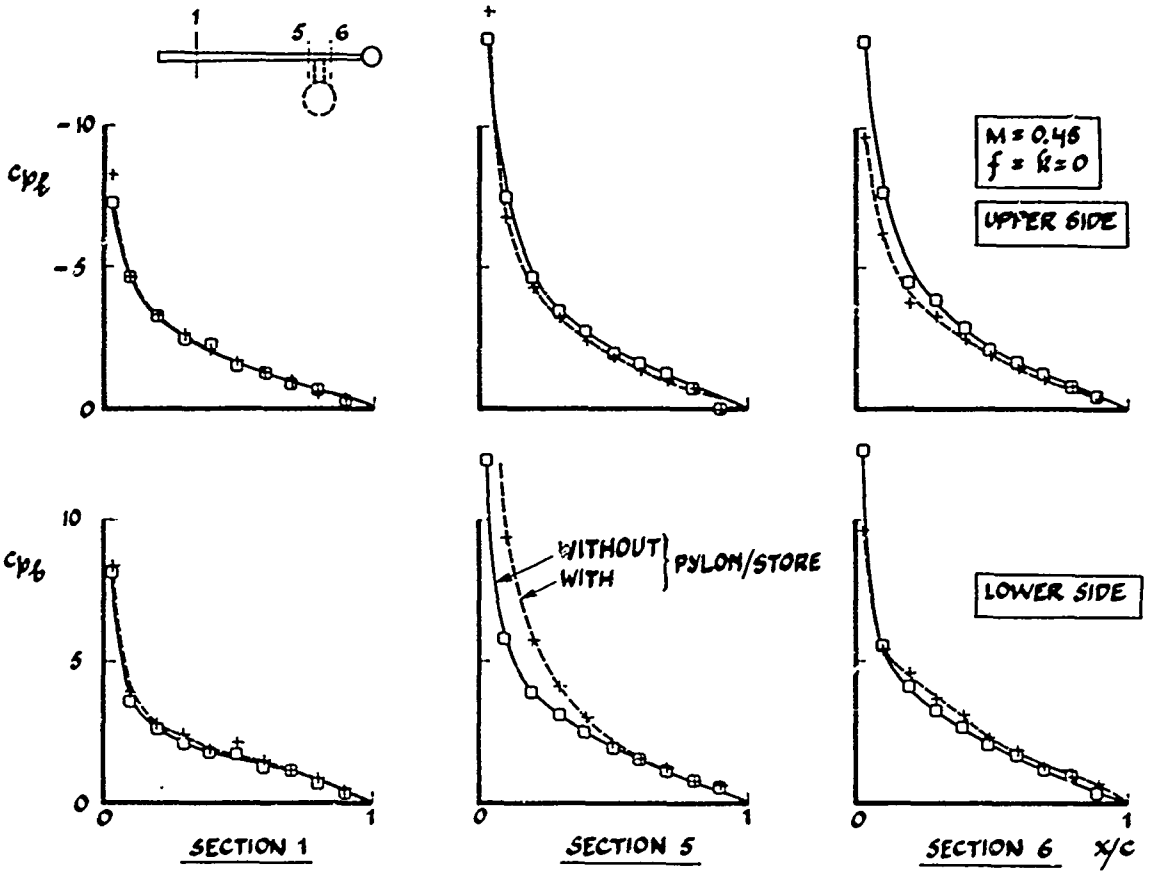

Fig.6 Influence of pylon and store on the quasi-steady chordwise pressure distributions on the wing in low subsonic flow.

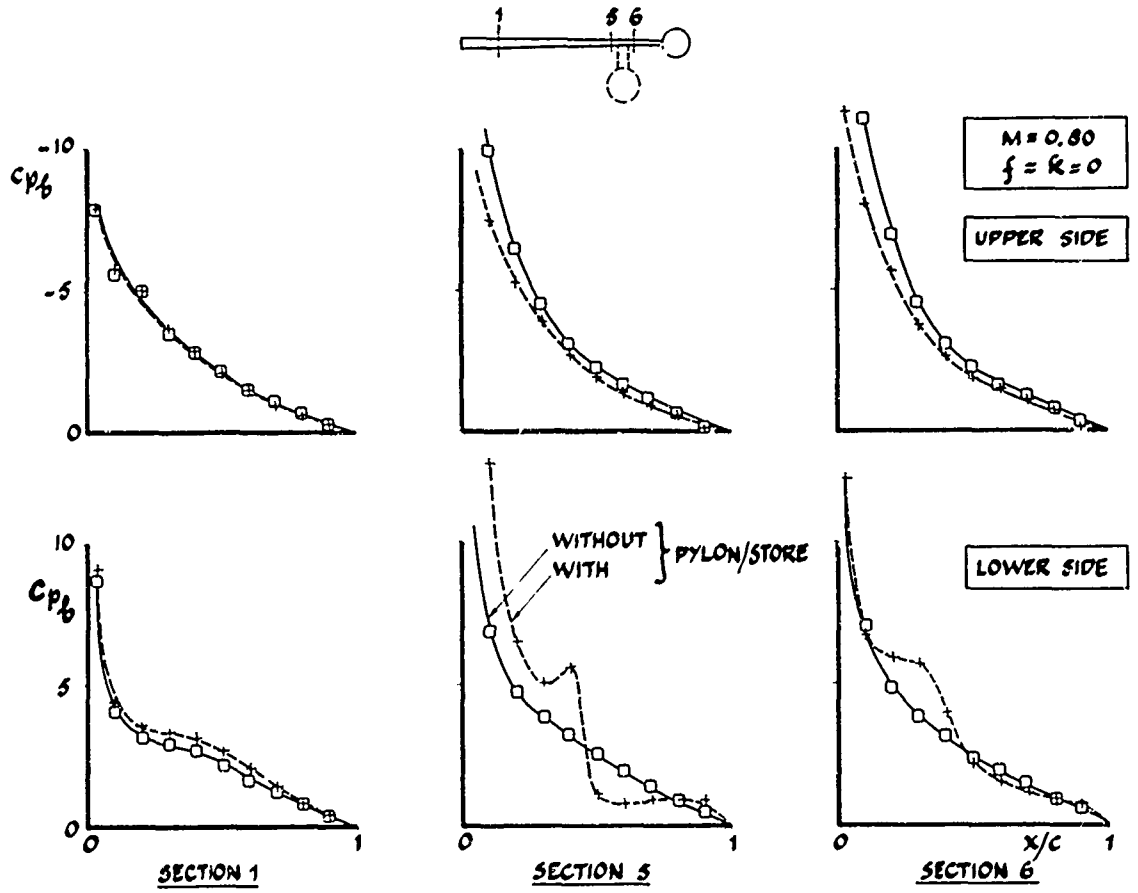

Fig.7 Influence of pylon and store on the quasi-steady chordwise pressure distributions on the wing in high subsonic flows.

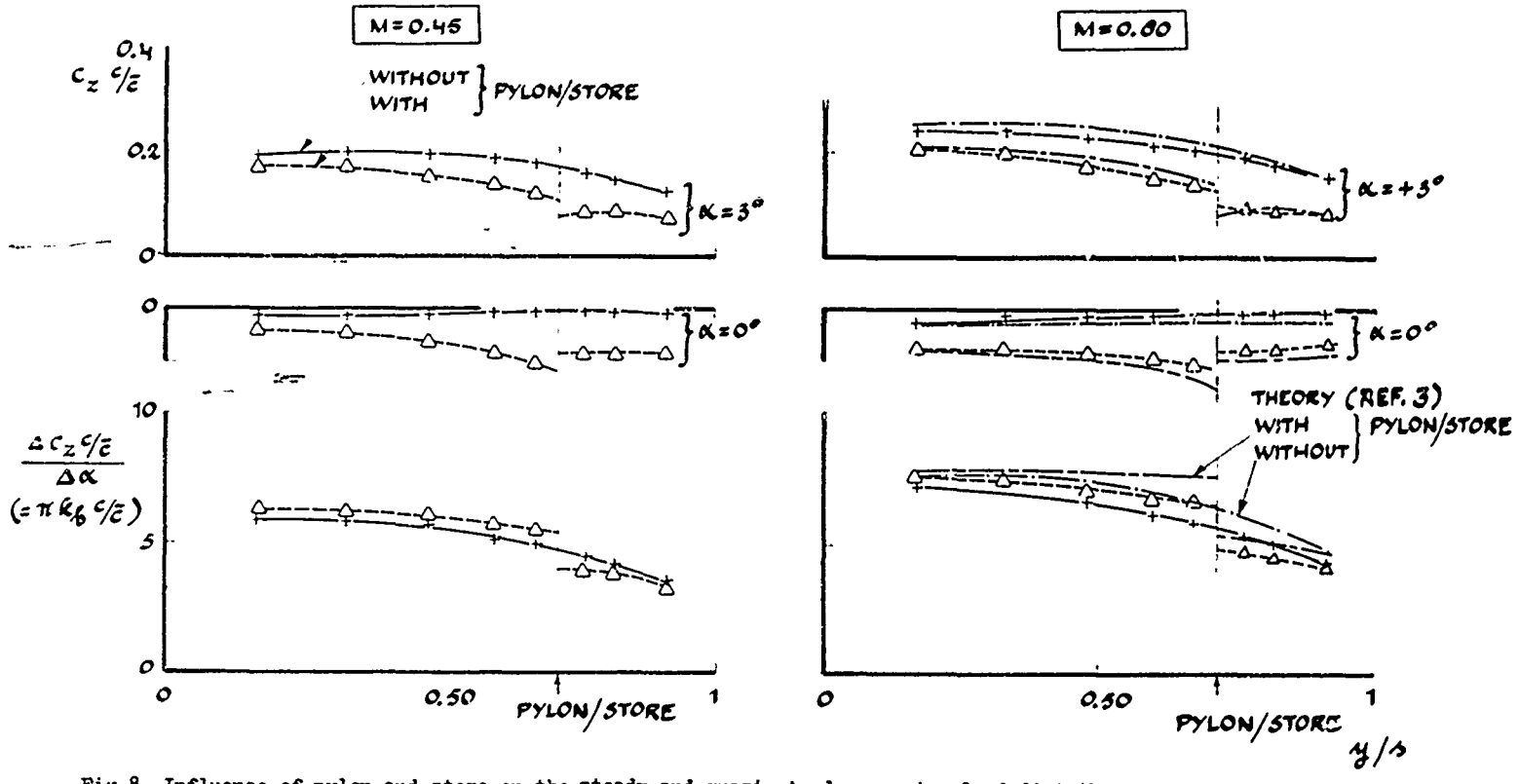

Fig.8 Influence of pylon and store on the steady and quasi-steady spanwise load distribution over the wing.

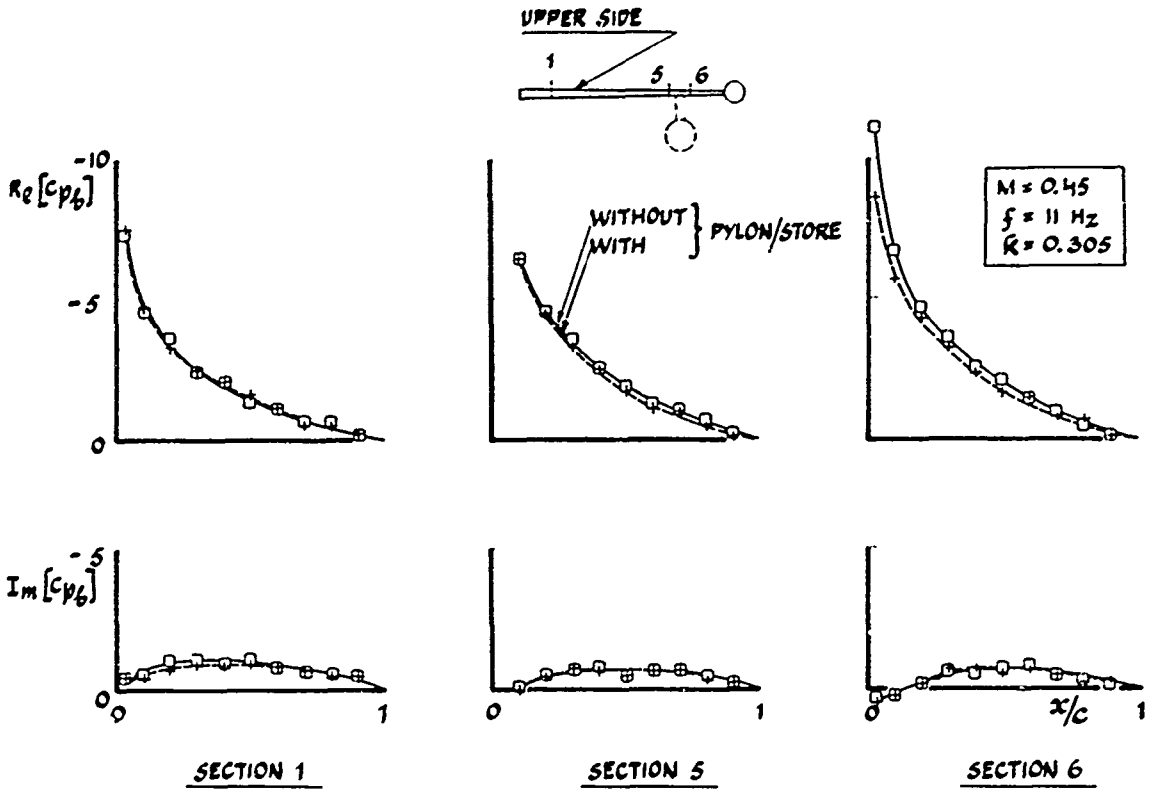

Fig.9a Influence of pylon and store on the unsteady chordwise pressure distributions at M = 0.45 and f = 11 Hz . wing upper side.

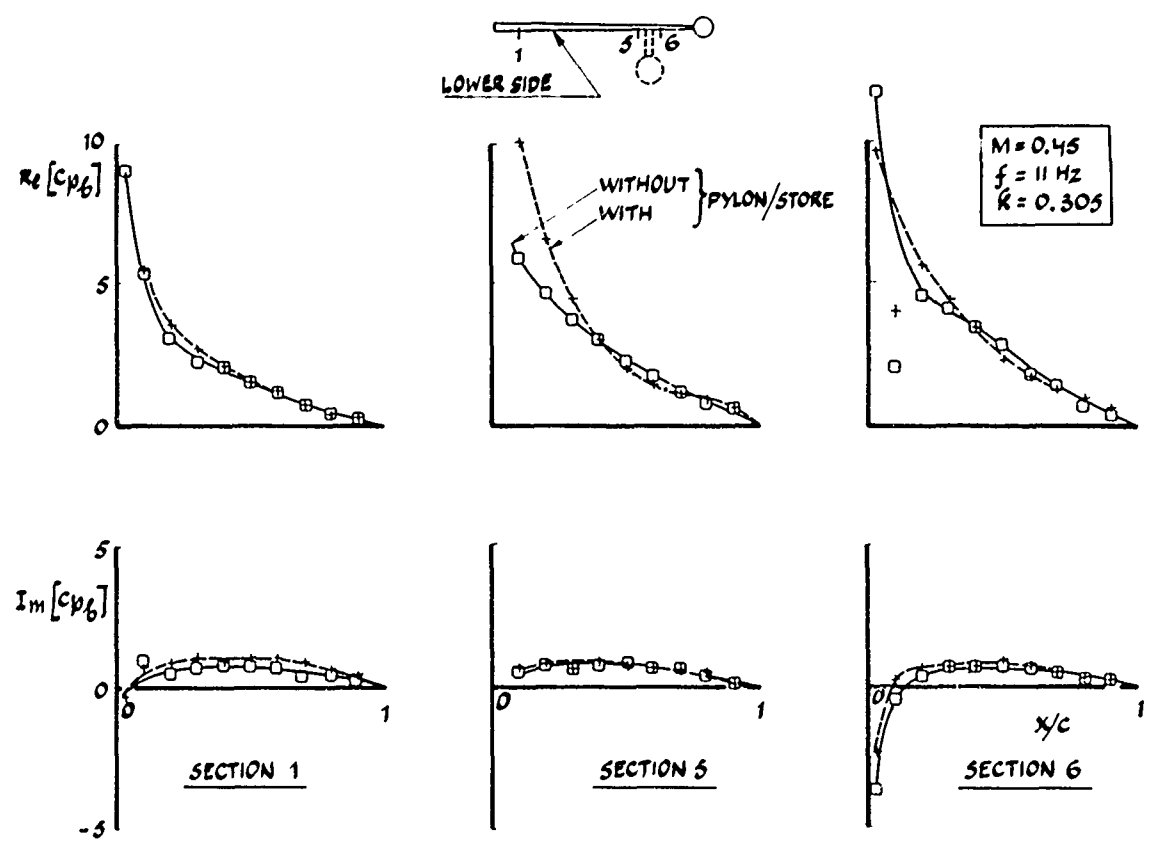

Fig.9b Influence of pylon and store on the unsteady chordwise pressure distributions at M = 0.45 and f = 11 Hz . wing lower side.

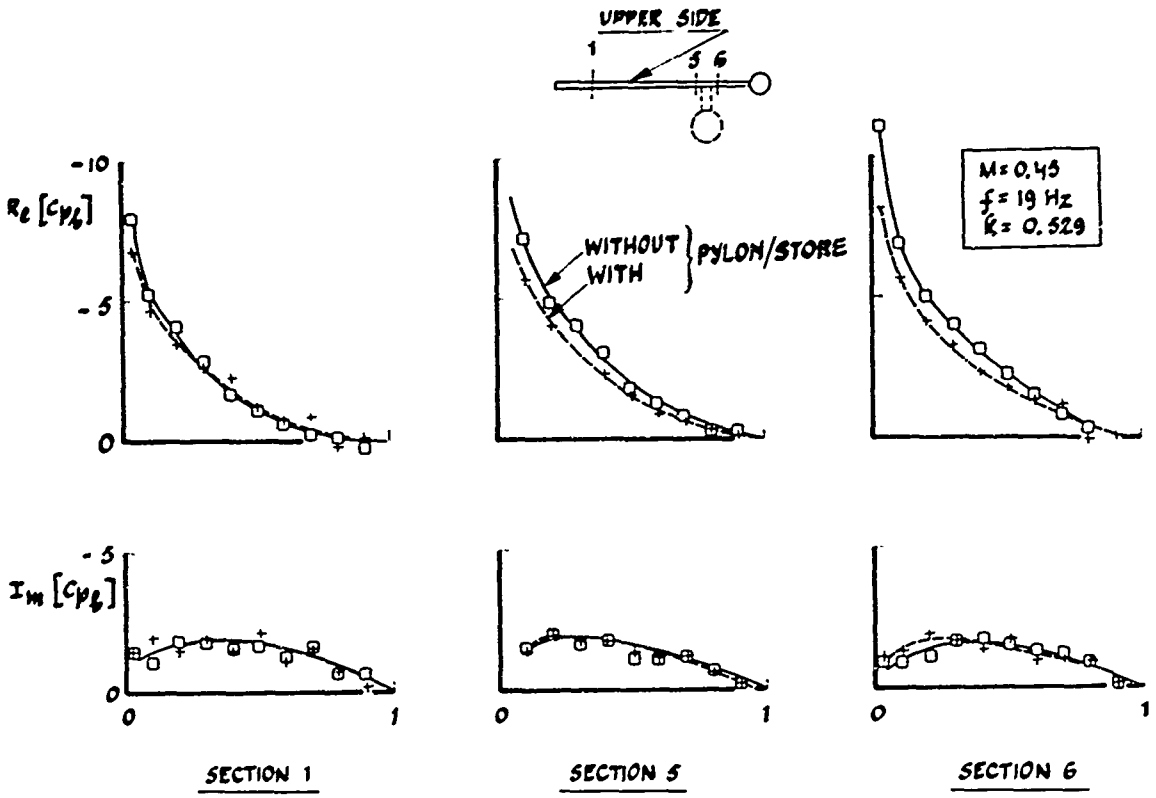

Fig. 10a: Influence of pylon and store on the unsteady chordwise pressure distributions at M = 0.45 and f = 19 Hz : wing upper side.

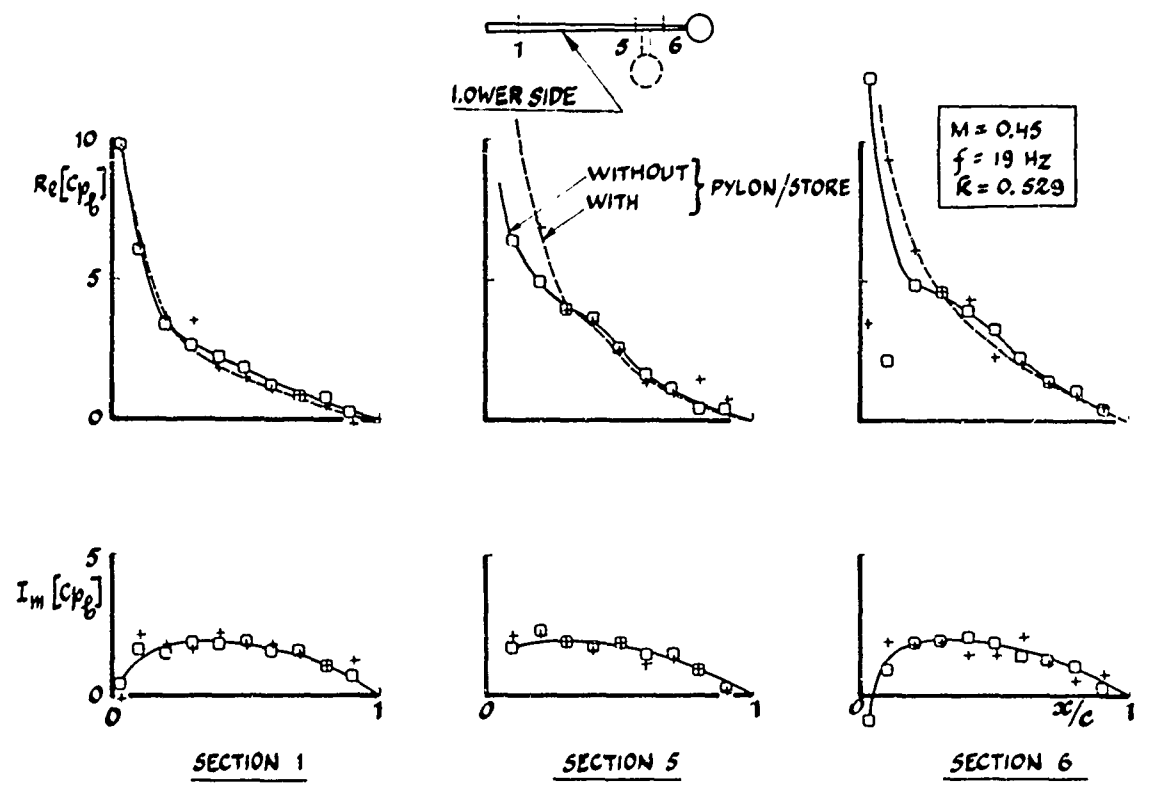

Fig.10b Influence of pylon and store on the unsteady chordwise pressure distributions at M = 0.45 and f = 19 Hz : wing lower side.

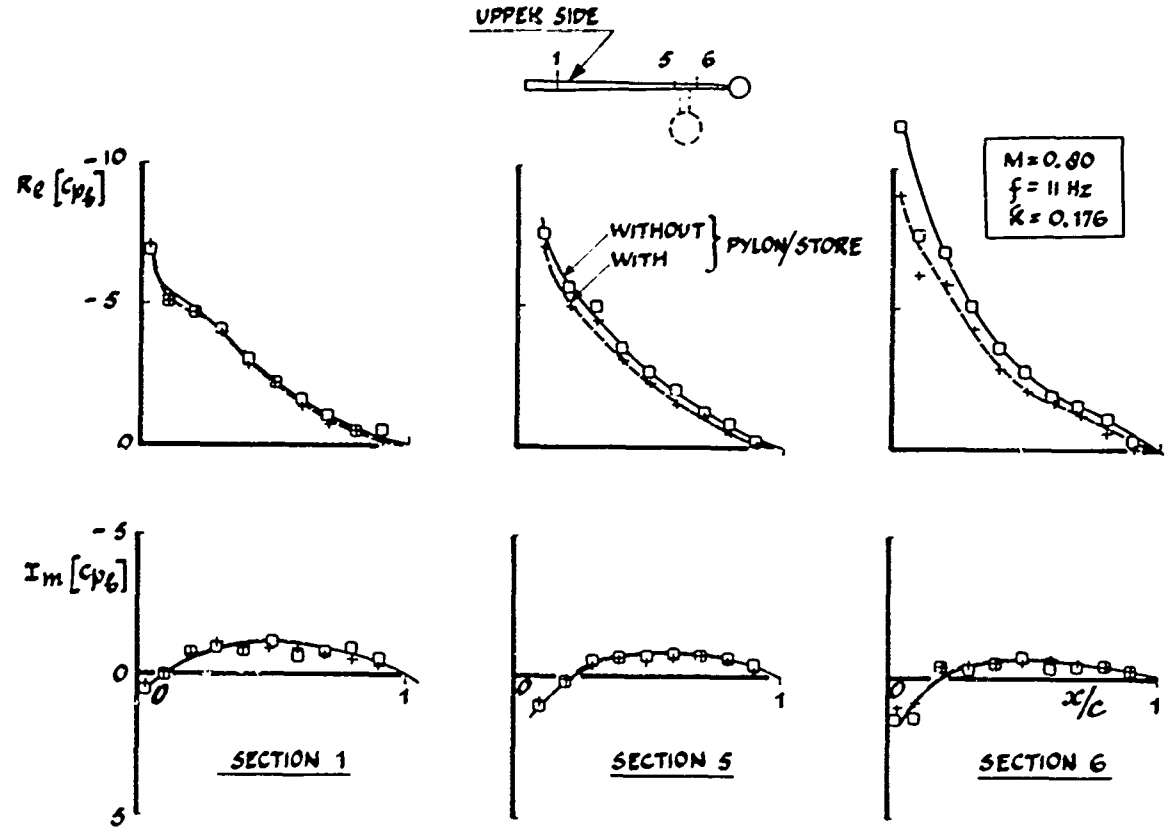

Fig.11a Influence of pylon and store on the unsteady chordwise pressure distributions at M = 0.80 and f = 11 Hz : wing upper side.

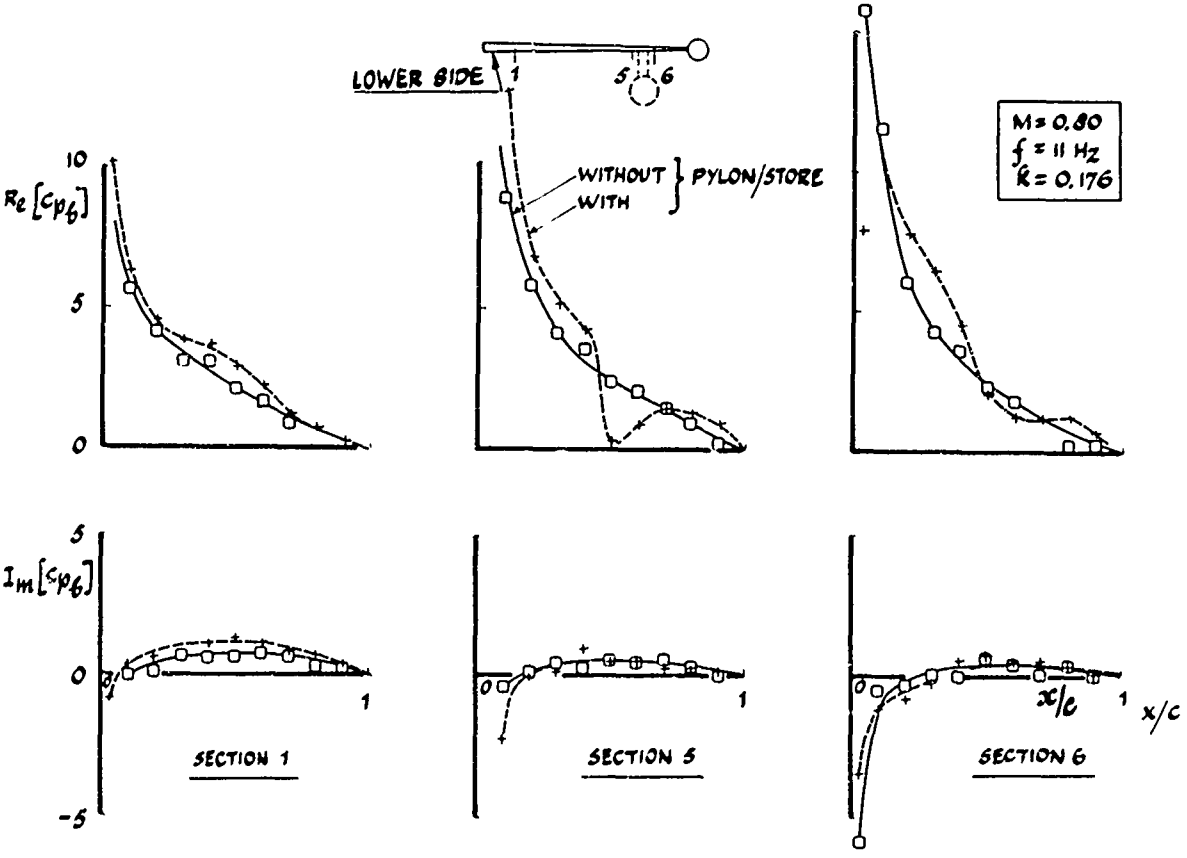

Fig.11b Influence of pylon and store on the unsteady chordwise pressure distributions at M = 0.80 and f = 11 Hz : wing lower side.

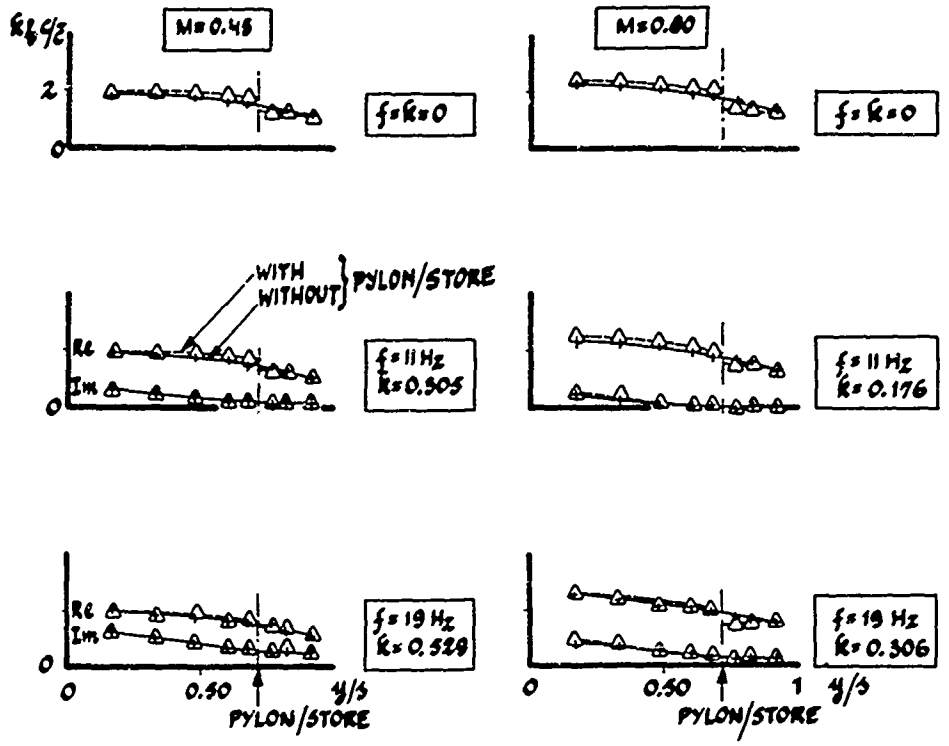

Fig. 12 Influence of pylon and store on the unsteady spanwise load distribution over the wing.

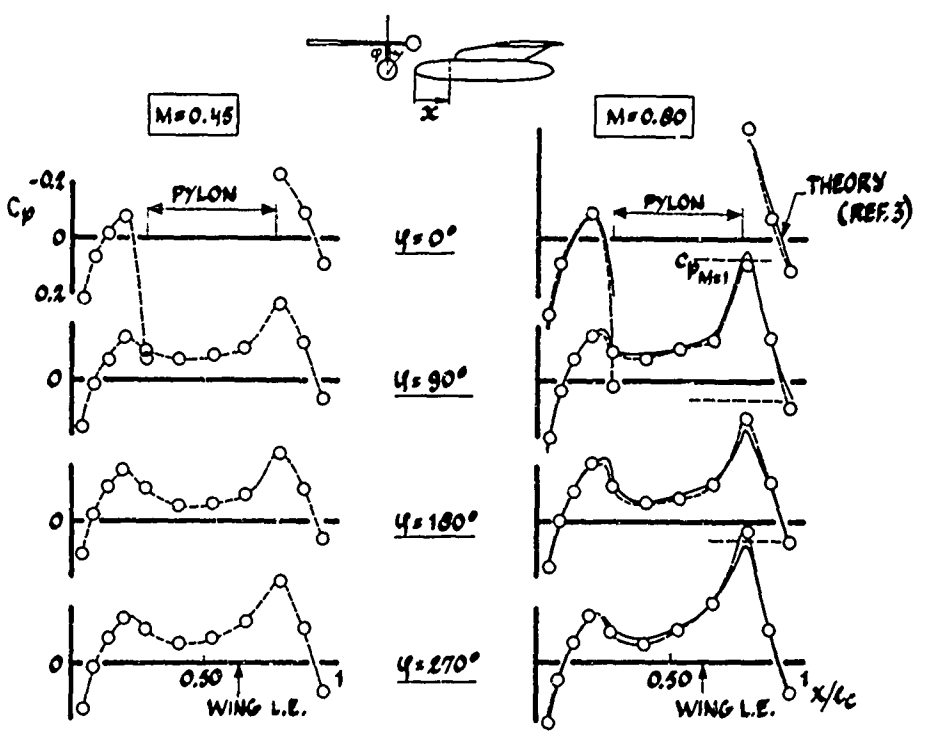

Fig. 13 Steady pressure distributions along the store.

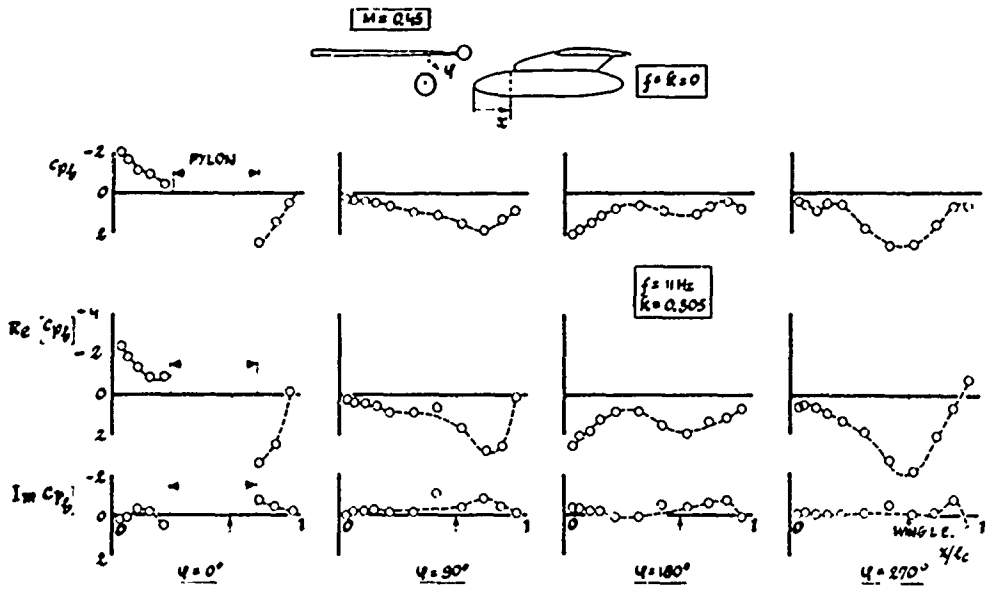

Fig. 14 Quasi-steady and unsteady pressure distributions along the store at low subsonic speed

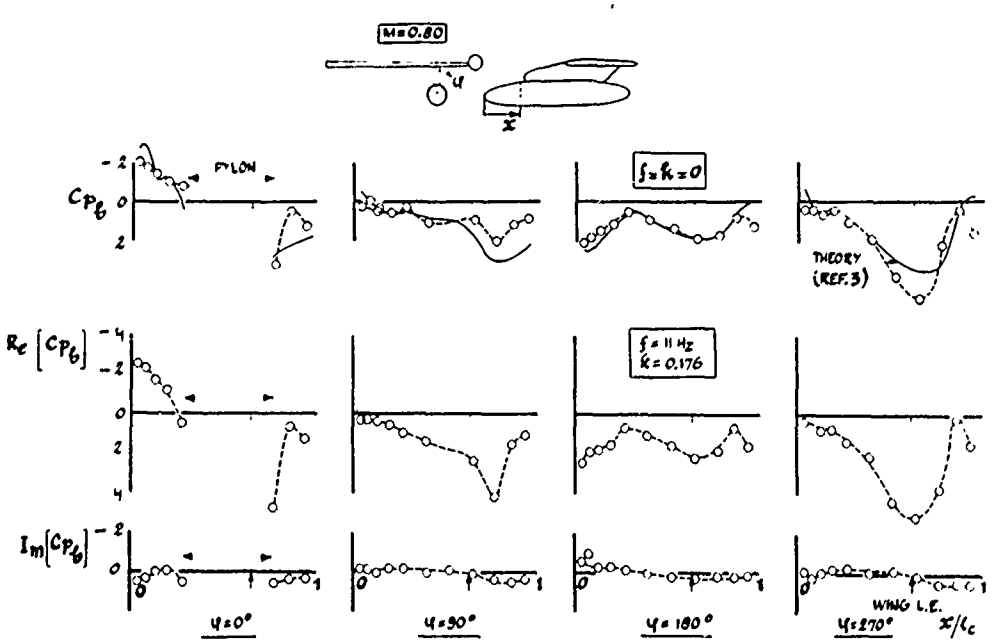

Fig. 15 Quasi-steady and unsteady pressure distributions along the store at high subsonic speed

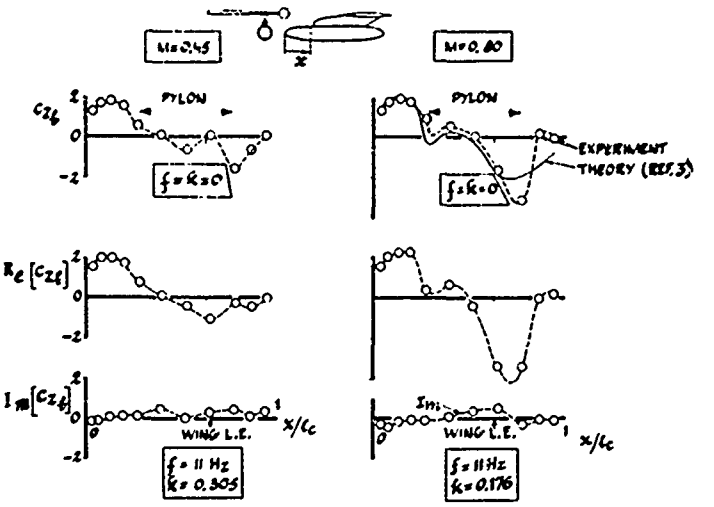

Fig. 16 Quasi-steady and unsteady normal force distribution along the store

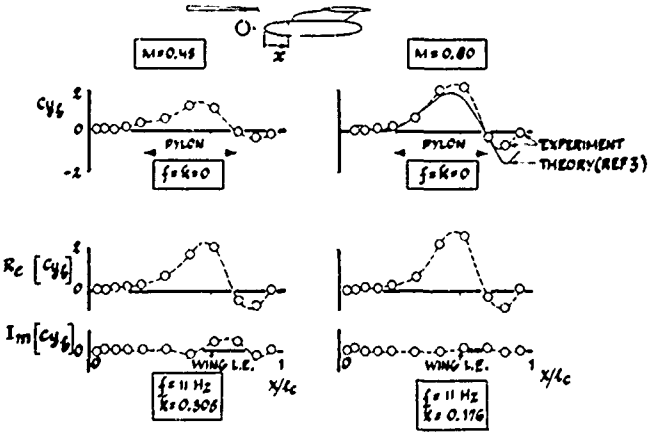

Fig. 17 Quasi-steady and unsteady side force distribution along the store

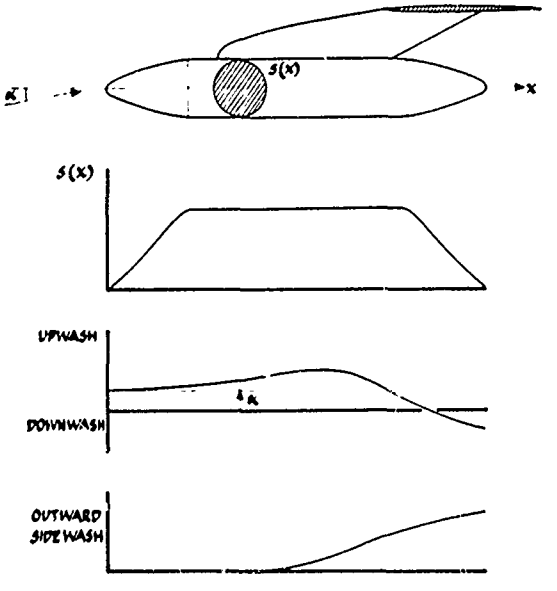

Fig. 18 Estaminated normal wash and side wash distribution along the store

WING WITH STORES FLUTTER ON VARIABLE SWEEP WING AIRCRAFT

by

O.Sensburg, A.Lotze and G.Haidl
Messerschmitt-Bolkow-Bloihm GMBH
Unternehmensbereich Flugzeuge · Entwicklung
Ottobrunn bei München

1. INTRODUCTION

The large number of wing mounted stores with varying mass and inertia properties for modern fighter concepts especially in conjunction with a variable wing geometry requires economical procedures for investigation of total airplane dynamics. There are two basically different analytical methods which are commonly used to explore wing-store flutter characteristics:

A) Determination of the stiffness matrix of the coupled system by application of subtructure techniques and calculation of normal vibration modes:

This method has the advantage that every degree of freedom is implemented (no truncation effects). There are two major disadvantages, namely that for total airplane analyses one must work with very large matrices and that for each mass variation leading to different normal modes the unsteady aerodynamic forces must be produced anew. For the latter reason the method is restricted to the application of two-dimensional unsteady aerodynamic forces with all known inaccuracies at high surface sweep angles. Use of correction methods to the unsteady aerodynamic forces reduces the error margin but still leaves uncertainties about the absolute error in prediction of flutter speeds.

B) Representation of the total aircraft dynamics by superposition of clean wing cantilever modes and cantilevered external store modes.

Here we have the advantage of wing branch modes and unsteady aerodynamic forces not changing with external store variation. As will be shown later convergence problems concerning the number of necessary wing branch modes will arise. If many higher order branch modes are utilized then the order of the eigenvalue problem increase and the amount of work which is needed for good definition of aerodynamic forces will be unacceptable.

It is also possible to use wing branch modes which incorporate the external mass rigidly attached to a wing point. This method contains the disadvantages of methods A and B since wing mode shapes will change with varying external stores thus requiring recalculation of unsteady aerodynamic forces and the convergence problems will not be alleviated.

Modified branch mode techniques are found to be most suitable to solve the problem. By this approach the frequencies and modeshapes of the coupled system are obtained by superposition of a limited number of clean wing normal modes and the so called junction modes, which are employed in order to improve the convergency of the results related to the number of cantilevered bare wing normal modes. The procedure, using modified branch mode techniques for the total airplane representation and crosschecking the solution of ground vibration and flutter calculations with total airplane model test results is considered to be the most efficient approach for obtaining reliable flutter results. It will be shown that only free-free dynamically scaled total aircraft models can give good correlation when tuning effects occur. The most efficient method of investigating flutter behaviour of asymmetrical store configuration is therefore the testing of this above mentioned model.

2. ANALYTICAL MODEL

Structural representation

For the representation of total airplane dynamics the following sets of finally retained generalized coordinates are considered for vibration and flutter analyses:

- Airplane rigid body modes
- Cantilevered fuselage normal modes

- o Cantilevered taileron normal modes and taileron attachment modes
- o Cantilevered fin normal modes and fin attachment modes
- o Cantilevered wing normal modes and wing attachment modes
- o Wing - external store junction modes
- o Cantilevered external store normal modes and pylon attachment modes

During early design stages each airplane component was represented by a simple beam structure to allow simple parameter variations. For initial investigations also the taileron and the fin were assumed to be rigid. After refinement of the design the fuselage, taileron and fin idealisation was replaced by a finite element representation, according to the complexity of the structure. For the cantilevered component modes a distinction is made between primary modes for a main structure as for the wing and secondary modes for substructures as for example an external store. Attachment modes, which are rigid body modes for components, are used to vary the connection stiffness of main structures with substructures. One attachment mode for each external store has been introduced to establish a yaw degree of freedom corresponding to the flexibility of the pylon control rod, which provides constant streamwise direction of the pylon for all wing sweep positions. It should be mentioned that according to the single point pylon attachment with free motion of the pylon in yaw relatively to the wing, the wing modes do not contribute to the pylon yaw displacements.

Determination of junction modes for the wing - external store attachment

Following the procedure, which has been developed for the dynamical coupling of substructures with statically undetermined attachments using constraint modes, (Ref. 1; 2; 3) junction modes can be derived from the stiffness matrix of the main structure and the stiffness matrix of the attached substructure respectively

$$\begin{Bmatrix} F^A \\ F^I \end{Bmatrix} = \begin{bmatrix} k^{AA} & k^{AI} \\ k^{IA} & k^{II} \end{bmatrix} \begin{Bmatrix} \delta^A \\ \delta^I \end{Bmatrix} \tag{1}$$

where the superscripts A and I refer to the freedoms of the attachment and the interior structure respectively. The coordinates δ are physical displacements of the attachment points and interior points. F and k describe the corresponding force vector and the stiffness elements respectively.

For the determination of junction modes the forces at all interior points are set to zero while the displacements of the attachment successively obtain unit values.

Using equation (1) this procedure leads to a number of junction modes corresponding to the number of attachment freedoms.

$$\begin{aligned} \left[\delta^I\right] &= -\left[k^{II}\right]\left[k^{IA}\right]\left[I\right] \\ \left[\delta^A\right] &= \left[I\right] \end{aligned} \tag{2}$$

I = unity matrix

Each column of $[\delta]$ refers to a junction mode

$$\begin{Bmatrix} \delta^I \\ \delta^A \end{Bmatrix} = \left\{ \Phi_J \right\} \cdot e^{i\omega t} \tag{3}$$

defining the displacements at the interior structure points and having unit displacement in one attachment freedom.

For the case in consideration, a wing with pylon mounted stores, equation (2) can be used to calculate the junction modes for the wing structure. Combined with all modes, which effect displacements on the wing structure, the resulting modal matrix produces a nondiagonal generalized mass and stiffness matrix.

A typical example of junction modes for a wing with a store connected at a wing inboard station in three attachment freedoms (roll, pitch and z-translation) is shown in Fig. 1.

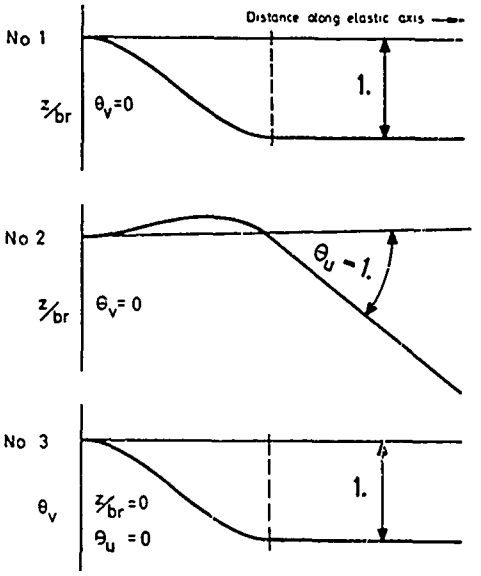

Fig. 1 Wing Junction Modes

For the connected substructure, the store having the flexibility of the pylon, the junction modes turn out to be rigid body modes, if the attachment between the main structure and the substructure is statically determined and the unit displacements at the attachment points do not produce deformations on the substructure.

Restricting our explanations to the wing-external store combination, the following generalized coordinates have to be introduced into the calculation:

- o Rigid wing modes (R. Wg)
- o Primary modes (P)
- o Wing junction modes (J)
- o Rigid store modes (R. St)
- o Secondary modes (S)

Compatibility conditions for the boundary

The compatibility equation

$$\left[\Phi^{A}_{RWG}\ \Phi^{A}_{P}\ \Phi^{A}_{J}\ \vdots\ \Phi^{A}_{RST}\ \Phi^{A}_{S}\right]\begin{Bmatrix} q_{RWG} \\ q_{P} \\ q_{J} \\ \hdashline q_{RST} \\ q_{S} \end{Bmatrix} = 0 \qquad (4)$$

ensure that the displacements on the boundary of the substructure match those of the primary structure on the attachment points. Before this operation can be performed, the motions of the store at the attachment points are to be expressed in terms of local wing coordinates. This can be achieved by a suitable transformation

$$\Phi^{A}_{STORE} = T_1\,\Phi^{A*}_{STORE} \qquad (5)$$

where Φ^{A*}_{store} represents the motion of the store at the attachment related to local store coordinates.

The compatibility equation (4) is used to eliminate dependent coordinates. Partitioning the generalized coordinates according to

$$q = \begin{Bmatrix} q_{depend} \\ q_{independ} \end{Bmatrix} \qquad (6)$$

equation (4) can be rewritten

$$\left[\Phi^{A}_{depend}\right]\left\{q_{depend}\right\} + \left[\Phi^{A}_{independ}\right]\left\{q_{independ}\right\} = 0 \qquad (7)$$

$$\begin{Bmatrix} q_{depend} \\ q_{independ} \end{Bmatrix} = \begin{bmatrix} -\left[\Phi^{A}_{depend}\right]^{-1}\left[\Phi^{A}_{independ}\right] \\ [\,I\,] \end{bmatrix}\left\{q_{independ}\right\} \qquad (8)$$

The transformation

$$q = T_2 \cdot q_{independ}$$

reduces the generalized coordinates to the finally retained coordinates $q_{independent}$, where T_2 is defined by equation (8). This operation also relates the displacements of the substructure to the generalized coordinates of the main structure. For convenience, the rigid store modes with unit displacement in pitch, roll and z-translation at the boundary can be considered as dependent modes. For total airplane calculations a similar treatment has to be performed for each connected component, as for example the rigid wing modes are used to satisfy the compatibility conditions for the wing-fuselage attachment.

System equation for vibration and flutter analyses

Applying the transformation matrix T_2, the generalized mass and stiffness matrix as used for vibration and flutter analyses of the complete system can be calculated from initially obtained generalized mass and stiffness matrices for the cantilevered components,

$$\left[M_{gen}\right]_{TOTAL} = \left[T_2'\right]\begin{bmatrix} M_{gen\,I} & \\ & M_{gen\,II} \end{bmatrix}\left[T_2\right] \tag{9}$$

$$\left[K_{gen}\right]_{TOTAL} = \left[T_2'\right]\begin{bmatrix} K_{gen\,I} & \\ & K_{gen\,II} \end{bmatrix}\left[T_2\right] \tag{10}$$

where the indices I and II denote the generalized coefficients of the main structure and the secondary structure.

The eigenvectors and frequencies of the coupled system are obtained by solving the eigenvalue problem

$$\left(\frac{\omega^2}{\omega_r^2}\left[M_{gen}\right]_{TOTAL} - \left[K_{gen}\right]_{TOTAL}\right)\left\{q_{indep}\right\} = 0 \tag{11}$$

The flutter problem is described by

$$\left[\frac{\omega_f^2}{\omega_r^2}\left[M_{gen}\right]_{TOTAL} - \left[K_{gen}\right]_{TOTAL}(1+jg) - \rho/2\,V^2\,\frac{A}{m_r\,\omega_r^2\,s}\cdot\right.$$
$$\left.\cdot\left(\left[C'_{gen}\right]_{TOTAL} + j\left[C''_{gen}\right]_{TOTAL}\right)\right]\left\{q_f\right\} = 0 \tag{12}$$

where : m_r, ω_r = reference mass and frequency

s = semispan of reference plane

A = area of reference plane

g = structural damping

v = true airspeed

ω_f = flutter frequency

q_f = flutter vector

C'gen. C'' gen. = real and imaginary parts of non dimensional generalized airforces defined for discret values of $k = \frac{\omega \cdot s}{V}$

Using the Q-R Algorithmus the flutter equation is solved for the equivalent amount of structural damping g necessary to provide harmonical oscillation.

The generalized airforces which are to be introduced into equation (12) can either be calculated directly for the constrained modes defined by equation (8) or be computed for the initially employed unconstrained modes and transformed by

$$[C_{gen}]_{TOTAL} = [T_2'] \begin{bmatrix} C_{genI} & \\ & C_{genII} \end{bmatrix} [T_2] \qquad (13)$$

Unsteady aerodynamic forces

3-dimensional unsteady aerodynamic forces are calculated according to the theories of (4), (5), (6), (7). Subsonic airforces including wing-tailplane-fin interference effects and supersonic aerodynamic forces considering wing-tailplane interferences can easily be introduced into flutter analyses by usage of branch modes.

Investigations show that there is little influence on flutter behaviour caused by unsteady aerodynamic forces on external stores and store-wing interference effects.

For comparison with flutter model test results in this paper only calculation for the subsonic region at Mach number 0.2 are discussed.

3. SUBSONIC WIND TUNNEL FLUTTER MODEL

A dynamically scaled free flying subsonic wind tunnel flutter model was bu lt at MBB and tested in the flutter tunnel of the Eidgenossisches Flugzeugwerk in Emmen, Switzerland.

The wings and the fuselage of this model are represented by elastic axis lumped mass systems. The fin and tailplane structure is simulated with a beam latice.

A set of stores with varying mass and inertia properties was fabricated and these stores could be quickly changed on the model. The store was attached to the wing by a beam representing the pylon stiffness.

The flutter speed and frequency of the model was found by increasing the tunnel speed up to the flutter speed and recording the frequency with accelerometers.

4. RESULTS

As already mentioned there is a huge variety of configurations, arising from the attachment of stores-largely differing in weight and inertia - to wings of variable sweep airplanes.

Fig. 2 illustrates a few major points. It shows flutter speed as a function of wing sweep angle for a store with a constant weight and variable radius of gyration. One can see, that the increments of flutter speed with wing sweep change with store radius of gyration. It is also important to note, that the minimum flutter speed occuring at different sweep angles changes with radius of gyration as is illustrated by curve 1 and 2 of Fig. 2. It is also possible that the flutter speed increment with wing sweep angle might not be sufficient, bearing in mind that the flight envelope is also extended for higher sweep angles. The flutter behaviour may look completely different for a store having another weight than that in Fig. 2.

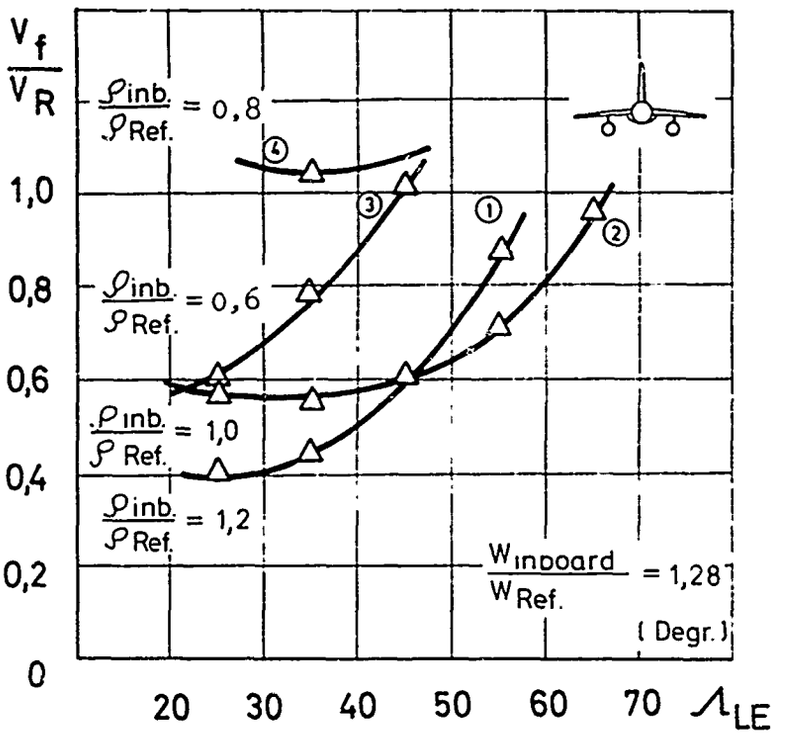

FIG. 2 FLUTTER SPEED VERSUS SWEEP ANGLE FOR DIFFERENT RADII OF GYRATION

An effective method is therefore necessary to cover all possible cases. A subsonic flutter model can be used and measured, flutter trends must be correlated with analysis results. Having had good correlation at low subsonic Mach numbers, the whole flight envelope with varying Mach numbers and altitudes can be covered analytically. All these analyses can be performed effectively with our developed branch mode system.

Correlation of test and analysis results

In order to prove the validity of a theoretical method it must be tested with the most severe boundary conditions. This is the case when a store is rigidly attached to a wing. We calculated the normal modes of this problem applying three different methods:

A. Exact solution

For this solution, the store mass properties were added to the wing mass matrix and the eigenvalue problem was solved.

B. Popular wing branch mode solution

The bare wing branch modes are used as assumed modes. A generalized mass matix is formed by pre and post multiplying of the store mass matrix. This generalized mass matrix is added to the wing generalized mass matrix. The eigenvalue problem is solved and the solution vectors are used to superimpose the clean wing modes, thus forming normal modes and a diagonal generalized mass matrix.

C. Combination of wing branch modes and junction modes.

The same solution method as for B is applied.

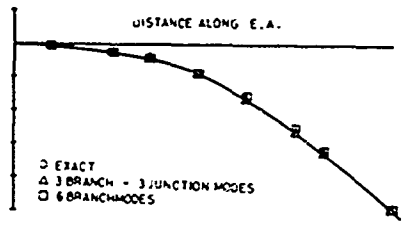

VERTICAL DEFLECTION $\frac{z}{b_r}$

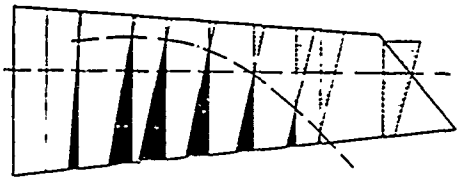

EXACT SOLUTION

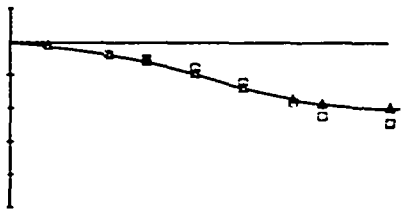

BENDING ANGLE Θ_u

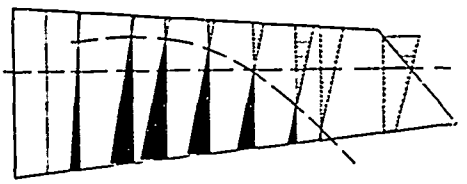

3 BRANCHMODES – 3 JUNCTION MODES SOLUTION

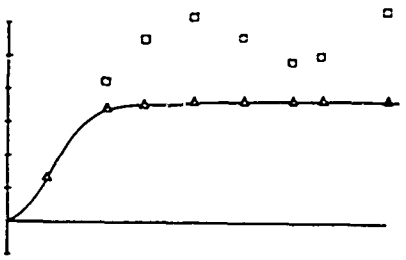

TORSION ANGLE Θ_v

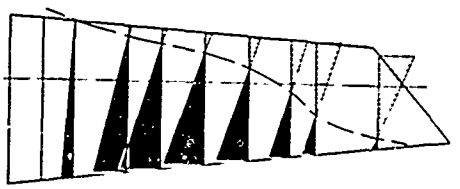

6 BRANCHMODES SOLUTION

FIG. 3 TORSION MODE SHAPE RESULTING FROM DIFFERENT APPROACHES FOR A CANTILEVERED WING WITH A RIGIDLY MOUNTED EXTERNAL STORE

	1st BENDING		1st TORSION		2nd BENDING		2nd TORSION	
	$\frac{f_1}{f_{exact}}$	$\frac{M_1}{M_{exact}}$	$\frac{f_2}{f_{exact}}$	$\frac{M_2}{M_{exact}}$	$\frac{f_3}{f_{exact}}$	$\frac{M_3}{M_{exact}}$	$\frac{f_4}{f_{exact}}$	$\frac{M_4}{M_{exact}}$
EXACT SOLUTION	1.0	1.0	1.0	1.0	1.0	1.0	1.0	1.0
3 JUNCTION MODES 3 BRANCH MODES SOLUTION	1.0	1.0	1.002	0.923	1.010	0.979	1.004	1.057
2 BRANCH MODES 1 JUNCTION MODE SOLUTION	1.005	0.979	1.005	1.078				
6 BRANCH MODES SOLUTION	1.005	0.955	1.099	1.435	1.044	0.944	1.034	1.028
3 BRANCH MODES SOLUTION	1.010	0.931	1.599	0.628				

FIG. 4 TABLE OF FREQUENCIES AND GENERALIZED MASSES

Results of these calculations are shown in Fig. 3 as deflections $\frac{z}{br}$, bending angles Θ_u and twist angles Θ_v along the wing elastic axis for the second torsion mode shape. Solutions with 6 branch modes and 3 branch and 3 junction modes are compared with the exact solution. Whereas the branch-mode junction mode system matches the exact solution very well, there is bad correlation with the 6 branch mode system for the twist angle which is very important because it forms to a large extent the generalized mass of this mode. From Fig. 3 it can be deduced that higher wing branch modes are not as well suited for representing a mode shape that features an increasing twist angle up to the store attachment point and has a constant angle from there on, than the torsion junction mode is, which has exactly those characteristic (see Fig. 1). For the other normal modes correlation of the three methods is much better - so they are not shown, but their generalized masses and frequencies are tabled in Fig. 4. This table proves again that only the branch mode-junction mode solution matches the exact solution accurately enough.

In this table it is also shown that the branch modes-junction mode solution converges rapidly. Only 2 branch modes and one junction mode are needed to get a reasonable match.

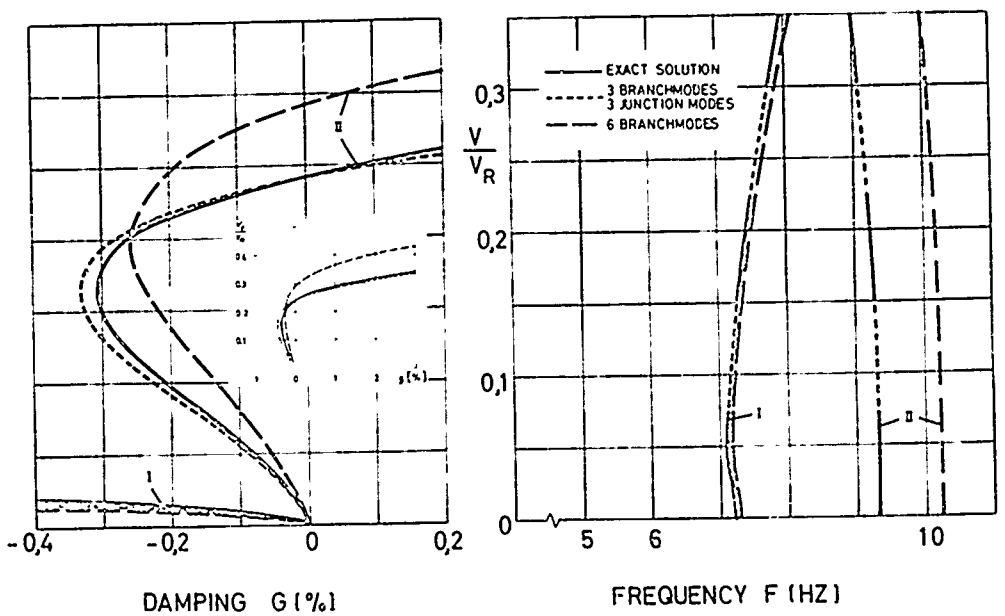

FIG. 5 FLUTTER SOLUTION RESULTING FROM DIFFERENT APPROACHES

Results of flutter calculations with the two different approaches are presented in Fig. 5. The classical wing bending torsion flutter problem occurs. With the branch mode system the flutter speed is unconservative 22 % for structural damping g = 0 and 25 % for g = 2 %. Again the branch mode-junction mode and the exact solution correlate very well.

It should be noted that we tested the method with a rigorous case i.e. rigid store attachment stiffness. For stores elastically attached to a wing the branch mode system should inevitably lead to better results because for the zero attachment stiffness case the clean wing modes are exact solutions.

The following pictures show the good correlation of analytical results with test results from a subsonic wind tunnel model.

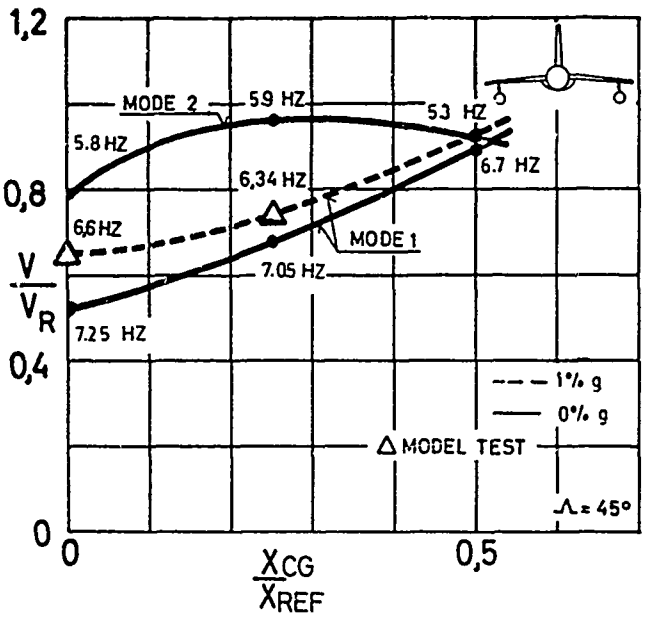

FIG. 6 FLUTTER SPEED VERSUS C.G. POSITION OF THE OUTBOARD STORE

Fig. 6 demonstrates how the fluttor speed of an outboard store increases with shifting its center of gravity forward of the elastic axis. It is interesting to note that no more increase in flutter speed can be expected by snifting the c.g. further forward than $\frac{x}{x_{ref}} = .5$ because another flutter mode, arising from detrimental coupling of the store yaw mode crosses over.

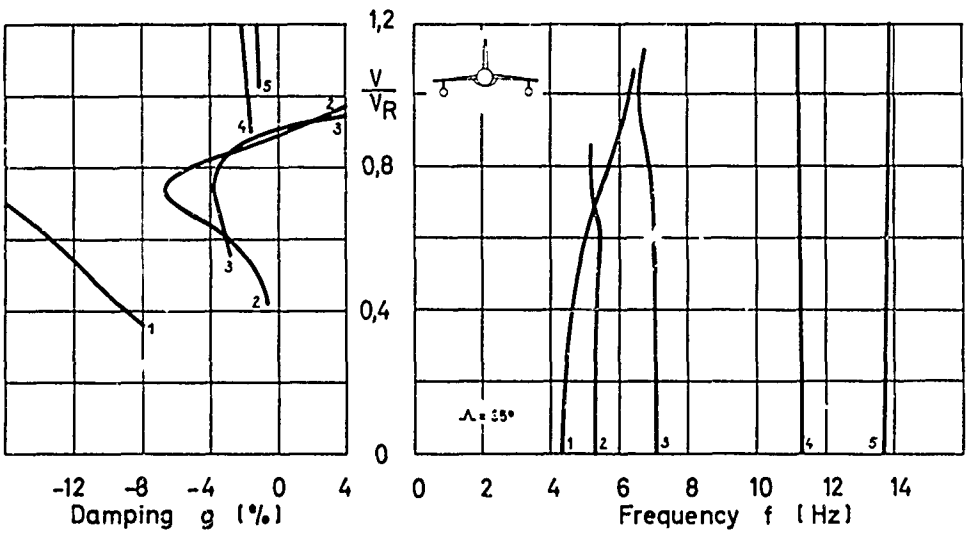

FIG. 7 FLUTTER SPEED VERSUS DAMPING AND FREQUENCY FOR TOTAL AIRPLANE WITH A STORE ATTACHED TO THE OUTBOARD WING

The V-g plot Fig. 7 depicts this behaviour at 0.5 c.g. shift. Bending mode and store pitch mode are producing flutter mode 1 and bending mode and store yaw mode produce flutter mode 2 of Fig. 6.

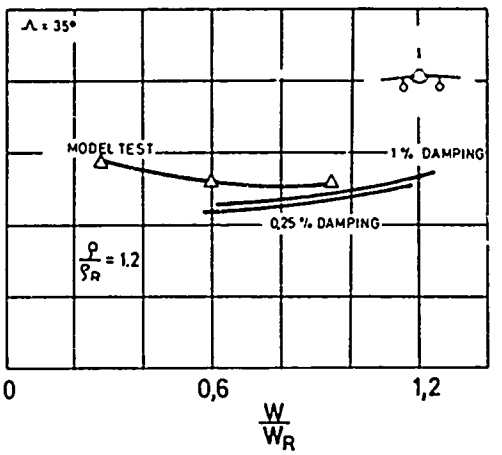

FIG. 8 FLUTTER SPEED VERSUS STORE WEIGHT FOR INBOARD STORE CONFIGURATIONS

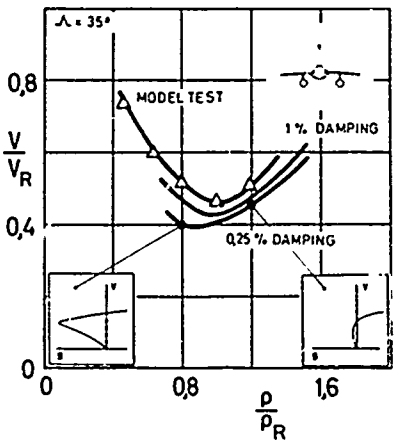

FIG. 10 FLUTTER SPEED VERSUS RADIUS OF GYRATION FOR INBOARD STORES

Fig. 8 illustrates, that there is little change of flutter speed with store weight for a certain inboard store (constant radius of gyration). This is attributable to the fact, that the inboard store weight changes the wing bending frequency very little. Fig. 9 shows the V-g plot for $\frac{W}{W_{Ref.}} = 0.886$. Here it can be seen that the flutter mechanism is wing bending store pitch coupling.(Mode 2, 3)

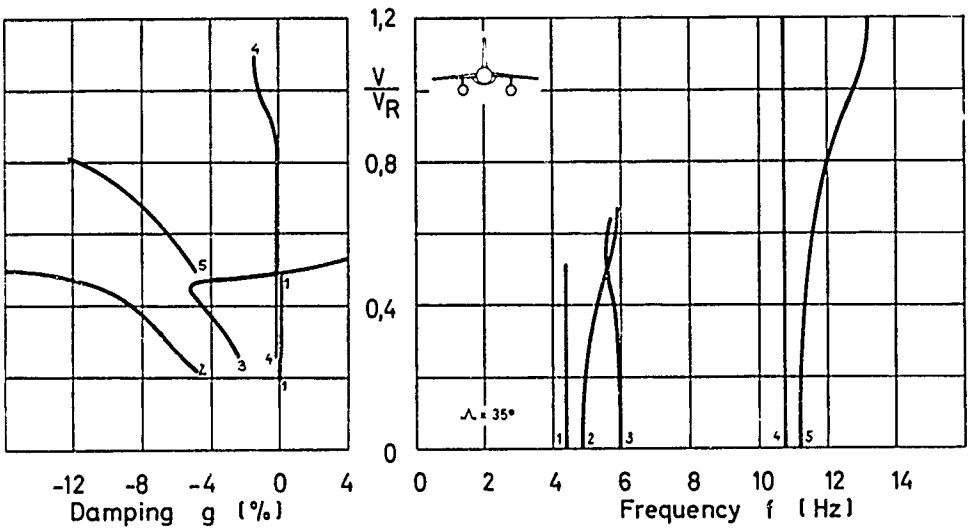

FIG. 9 FLUTTER SPEED VERSUS DAMPING AND FREQUENCY FOR TOTAL AIRPLANE WITH A STORE ATTACHED TO THE INBOARD WING

Fig. 10, showing flutter speed versus inboard store radius of gyration, proves the well known fact, that the lowest flutter speeds occur when the store pitch frequency matches the wing bending frequency. The two small V-g plots in Fig. 10 demonstrate that the flutter cases for store pitch frequency below wing bending frequency are mild whereas strong flutter occurs for the opposite frequency ratio.

Fig. 11 shows a strong dependency of the flutter speed of two stores inboard and outboard on a wing with inboard store weight. The V-g plot for a $\frac{W}{W}_{Ref.}$ = 0.886 is given in Fig. 12.

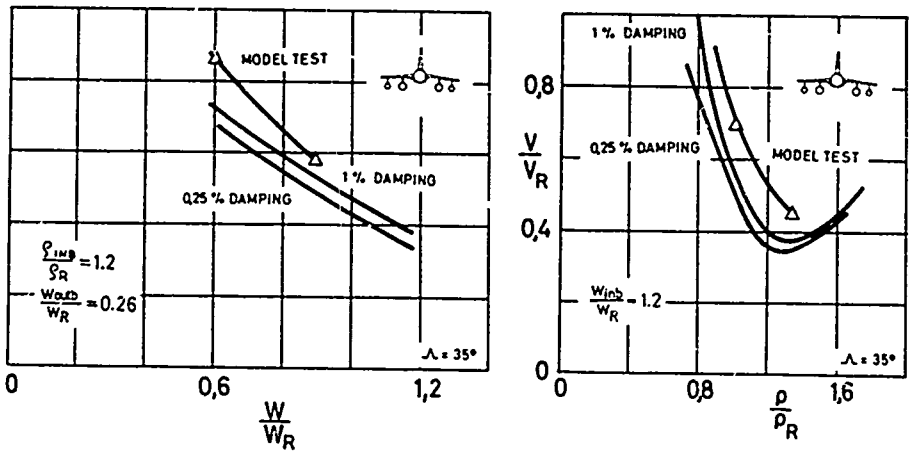

FIG. 11 FLUTTER SPEED VERSUS INBOARD STORE WEIGHT FOR VARYING INBOARD STORES AND CONSTANT OUTBOARD STORE

FIG. 13 FLUTTER SPEED VERSUS INBOARD STORE RADIUS OF GYRATION FOR VARYING INBOARD AND CONST. OUTBOARD STORE

In Fig. 13 variation of flutter speed of an airplane with two stores mounted on each wing as a function of radius of gyration of the inboard store is depicted.

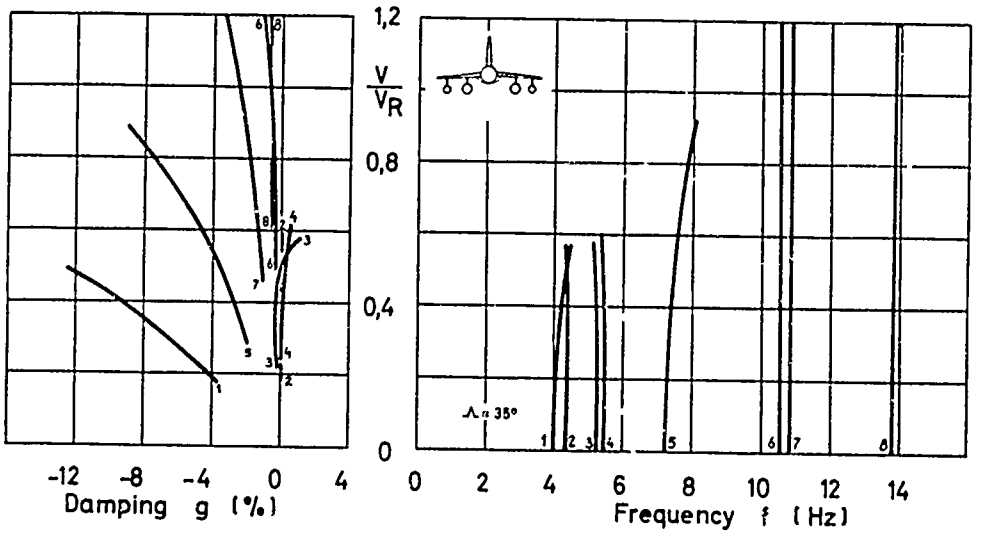

FIG. 12 FLUTTER SPEED VERSUS DAMPING AND FREQUENCY FOR TOTAL AIRPLANE WITH ONE STORE ON THE INBOARD WING AND ONE STORE ON THE OUTBOARD WING

Influence of flutter model suspension system

Most of the flutter cases, experienced during our tests were symmetrical cases, but we have also encountered antisymmetrical flutter cases. We have also found, that there can be a strong influence of fuselage tuning effects upon store flutter cases, fluttering symmetrically. For these two reasons we recommend to use a freely suspended total aircraft wind tunnel model for wing-store flutter investigation. In the next figures the effect of boundary conditions on the flutter speeds wing-store configurations will be illustrated. These pictures also prove, that the usage of uncorrected two-dimensional unsteady air forces may lead to large errors in flutter predictions.

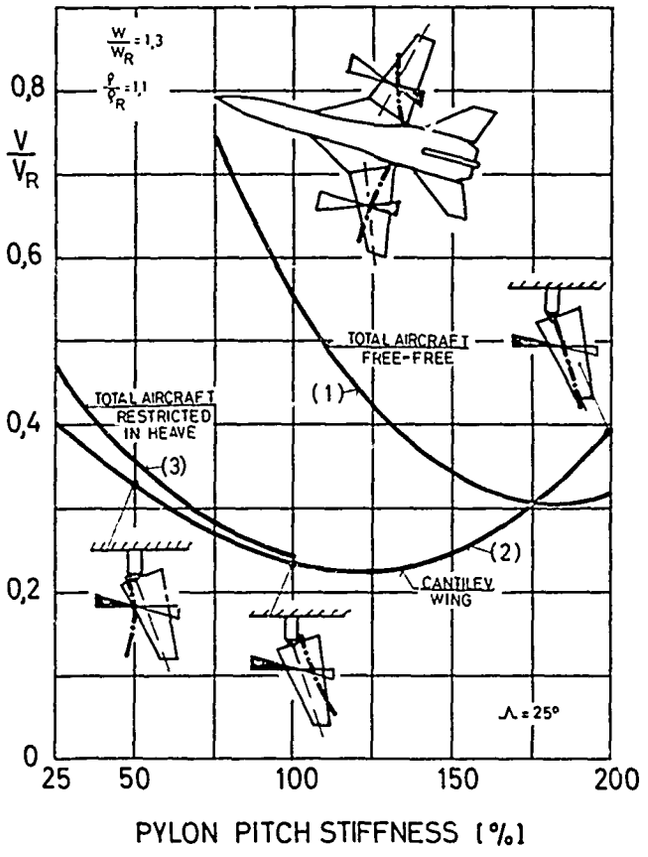

FIG. 14 FLUTTER SPEED VERSUS PYLON PITCH STIFFNESS FOR FREE AND RESTRICTED AIRPLANE

Fig. 14 shows the differences in flutter speed for varying boundary conditions as a function of pylon pitch stiffness. Curve (2) illustrates how the flutter speed of a cantilevered wing with an external store varies with pylon pitch stiffness. The important store pitch mode shape is presented for different pylon pitch stiffness. These mode shapes allow a qualitative assessment of flutter behaviour. The mode shape for 100 % pylon pitch stiffness shows a nodal line at about three quarter wing chord. Both nodal lines for 50 % end 200 % pylon pitch stiffness are further forward on the wing chord, thus leading to higher flutter speeds. The free-free aircraft flutter model has a different flutter behaviour versus pylon pitch stiffness (Curve 1). This time the nodal line is forward for 100 % pylon pitch stiffness. When the heave mode of the total airplane model is restricted (Curve 3), than the model behaves as the cantilevered wing. From Fig. 14 it can be learned, that the flutter speed can be largely underestimated with cantilevered wing models for certain pylon pitch stiffness.

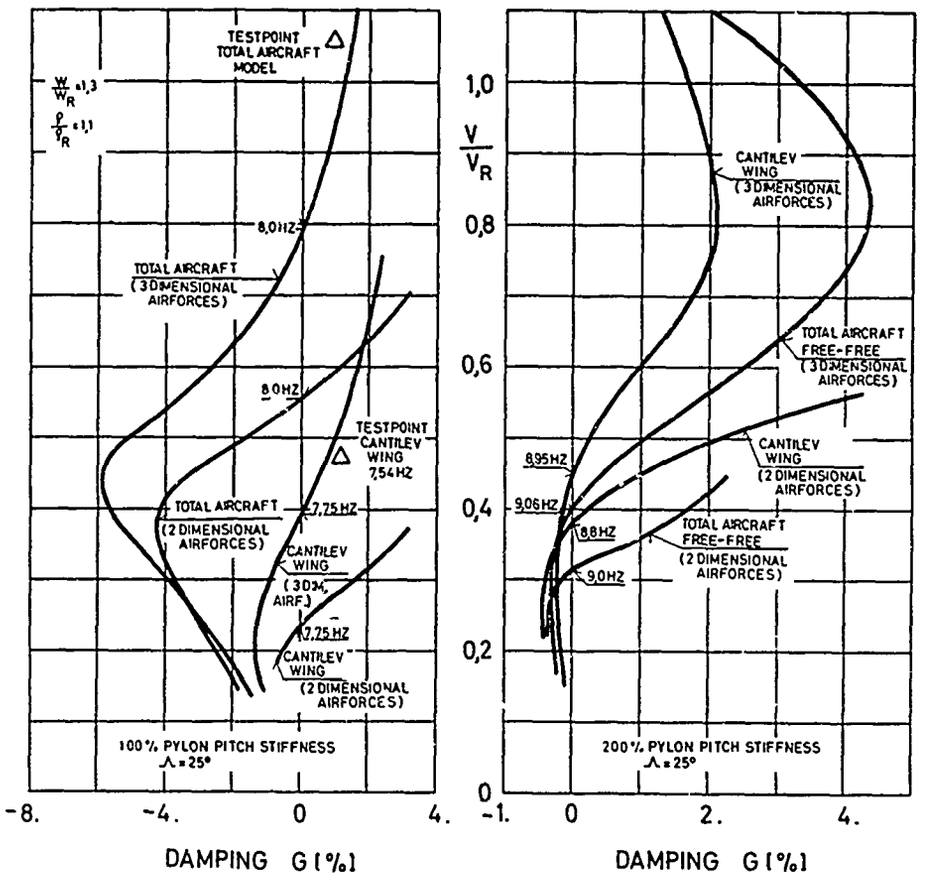

FIG. 15 FLUTTER SPEED VERSUS DAMPING FOR FREE AIRPLANE AND CANTILEVERED WING FOR TWO DIFFERENT PYLON PITCH STIFFNESSES

V-g plots for different boundary conditions and two pylon pitch stiffnesses are given in Fig. 15. The large differences in flutter speed for cantilevered wing and total airplane with two-dimensional and three-dimensional air forces are striking for the case with 100 % pylon pitch stiffness. Much smaller differences are apparent for 200 % pylon pitch stiffness.

Flutter of asymmetrical external store configurations

This phenomenon can only be investigated with total airplane flutter models. Asymmetrical store configurations are possible for an airplane carrying bombs and missiles.

Fig. 16 shows, that it is possible to have increases or decreases of flutter speeds with sweep angles for asymmetrical store configurations compared with symmetrical store configuration. Whereas Fig. 16 a shows higher flutter speeds for a store with a high radius of gyration on one wing than for the same store on two wings, Fig. 16 c demonstrates the opposite. A different behaviour occurs for two stores on the wing (Fig. 16 d, 16 e, 16 f).

Couplings of three different vibration modes are feasible. These vibration mode shapes are shown in Fig. 17. In Fig. 17 a first wing bending, in Fig. 17 b store pitch and in Fig. 17 c store roll is represented. The mode shapes, considering only the right side wing change little for symmetrical and asymmetrical configurations, but the frequencies vary.

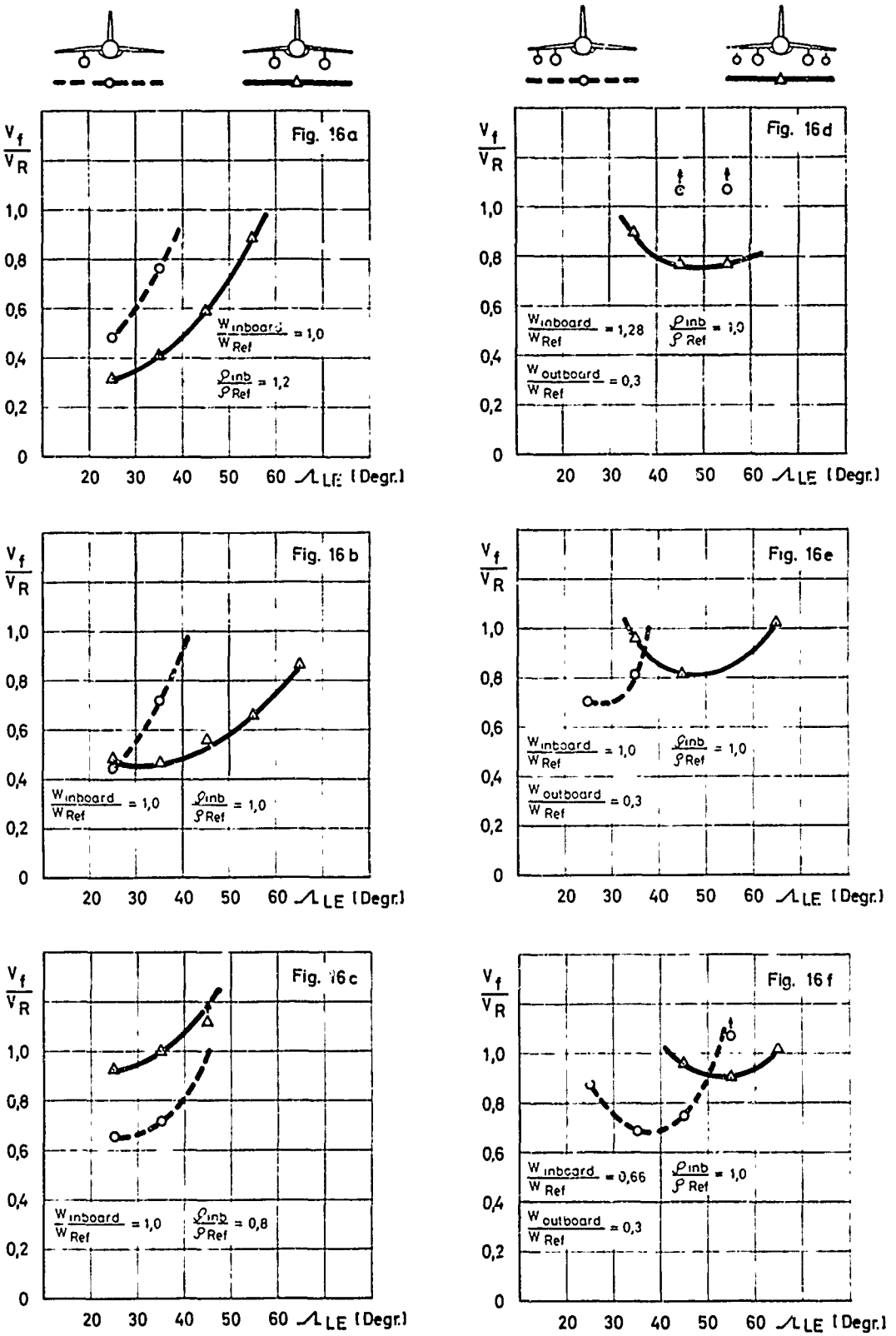

FIG. 16 FLUTTER SPEED VERSUS WING SWEEP ANGLE FOR SYMMETRICAL AND ASYMMETRICAL STORE CONFIGURATION

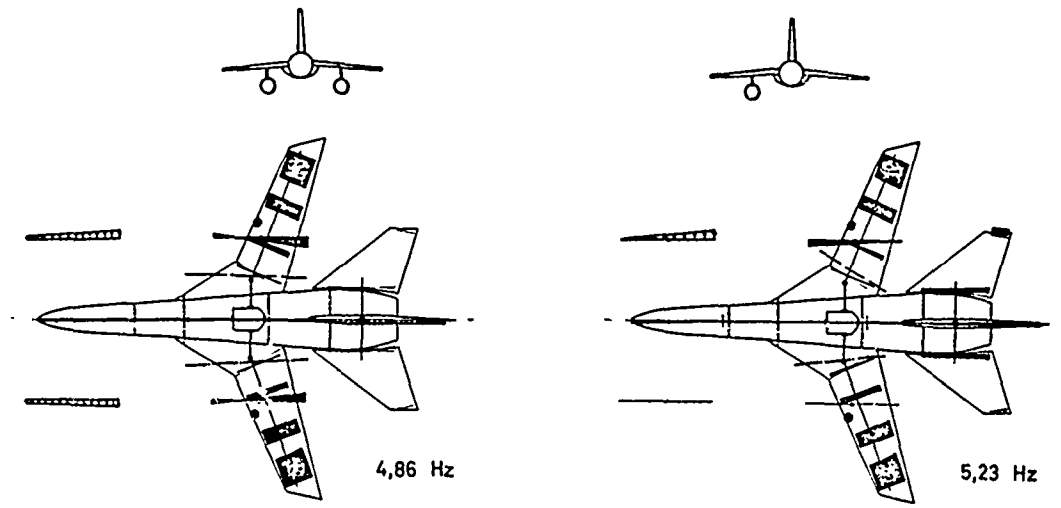

Fig. 17a FIRST WING BENDING

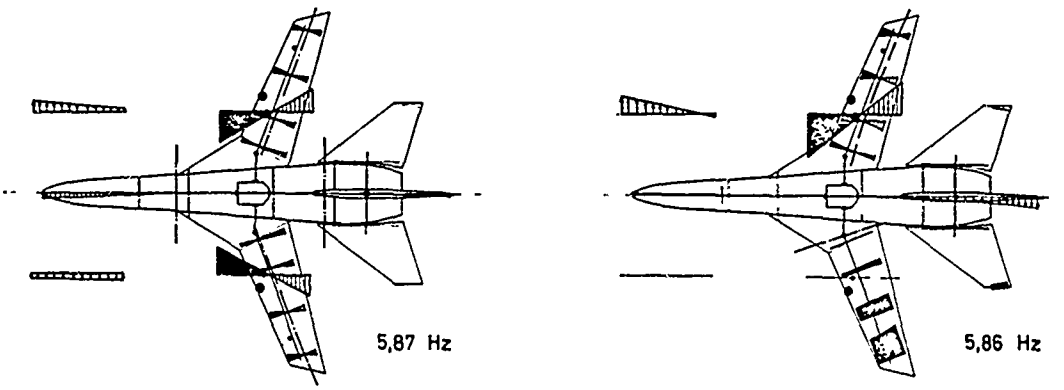

Fig. 17b INBOARD STORE PITCH

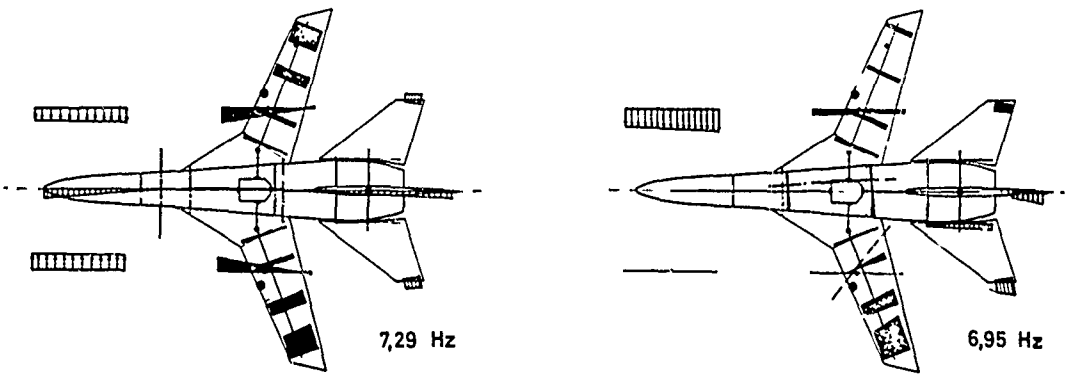

Fig. 17c INBOARD STORE ROLL

FIG. 17 VIBRATION MODE SHAPES FOR SYMMETRICAL AND ASYMMETRICAL STORE CONFIGURATION

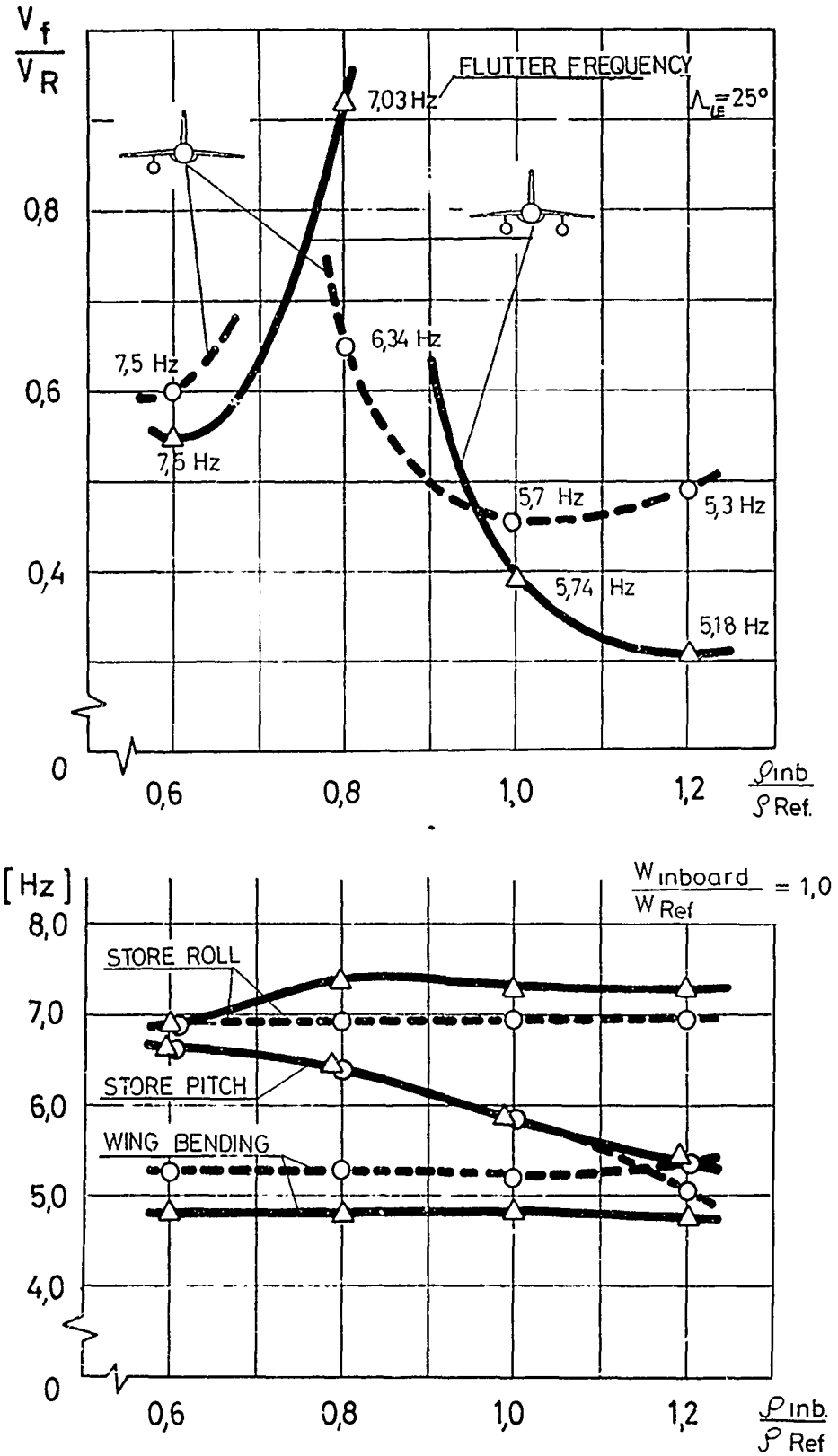

FIG. 18 FLUTTER SPEED AND MODAL FREQUENCIES VERSUS RADIUS OF GYRATION

An explanation of the flutter mechanism will be given using the following figures for the inboard store configuration. In Fig. 18 a the flutter speeds for a symmetrical and asymmetrical store configuration are drawn versus radius of gyration of this store for a constant sweep angle $\Lambda_{LE} = 25^{\circ}$ (they are taken from Fig. 16 a, 16 b, 16 c).

Fig. 18 b presents the frequencies of the different modes varying with radius of gyration.

For $\frac{\rho}{\rho_{ref}} = 12$ one can see, that the asymmetrical store pitch frequency is below the asymmetrical wing bending frequency. This leads to a milder flutter case than that of the symmetrical configuration where store pitch frequency is above wing bending frequency. For this reason we get a higher flutter speed for the asymmetrical configuration. For $\frac{\rho}{\rho_{ref}} = 0.7$ to $\frac{\rho}{\rho_{ref}} = 0.9$ the wing bending-store pitch flutter is detuned and a mode coupling store pitch with store roll is tuned in. When store pitch and store roll mode have the same frequency at $\frac{\rho}{\rho_{ref}} = 0.6$ the lowest flutter speed for this coupling occurs.

The different behaviour of the symmetrical and a asymmetrical configurations may be explained by the different mode frequencies of these configurations.

REFERENCES

1. HURTHY, W.C. — Dynamic Analysis of Structural Systems Using Component Modes. AIAA Journal, Vol. 3, No. 4, April 1965, pp. 678 - 685

2. CRAIG, R.R.; BAMPTON, M.C.C. — Coupling of Substructures for Dynamic Analyses. AIAA Journal, Vol. 6, No. 7, July 1968 pp. 1313 - 1319

3. LOTZE, A.; GARR, R. — Eigenschwingungsberechnung statisch unbestimmt verbundener Unterstrukturen mittels dynamischer Kopplung. (Aeroelastik-Kolloquium TU Berlin Juli 1971). MBB-Report UFE-733-71

4. LASCHKA, B. — Zur Theorie der harmonisch schwingenden tragenden Fläche bei Unterschallanströmung. Zeitschrift für Flugwissenschaften Vol. 11, 1963, p. 265.

5. STARK, V.J.E. — Calculation of Aerodynamic Forces on Two Oscillating Finite Wings at Low Supersonic Mach Numbers. Saab TN 53 (1964)

6. BECKER, J. — Instationäre Luftkräfte an Flügel-Außenlast-Systemen. MBB Report UFE-812-71

7. RODDEN, W.P.; GIESING, J.P.; KALMAN, T.P. — New Developments and Applications of the Subsonic Doublet-Lattice Method for Nonplanar Configurations.

8. SENSBURG, O.; LASCHKA, B. — Flutter Induced by Aerodynamic Interference between Wing and Tail. Journal of Aircraft, Vol. 7, No. 4, July-August 1970.

9. SEIDEL, W. — Flatteranalyse im frühen Entwurfsstadium mit Hilfe eines Unterschallflattermodells und parallel laufender Rechnungen. Jahrbuch 1967 der WGLR

10. HONLINGER. H. — Bauweisen aeroelastischer Modelle für eine rationelle Flatteruntersuchung moderner Flugzeugkonzeptionen. (4. Jahrestagung der DGLR, Baden-Baden Oktober 1971). MBB-Report UFE-786-71

11. THIEL, M.; SCHNEEBERGER, B. — Ground Vibration Test of Flutter Model Intern MBB-Report March 74

A PARAMETRIC STUDY OF WING STORE FLUTTER

by
L. CHESTA
AERITALIA S.p.A. - TORINO

INTRODUCTION

At Aeritalia an intensive study program based on tests and calculations on a sweepable wing model has been carried out in the past years and is still in progress.
Most of the work has been devoted to the stores problem to study the influence of different parameters in order to optimize the flutter performance of a wing with stores.
More than 3000 configurations have been tested in the wind tunnel and many computations have been done to extend the research to parameters that were difficult to simulate on the models.
Fig. 1 shows the geometry of one of the models used.
The model has been built in the classical way with a spar simulating the bending and torsional stiffnesses and nine sections simulating the inertia of the wing.
The pivot and fuselage flexibilities have been simulated by a beam clamped to a rigid rig fixed to the tunnel roof.
It was possible to change the sweep angle by a screw with a spring incorporated in order to simulate the rigid wing fore and aft mode.
Two pylon stations have been provided at suitable positions and the two pylons have been simulated by beams of different pitch, lateral and yaw stiffnesses.
The store C.G. position, weight and moment of inertia were simulated by two variable masses mounted on a beam at seven standard positions without any aerodynamic shape simulation.

TESTS PROCEDURES

A complete investigation has been performed on the following parameters :

- Store mass
- Store radius of inertia
- Store C.G. longitudinal position referred to the pylon attachment point
- Pylon pitch stiffness
- Wing sweep angle

Moreover a limited analysis has been done to evaluate the influence of parameters such as: Pylon length, pylon lateral stiffness, fuel in the wing, fore and aft rigid wing stiffness, open flaps and slats, pivot backlash, stores aerodynamic shape and the size of the stores vanes.

RESULTS

Most of the studied configurations showed a flutter induced by the coupling of the wing fundamental bending and the store pitch modes.
Fig. 2 left shows a typical contour diagram obtained for a configuration with the inboard station loaded and a wing sweepangle of 25 degrees.
Equal speed lines are drown with reference to the max wind tunnel speed in the store weight -radius of gyration plane.
On the right side of the figure a section of the diagram for fixed weight is shown together with the frequency behaviour of the relevant flutter modes.
It can be readily seen that the flutter speed decreases increasing the store radius of inertia until the frequency of the store pitch mode is higher than the fundamental bending and starts again to increase as soon as the pitch frequency becomes lower than the fundamental.
This second type of flutter is normally very mild; it is very difficult during the test to define correctly the flutter speed, and consequently to make a correct comparison with the computation without a careful evaluation of the model damping.
On Figure 3 the results obtained for the basic configurations with only one store at the inboard pylon are shown.
The figure is a composition of many diagrams like that one shown on Fig. 2.
The diagrams are set from left to right, in order of increasing values of the C.G. forward shift and from top to bottom, in order of increasing swee angle.
It is clear that for all the sweep angles the forward C.G. shifting produces a slight reduction of the value of the minimum flutter speed associated with a reduction of the area encircled by a defined constant speed line. Such area increasing the C.G. shift is progressively reduced to the region of stores with small weight and large radius of inertia.

An increase in the sweep angle produces a rise of the value of the minimum flutter speed and the reduction of the effectiveness of the C.G. shift.
Fig. 4 shows a similar diagram obtained for a configuration with a pylon pitch stiffness four time the one used in fig.3
Comparing the two figures it is possible to see that an increase of the pylon pitch stiffness does not change the value of the minimum flutter speed but shifts it towards stores of higher weight and radius of inertia and reduces the effectiveness of the forward shifting of the C.G. -

On Fig. 5 and 6 the effects of the same parameters for a configuration with a store at the outboard station are presented. The trend is the same as before, only the effect of the pylon pitch stiffness is less important, because the total deformability of the wing pylon system from the root to the store attachment does not change toomuch multiplying the pylon nominal pitch stiffness by four.

Fig. 7 and 8 show the effect on the flutter speed of a fixed and inertially well defined store at the outboard pylon for the same wing sweep angles and inboard store parameters previously analyzed.
The configuration chosen for the outboard store was inherently very stable and therefore the result was only a shifting of the minimum flutter speed toward the region of the large store weights and radii of inertia.

The diagram presented before could be considered in many aspects ideal because only one type of flutter occurred in the configurations chosen.
Some different types of flutter can appear changing other parameters.

The lateral stiffness of the pylons comes out as a very important parameter for heavy stores with a small radius of inertia like bombs mounted on double or triple carriers.
In these cases a flutter due to the coupling between the lateral pylon bending and the pylon pitch modes can appear.
Fig. 9 shows nine contour plots, obtained for the same wing configuration and for different pylon stiffnesses and C.G. position, in which the distorsions of the equal speed lines due to the presence of different flutter modes are evident.
On top of fig. 10 three sections of these diagrams for a constant store weight are presented together with the frequency trends of the most interesting modes.
Pylon C1 presents the normal behaviour because the lateral pylon mode has alway a frequency higher than the pitch mode.
Pylon B01 has the same pitch stiffness but a lower lateral stiffness so that the pitch and lateral mode frequencies are very close for the first two test point and a flutter due to the coupling of these modes appears at speed lower than espected.
Pylon B02 has about the same lateral stifiness as pylon B01 but a larger pitch stiffness and also in this case when the frequency of the lateral bending mode is lower or close to that one of the pitch mode the same type of flutter appears at speed lower than expected.

Also when both stations are loaded the lateral bending stiffness of the inboard pylon has been found important; Fig. 11 shows a configuration in which some cases of flutter due to the coupling of the lateral bending of the inboard pylon with the pitch mode of the outboard pylon are present.
In this configuration the outboard pylon yaw mode some times has nearly the same frequency as the flutter mode and therefore a rotating motion of the outboard pylon may appear during the flutter.

The most peculiar flutter found is however that one originated by the rigid fore and aft motion of the wing.
This mode couples itself very strongly with the wing torsion when a store is fitted on the pylon because of the large vertical distance between the wing and the store C.G. - Therefore, if the frequency of the uncoupled fore and aft mode is low enough, a new mode at a lower frequency with a large amount of torsion may appear inducing a flutter at a lower speed.
On Fig. 12 bottom the frequency trends with the radius of inertia of the relevant modes for two cases with and without fore and aft motion are presented together with the corresponding flutter trends on the top of the figure.
It is clear that for heavy stores with a small radius of inertia the wing fore and aft mode has a frequency lower than the store pitch and couples itself with the fundamental wing bending at a lower speed. This is made evident on figs. 13 and 14 where the modes nodal lines together with the V-g plots for two typical cases are shown.

Apparently the aerodynamic shape is not a very important parameter, only if the store is very large and light a small increase in the flutter speed has been found (see Fig. 15).
Also the vanes may increase slightly the flutter speed when the flutter is mild as shown in fig.16.

CONCLUSIONS

The diagrams shown are only a few sample of the results obtained in the work; unfortunately the short time available allows only the presentation of some highlights and their discussion in a very arid way.
It is anyway possible to summarize here some important general conclusions reached during the progress of the study.

If an aircraft carrying many underwing store configurations must be developed a complete flutter analysis should be done taking into account the effect of the variation of as many parameters as possible .
In fact, with an analysis limited to the required store configurations or, much worse, only to the configurations considered critical, it is impossible to extrapolate the value of the flutter speed even for very similar configurations and to make any forecast of the critical speed trends if some parameter is changed.
The evaluation of the effect of a change of the value of some parameters is the normal work, during the development of an aircraft, but this is very cumbersome and difficult to do if many underwing store configurations have to be cleared together . In fact an increase of the value of one parameter, for example the pitch pylon stiffness, may be beneficial for one store and simultaneously unfavorable for another store only slightly differing in the inertia characteristics.
To be able to judge about the convenience of a modification of a parameter it is therefore necessary to have well in mind how the overall picture, and not only the single points, changes with that parameter.
This is even more complicate for an aircraft with a variable sweep wing where it is necessary to get a good compromise with the different flight envelope requirements at each sweep angle.

In the design of the wind tunnel models and in the definition of the mathematical models for the computations it is important to take into account all the degrees of freedom, also those normally neglected like the in-plane flexibility of the wing, the lateral and yaw flexibilities of the pylons.
In particular for the computations, it is necessary to obtain a good accuracy in the representation of the wing modes. In fact most of the discrepancies found in the cross checks between tests and computations were due to inaccuracies in the modes definition specially in the earlier calculations when the method of the branch modes, without junction modes was used.
For this reason all the flutter computations have been done using wing-pylons normal modes computed for each specific configuration reaching in this way a good agreement between test and calculation, notwithstanding some further difficulty in the correlation due to a structural damping of the model. In fact if the flutter is mild, and normally it is, a small amount of damping is sufficient to increase very much the value of the flutter speed; moreover the definition of the flutter speed in the wind tunnel may get, in these cases, inaccurate since it is difficult to define the point of the flutter onset. Anyway a good comparison has always been found introducing the measured value of the flutter mode damping.

As a last sentence it has been found very convenient and powerful to use a mixed wind tunnel - computation flutter analysis. In fact, as both methods have been proven equivalent in the accuracy of the results it has been possible in this way to reach an optimum between the time necessary to get the results and the difficulties to represent some parameter either on wind tunnel or mathematical models.

ACKNOWLEDGMENTS

The author wishes to express his appreciation to the Aeritalia Dynamic Office for their support and is specially indebted to Mr. G. DANIELI for his contribution during all the studies described in the paper.

REFERENCES

- E. Morelli - G. Carrà - AIT Report F 70145-Model 16 C - Flutter tests results
- E. Morelli - G.De Ferrari - AIT Report F 74023-Model 16W - Flutter Tests results
- G. Mattea - C. Bertero - AIT Report F 72034 - Part 1,2,3 - Model 16 Flutter Analysis

LIST OF SYMBOLS

C_R	=	Reference chord
IPL	=	Inboard pylon lateral mode
IPP	=	Inboard pylon pitch mode
IPY	=	Inboard pylon yaw mode
OPL	=	Outboard Pylon lateral mode
OPP	=	Outboard pylon pitch mode
OPY	=	Outboard pylon yaw mode
V_{max}	=	Max wind tunnel speed
V_F	=	Flutter speed
VBII	=	Wing second bending
WFA	=	Wing fore and aft
WFB	=	Wing fundamental bending
W_{ISm}	=	Inboard store weight (model)
λ	=	Sweep angle
ω_F	=	Flutter frequency
ω_m	=	Model frequencies

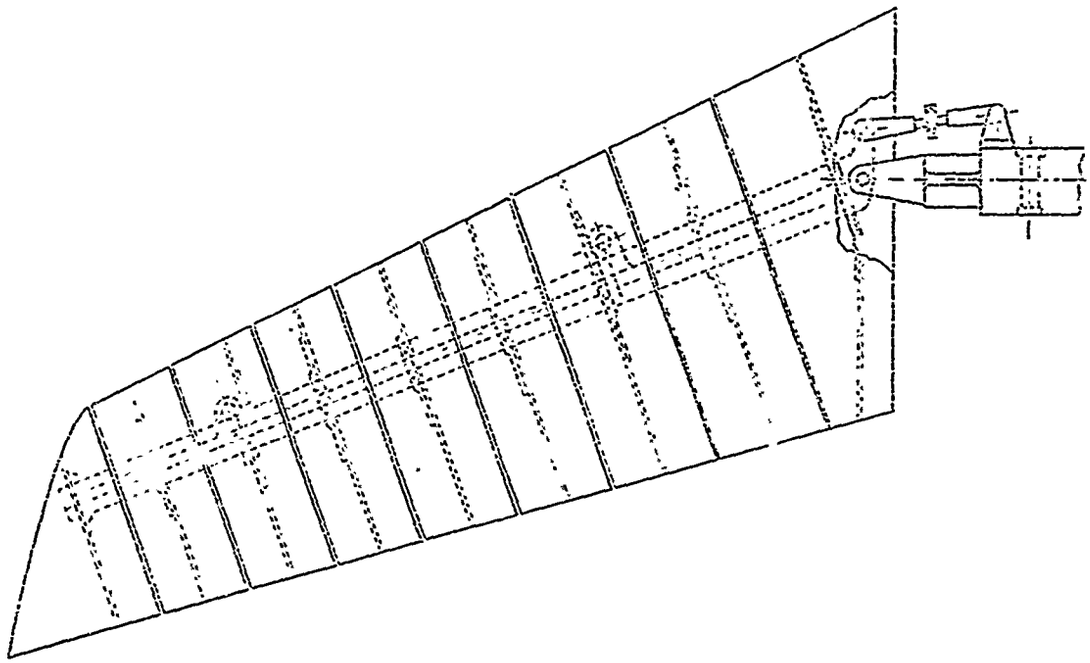

Fig. 1 - Sketch of the wing model

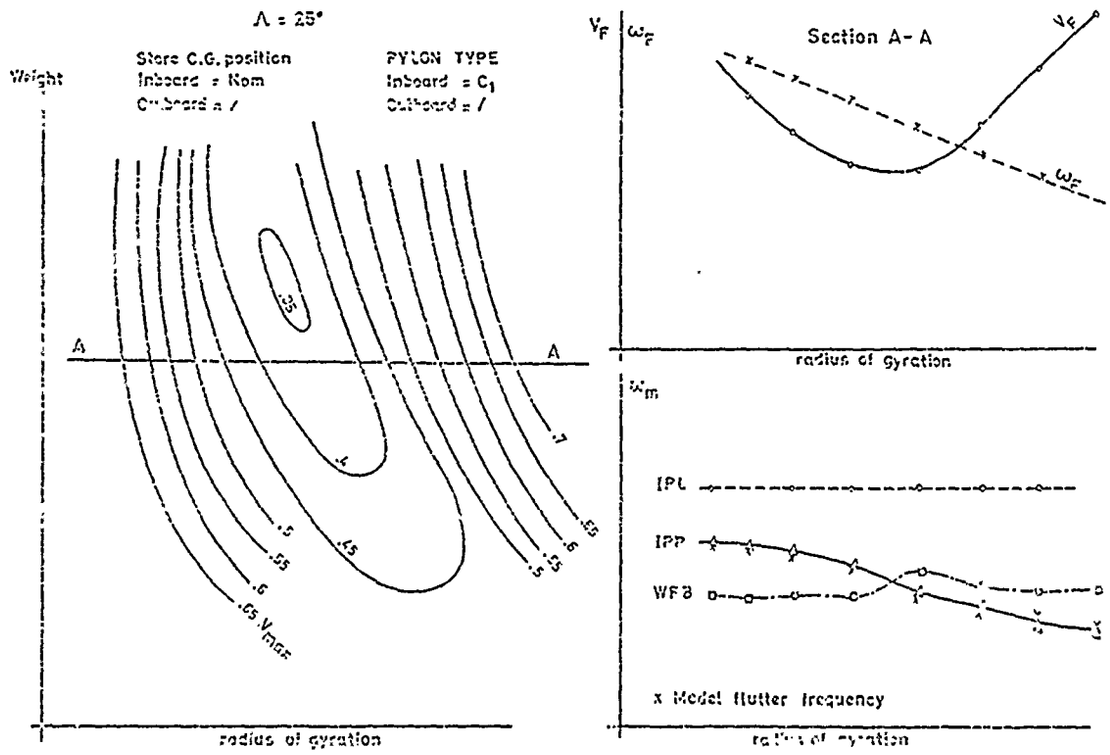

Fig. 2 - Influence of inboard weight and radius of inertia
- Typical contour plot

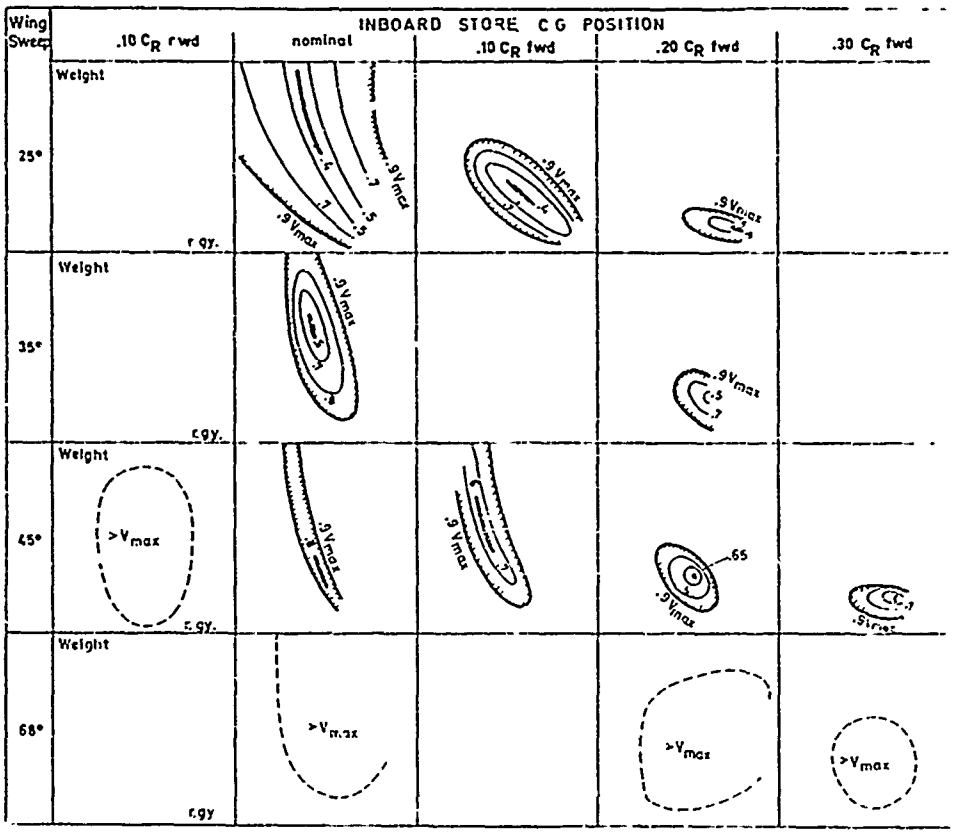

Fig. 3 - Influence of store C.G. position and wing sweep angle
- Store at the inboard station
- Nominal pylon pitch stiffness

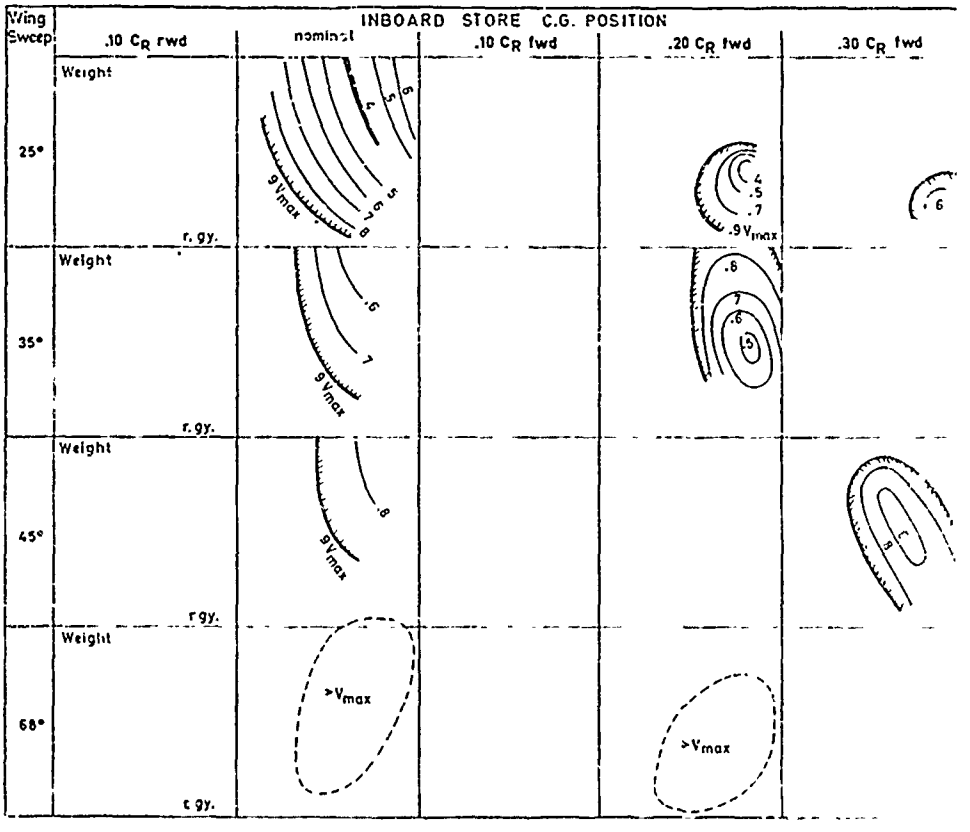

Fig. 4 - Influence of store C.G. position and wing sweep angle
- Store at the inboard station
- 4X Nominal pylon pitch stiffness

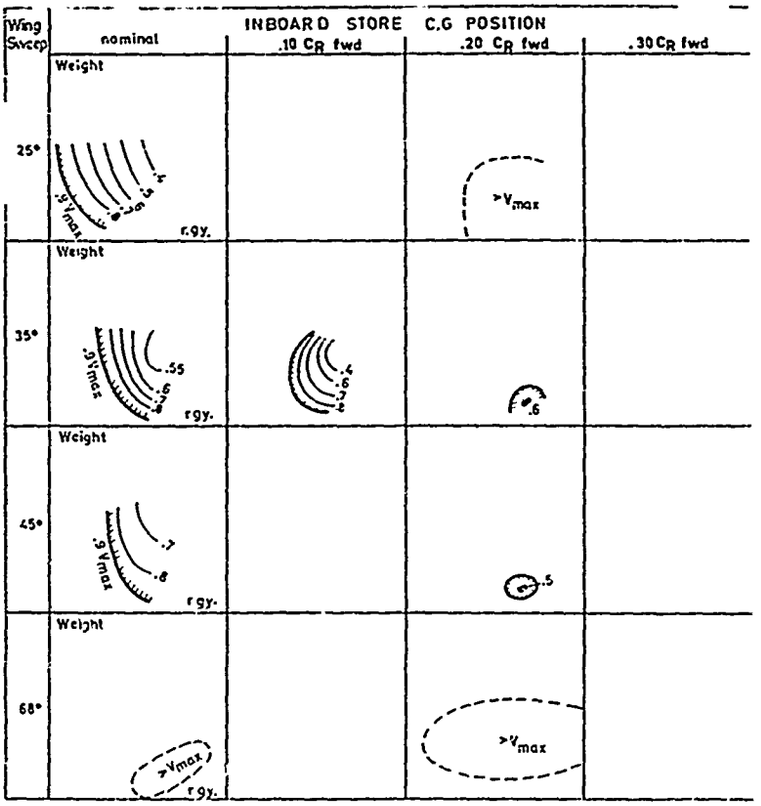

Fig. 5 - Influence of store C.G. position and wing sweep angle
- Store at the outboard station
- Nominal pitch pylon stiffness

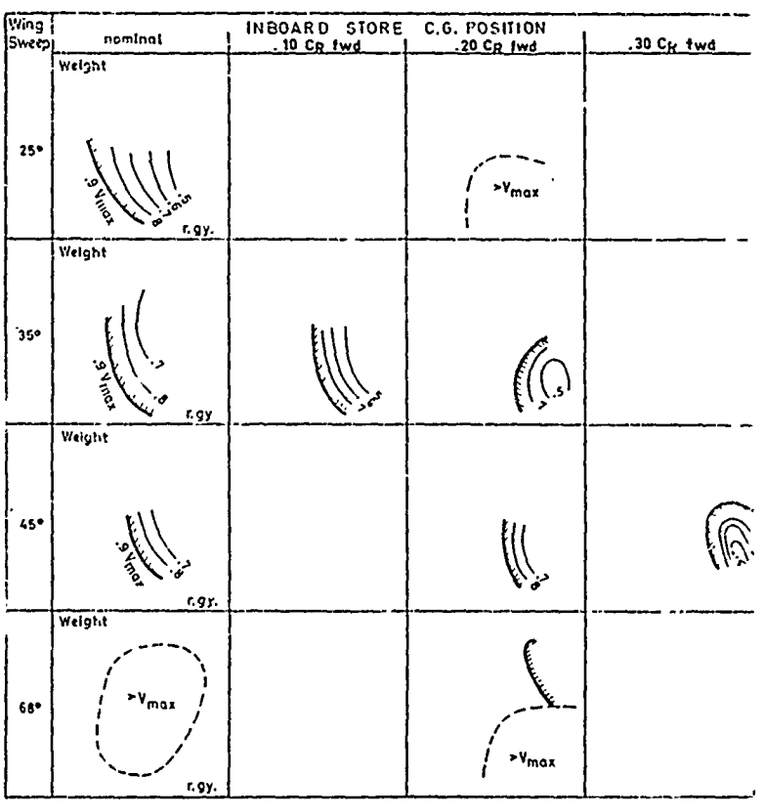

Fig. 6 - Influence of store C.G. position and wing sweep angle
- Store at the outboard station
- 4X Nominal pylon pitch stiffness

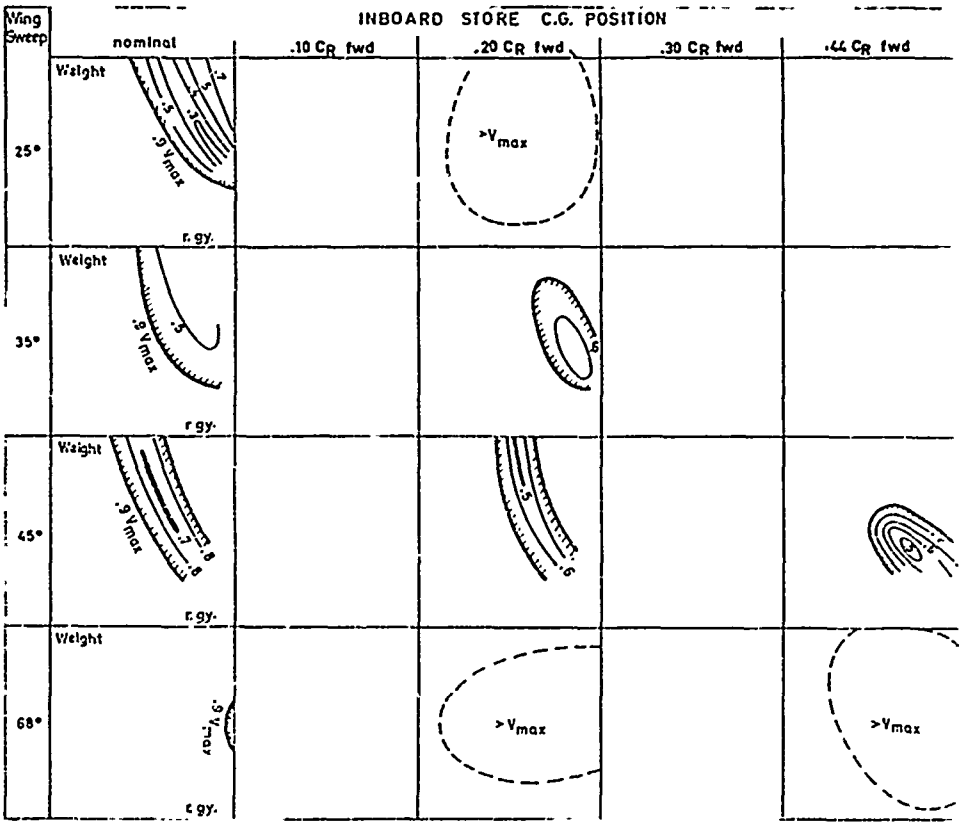

Fig. 7 - Influence of store C.G. position and wing sweep angle
- Store at inboard and outboard station outboard store C.G. position .20 C_r fwd
- Nominal pylon pitch stiffness

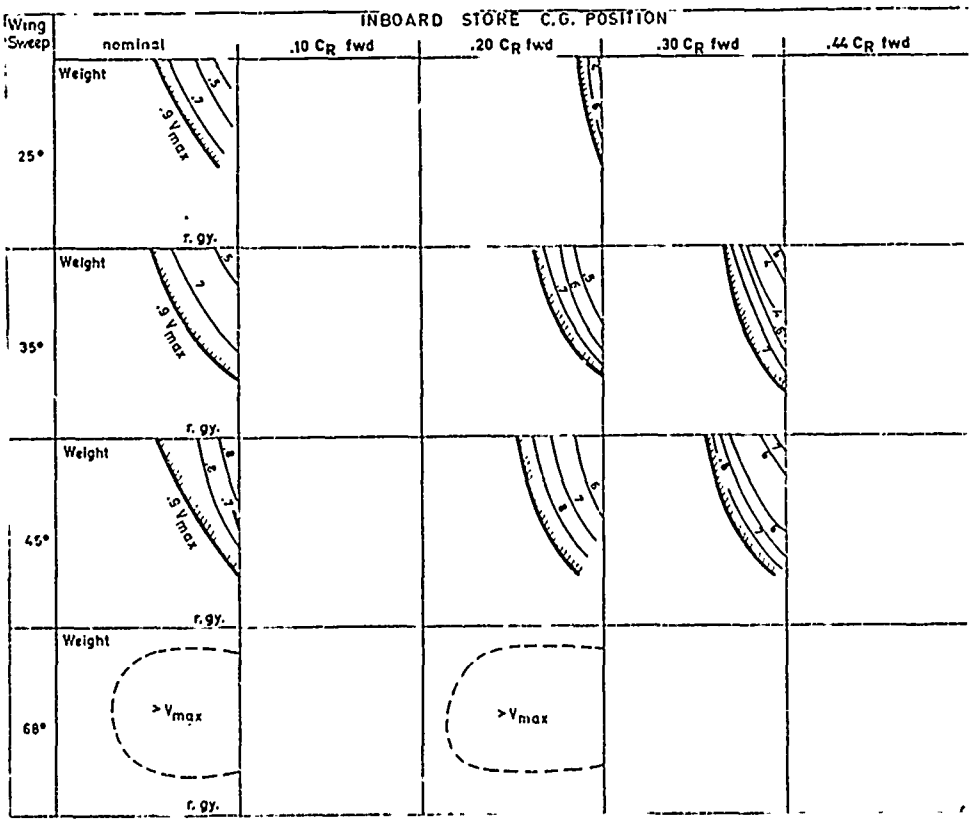

Fig. 8 - Influence of store C.G. position and wing sweep angle
- Store at inboard and outboard stations outboard store C.G. position .20 C_r fwd
- 4X Nominal pylon pitch stiffness

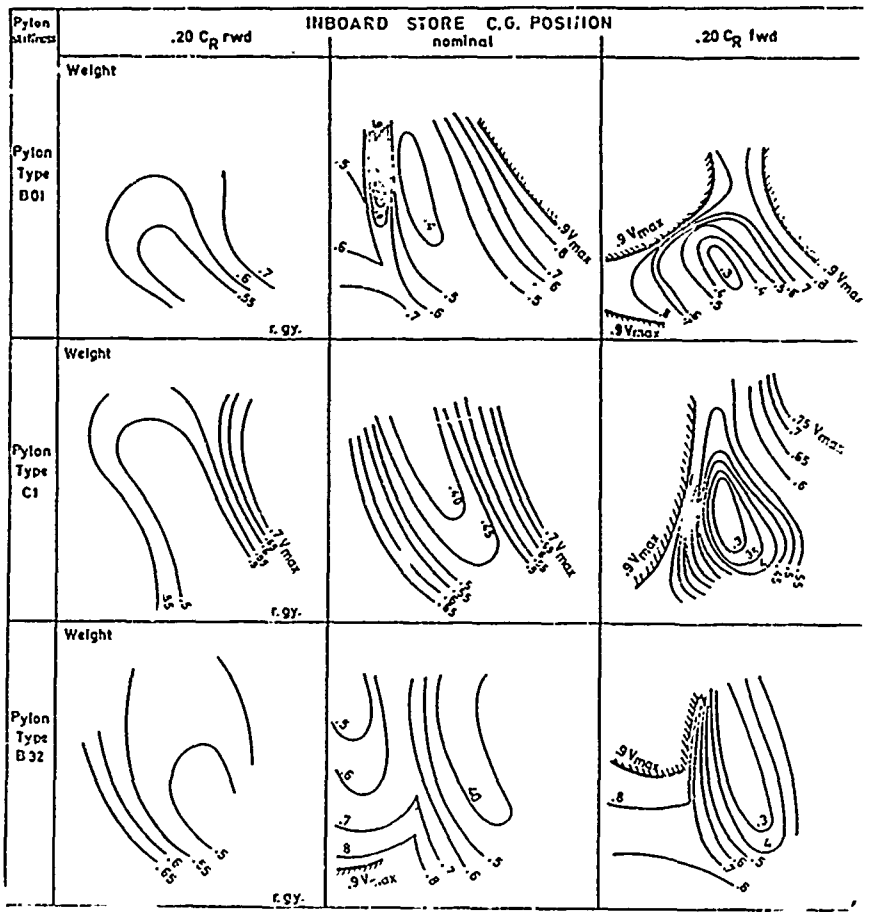

Fig. 9 - Influence of pylon lateral stiffness and store C.G. position
- Store at the inboard pylon
- Wing sweep 25°

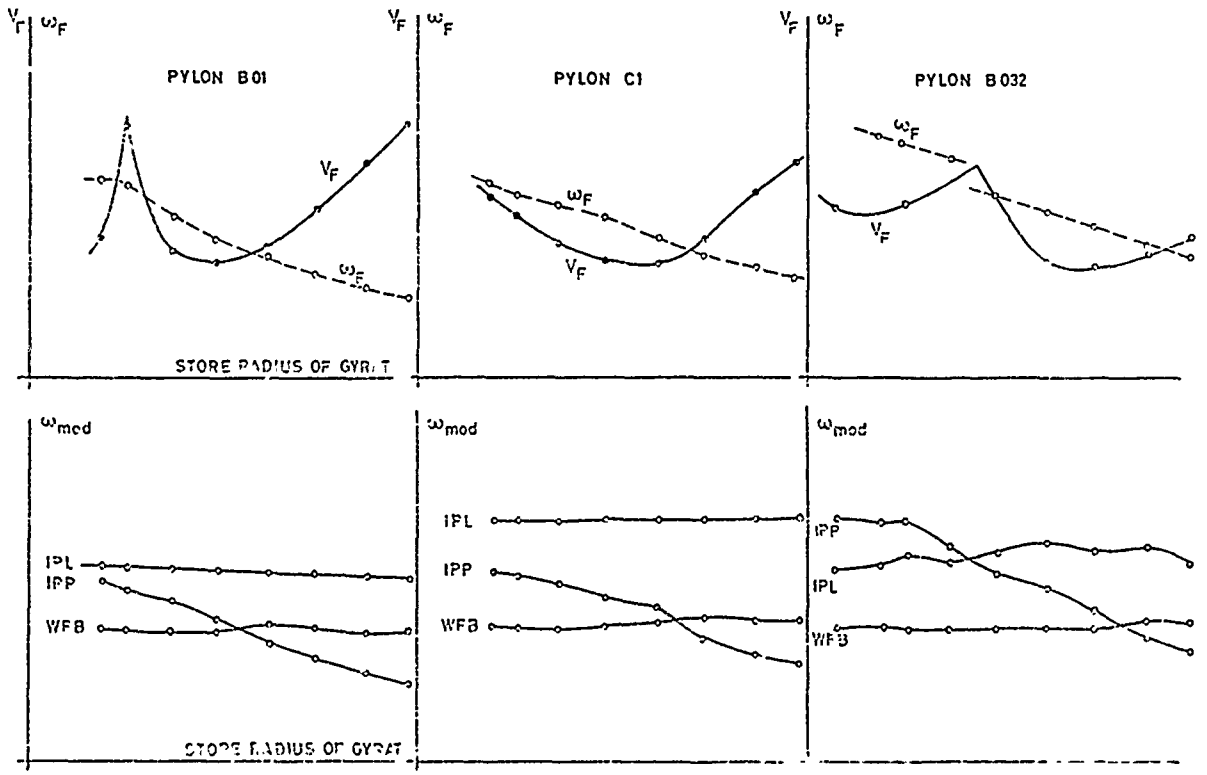

Fig. 10 - Influence of pylon lateral stiffness
- Store at the inboard pylon
- Wing sweep 25°

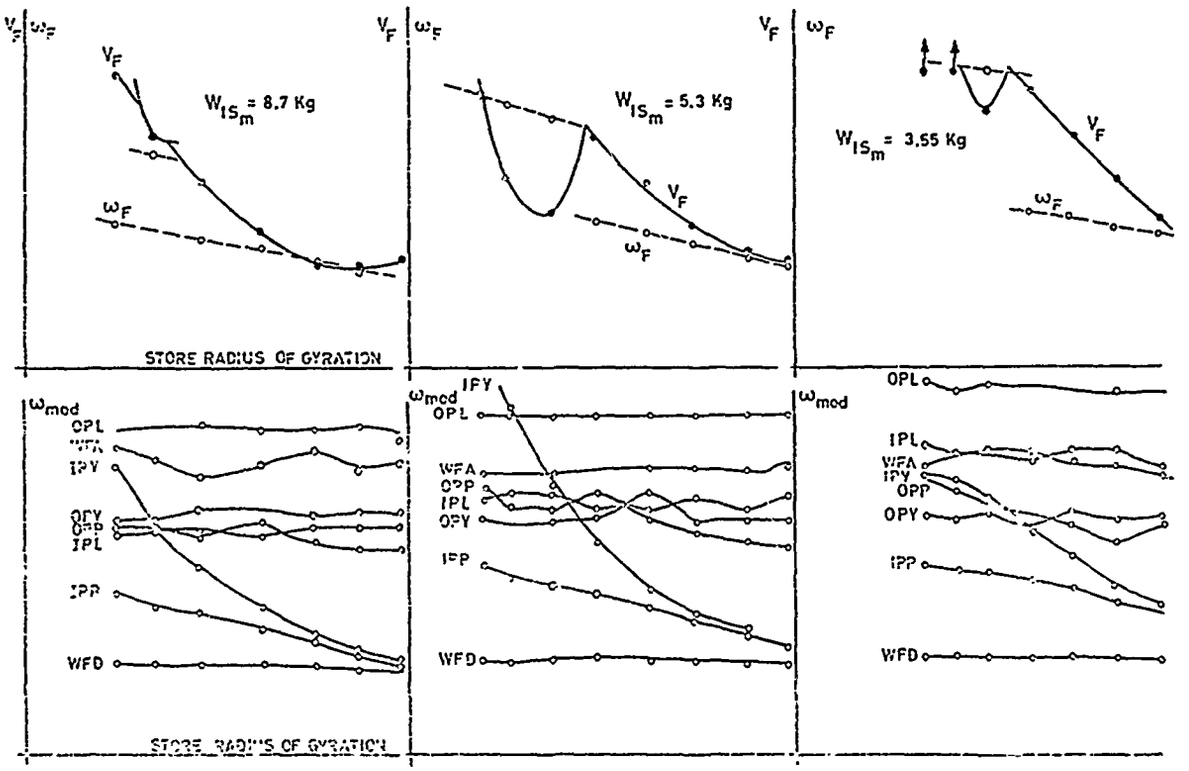

Fig. 11 - Influence of lateral pylon stiffness
- Wing sweep 25°
- I/b and O/b stations loaded

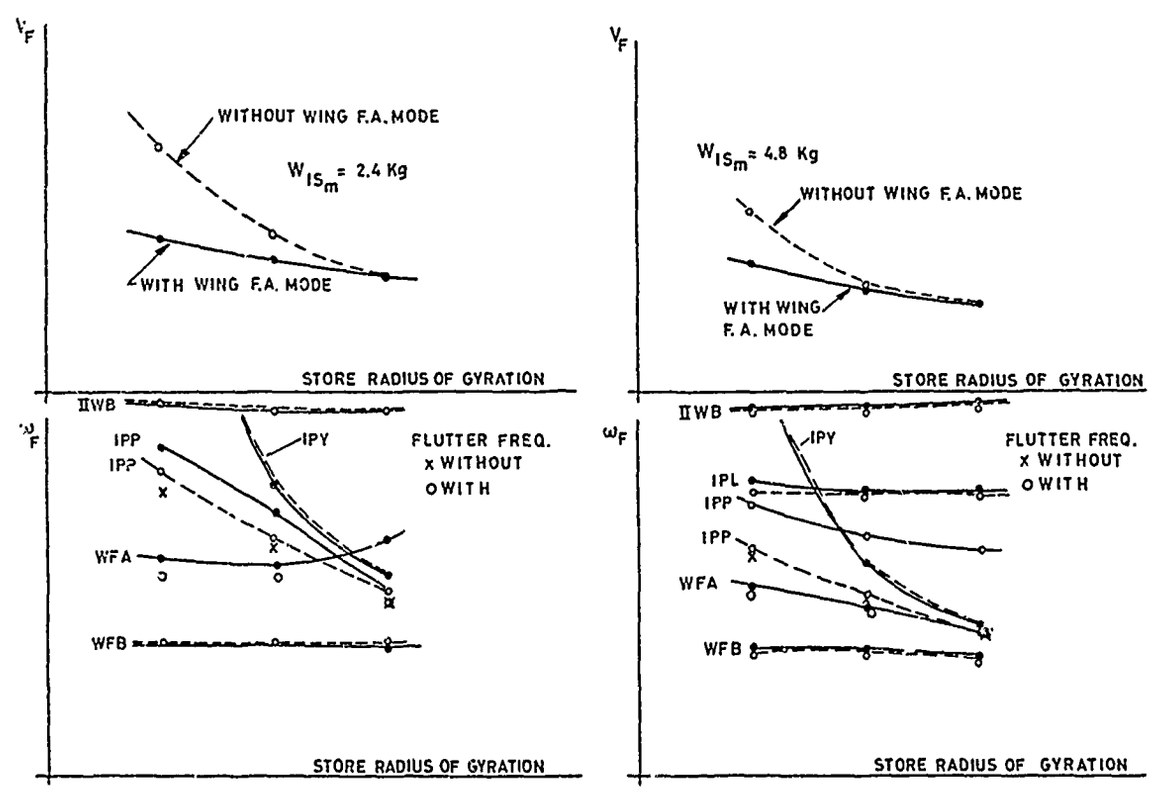

Fig. 12 - Influence of the wing fore and aft flexibility
- Store at the inboard pylon
- Wing sweep 25°

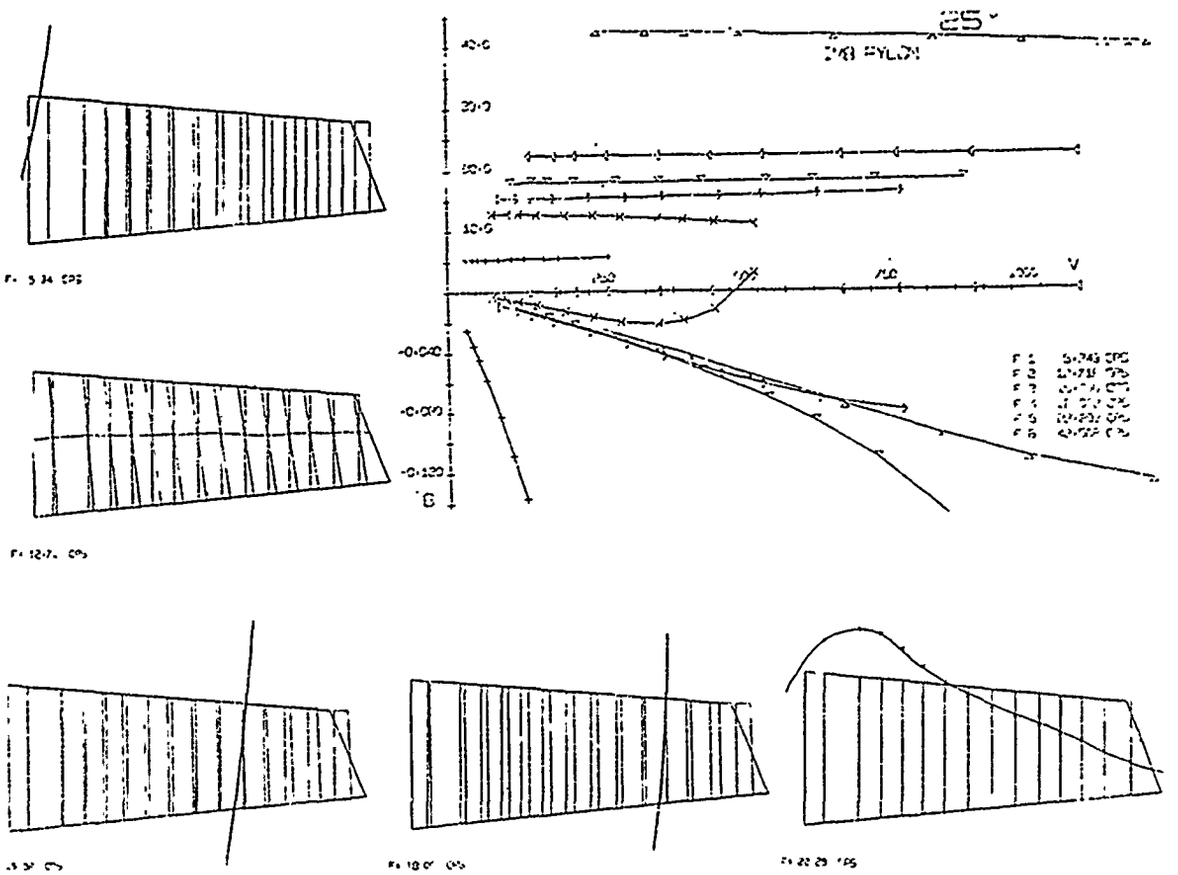

Fig. 13 - Wing without rigid fore and aft motion
- V-g plots and modes nodal lines

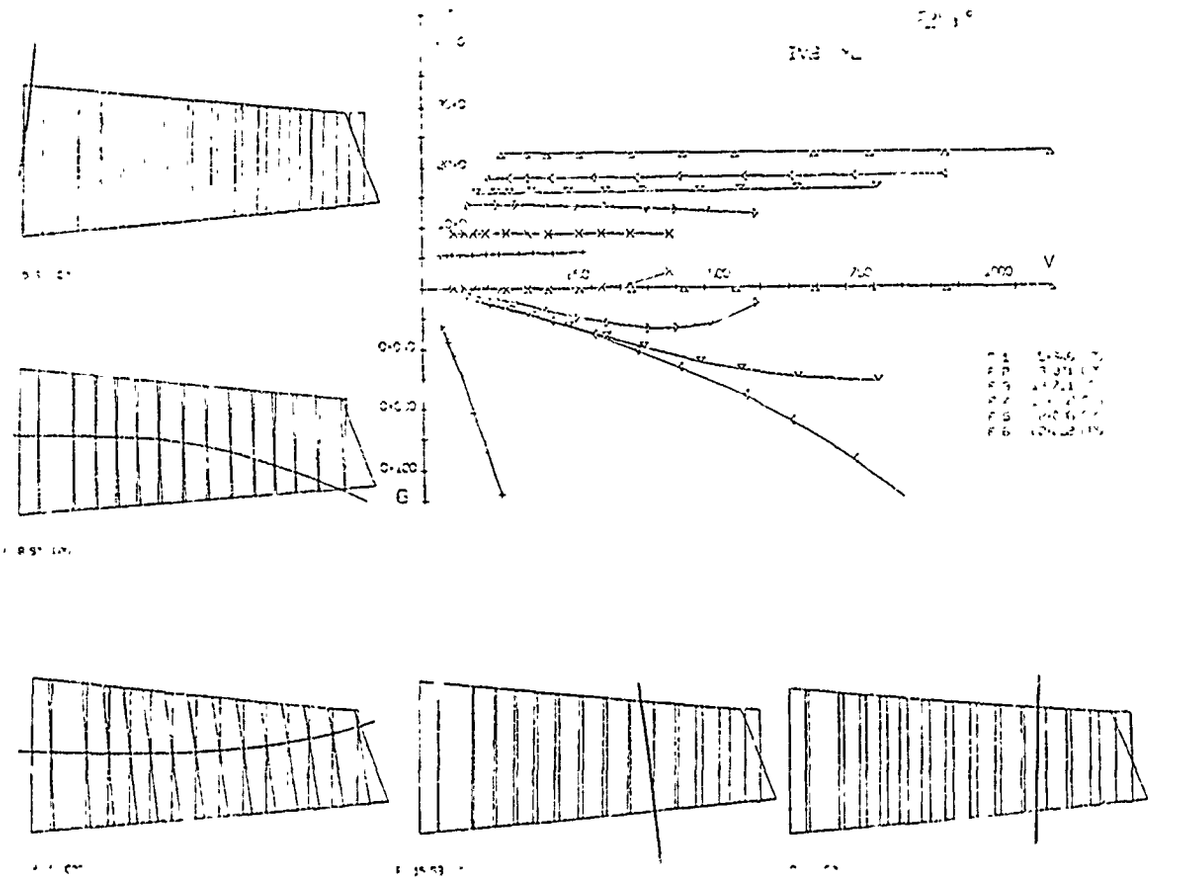

Fig. 14 - Wing with rigid fore and aft motion
- V-g plots and modes nodal lines

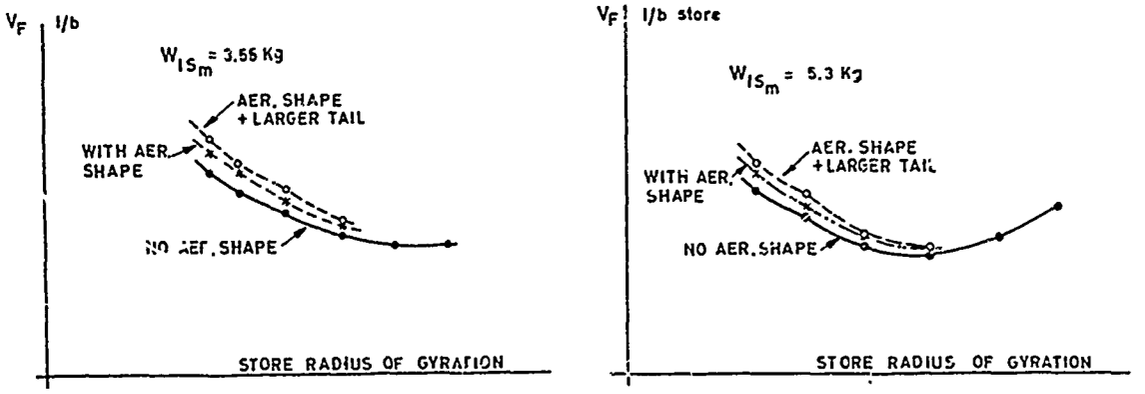

Fig. 15 - Influence of store aerodynamic shape and tails

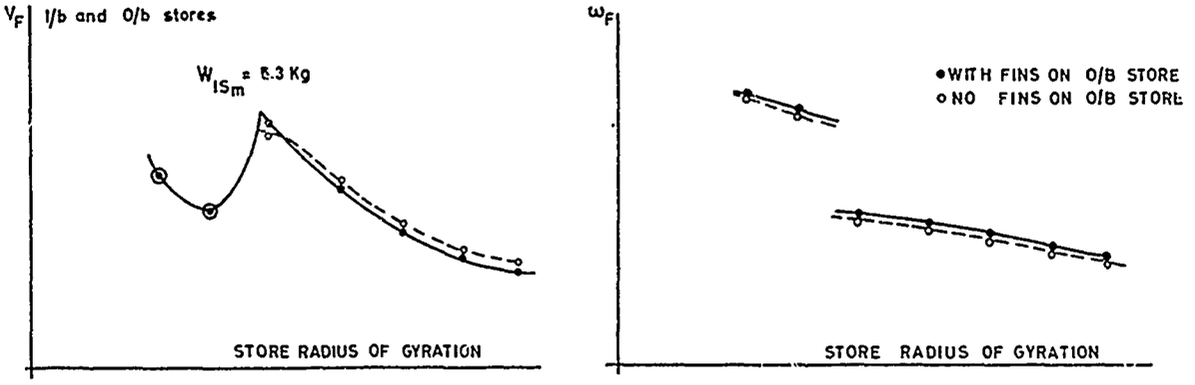

Fig. 16 - Influence of outboard store fins

RECENT OBSERVATIONS ON EXTERNAL-STORE FLUTTER

Eugene F. Baird and William B. Clark
Grumman Aerospace Corporation
Bethpage, New York 11714

INTRODUCTION

The problem of wing flutter with external stores is generally regarded as one of the most complex flutter-prevention considerations. The sheer magnitude of the number of configurations to be studied, Figure 1, all too often staggers the imagination of the flutter engineer; it places him in a state of near-exhaustion, contemplating the number of analyses he must perform to fully understand the problem. Often, one of the main dilemmas is just where to start. This paper attempts to show how this problem can be approached realistically and how its magnitude can be reduced to manageable proportions. The paper first discusses the current approach to external-store flutter, and then touches on some of the recent developments being made to better cope with this complex problem.

As is well known, classical wing flutter involves the coupling of at least two degrees of freedom, one or more of which must contain motion of the wing in angle of attack. Wing external-store flutter is no exception to this rule. The basic mechanism of external-store flutter can be thought of as the coupling of wing modes with store modes which produce wing angle-of-attack motion. Most external-store flutter problems occur either as an existing bare-wing flutter mode, modified by the addition of store mass and inertia on a relatively stiff pylon, or as a new flutter mode introduced by the addition of the store on a relatively flexible pylon. The occurrence and characteristics of either type of flutter are very much a function of aircraft configuration, store location relative to the aircraft, and system mass and elastic properties. It is, obviously, impractical to provide detailed design charts for any and all possible combinations of these parameters. This paper will show how the problem can be approached and interpreted in a manner sufficient to gain the understanding required for a realistic problem solution.

EARLY TRADEOFF DESIGN CONSIDERATIONS

In the early design stages of an aircraft, the flutter analyst is generally asked to provide configuration tradeoff information necessary to arrive at an optimum overall design. Analyses are usually based on very preliminary design data and little or no test information. This problem is greatly complicated when the aircraft being designed is required to carry a large variety of wing-mounted external stores. If the design happens, for example, to be a strike fighter, then the tradeoffs between the fighter configuration, which is required to carry a few air-to-air missiles, and the attack version, which most likely must carry a large assortment of heavier air-to-ground stores, become a major design consideration. How much weight penalty should be imposed on the fighter version to have a satisfactory attack capability? Early design flutter studies of a reasonable number of store configurations with a strength-design wing will indicate quickly the scope of the problem. It is not unreasonable to find a ratio in flutter speeds of two or more between the bare wing and the wing heavily loaded with stores. Such a ratio would surely require that the torsional stiffness of the wing be increased. The additional stiffness required will then depend on exactly what performance is needed for the attack mission. An early check on the aircraft performance with the added store drag is certainly a calculation which should be made. These results help the analyst decide just what level of stiffness is needed to satisfy the various mission profiles.

The most gratifying approach to carrying external stores to come along in a long while is the concept of conformal weapon carriage, Figure 2. This concept provides for the mounting of stores within a pallet that fits along the bottom of the aircraft fuselage. The stores are submerged and held in place by ejector racks within the pallet. Flight tests have demonstrated substantial performance improvements with the conformal carriage pallet. Results indicate a very dramatic reduction in the drag associated with external stores. However, because the trends in weapon development are toward very large, heavy, sophisticated bombs, the use of the pallet will be limited. Because sophisticated weapons have aerodynamic fins for controllability and will be elongated with complex guidance units, the installation of these bombs into the pallet may not be possible. Therefore, satisfactory operation of sophisticated bombs will still require the use of wing pylon mounting.

Unfortunately, there is little hope of ever having enough quantitive data to set down a complete set of guidelines for the optimum arrangement of external stores on a wing. Some obvious general guidelines to follow in the design of a new aircraft which carry many external-store configurations are:

- Keep all store stations as close to the fuselage as possible, as shown in Figure 3
- If store stations outboard of about the wing mid-span are required, minimize the possible mass / inertia variations at these stations
- Obtain as high a bare-wing flutter speed as is practical, an example of which is shown in Figure 4

Once the configuration has been established, some preliminary analyses must be performed to establish what the critical flutter modes are and an idea of what the critical parameters are. The amount of work necessary in this preliminary study will depend to a large extent on the configuration to be analyzed.

CURRENT APPROACH

Mission-Loading Definition

The mission store-loading requirements for a new aircraft are generally well defined in the specifications. Here, the various roles of the aircraft are detailed and the armament specified. For example, a strike fighter will, typically, perform a fighter escort mission for which a few relatively light air-to-air weapons are carried. This same aircraft might well be required to also perform an interdiction mission carrying a much heavier assortment of external stores and a close-air-support mission with a still heavier load of wapons. If all the possible mission and weapon requirements of the aircraft are set forth, one soon begins to realize the scope of the problem that faces the flutter analyst. The enormous number of possible wing-store combinations is the central problem to most wing-store flutter studies.

The first job of the flutter analyst is to reduce this seemingly infinite problem to one of manageable size. Generally, this task is begun by discussing mission loadings with both the contracting agency and the operational squadrons. In the case of the hypothetical strike fighter, it is not unreasonable to expect that out of these discussions will emerge six or eight mission loadings which must be thoroughly analyzed to establish stiffness levels necessary for proper flutter margins throughout the defined flight profiles; that is, the wing should be designed to carry these basic mission loadings and their subsets to specified limit speeds.

The problem then becomes one of minimizing the number of subsets which must be analyzed to clear an entire loading. An effective way of accomplishing this reduction is to make use of inertial similarity. This procedure is based on the establishment of a relationship between store inertial properties and wing flutter characteristics. This is accomplished by plotting the inertial properties of all possible stores within a mission loading at a given station, as shown in Figure 5. Examination of this plot reveals important areas where analysis of a few cases is representative of a larger number. Consideration of plots of this type for each station and each loading will lead to a list of cases which, when analyzed, will represent the entire array. This list becomes the basis for the preliminary analysis.

Analysis

A successful theoretical analysis is one which initially identifies problem areas, categorizes them in terms of impact on design and performance, and provides detailed relationships between stiffness, weight, and flutter margin to the designer. The accurate identification of a wing-store flutter problem at an early stage of development is essential for a minimum-impact solution.

A search for problem areas can be undertaken as soon as a tentative strength design has been determined. The clean wing is analyzed, of course, in each of its possible modes: cantilever, symmetric and antisymmetric; with and without wing fuel; at various wing sweeps, if movable; and at several key Mach numbers. The wing flutter speed(s) should be considered in terms of gradients. If flutter speed changes rapidly with respect to any important parameter (fuel, wing sweep, root attachment stiffness, outer panel stiffness, altitude, Mach number, fuselage inertia, etc.), the phenomena should be studied in more detail.

As a next step, candidate stores from the mission loadings described above are introduced into the analysis, one station at a time. The effect of their weight and inertia on the clean wing should, initially, be determined by making the attachment stiffness infinite. (A typical flutter velocity contour is shown in Figure 6.) The modes obtained in this way are an excellent set of generalized coordinates for later use when store flexibilities are first evaluated. Combinations of rigidly attached stores should also be analyzed using the mission loadings as a guide. Rather extensive modifications to the clean-wing flutter results can be expected, especially for those stores most outboard on the surface. As above, steep gradients in flutter speed as a function of mass or inertia at a certain wing station should be studied and the phenomena properly identified and understood.

The introduction of pylon flexibilities is next undertaken. It is suggested that cantilever pylon modes (relative to the fixed wing) be coupled to the modes above (wing with rigid store attachments) directly in the flutter determinant during these early design studies when little data are available for precise prediction of coupled modes. The flutter determinant shown in Figure 7 can be configured such that it is necessary only to change a single diagonal element to change a particular flexibility; if store aerodynamics are ignored, only mass coupling exists between the store and wing coordinates. Flutter trends vs pylon flexibility can thus be obtained very efficiently and effectively. The hopeful result of these trend studies would be ranges of pylon stiffness where acceptable flutter margins exist. If satisfactory margins cannot be predicted, the entire analysis should form a basis for reevaluation of the situation and reconfiguration of the design.

The analyses described to this point can be regarded as a study, the output of which is a description of the flutter behavior of a particular aircraft when external stores are introduced. The knowledge accumulated to this point should be sufficient to plan the remainder of the theoretical analysis program. A relatively small number of cases should be chosen as representative and a detailed analysis of each performed. These cases will be a basis for monitoring the design as it progresses.

Flutter-Model Tests

Having completed the preliminary theoretical analysis, a flutter-model test program can be planned. An early goal of this program should be identification of the transonic flutter characteristics due to the presence of a store shape near the wing. Component models tested in a small, high-density blowdown tunnel are useful to this end. (See Figure 8.) The component models are not necessarily dynamically similar, but should have node lines similar to full scale and the proper thickness distribution. A vibration test is performed before tunnel testing so that an accurate determination of generalized mass and stiffness can be made for theoretical analyses of the models. A clean-wing flutter boundary is first obtained and the test repeated with a very lightweight store shape added to the model. The store is kept light so that only small changes in the wing modes occur, ensuring flutter at nearly the same tunnel condition. The difference between the two boundaries is now primarily a measure of the change in aerodynamics due to the presence of the store.

A large, low-speed flutter model, such as the one shown in Figure 9, is the most useful experimental tool to determine increments in flutter speed for a large variety of stores. This type of testing can be accelerated greatly with the use of a variable-inertia store whose internal weights can be positioned remotely for variations in store center of gravity and inertia. The use of a low-speed model is also an excellent way of assessing the influence of nonlinearities, such as free play, on store-flutter mechanisms. Low-speed models should be cable- or rod-mounted so that body freedoms are relatively uninhibited.

Free-flying transonic flutter models, such as those flown on cables in the NASA Langley 16-foot Freon Tunnel (Figure 10), are best suited to demonstrating margins in the transonic regime and investigating special problems associated with Mach number and altitude. The complex design problems and high fabrication and test costs associated with these models do not make them attractive for tests of more than a very few store configurations.

Ground Vibration Tests

The ground vibration survey of the flight article is traditionally performed just before first flight. It is costly, time-consuming, and complex, and it is unreasonable to perform complete aircraft vibration tests for each external-store configuration of interest.

An effective way of alleviating this situation is to perform vibration tests of isolated pylon/store configurations and couple these measured modes analytically to either calculated or measured modes of the aircraft without stores. A fixture must be provided which properly simulates the wing pylon attachment into a fixed base. (See Figure 11.) These measured modes are comparable to those used in the theoretical study described above. The aircraft modes should include those at least as high in frequency as wing second torsion so that enough wing deformation shapes are available as coordinates. The pylon store modes can be measured whenever the stores are available without access to the aircraft itself. When this approach is employed, several of the most critical cases should be checked by performing ground vibration tests on the fully loaded aircraft to demonstrate the accuracy of this analytical procedure. (Figure 12 shows a heavily loaded aircraft during a ground vibration survey.)

Flight-Flutter Tests

It is obvious that only a relatively small number of store configurations can be flight-flutter tested. To this end, it is important that an identification be made, based on all the analyses described above, of a few configurations which, when demonstrated in flight, will clear all remaining configurations of interest. This difficult and seemingly idealistic task can be accomplished if the flutter mechanisms are thoroughly understood and the pertinent parameters have been monitored throughout the design process. Put another way, money well spent to support the engineering analysis is money saved many times over in flight testing.

To make the flight test program as brief as possible, it is recommended that a dedicated control surface be installed on each wing to act as an exciter. A surface of this type is very effective in the frequency spectrum of interest. Ample excitation of the stores themselves can be achieved in this manner. Data acquisition methods should be comparable to those used for the clean aircraft, e.g., those described in Reference 1.

RECENT DEVELOPMENTS

In the past few years there have been some noteworthy developments in several areas which we believe will greatly ease the burden of the flutter analyst in his quest for a more practical solution to the wing-store flutter problem. Generally, these developments fall into three main categories: active flutter suppression, fast flutter routines, and flutter optimization.

The most promising application of active flutter suppression is to problems of wing external-store flutter, Reference 2. A considerable amount of analytical work, wind tunnel testing, and flight testing has been performed in the United States on this approach. Figure 13 is a schematic of the flutter-suppression system used in one of the studies. Active flutter suppression is attractive for store-flutter problems for three main reasons: store flutter instabilities are commonly very mild, which suggests that large increases in flutter speed are potentially achievable; a flutter-suppression system is adaptable to store loadings not covered in the original aircraft specifications and, accordingly, not covered by the original flutter-prevention program; and a wide variety of store-flutter mechanisms can conceivably be suppressed by properly adapting the electronically compensated feedback network.

In the field of fast flutter routines, two promising methods have been developed: one by McDonnell Douglas (Reference 3) and one by Northrop (Reference 4).

McDonnell Douglas has developed a high-speed wing-store flutter analysis program which features a data storage and retrieval system and diagnostic and interpolation subprograms. A classical vibration and flutter analysis routine which has been configured to treat wing-store cases in an optimum fashion is the central program in the group. Results from this program are permanently stored for later use. When a significant amount of data have been stored, the diagnostic program is used to provide information such as minimum flutter speed or flutter-speed gradient vs some pertinent parameter. When a new store is to be analyzed, the interpolation program is used to estimate the flutter speed instead of performing a complete analysis. The entire system is tied to a cathode-tube display and real-time control panel providing the flutter engineer with a powerful analysis tool.

Northrop engineers Cross and Albano have shown that computing time can be reduced considerably by using perturbation theory to find flutter speeds of wing-store combinations. The savings are accomplished by avoiding the repetitive and time-consuming operations of extracting eigen data from real dynamic matrices (vibration) and complex flutter determinants. A representative case is first solved by classical methods; a new store mass (or flexibility) representation is then chosen, which is expressed as an incremental change in the dynamic matrix; the roots and vectors for the new case are computed directly in terms of the original values and the incremental dynamic matrix using elementary algebraic relationships; an incremental flutter determinant is then derived from the new vectors, etc., and the perturbation equations are applied again. Northrop has been able to solve 1000 analyses per hour on an IBM 370/165 computer with this method.

These recent developments in wing-store flutter prevention have been directed mainly toward increasing the efficiency of flutter-speed computations for variations in design parameters, the so-called fast-flutter techniques. Although these techniques aid significantly in establishing flutter-speed/store-parameter trends, definition of the most critical design cases remains based largely on interpolation of the computed data. This implicit dependence on the extensive "mapping" of flutter-speed "contours" leads to considering the feasibility of utilizing a more direct numerical search procedure. The relatively recent derivation of an exact expression for the derivative of flutter velocity (Reference 5) with respect to design parameters leads to the possibility of employing a flutter-velocity gradient search to determine the critical (minimum flutter speed) configurations. Pylon stiffness, store mass, and store inertia would be considered as continuous design variables within the prescribed envelope of permissible values. Pylon stiffness parameters would be constrained not to fall below their strength-required values. The gradient-search approach would be used to determine directly a minimum flutter speed condition without the requirement for extensive contour mapping. For cases where more than one critical root exists for a given flight condition, the gradient search would necessarily be applied to each root separately to find the respective worst cases.

Having somehow arrived at a critical wing-store configuration, the next logical step in the design process is that of determining a "fix" to achieve a specified flutter-speed margin for selected critical cases. Up to now, this process has tended to rely rather heavily on engineering judgment. An automated procedure (Reference 6) has been developed recently for resizing a structure to meet both flutter and strength requirements for minimum weight increase. Although the reported method is currently being applied to structures having a single critical flight-flutter condition, it could be extended to multiple conditions, more typical of the store flutter problem, by holding the increased gage sizes resulting from redesign for one critical case as minimum gage for redesign for any subsequent case.

CONCLUDING REMARKS

We have attempted to show how the problem of aircraft/external-store flutter can be handled in a realistic and practical manner and how the magnitude of the problem can be reduced to manageable proportions. We have also touched on what we feel is the current approach in the United States to the design of aircraft which are required to carry a large assortment of external stores. Finally, some remarks on several promising new developments have been presented which provide the authors with some hope that in the future aircraft designers will be able to cope with this formidable problem in a more sophisticated manner.

REFERENCES

1. Baird, E.F., and Clark, W.B., "Recent Developments in Flight Flutter Testing in the United States," Presented at the 34th Meeting of the AGARD Structures and Materi..l Panel Lyngby, Denmark, 9-14 April 1972

2. Triplett, W.E., Kappus, H.P.F., and Landy, R.J., "Active Flutter Control - An Adaptable Application to Wing Store Flutter," A.I.A.A. Journal of Aircraft, November 1973

3. Ferman, M.A., "A Rapid Method for Flutter Clearance of Aircraft with External Stores," Air Force Flight Dynamics Laboratory Technical Report AFFDL-TR-73-74, Volume I, September 1973

4. Cross, A.K., and Albano, E.A., "Computer Techniques for the Rapid Flutter Clearance of Aircraft Carrying External Stores," Air Force Flight Dynamics Laboratory Technical Report AFFDL-TR-72-114, February 1973

5. Rudisill, C.S., and Bhatia, K.G., Optimization of Complex Structures A.I.A.A. Journal, Volume 9, Number 8, August 1971

6. Wilkinson, K, Lerner, E., and Taylor, R.F., "Practical Design of Minimum Weight Aircraft Structures for Strength and Flutter Requirements," Presented at the A.I.A.A. 6th Aircraft Design, Flight Test, and Operations Meeting, Los Angeles, California, 12-14 August 1974

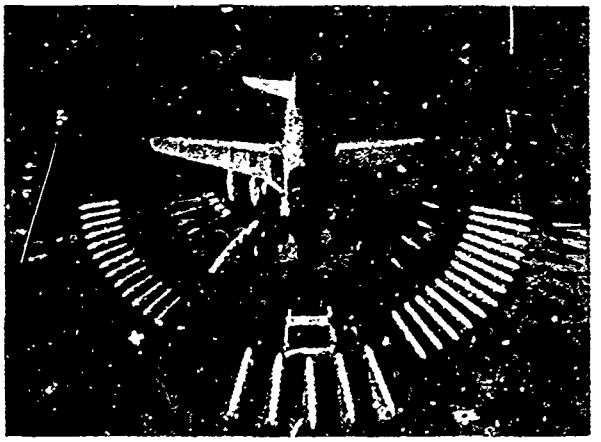

Figure 1

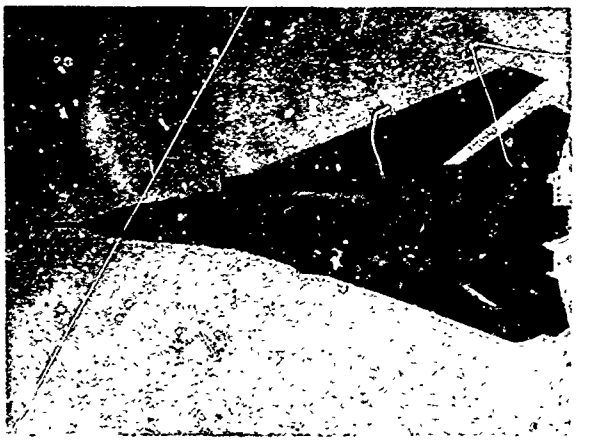

Figure 2

Figure 3

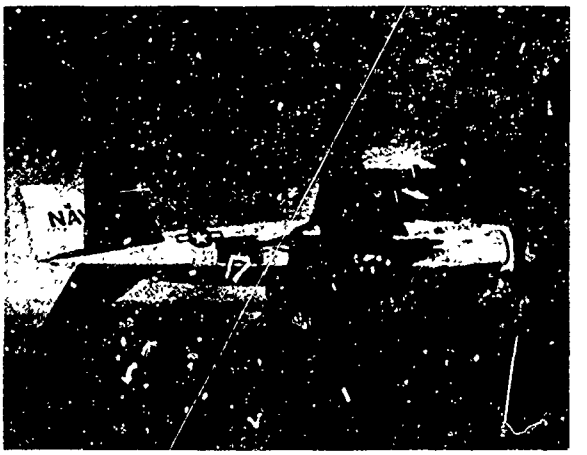

Figure 4

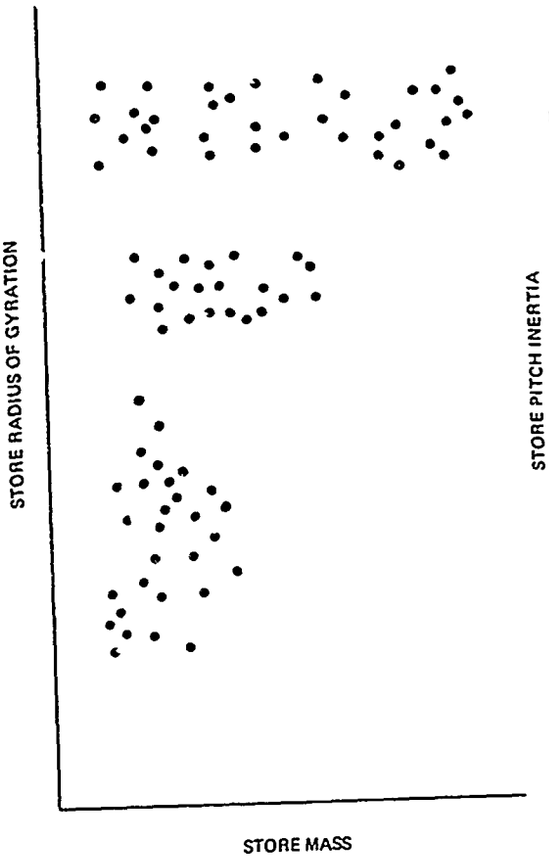

Figure 5

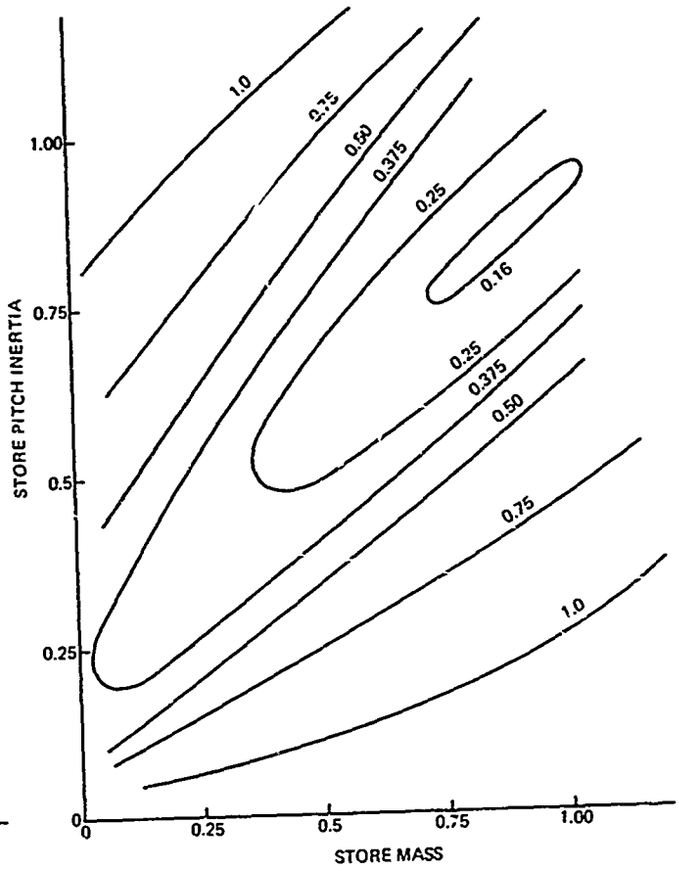

Figure 6

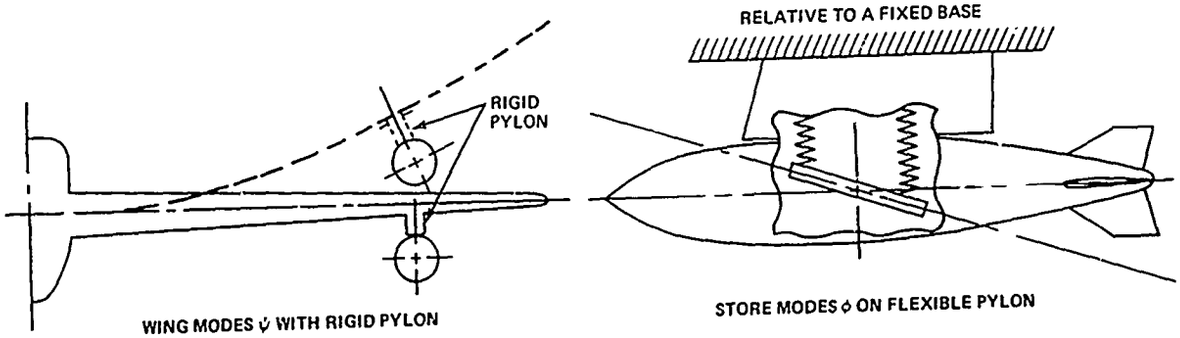

$$q = \begin{bmatrix} \text{WING MOTION} \\ \text{STORE MOTION} \end{bmatrix} = \begin{bmatrix} \psi & 0 \\ 0 & \phi \end{bmatrix} \xi$$

FLUTTER DETERMINANT $D = [M + A - \Omega K]$

WHERE:

$$M = \begin{bmatrix} M_W & M_{WS} \\ M_{WS}^T & M_S \end{bmatrix} \quad A = \begin{bmatrix} A_W & 0 \\ 0 & 0 \end{bmatrix} \quad K = \begin{bmatrix} K_W & \\ & K_S \end{bmatrix}$$

Figure 7

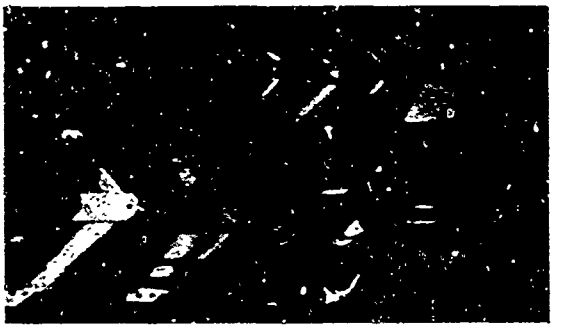

Figure 8

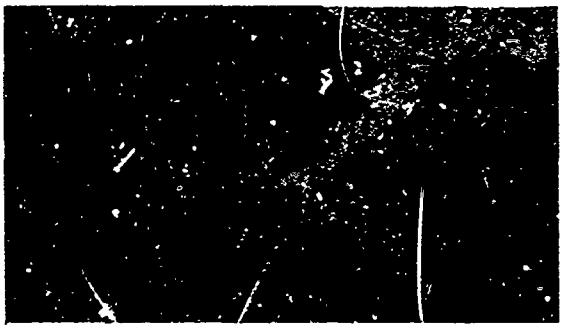

Figure 9

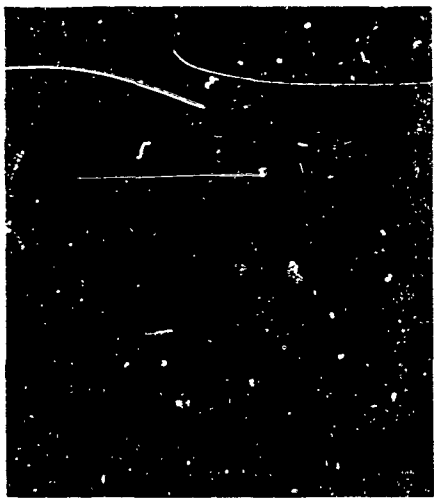

Figure 10

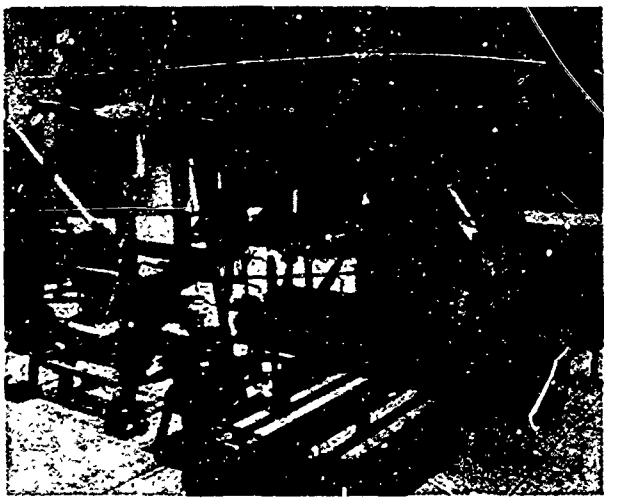

Figure 11

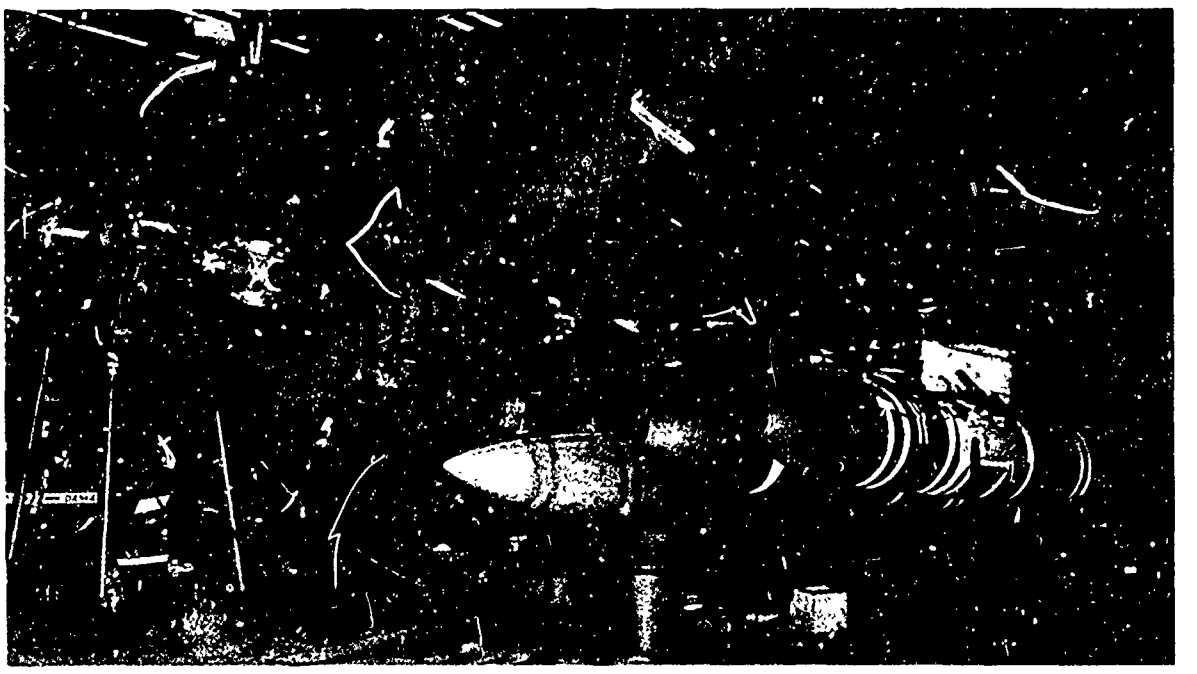

Figure 12

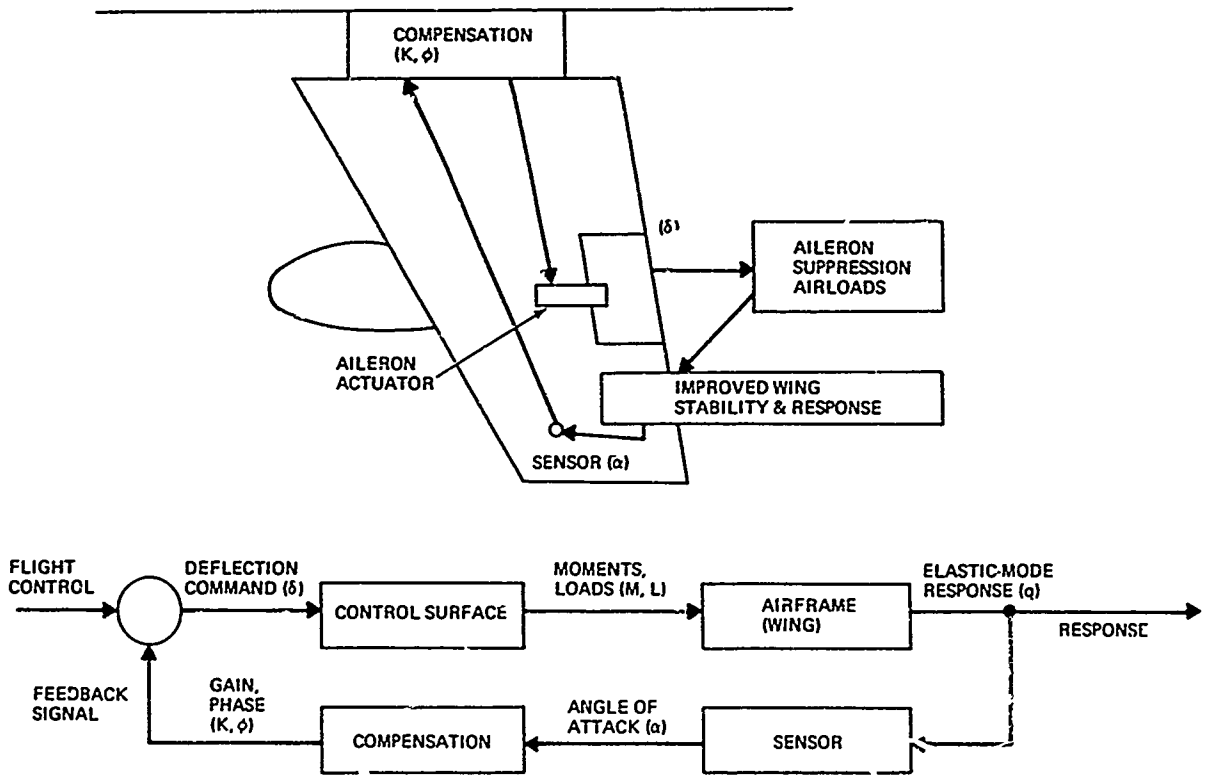
COMPENSATION
(K, ϕ)
(δ)
AILERON
SUPPRESSION
AIRLOADS
AILERON
ACTUATOR
IMPROVED WING
STABILITY & RESPONSE
SENSOR (α)
FLIGHT
CONTROL
DEFLECTION
COMMAND (δ)
CONTROL SURFACE
MOMENTS,
LOADS (M, L)
AIRFRAME
(WING)
ELASTIC-MODE
RESPONSE (q)
RESPONSE
FEEDBACK
SIGNAL
GAIN,
PHASE
(K, ϕ)
COMPENSATION
ANGLE OF
ATTACK (α)
SENSOR

Figure 13

RECENT ANALYSIS METHODS FOR WING-STORE FLUTTER

by
Walter J. Mykytow
Assistant for Research and Technology
Vehicle Dynamics Division
Air Force Flight Dynamics Laboratory
Wright-Patterson Air Force Base, Ohio
USA

SUMMARY

This paper first presents a summary or overview gleaned from a brief review of some of the literature on the practical aspects of wing-store flutter prediction and prevention. Brief comments are given on the advantages and disadvantages of various aspects of analytical and test procedures. Descriptions of improved analytical procedures developed for the United States Air Force is then given. Two methods are described in some detail and the results of the investigators are outlined. One is a rapid special purpose wing-store flutter analysis program called FACES. It has data storage and retrieval capabilities which together with a diagnostic and interpolation/extrapolation procedure estimate the flutter speed of new, similar stores. The system can be coupled to a cathode ray tube to increase man/machine interaction and reduce decision times. The other analysis method described is based on the perturbation approach. Computation times can be reduced 90% by using the previously available data. The method produces good results when the mass or stiffness changes are small so that in turn, eigenvalue and eigenvector changes are small. A graph of flutter speed versus important parameters can be produced in one minute on a modern computer. Limitations of the method are discussed.

INTRODUCTION

Modern capabilities in flutter analyses and subsonic and transonic wind tunnel flutter model techniques are used in the mid-term design period to determine the optimum location of pylon mounted jet engines on transports from a flutter avoidance standpoint. The chordwise and spanwise locations of the propulsion systems, and natural frequencies of their suspension systems, are selected to provide higher flutter speeds and avoid valleys of low flutter speeds. Such action is possible for a select critical number of "external stores" on fighters. However, this procedure is not possible for the vast number of externally mounted stores or weapons, since many other technical considerations force placement of stores on fighter wings at positions which adversely affect flutter characteristics. Fighter flutter speed placards on many stores are frequently in the speed range near M = 0.8 and thereby restrict and constrain the speed-altitude mission envelope which otherwise might be available to a field commander (Reference 1). Another adverse effect of the performance limiting placard is a noticeable reduction in survivability. Some relative evaluations indicate that moderate increases (12-15%) in speed near M = 0.8 at low altitude can almost double the survivability against anti-aircraft guns.

Another serious consideration for the engineer concerned with the prediction and prevention of flutter of wings carrying external stores is the potentially overwhelming magnitude of different store combinations that could be carried. It would not be unusual to be concerned with several thousand (10,000) realistic cases in analysis which are further evaluated and narrowed down by subsonic model tests to several hundred more critical cases. These cases in turn are reduced further to the most critical which are investigated by transonic-low supersonic speed model tests and additional final analyses. A limited number of representative stores exhibiting the main highlights are selected for flight flutter checkouts to substantiate safety and prove out the reliability of the process. Store inertia-flutter mode characteristic similarities are sought out to reduce the number of individual store investigations. However, the process is extensive, time and labor consuming and expensive.

The above briefly summarizes the balanced analytical-flutter model approaches used by most of the US contractors for wing-store flutter prediction and prevention. The spectrum of store loadings and flutter critical store loadings can be reduced by early discussions with the Air Force engineering and procurement agencies, the aircraft manufacturer and the using Air Force command. This includes a discussion of best pylon and suspension for critical stores and store release sequences to minimize speed restrictions. The dialogue should be maintained throughout the design and early life of the aircraft. This obvious type of action must be given priority and contacts must be renewed to arrive at the store (mass-inertia) loading spectrum possible on each pylon and rack.

Another essential aspect is a complete understanding of the physical-mathematical model for the subject aircraft with stores and the cause for the flutter conditions as a function of the store variations. Exploratory zero airspeed vibration and flutter calculations covering a reasonable part of the store mass-inertia matrix are absolutely necessary to locate modes which could couple due to frequency proximity (frequencies versus store parameter) and to obtain experience about the relative magnitudes of mass (or elastic) couplings which induce the flutter causing wing twist and also the subsequent adverse aerodynamic couplings. These calculations will then shed light on the more critical conditions and further calculations needed. They also can confirm or refute "rule of thumb" statements such as "locate heavy stores in-board and forward", which could produce more critical conditions for some aircraft.

This introduction ends by summarizing the highlights of a brief but not encompassing review of some literature on engineering prediction and prevention of flutter of wings with stores. The overview includes some recent comments by a few specialists and is given in the following Table I. One important new development is the potential use of active controls to suppress wing-store flutter (Reference 1). Comments on recent United States Air Force research on wing-store flutter analyses then follow in subsequent sections.

TABLE I. COMMENTS ON THE WING-STORE FLUTTER PREDICTION PROCESS

TOPIC	COMMENTS	REFERENCE
Computer Methods	Most analyses are conducted with digital computers. General Dynamics uses the Direct Analog Electric Analog Computer also in a parametric approach to obtain flutter boundaries rapidly and economically in terms of inertia versus weight for various c.g. conditions and velocities	2
	LTV employed a data storage and search system to evaluate different stores on the basis of inertial similarity. A library stores wind tunnel and flight data. Decisions are based on the evaluating engineer's experience and the location of the store's characteristics within an acceptable inertial similarity field.	3
Inertia Characteristics of Inert Bombs	Weight and inertia can vary 18%. Variations should be covered in analyses. Flutter speed could be very sensitive to and drop sharply with a moderate change in bomb weight for flutter modes involving rack bending, store pitch, and wing twist.	4 and 5
Fuselage Dynamics	The fuselage is sometimes relatively stiff so coupling is not large. However, in some cases, fuselage frequencies are in the range of wing-store flutter frequencies. The effective wing bending-to-torsion frequency ratio or root impedance is changed. Also, fuselage deformations produce a wing angle of attack at the root and cause aerodynamic coupling. This is very important for low aspect ratio wings with long root chords and can produce fuselage induced wing pitch and wing bending flutter. Active flutter control could be a good prevention approach in such case. Detailed finite element methods are sometimes necessary to predict fuselage and carry-through stiffness and dynamics.	Personal Comment
Pylon-Store Dynamics	This is the prime cause of flutter through production of mass coupling and adverse frequency ratios. Store motions including pitch produce wing twisting and aerodynamic coupling. Critical frequency ratios exist where bending type wing modes coalesce with higher torsion mode. Pylon or rack modes change effective critical wing bending torsion frequency ratios.	
	Flutter modes can occur which seem to be mostly confined to the stores. Modes are influenced by store aerodynamics and the use of fins is beneficial for preventing flutter.	6
	A good definition of the store-pylon dynamics including wing connections is essential but can be complicated for higher complex rack modes. Ground vibration and stiffness tests and analytical correlations are essential, but cause a problem in that test data cannot be obtained early for analyses and model tests. Wing, pylon, fuselage and carry-through stiffness coefficients can be approximated early by finite element models.	
	Cantilevered store-pylon tests can be conducted to determine resonant frequencies and back-calculate influence coefficients.	7 3 and 8
	Proper dynamic simulation of tip missiles and launcher rails through similar tests are required. Tip modal deflections are important for proper estimation of aerodynamic coupling.	7
	Cantilever pylon-store tests, while useful, can be influenced by too much flexibility in short wing section-sturdy jig tests. Centerline pylon-store modes were developed successfully from vibration tests with wing and fuselage on jacks, however. Pylon and rack stiffness characteristics can be non-linear (buckling). Effective fuel inertia characteristics can be approximated by conducting tests on empty and partially full fuel tanks and using the stiffness data determined from the empty tank vibration tests.	7
Model Tests	Both subsonic and transonic tests are employed generally with analyses for balanced approach. Lower frequency fuselage degrees of freedom are included as well as lower mode pylon or rack-store freedoms.	3,5,6,7,8,9, etc.

TABLE I. COMMENTS ON THE WING-STORE FLUTTER PREDICTION PROCESS (Cont'd)

TOPIC	COMMENTS	REFERENCE
	Special tanks or shells are used together with variable or movable masses to cover inertia-mass range of stores. This may not be a sufficiently detailed representation of bombs on Multiple Ejection Racks. Perisho mentions that a shell model with coarse variations of inertia did not produce acceptable results. Use of fore and aft bombs on model MER rack produces mild store flutter mode involving S shaped lateral bending mode of rack. Bomb nose changes and bomb fins eliminate flutter. Thus higher order rack modes and store dynamics can be important.	6
	Following initial model program with extensive analysis to define flutter modes which have gradual loss in damping and the symmetry, LTV uses half-span symmetric model as main source of flutter data. Full span tests showed flutter velocity is extremely sensitive (+40% increase) to 10% (+5%) asymmetrical (LH/RH) difference in pylon frequencies. Also, velocity is very sensitive to small pylon c.g. (1/4 inch on aircraft) asymmetry. Planform symmetry adjustments improve model behavior significantly also, and provide some different results. Pylon dynamics are critical and require accurate determination from stiffness and ground vibration tests. TER flexibilities modeled from ground vibration test results. Rigid TER tests are conservative generally, but one long store model test without fin shows unconservative results (no flutter on rigid TER). Flexible TER model and flight tests confirm limited rack-store flutter. LTV has probably now evaluated approximately 10,000 store combinations for subject aircraft. Clean wing flutter speed well above limit dive speed.	3 and 8 5 3 and 8
	LTV later conducts half-span subsonic and larger transonic model tests. Due to sensitivity of flutter to store rack parameters, rack influence coefficients are obtained from rack vibration data rather than stiffness tests. Pylon discrepancies on previous smaller transonic model are eliminated. Low speed and transonic model test results agree rather well with flight data, although transonic model results indicate somewhat conservative results.	8
Store Aerodynamics	Frequently, store aerodynamics are not included in analyses and lowly damped modes are evaluated with some apprehension pending test data. However, subsonic unsteady aerodynamic methods now exist for reasonable approximation of pylon-store aerodynamics. Effects are expected to be small in many cases.	10
	Tip missile unsteady aerodynamics are difficult to predict but are important. Flow separation effects at transonic speeds could be important but are difficult to approximate Calculations for various wing mounted store and tip missiles do not produce consistent results.	7
	Some flutter modes occur which seem to be confined to motion of stores and are influenced by store aerodynamics. Use of fins is beneficial.	6 3
	Interference was suspected between fuselage nacelle ducts and inboard pylon-store. Flow-through-nacelle-duct might change flutter speed of inboard pylon on transonic model and therefore was employed. Proper simulation of fuselage-wing cavity seals is important.	9
Store Loadings	Individual pylon loadings do not produce independent flutter effects. Frequency proximities, mass coupling and aerodynamic coupling can produce widely varying results for different airplanes	
	Some comments made by S. Schwartz for one aircraft are:	7
	1. Careful attention is required for light tip stores with heavy inboard stores. Results are sensitive to the centerline store carried.	
	2. High flutter speeds result with heavy tip stores with forward cg and with inboard stores.	
	3. Analyses are less likely to accurately predict tip store and outboard store cases than other cases.	

TABLE I. COMMENTS ON THE WING-STORE FLUTTER PREDICTION PROCESS (Cont'd)

TOPIC	COMMENTS	REFERENCE
	4. Flutter speeds with all stores loaded were most difficult to predict but satisfactory target or placard speeds could be established based on mission performance requirements and lower store limitations and speeds.	
Coupling with Control System	Heavy stores or moderate to light tip stores reduce the natural frequencies of the wing-store system significantly so that coupling with the natural frequencies of the control system are possible. Brock covers a static or mechanical coupling problem. However, as is well known, dynamic coupling is possible and needs to be predicted and prevented. Aeroservo-elastic prediction methods are available and are not discussed here. A closely related and reverse problem to aeroservoelasti-city is active flutter control where a high frequency SAS system is used a priori to advantage.	11 1

THE FACES WING-STORE DIGITAL COMPUTER - CRT SYSTEM

Fast computer programs are required to reduce the cost and time of extensive analyses for very large numbers of stores, to determine the more critical stores and their flutter speeds, and to reduce number and costs of flutter model tests and flight tests. One such research-development program was conducted for the Air Force Flight Dynamics Laboratory (AFFDL) by Ferman et al., of the McDonnell Aircraft Company and is reported fully in Reference 12 and summarized in Reference 13. Later figures are excerpts from these documents.

In addition to the development of a fast flutter routine, the AFFDL considered that R&D was needed for systematic accumulation and retrieval of the large quantities of data which were too great for one or two individuals to recall and use from human memory. Furthermore, difficulties were frequently caused by transfer of key flutter engineering personnel when the aircraft was in main use leading to delays and difficulties in flutter decisions and considerable repeating of previous indoctrination and training. Other R&D requirements specified by AFFDL were the development of an interpolation-extrapolation procedure for new but similar stores and investigation of the potential of man-machine interfaces using the cathode ray tube and associated controls. The data storage retrieval, diagnostic-interpolation-extrapolation, and CRT control developments were of moderate scope in view of the resource limitations. However, they proved successful. The CRT aspect proved very valuable for a priority flutter prevention study on a different problem for a new design.

The above requirements resulted in a computer system called FACES (Flutter of Aircraft with External Stores). The procedures have been checked out and the computer program is being employed extensively now by several USAF contractors and USAF organizations. Well over 5000 store configurations have been recently investigated using this system for several aircraft. This program or system is outlined on Figure 1.

The main characteristics of the Fast Flutter Routine are outlined in Table II. The wing simulation is based on sectionalized chordwise rigid strips. This beam procedure has been found to be generally adequate for fighters. However, the program can also accept mode shapes and frequencies from external inputs in case chordwise deformations are present on lower aspect ratio wings. The incorporation of a mini-finite element structural analysis module is a future possibility. The Fast Flutter Routine (FFR) can use subsonic strip, subsonic lifting surface, or supersonic piston theories. Other aerodynamic information can be inserted from other external sources. Notice that the program can handle five pylons per side. Each pylon is represented as a rigid body restrained at top and bottom with six degrees of freedom, whereas each Multiple Ejection Rack (MER) has six degrees of freedom to represent three rigid sections which are elastically connected.

Figure 2 shows the Data Storage and Retrieval System flow. It accepts data internally from the Fast Flutter Routine for the four modes with the lowest flutter speeds or from other external data, either theoretical or experimental. The data control is accomplished by KEYS which are groupings of five two-digit words. The ten digit words code five physical properties. The number of words required increases with the number of stores carried. If the key code matches, stored data information is listed as a result of the retrieval request. Otherwise, DSRS can be used in a further process with diagnostic and interpolation-extrapolation procedures described next.

The Diagnostic Process (DIAPR) and the Calculation Interpolation Decision Process (CID) operate as a combined process. Table III shows the sensitivity information used as engineering reminders and for aiding engineering evaluations. Sensitivity criteria are built into the program. If a new store satisfies these criteria, then CID uses these stored data to estimate the similar but new store's flutter speed. The user is notified regarding satisfaction of acceptance or sensitivity criteria. Figure 3 is a carpet type diagram and outlines a limited but successful application of the data storage and retrieval system. The various cases show that stored data are retrieved and listed when data matches exist. Two cases show no data are retrieved (paths 4 or 6) if there is no parameter match. If no exact match results, the combined DIAPR/CID module can be asked to delete a variable and perform a trend study. Three or more matches from a trend study are required to estimate flutter speeds of new stores. Simple (parabolic) curve fittings are used for estimates. Extrapolations are acceptable if the parameter is within 20% of maximum or minimum values of the parametric stores data and if flutter velocity derivative data or

acceptance criteria are within specified ranges (velocity-damping crossing is not too shallow or velocity does not vary too rapidly with the parameter). The 260 knot estimated flutter speed at a pitch inertia of 2 X 10^6 lb inches^2 and 600 lbs was extrapolated but was questioned by the acceptance criteria because the pitch inertia of the store was well outside the 20% data range criterion.

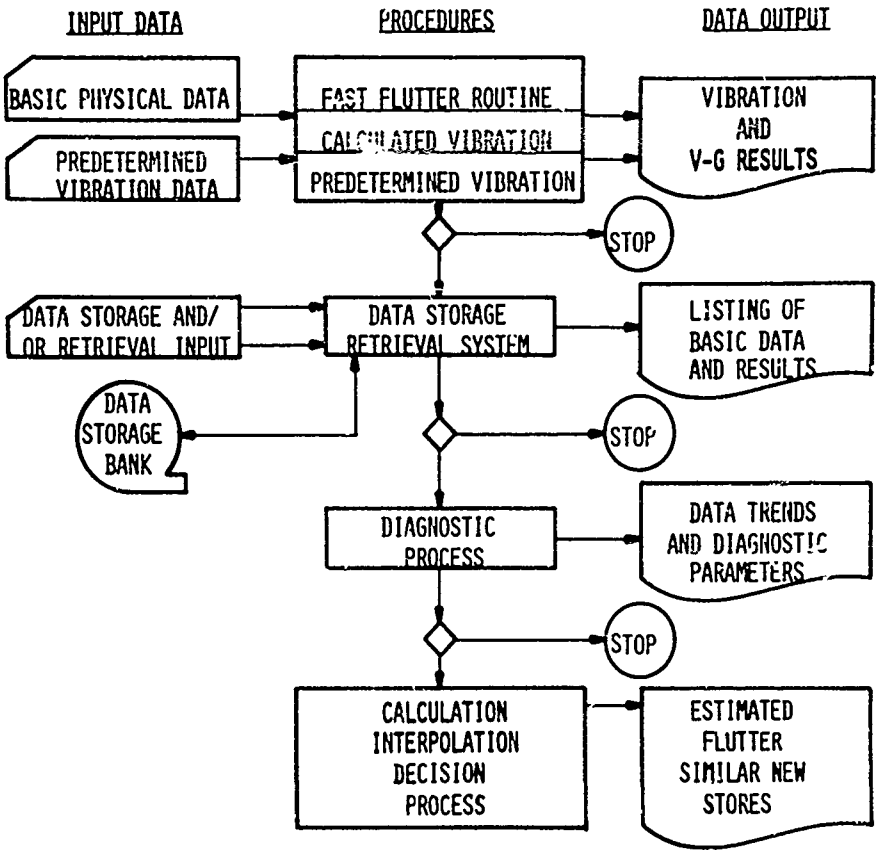

FIGURE 1. BLOCK DIAGRAM FOR FACES DIGITAL COMPUTER PROGRAM

TABLE II: OUTLINE OF FAST FLUTTER ROUTINE CHARACTERISTICS

- CANTILEVER, SYMMETRIC, ANTISYMMETRIC
- 14 WING SECTIONS - SERIALLY KINKED ELASTIC AXIS
- STREAMWISE MASS, ELASTIC AXIS MASS
- TWO WING-ROOT FREEDOMS, STIFFNESS OR INFLUENCE COEFFICIENTS
- WING EI AND GJ STIFFNESS OR INFLUENCE COEFFICIENTS
- FIVE PYLONS PER SIDE - - MER, TER, SINGLE STORES
- 5 FREEDOMS, SPRINGS, INFLUENCE COEFFICIENTS FOR EACH PYLON
- 6 FREEDOMS, SPRINGS, INFLUENCE COEFFICIENTS FOR EACH MER RACK
- SAVE WING MASS, STIFFNESS, EFFECTIVE MASS
- STRIP THEORY, LIFTING SURFACE AND STORE AERO, PISTON THEORY
- MULTICASE OPTIONS: (FLUTTER)

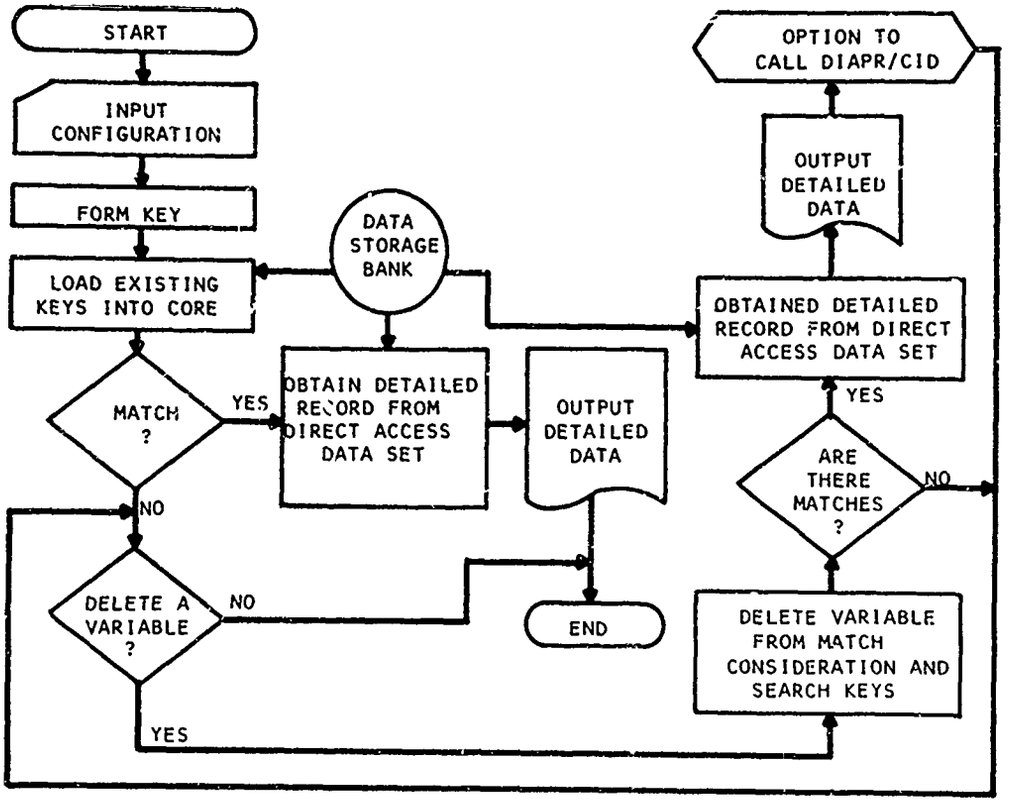

FIGURE 2. DATA RETRIEVAL FLOW

TABLE III. DESCRIPTION OF DIAGNOSTIC PARAMETERS

SYMBOL	NAME	FUNCTION
$(V_F)_M$	MINIMUM FLUTTER SPEED	TO ESTABLISH THE MINIMUM FLUTTER SPEED SPEED FROM A FLUTTER SPEED TREND VS A PARAMETER
$(V_F)_R$	REQUIRED FLUTTER SPEED	USED TO ESTABLISH FLUTTER CLEARANCE
$(V_F)_A$	ASYMPTOTIC FLUTTER	TO ESTABLISH THE FLUTTER SPEED ASYMPTOTE
$(\zeta_F)_A$	ASYMPTOTIC ζ	TO ESTABLISH THE PARAMETER VALUE ζ_A WHERE $\Delta V/\Delta\zeta \to \infty$
$\Delta V/\Delta G$	FLUTTER SENSITIVITY	TO ESTABLISH FLUTTER SPEED GRADIENT WITH DAMPING
$(\Delta V/\Delta\zeta)^*$	FLUTTER GRADIENT	TO ESTABLISH FLUTTER SPEED GRADIENT WITH CHANGES IN A PARAMETER
F_C	FLUTTER CLEARANCE FACTOR	TO ESTABLISH FLUTTER SPEED CLEARANCE IN PERCENT, EQUALS $[(V_F)_M - (V_F)_R] \quad (100)/(V_F)_R$
ACT	ACCEPTANCE CRITERIA	EVALUATES FLUTTER SENSITIVITY BEHAVIOR AND ESTIMATED FLUTTER

$$\frac{\Delta V}{\Delta G} = \frac{V_J - V_{J-1}}{G_I - G_J - 1} \qquad \left(\frac{\Delta V}{\Delta \zeta}\right) = \frac{(V_J - V_{J-1})/V_J}{(\zeta_J - \zeta_{J-1})/\zeta_J}$$

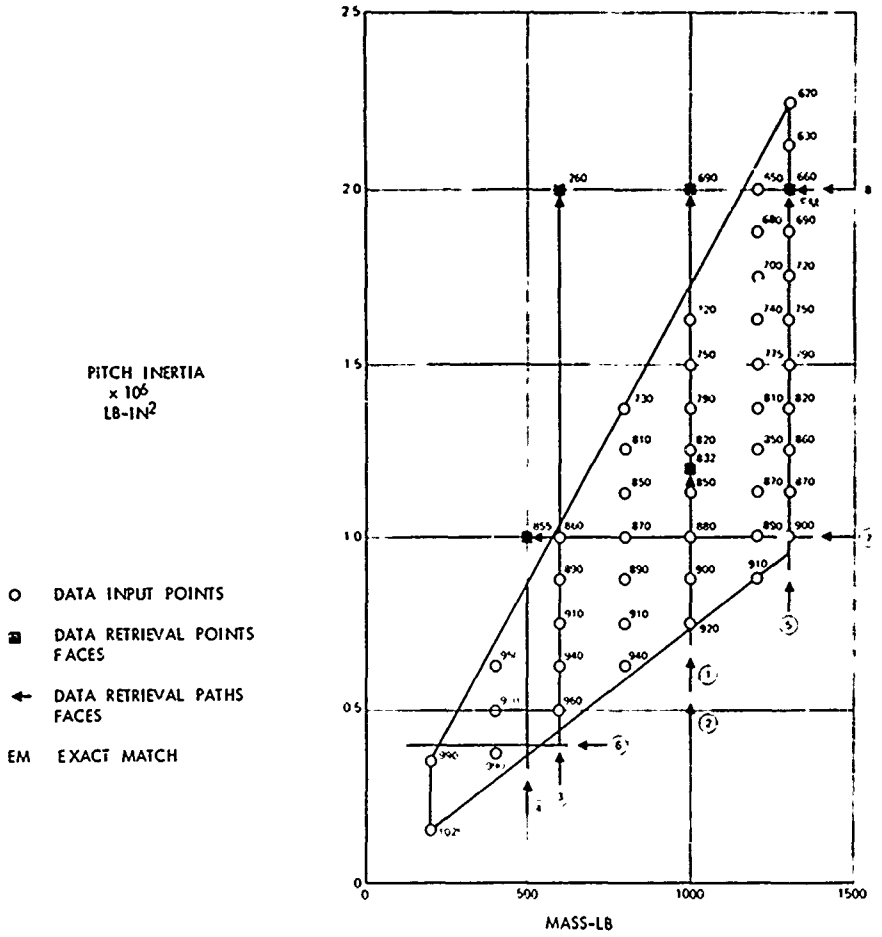

FIGURE 3. DSRS RESULTS FOR FIGHTER WITH POD AT 60% SEMISPAN

One version of FACES is coupled to a cathode ray tube system to increase interface between engineer and the computer, control computations, accomplish rapid variations of parameters, display results and accelerate turn-around time and engineering decisions. Flutter data from the CRT mode of operation are incorporated into the storage system.

The CRT system can display a list of natural frequencies and as shown in Figure 4, also display mode shape information. Such data should be valuable in indicating the likelihood of flutter due to proximity of frequencies of important modes and the amount of response coupling between wing-pylon-store components in a mode as well as the amount of relative wing twisting. The latter could be an indication of aerodynamic coupling. The CRT user options are: Display Eigenvectors, Display Deflections, Plot Deflections, Change Input Matrix Data, Change MER Rack Configuration, Redisplay Frequencies, Rerun Vibration, and Vibration Analysis Complete. The program also displays flutter mode crossing in terms of mode number, flutter speed and frequency. Damping versus velocity and frequency versus velocity trends are displayed. Root sorting is employed to track modes. These capabilities are shown in Figure 5 which also simulates an actual application case. Figure 6 shows a simulation of an actual display of data retrieval, flutter speed estimates and diagnostic information. The acceptance criteria reject the estimates because the required flutter speed is too close to the minimum flutter speed for the parameter. Also, the estimated flutter speed could be adversely affected by damping uncertainty caused by a shallow g-V curve. Figure 7 shows some comparisons of FACES data with data from other methods and the trend of flutter speed with bomb ejection sequence. However, it could be an illustration of a future capability in machine/flutter engineer interaction and fast flutter evaluations.

As previously mentioned, the wing-store flutter analysis system called FACES has been checked out by many comparisons with results from other computer programs. It is in extensive use today at several industrial firms and US Government organizations, and is an extremely valuable tool for screening many store combinations to determine satisfactory or critical store combinations. The time and cost savings of the FACES program have been evaluated relative to a similar method. The same engineering skill and wing finite section approach was used to provide a fair comparison. Figure 8 shows that a 2 to 1 reduction in costs and core occupancy in favor of FACES results when carrying two stores per side. The advantage increases to 3 to 1 for four stores per side. Other special purpose programs could, of course, reduce the advantage.

Future improvements could include a mini-finite element structural analysis method for wing, wing root, pylon and rack. Any fast finite element structural model should avoid extreme detail in favor of speed. Other future possibilities are incorporation of low supersonic Mach number aerodynamics; improved procedures in data storage-retrieval, diagnosis, and interpolation and extrapolation; incorporation of pitch inertia-mass carpet plot capability (displaying points or contours of constant velocity in the inertia-mass plane); a multi-surface fit for estimating flutter characteristics for new stores in lieu of a curve

fit; and display of plots of store deflections relative to the wing on the CRT. More applications of data storage, retrieval, new store flutter evaluations and the CRT capability are certainly needed and some will be performed by AFFDL.

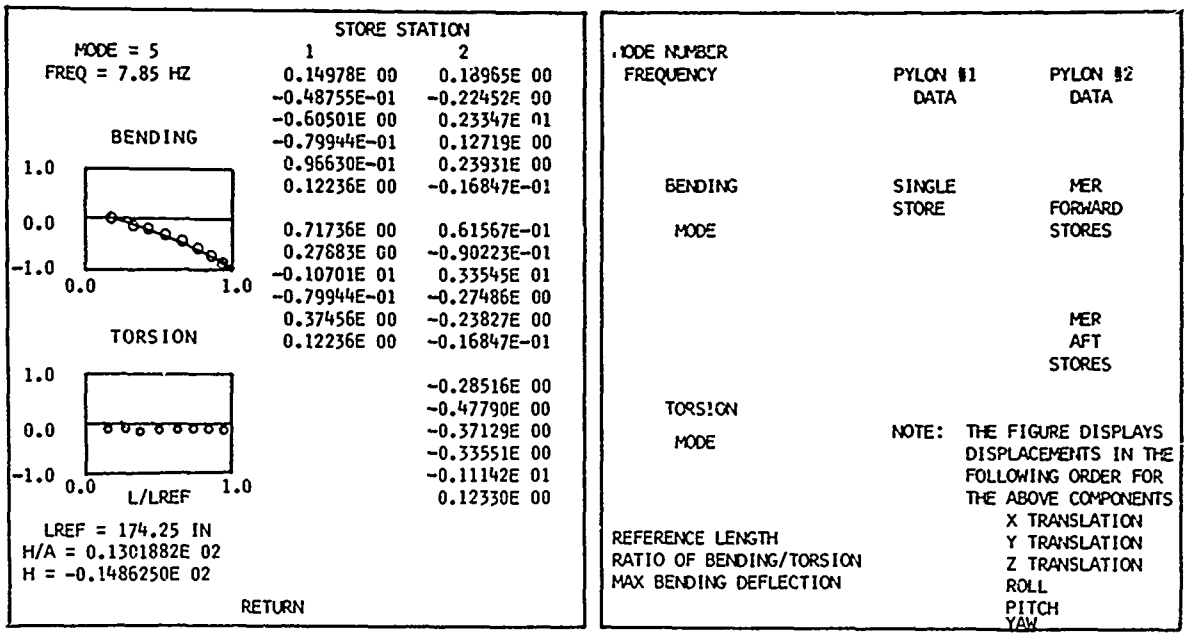

FIGURE 4. CRT GRAPHICS VIBRATION DATA FOR FIGHTER WITH STORES ON TWO PYLONS PER SIDE

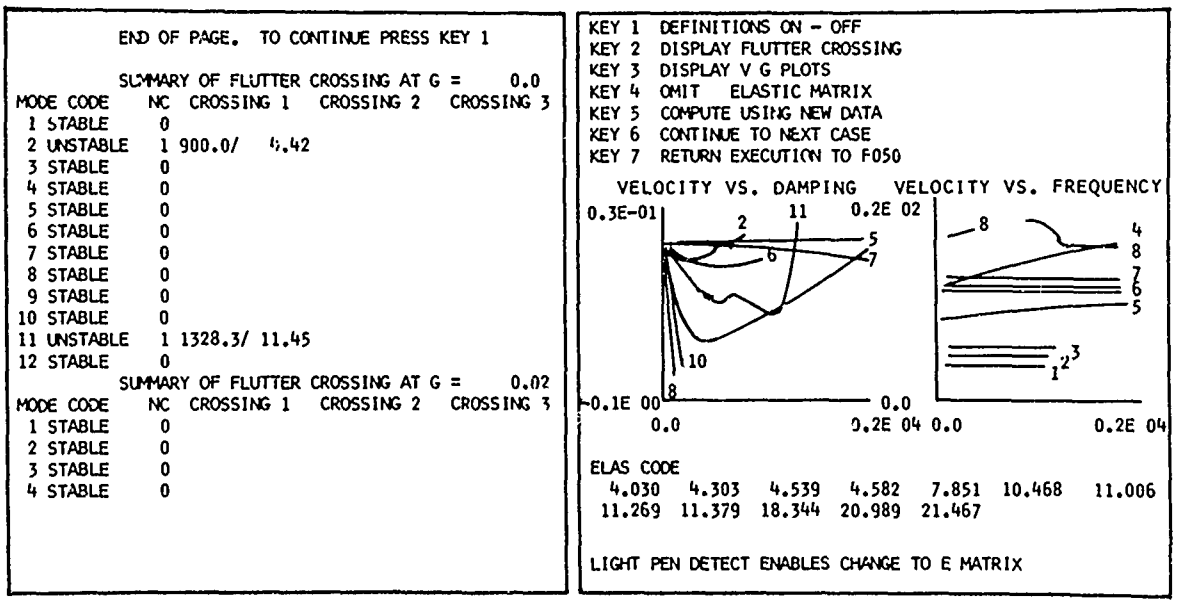

FIGURE 5. CRT GRAPHICS FLUTTER DATA FOR FIGHTER WITH STORES ON TWO PYLONS PER SIDE

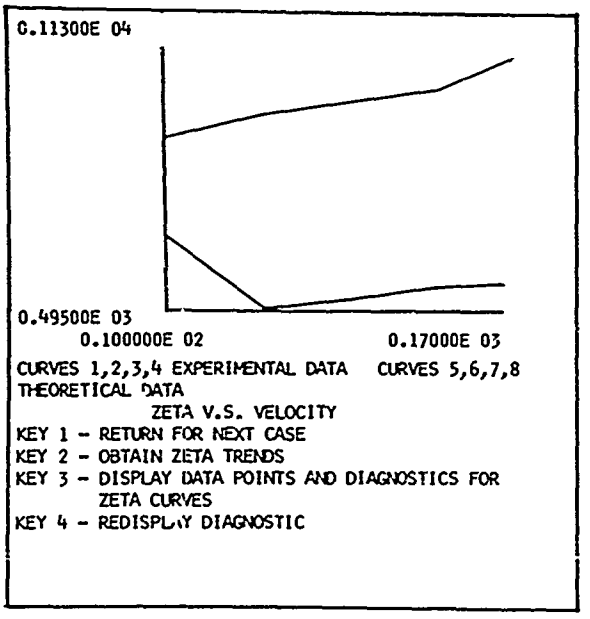

THEORETICAL CURVE NO. 5 INFORMATION
RETRIEVED DATA

SPEED	ZETA	DV/DG	FREQ
595.0	0.10000E 02	100000.0	8.5000
495.0	0.50000E 02	100000.0	8.5000
502.0	0.10000E 03	100000.0	8.5000
530.0	0.15000E 03	100000.0	8.5000
535.0	0.17000E 03	100000.0	8.5000

HORIZONTAL ASYMPTOTE V = 595.00 ZETA = 0.1000E 02
NO VERTICAL ASYMPTOTE
MINIMUM FLUTTER SPEED = 480.0 CORRESPONDING VALUE DV/DG
99999.9 ZETA = 0.72614E 02
DIAGNOSTICS FOR REQUESTED ZETA = 0.20000E 03
ESTIMATED FLUTTER SPEED = 535.9
ESTIMATED DV/DG = 100000.0
REQUIRED FLUTTER SPEED = 550.0
FLUTTER CLEARANCE FACT = -2.57
THIS CURVE FAILED SENSITIVITY CRITERIA
DV/DG.GE.2500.0, FIXED ZETA, -1 PERCENT.FE.FC.LE10 PERCENT
KEY 1 - RETURN FOR NEXT CASE
KEY 2 - OBTAIN ZETA TRENDS
KEY 3 - DISPLAY DATA POINTS AND DIAGNOSTICS FOR ZETA CURVES
KEY 4 - REDISPLAY PLOT

FIGURE 6. DISPLAY OF CRT DATA STORAGE-RETRIEVAL AND CALCULATION INTERPOLATION DECISION PROCESS

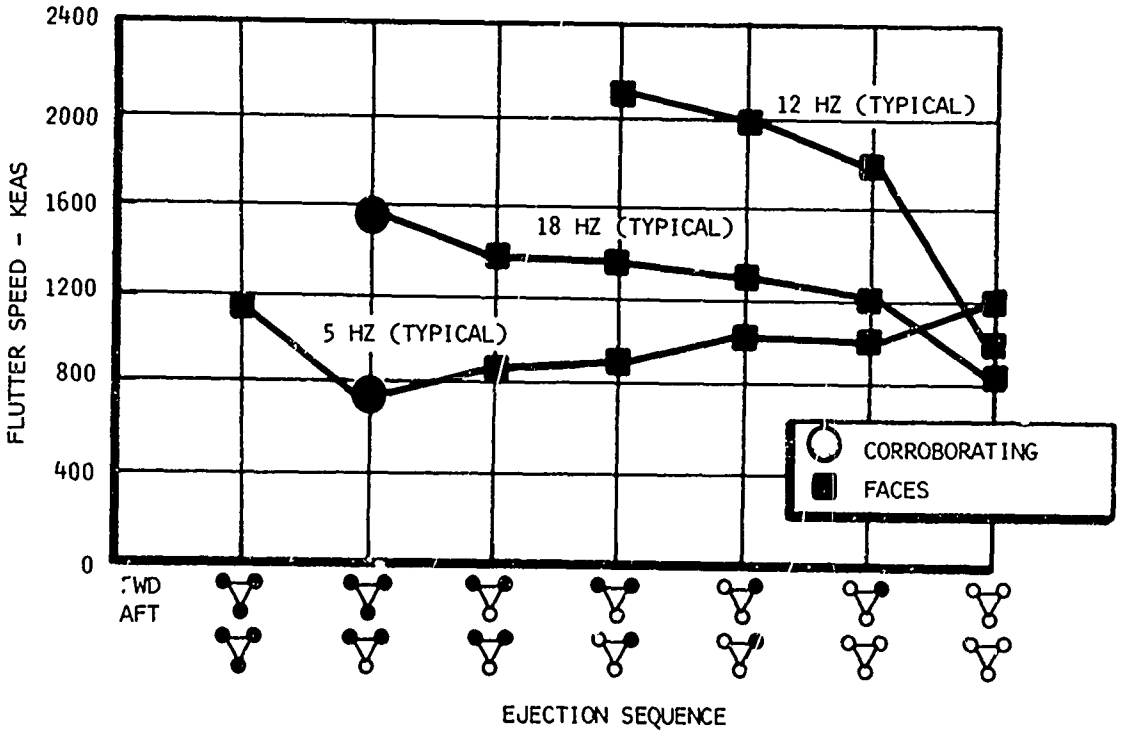

FIGURE 7. FLUTTER SPEED FOR BOMB EJECTION SEQUENCE FROM ONE AIRCRAFT PYLON

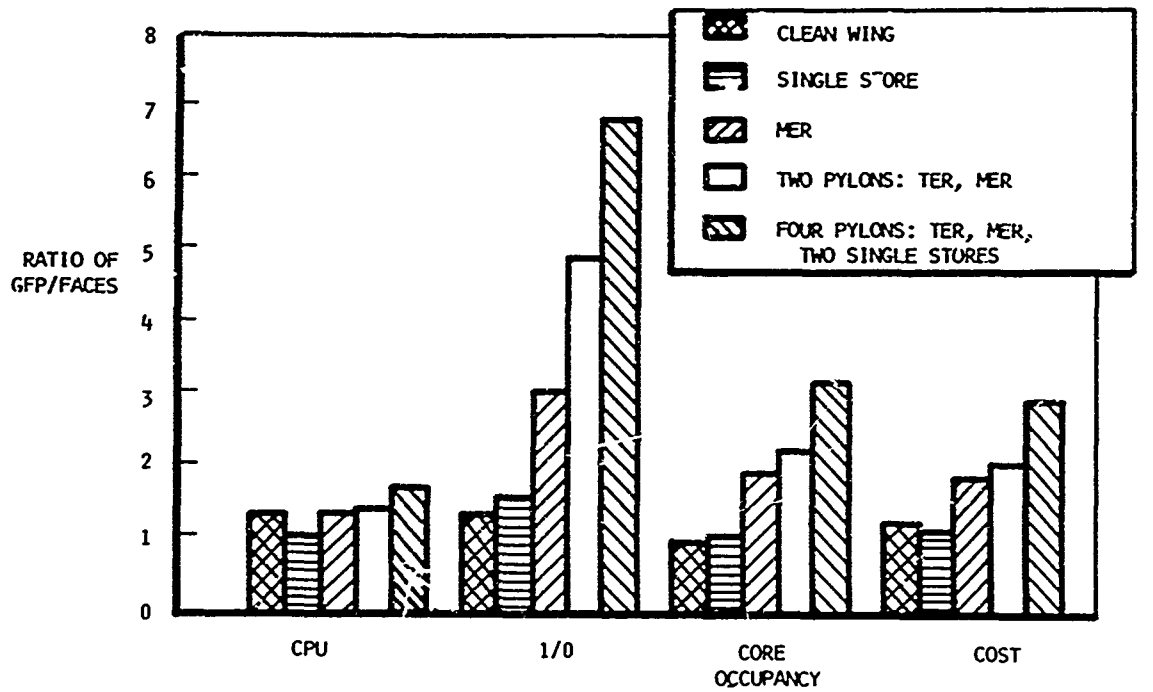

FIGURE 8. TIME AND COST COMPARISON GENERAL FLUTTER PROGRAM AND FACES

THE PERTURBATION METHOD

Another approach which could expedite the flutter analyses of wings which carry many store combinations is the perturbation method. The potential of this method for dynamic analyses has been discussed by van de Vooren, Scrbin, Flax, and Siegel and Andrew (References 14 to 19). Cases exist where changes to planform, inertia, or stiffness parameters are sufficiently small so that corresponding changes in the flutter and vibration eigenvalues and eigenvectors are also small. Then the new values can be approximated through perturbation methods using a considerable amount of the previous data and approximating the increments without eigenvalue extractions. This can be accomplished with considerably less work and cost.

At the request of AFFDL, Cross and Albano of the Northrop Corporation, developed a third order perturbation method for predicting the vibration and flutter characteristics of aircraft with wing stores (Reference 20). It simulates the free flight condition and accounts for rigid body freedoms. Perturbation flutter analyses are made only if the zero airspeed vibration modes have converged. Second order terms for the eigenvectors are used in the perturbation vibration and flutter analyses to estimate effects of moderate changes in parameters. The third order flutter eigenvalue term is used to evaluate convergence. The perturbation method developed was applied to eight series of wing-store combinations having 63 elastic degrees of freedom and 3 rigid body freedoms for each symmetry. Up to four underwing stores per side were used in some applications having 24 store-pylon degrees of freedom.

Some of the results obtained by Cross and Albano will now be presented and discussed. For many cases there was very little difference between results from exact (classical) methods and those from the perturbation method. However, in some cases involving larger perturbations or complications due to proximity of modes, the perturbation method did not give converged results.

Results for variations in the chordwise location of a tip missile are shown in Figure 9. The perturbation method results are in excellent agreement with corresponding data from classical methods. For the minus 20% chordwise location of the tip missile cg there is a switch in flutter mode compared to the basic 0% chordwise case. Figure 10 shows the g-V curves for both cases and the mode switch. Both modes are well predicted using the same basic case as a start. Use of more modes (12 in lieu of 9) improves the agreement.

Figure 11 shows another good agreement between methods for the case of tip missile inertia variation (for different missiles) and when an outboard store is carried. Similar good agreement is obtained for variable tip store pitch inertia while carrying an inboard store.

Coupling between inboard and outboard stores can produce close proximity of baseline frequencies and a lack of convergence in the perturbation techniques. Smaller perturbations could obtain better trends. Figure 12 shows non-converged results when baseline vibration frequencies have 3% separation. The 160 slug-ft^2 pitch inertia symmetric perturbation case compares well with data from conventional procedures. However, there is a rapid rise in flutter speed on each side of the basic case. The lack of convergence indicates a steep gradient. The antisymmetric case gives somewhat better results but agreement is handicapped by changing conditions near a pitch inertia of 110-120 slug-ft^2. However, flutter velocities are extremely high and well above practical values.

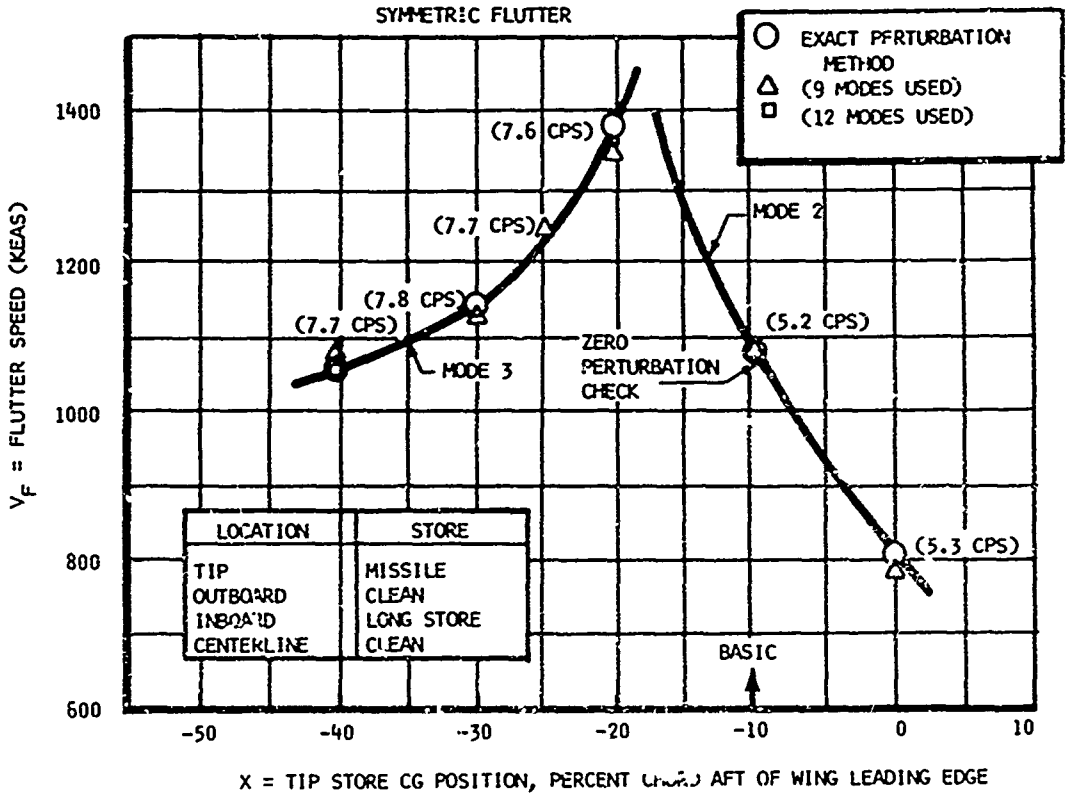

FIGURE 9. COMPARISON OF RESULTS FOR TIP STORE CENTER OF GRAVITY VARIATION

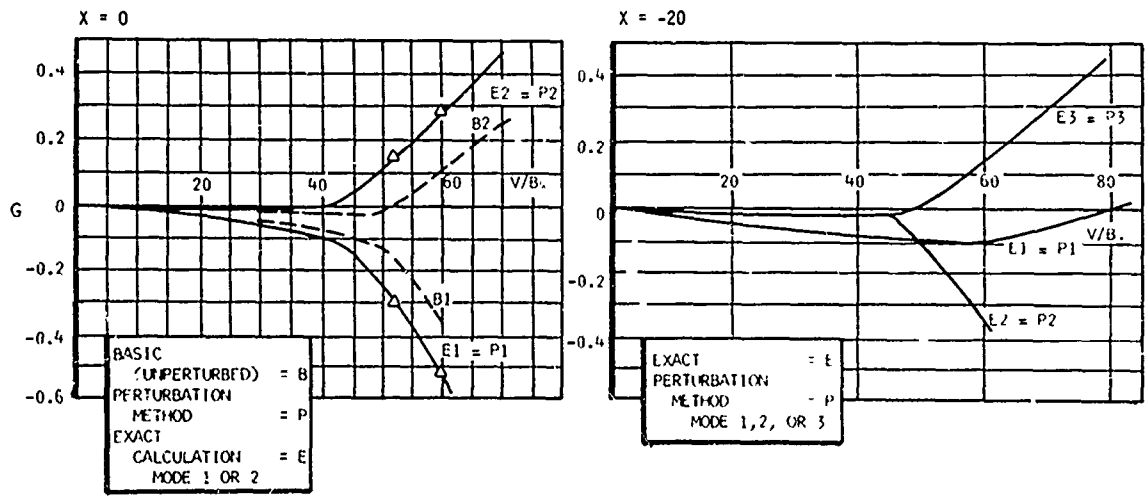

FIGURE 10. V-G CURVES FOR TIP MISSILE C.G. AT X = 0 AND -20 PERCENT CHORD AFT OF LEADING EDGE

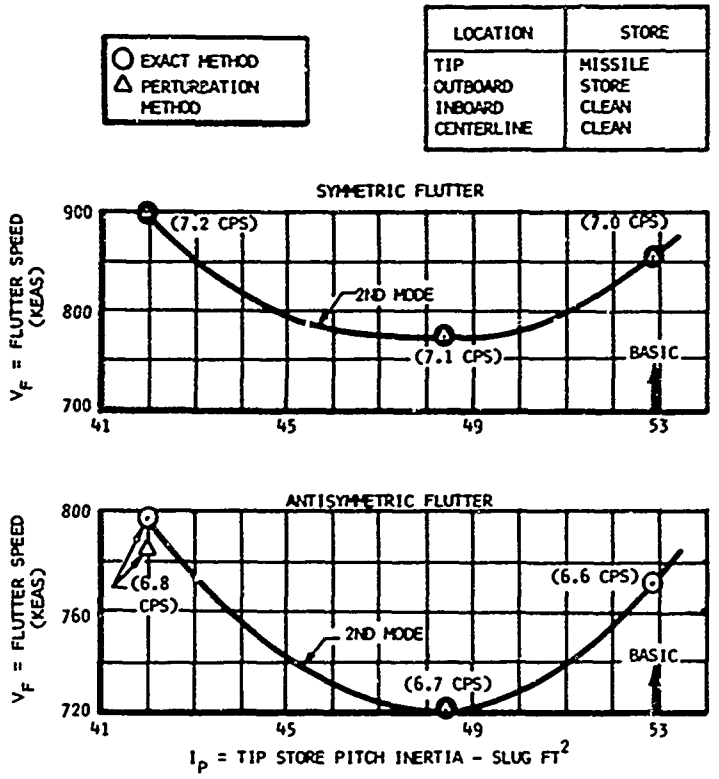

FIGURE 11. COMPARISON OF RESULTS FOR VARIABLE TIP STORE INERTIA

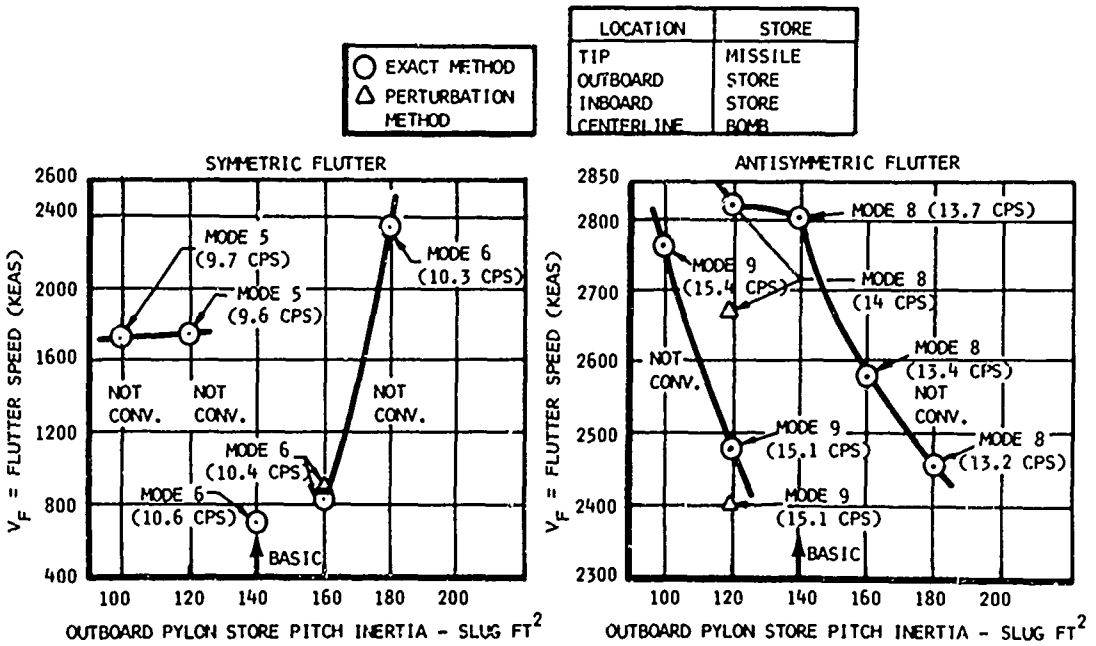

FIGURE 12. COMPARISON OF RESULTS FOR CONDITION WITH TIP, OUTBOARD, INBOARD AND CENTERLINE STORES.

In connection with the above series of calculations, one perturbation proceeded from a 2000 pound bomb at the centerline to a full tank at the centerline with the same weight but with 2.4 times the pitch inertia. This produced a lower frequency mode differing radically from those baseline modes with the centerline bomb. Not unsurprisingly, the perturbation method produced nonconverged results.

Figure 13 shows relatively good agreement for the case of tip missile with outboard store. The antisymmetric mode 8 is reasonably well predicted and needs to be located to assure high flutter speeds since it is violent. The higher pitch inertia conditions probably produced perturbations which were too large. Improvements are expected with smaller perturbations.

Figure 14 shows the difficulties encountered when two symmetric modes, the fourth and fifth, are within 1.4% in frequency so that convergence is poor. Furthermore, these modes coalesce, possibly switch and are lightly damped, adding to the difficulty. Mode 3 diverges more rapidly and is better predicted. The antisymmetric modes are well separated (5%) in frequency. An agreement between perturbed and exact results is generally excellent except for the 100% pitch inertia change. Flutter speeds are very high.

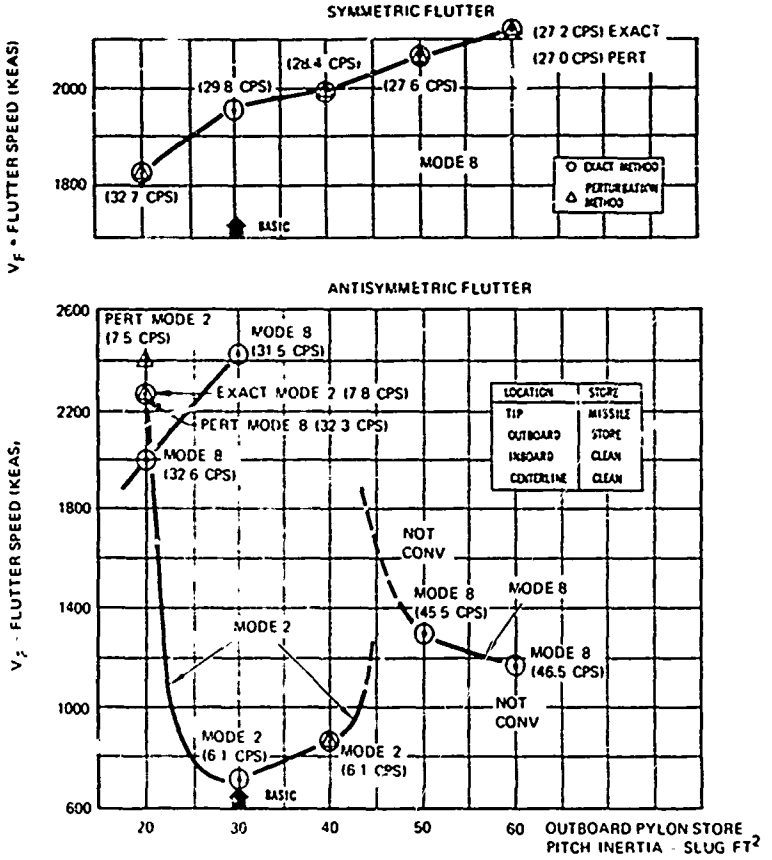

FIGURE 13. COMPARISON OF RESULTS FOR TIP MISSILE AND VARIABLE OUTBOARD STORE

The following conclusions are drawn:

a. When the changes in parameters are small so that eigenvalues and eigenvector changes in turn are small, the perturbation technique yields reliable results.

b. A 90% savings in execution time is possible.

c. The perturbation method is very effective in screening and locating critical cases. It can also be employed to determine best pylon-store dynamic characteristics (suspension tuning).

d. A complete flutter trend versus a controlling parameter (Figure 9) can be obtained in one minute using a modern computer and could be displayed on a cathode ray tube for quick engineering decisions.

e. Difficulties are caused in convergence when:

(1) A flutter velocity-frequency curve crosses another mode and flutter mode dampings are low.

(2) A new lower and radically different mode is introduced by a large perturbation.

(3) The baseline frequencies are in close proximity.

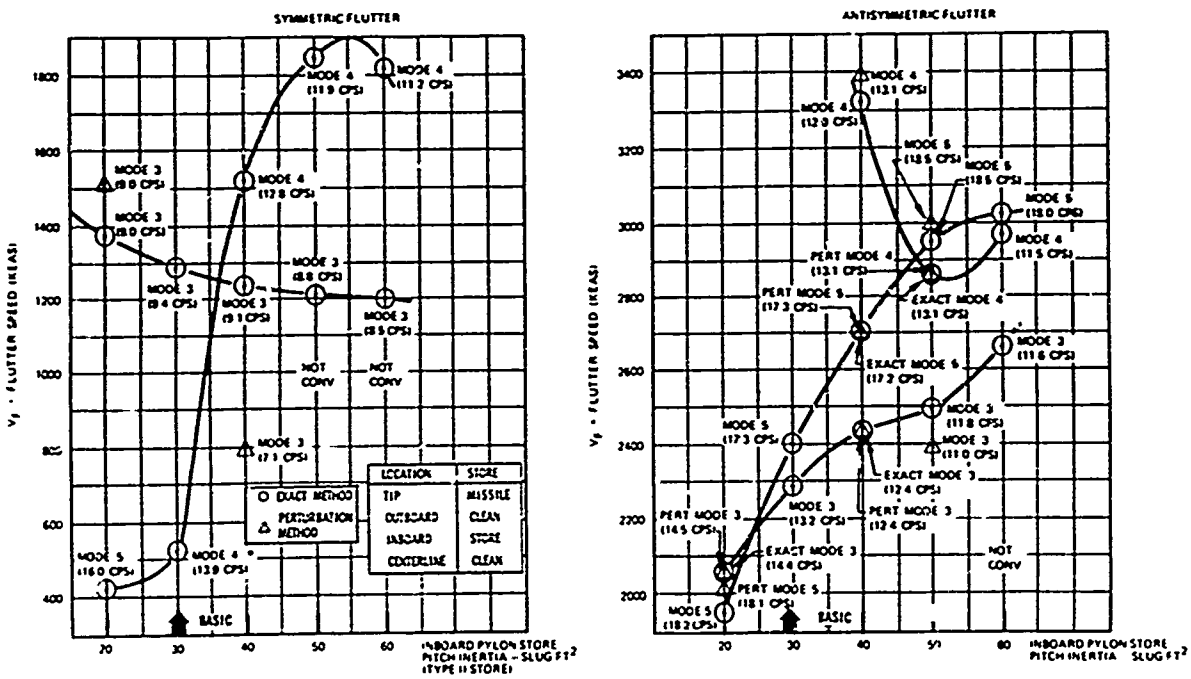

FIGURE 14. COMPARISON OF RESULTS FOR TIP MISSILE WITH VARIABLE INBOARD STORE

f. Smaller perturbations, more modes and more reduced frequencies could alleviate some of the above problems.

g. The perturbation method can be a useful and economical tool for flutter analyses involving changing parameters or determining optimum designs.

REFERENCES

1. Noll, T.E., Felt, L.R., Mykytow, W.J., Russell, Major H.L., "Potential Application of Active Flutter Suppression to Future Fighter Attack Aircraft", Presented by US AFFDL at Aircraft/Stores Compatibility Symposium, September 1973.

2. Epperson, T.B , "A Different Approach to the Problem of Flutter of Aircraft with External Stores", Ft. Worth Division of General Dynamics, Presented at Aircraft/Stores Compatibility Symposium, August 1972.

3. Chaney, J.D., and Storey, W.W., "A Review of Flutter Clearance Methods Employed on A-7 Aircraft", LTV Aerospace Corporation, Presented at Aircraft/Stores Compatibility Symposium, November 1969.

4. Moore, J.E., and Bunton, R.W., "United States Air Force Armament Laboratory Flutter Program", US Air Force Armament Laboratory, Eglin Air Force Base, Presented at Aircraft/Stores Compatibility Symposium, November 1969.

5. Katz, H., "Flutter of Aircraft with External Stores", McDonnell Aircraft Company, Presented at Aircraft/Stores Compatibility Symposium, November 1969.

6. Perisho, C., Letter on MER Rack Lateral Bending Mode Shape, McDonnell Aircraft Company, July 1974.

7. Schwartz, S., Letter on Wing-Store Flutter Clearance Methods, Northrop Corporation, August 1974.

8. Storey, W.W., "A-7 Flutter Model Results, Comparison of Low Speed, High Speed, Full Span, and Semi Span Results with Flight Test Results", LTV Aerospace Corporation, Presented to Aircraft/Stores Compatibility Symposium, August 1972.

9. Ness, H.B., Murphy, A.C., and Wilson, L.E., "The Experimental Program for Flutter Prevention on the F-111 with Wing Mounted Stores", Ft. Worth Division of General Dynamics Corporation, Presented at Aircraft/Stores Compatibility Symposium, November 1969.

10. Giesing, J.P., Kalman, T.P., Rodden, W.P., "Subsonic Unsteady Aerodynamics for General Configurations, Part I, Direct Application of the Non-planar Doublet Lattice Method", AFFDL-TR-71-5, Part I, February 1971.

11. Brock, B.J., "Investigation of an Aeroservo-Elastic Instability in an Aircraft with External Stores", LTV Aerospace Corporation, Presented at Aircraft/Stores Compatibility Symposium, November 1969.

12. Ferman, M.A., "A Rapid Method for Flutter Clearance of Aircraft with External Stores", AFFDL-TR-73-74, Volume I, September 1973.

13. Ferman, M.A., and Unger, W.H., "A New Approach for Rapid Flutter Clearance of Aircraft with External Stores", McDonnell Aircraft Company, Presented to Aircraft/Stores Compatibility Symposium, September 1973

14. van de Vooren, A.I., "A Method to Determine the Effects of Small Changes in the Mechanical System on Changes in Flutter Speed", National Luchtvaart Laboratory Report V1366, 1947.

15. van de Vooren, A.I., "Theory and Practice of Flutter Calculations for Systems with Many Degrees of Freedom', Technische Hogeschool Te Delft, (Delft University of Technology, Delft), Published by E.Ijdo N.V., Leyden, Holland.

16. Serbin, H., "The Response of an Aerodynamic System under an External Harmonic Force", J. Appl. Physics, Vol. 22, 1951, pp 1307.

17. Flax, A.H., "Aero and Hydroelasticity", Structural Mechanics, Presented to the Proc. of the First Symposium on Naval Structural Mechanics Program, Pergamon Press, 1960, pp. 285-333.

18. Andrew, L.V., "Evaluations of Methods to Predict Flutter of Wings with External Stores", North American Rockwell Corporation, Presented at Aircraft/Stores Compatibility Symposium, November 1969.

19. Siegel, S., and Andrew, L.V., "Evaluation of Methods to Predict Flutter of Wings with External Stores", AFFDL-TR-69-101, May 1970.

20. Cross, A.K., and Albano, E.A., "Computer Techniques for the Rapid Flutter Clearance of Aircraft Carrying External Stores, Part I. Perturbation Theory and Applications", AFFDL-TR-72-114, Part I, February 1973.

REPORT DOCUMENTATION PAGE

1. Recipient's Reference	2. Originator's Reference	3. Further Reference	4. Security Classification of Document
	AGARD-CP-162		UNCLASSIFIED

5. Originator	Advisory Group for Aerospace Research and Development North Atlantic Treaty Organization 7 rue Ancelle, 92200 Neuilly sur Seine, France
6. Title	Wing-with-Stores Flutter
7. Presented at	Munich, Germany
8. Author(s)	Various
9. Date	April 1975
10. Author's Address	Various
11. Pages	134
12. Distribution Statement	This document is distributed in accordance with AGARD policies and regulations, which are outlined on the Outside Back Covers of all AGARD publications.

13. Keywords/Descriptors		14. UDC
Wings	Tactical aircraft	533.695.9:533.6.013.422
External stores	Design	
Flutter	Proceedings	

15. Abstract

The carriage of stores on wings significantly changes their dynamic characteristics and often adversely affects their flutter properties through drastically reduced flutter speeds. Placarding of aircraft is frequently required because of flutter limitations, and these limitations often drastically restrict potential speed and mission performance. The large number of stores that can be carried by most tactical aircraft means that a very high number of potentially flutter critical store combinations must be evaluated. This Conference Proceedings consists of nine papers which deal with the difficult problem of Wing/Store Flutter. The latest state-of-the-art is examined, improved methods for avoiding restrictive placarding and for rapidly and economically evaluating the many possible store combinations are presented, and possibilities for optimizing the design procedure with regard to wing/store combinations are discussed.

Papers presented at the 39th Meeting of the Structures and Materials Panel in Munich, Germany, 6-12 October 1974.